An Integrated Design Approach for Improving Drinking Water Ozone Disinfection Treatment Based on Computational Fluid Dynamics

by

Jianping Zhang

A thesis

presented to the University of Waterloo

in fulfilment of the

thesis requirement for the degree of

Doctor of Philosophy

in

Civil Engineering

Waterloo, Ontario, Canada, 2006

AUTHOR'S DECLARATION

I hereby declare that I am the sole author of this thesis. This is a true copy of the thesis, including any required final revisions, as accepted by my examiners.

I understand that my thesis may be made electronically available to the public.

ABSTRACT

Ozonation is currently considered as one of the most effective microbial disinfection technologies due to its powerful disinfection capacity and reduction in levels of chlorinated disinfection by-products (DBP). However, ozonation of waters containing bromide can produce bromate ion above regulated levels, leading to tradeoffs between microbial and chemical risks. In efforts to meet increasingly stringent drinking water regulations and to be cost-effective, water suppliers are required to optimize ozone dosage. Therefore, there is a need to develop a robust and flexible tool to accurately describe ozone disinfection processes and contribute to their design and operation. Computational fluid dynamics (CFD) has come into use recently for evaluating disinfection systems. However, the focus of its application has been largely on modelling the hydraulic behaviour of contactors, which is only one component of system design.

The significance of this dissertation is that a fully comprehensive three dimensional (3D) multiphase CFD model has been developed to address all the major components of ozone disinfection processes: contactor hydraulics, ozone mass transfer, ozone decay, and microbial inactivation. The model was validated using full-scale experimental data, including tracer test results and ozone profiles from full-scale ozone contactors in two Canadian drinking water treatment plants (WTPs): the DesBaillets WTP in Montréal, Quebec and the Mannheim WTP in Kitchener, Ontario. Good agreement was observed between the numerical simulation and experimental data.

The CFD model was applied to investigate ozone contactor performance at the DesBaillets WTP. The CFD-predicted flow fields showed that recirculation zones and short circuiting existed in the DesBaillets contactors. The simulation results suggested that additional baffles could be installed to increase the residence time and improve disinfection efficiency. The CFD model was also used to simulate ozone contactor performance at the Mannheim Water Treatment Plant before and after installing new liquid oxygen (LOX) ozone generators and removing some diffusers from the system. The modelling results indicated that such changes led to an increase in effective residence time, and therefore an adjustment to operational parameters was required after system modification.

Another significant contribution is that, for the first time, the Eulerian and Lagrangian (or particle tracking) approaches, two commonly utilized methods for predicting microbial inactivation efficiency have been compared for the study of ozone disinfection processes. The modelling results of two hypothetical ozone reactors and a full scale contactor suggested that the effective CT values predicted by the Lagriangian approach were slightly lower than

those obtained from the Eulerian approach but their differences were within 10%. Therefore, both approaches can be used to predict ozone disinfection efficiency. For the full scale contactor investigated, the tracer residence time distribution predicted by the Euerlian approach provided a better fit to the experimental results, which indicated that the Eulerian approach might be more suitable for the simulation of chemical tracer performance. The results of this part of work provided important insight in understanding the complex performance of multiphase ozonation systems and played an important role in further improving CFD modelling approaches for full-scale ozone disinfection systems.

The third significant contribution of this work is that a CFD model was applied to illustrate the importance of ozone residual monitoring locations and suggest an improved strategy for ozone residual monitoring. For the DesBaillets ozone contactors, the CFD modelling results showed that ozone residuals in the cross section of the outlets of some contactor chambers differed by an order of magnitude. The "optimal" area of monitoring locations however varied at different operational conditions. Therefore, it was suggested that multiple ozone residual sampling points should be installed based on CFD analysis and experimental studies, to provide more accurate indicators to system operators. The CFD model was also used to study the factors affecting the residence time distribution (RTD). The results suggested that the selection of the tracer injection locations as well as tracer sampling locations might affect the RTD prediction or measurement. The CFD-predicted T_{10} values at different outlet locations varied by more than 10% variation. It is therefore recommended that CFD modelling be used to determine tracer test strategy before conducting a full-scale tracer test, and multiple sampling points should be employed during tracer tests, if possible.

In addition, a research based on full-scale investigation has also been done to compare the three different CT prediction approaches: CT_{10}, integrated disinfection design framework (IDDF), and CFD, to determine the most appropriate method for design and operation of ozone systems. The CFD approach yielded more accurate predictions of inactivation efficacy than the other two approaches. The current results also suggested that the differences in the three approaches in CT predictions became smaller at higher contactor T_{10}/T ratios conditions as the contactors performed more closely to ideal plug flow reactors.

This study has demonstrated that the computational fluid dynamics (CFD) approach is an efficient tool for improving ozone disinfection performance of existing water treatment plants and designing new ozonation systems. The model developed in this study can be used for ozone contactor design, evaluation, and troubleshooting. It can also be used as a virtual experimental tool to optimize ozone contactor behaviour under varying water quality and operational conditions.

ACKNOWLEDGEMENTS

First and foremost, I would like to express my sincere gratitude and appreciation to my supervisors Dr. Peter Huck and Dr. Gordon Stubley, for their knowledge and guidance to my research. Over the past four years, Dr. Huck has been providing me strong continuous support both scientifically and personally. This dissertation would have been impossible without his great efforts, encouragement, trust, and patience. I also thank him for teaching me not only drinking water treatment principles but also the great skills in producing a quality work. Dr. Stubley's creativity, inquisitive nature and incredible dedication to his work are all qualities to which I aspire. I greatly appreciate his strong support, patience and speedy replies to my numerous computational fluid dynamics queries. His expertise, feedback and guidance were crucial to the completion of my thesis.

I would also like to express my special and great thanks to Dr. William B. Anderson for his valuable advice and friendship throughout my study. I appreciate his important suggestions and countless patient hours spent on my thesis work. His unrelenting support and outstanding work ethic also made the work much enjoyable.

My sincere thanks are extended to the other members of my advisory committee for their constant interest in my work and for many useful comments during this research. They are: Dr. Susan Andrews, Dr. Neil Thomson, Dr. William Anderson and Dr. Hans van Dijk.

I would also like to gratefully acknowledge the contributions of Dr. Benoit Barbeau, Mr. Franklyn Smith, and Mr. Abhay Tadwalkar for their continuous support with respect to data collection and field investigation of the DesBaillets, Mannheim and City of Toronto Water Treatment Plants. I am very thankful for the exceptional technical support afforded by Mark Sobon and Bruce Stickney in the laboratory to this research project. I appreciated their patience and strong problem solving ability.

The financial support of the following organizations for this research is greatly acknowledged: the partners of the Natural Sciences and Engineering Research Council of Canada (NSERC) chair in Water Treatment at the University of Waterloo, and the Canadian Water Network.

My great thanks also go to all of the Water Resources Civil and Environmental Engineering Graduate students for their help, the laughs, and the memories.

Finally, I would like to express my most sincere gratitude to my parents, my wife and my son, for their unconditional encouragement, inspiration and support to my research. Their love and support is the foundation for all that I am, do, and that to which I aspire.

To my parents, to Shujun and Andrew

TABLE OF CONTENTS

LIST OF FIGURES

LIST OF TABLES

CHAPTER 1 INTRODUCTION

1.1 Research Motivation

The primary goal of drinking water treatment is to protect public health by supplying water with acceptably low concentrations of microbial and chemical contaminants. Ozone is a strong oxidant and a powerful disinfectant. It has been used in drinking water treatment for close to one hundred years (Rakness, 2005). In recent years, the application of ozone as a disinfectant has become increasingly common because of its effectiveness in treating pathogens such as oocysts of the protozoan parasite *Cryptosporidium parvum*, which are resistant to free chlorine and monochloramine at concentrations used in drinking water treatment. In addition, due to stringent regulations for trihalomethanes and other halogenated disinfection byproducts (DBPs), ozone has been identified as an effective alternative to free and combined chlorine (Finch et al., 2001; Rakness et al., 2005). Ozonation of waters containing bromide however can produce other types of DBPs (including bromate, aldehydes, and carboxylic acids) above regulated levels, leading to tradeoffs between microbial and chemical risks (Amy et al., 2000; Bellamy et al., 1998). To meet increasingly stringent drinking water regulations and to be cost-effective, water suppliers are required to optimize ozone dosage.

The current commonly used design approaches for ozone disinfection processes involve application of a CT concept, where C is the ozone residual concentration in the contactor and T is usually represented by T_{10}, which is defined as the detention time for ten percent of the water to pass through a disinfection contactor (USEPA, 1991). The

CT approach is a simple way to evaluate disinfection treatment efficiency; however, it has two important drawbacks. One is that the effect of ozone contactor hydraulics is described by a single parameter, T_{10}. Such a simple parameter cannot reveal all the underlying factors governing hydrodynamic behaviour (Greene, 2002). The other significant drawback is that the CT approach ignores the details of other important components which may affect the efficiency of ozone disinfection, including ozone mass transfer, ozone demand and decay, microbial inactivation, and bromate formation kinetics. Previous research has demonstrated that application of the CT approach may result in inaccurate estimation of the ozone disinfection efficiency (Bellamy et al., 1998).

The more recently developed Integrated Disinfection Design Framework (IDDF) is a somewhat more sophisticated approach for designing ozonation processes (Bellamy et al., 1998). The IDDF approach incorporates four components in one model, including a contactor hydraulic module, a disinfectant decay kinetics module, a pathogen inactivation module and a DBP formation module. It has been shown that the IDDF method is more accurate than the CT method in predicting ozone disinfection efficiency (Carlson et al., 2001). The IDDF approach employs the tracer residence time distribution (RTD) together with a disinfectant decay kinetic model to predict disinfection efficiency in a chemical disinfection process. However, the use of the RTD ignores the complex three dimensional flow behaviour within a contactor. Additionally, the IDDF approach uses the assumption that fluids in the disinfection contactor are completely segregated. This assumption may over- or under-estimate disinfection efficiency (Greene 2002). Therefore, there is a need to develop a more accurate approach to contribute to the design and operation of ozone disinfection processes.

Other reported studies have concentrated on modeling the hydrodynamics and disinfection performance using reactor theory models, such as continuous stirred-tank

reactor (CSTR), plug flow reactor (PFR), CSTR cascade, axial dispersion reactor, back-flow cell, and various combinations of these models (Zhou and Smith, 1994; Chen, 1998; Roustan et al., 1999; Kim, 2002). The advantage of these models is their simplicity and hence eases of solving. However, they do rely on empirical inputs, such as axial dispersion coefficients (Chen, 1998; Kim, 2002). These empirical inputs are case dependent and cannot be extrapolated to other geometries, scales, and operating conditions (Cockx et al., 1997). Therefore, there is a need to develop a more robust and flexible modelling tool to fully describe ozone disinfection processes and contribute to their design.

Computational fluid dynamics (CFD) is the science of predicting fluid flow, mass transfer, chemical reactions, and related phenomena by solving the mathematic equations governing these processes using numerical algorithms (Versteeg et al., 1995). One of the main advantages of CFD is its ability to test a large number of variables at a much lower cost than with experimental models (Hossain, 2005). Another advantage of the CFD approach is its ability to resolve small scale phenomena and its efficiency to simulate both small scale (laboratory pilot units) and large scale (full-scale reactors) facilities without the use of particular scale-up laws. Thus, the predictions of the CFD tool can be used to obtain more accurate information about the performance of the process units; and to find rapid design solutions for optimization (Do-Quang et al., 1999). CFD has gained large popularity during the last two decades due to the development of advanced commercial CFD codes and increasing power of computational resources. Applications of CFD are common in industries as diverse as the auto industry, the aerospace industry, and in the medical/biological/chemical research field. It also has been used somewhat sporadically in the drinking water field for the past decade or so, including study of mixing in reservoirs, design of clearwells and contact tanks, and optimization of design parameters for flocculators and sedimentation tanks (Grayman et al., 2003; Zhang et al., 2006e). CFD is now being

used to evaluate disinfection systems, including chlorination, ultraviolet (UV), and ozonation processes (Lyn et al. 1999; Greene, 2002; Do-Quang et al., 1999; Zhang et al., 2005).

CFD modelling of ozonation processes appears more complicated than modelling of chlorination and UV processes, because the ozonation processes include more complicated phenomena, such as interphase mass transfer, multiphases, reactions, etc.. Several researchers (Murrer et al., 1995; Peltier et al., 2001; and Huang et al. 2002) tried to simplify the problem by developing mono-phase CFD models to simulate the ozone contactors and apply their models to optimize the ozone contactor hydraulics. These models did not consider the effects of the gas phase on contactor hydraulics, so they are not capable of predicting the effects of gas flow rate, gas concentration, and gas injection locations on the contactor flow patterns.

Henry and Freeman (1995) provided a two-phase two dimensional (2D) CFD model to track ozone bubble trajectories and their influence on the velocity and pressure distribution of the mean flow field. A tracer test simulation was conducted using a transient advection-diffusion analysis and the simulation results were validated by tracer tests. The effects of the gas/liquid ratio and addition of vanes, corner fillets and wall foils were analyzed to optimize the contactor design. Ta and Hague (2004) used similar approach in a three dimensional (3D) CFD modelling of full-scale contactor. The focus of their study is only on contactor hydraulics. No attempt was performed to simulate ozone profile and pathogen inactivation performance.

Kamimura et al. (2002) developed a mono-phase CFD model for an O_3/UV reactor based on CFD analysis. The mono-phase fluid dynamics model is combined with a complex radical reaction model. This radical model consists mainly of two processes, i.e., the photochemical reaction process and the O_3/UV reaction process. The validity

of the radical reaction model was evaluated by comparing the simulated concentrations of total organic carbon (TOC), H_2O_2, and dissolved ozone with experimental data obtained from a bench-scale CSTR. Once the radical reaction model was validated, CFD simulation was executed to obtain the distribution of the concentration of TOC, ozone, $OH^{\cdot}$ and other substances in the reactor. The CFD model was used for optimizing the reactor configuration and operational conditions, to reduce the ozone demand required for decomposing TOC. The weaknesses of this model include that it is a single phase model and the model relies on details of very complex ozone reaction kinetics. Such information is difficult to obtain at site-specific conditions.

Do-Quang et al. (1999) formulated an ozone disinfection model for a two-phase ozone disinfection system. Water velocity and ozone gas hold-up fields were numerically estimated from a two phase, Eulerian flow sub-model. Ozone concentrations in the water phase were then predicted by solution of coupled mass transfer and first-order ozone decay expressions. It was reported that predicted reactor ozone concentrations correlated well with experimental results. However, the authors did not investigate the sensitivity of some important factors (such as mesh density, turbulence model slection and bubble size) on the modelling. No attempt was performed to use Lagrangian approach to simulate pathogen inactivation.

As discussed above, previous researchers have demonstrated the capabilities of CFD, however the focus of its application has been largely on modelling the hydraulic behaviour of contactors, which is only one component of system design. There are few studies considering the effects of water quality on the CFD model and there is limited information on applying a CFD model to optimize the operation of ozone contactors at varying operational conditions. No model has been reported to compare the Eulerian and Lagrangian approaches for predicting ozone disinfection efficiency. No reported

studies have compared the CFD approach with two commonly used disinfection design approaches: CT_{10} and IDDF approaches.

1.2 Research Objectives

The goal of this thesis was to develop an integrated CFD model to predict ozone disinfection performance and to assist with the design and operation of full-scale ozone contactors. The specific objectives of this research were to:

(1) develop a comprehensive multiphase CFD model to address all the major components of ozone disinfection processes: contactor hydraulics, ozone mass transfer, ozone demand and decay, microbial inactivation, and disinfection by-product formation kinetics.

(2) validate the CFD model using full-scale experimental data, including tracer testing results, ozone profiles, and microbial inactivation tests of full scale ozone contactors in two Canadian water treatment plants: the DesBaillets WTP in Montréal, Quebec and the Mannheim WTP in Kitchener, Ontario.

(3) compare the Eulerian and particle tracking approaches for the prediction of microbial inactivation efficiency of ozone contactors.

(4) improve ozone monitoring and tracer test strategies based on CFD analysis to assist with ozone contactor operation and ozone disinfection efficiency prediction.

(5) investigate the effects of water quality (represented by ozone demand, decay kinetic constants and temperature etc.) on ozone disinfection performance based on CFD modelling.

(6) use the model to predict the effective CT of ozone disinfection processes and compare the results with the results calculated from conventional design approaches, including CT_{10} and IDDF approaches.

Objectives (1) and (2) include significant improvements over previous CFD modelling approaches. Objectives (3), (4), (5) and (6) are original contributions in the field of numerical modelling of ozone disinfection processes.

1.3 Scope of Thesis

This thesis consists of seven additional chapters, as follows.

Chapter 2 Background and Literature Review: examines the most important factors affecting ozone disinfection performance, reviews the pros and cons of currently used design approaches for ozone disinfection processes, and discusses the historical CFD modelling studies for predicting the performance of drinking water treatment units.

Chapter 3 Experimental approach: presents the experimental methodologies for tracer testing, ozone demand and decay kinetics testing, ozone profile monitoring, and microbial inactivation determination experiments performed by the École Polytechnique de Montréal and the author.

Chapter 4 Development and validation of CFD model: summarizes the mathematical equations and inputs of the multiphase CFD model for ozone processes, and also provides relevant background that shaped this investigation. Presents and discusses the results including model validation and applications through two case studies.

Chapter 5 Improving ozone residual monitoring and tracer test strategies: presents the results of the sensitivity study of ozone residuals corresponding to monitoring locations and proposed ozone monitoring strategy. Discusses the effects of tracer input methods and sampling strategy on residence time distributions and T_{10} predictions.

Chapter 6 Comparison of Eulerian and Particle tracking methods in prediction of disinfection efficiency: presents the two CFD modelling approaches, compares and discusses the predicted disinfection results.

Chapter 7 A comparison of CT_{10}, IDDF, CFD approaches: presents and discusses the prediction results of disinfection performance by three different approaches.

Chapter 8 Conclusions and future work: provides the conclusions from the research and presents the recommendations for future work.

1.4 Significant Contributions of This Work

The most significant contribution of this work is that, a fully comprehensive computational fluid dynamics (CFD) model has been developed, validated and applied to quantitatively evaluate the effects of water quality and operational parameters on ozone disinfection and bromate formation.

Another significant contribution of this work is that, for the first time, the CFD modelling approach was used to assist with the optimization of the locations of ozone monitoring points to provide more accurate information for system operators.

Other contributions include: the Lagrangian approach was introduced to the modelling of ozone disinfection performance and compared the results with that of Eulerian

approach; Conducted investigation to compare CT_{10}, IDDF and CFD approach; and the effects of water quality and operational parameters on ozone disinfection performance were studied.

The work has demonstrated that the CFD approach is an efficient tool for improving the ozone disinfection performance of existing water treatment plants and designing new ozonation systems.

CHAPTER 2 BACKGROUND

Modelling ozone disinfection processes requires some understanding of background information including: 1) drinking water regulatory issues regarding disinfection and disinfection by-product (DBP) requirements; 2) ozone chemistry; 3) components of ozonation processes and factors affecting ozone disinfection processes 4) current design and modelling approaches; and 5) the background of multiphase computational fluid dynamics (CFD) and previous studies on CFD modelling of water treatment processes especially disinfection treatment systems. Each of these items is addressed in the following literature review.

2.1 Regulations for Disinfection and Disinfection By-products

Disinfection can effectively reduce the health risks caused by pathogenic microorganisms in drinking water. However, disinfectants themselves can react with naturally-occurring materials in water to form unintended organic and inorganic byproducts which may pose health risks. Therefore, the major purpose of current drinking water regulations related to disinfection is to ensure that drinking water is microbiologically safe for drinking purposes while at the same time reducing health risks resulting from the consumption of disinfectant residuals and disinfection by-products (USEPA, 1994; USEPA, 1996).

2.1.1 Regulations in the United States

In the United States, regulations for drinking water treatment by the US Environmental Protection Agency (USEPA) have directly affected the use of ozone (Rakness, 2005). These USEPA regulations include:

The Surface Water Treatment Rule (SWTR): The SWTR was promulgated in 1989 and made effective in December 1990 (USEPA, 1991). It applies to all public water systems using surface water sources or ground water sources under the direct influence of surface water. The SWTR requires that treatment plants should achieve a minimum of three logs (99.9%) and four logs (99.99%) removal and/or inactivation of *Giardia cysts* and viruses, respectively (USEPA, 1991). The SWTR guideline manual discussed ozone CT values for inactivation of *Giardia* and viruses. Ozone CT is defined as ozone residual times contact time, which is similar in concept to chlorine CT (Rakness, 2005). Consequently, the SWTR is based on the approach of specifying treatment requirements instead of the regulatory approach used in some other conditions of establishing maximum contaminant levels (MCLs) for target pathogenic microorganisms.

Interim Enhanced Surface Water Treatment Rule (IESWTR): The IESWTR was promulgated in December 1998 and made effective in February 1999 (USEPA, 1999). It applies to systems using surface water, or ground water under the direct influence of surface water that serve 10,000 or more persons. The rule built upon the treatment technique requirements of the Surface Water Treatment Rule with the following key additions and modifications: i) it introduced a maximum contaminant level goal (MCLG) of zero for *Cryptosporidium*; ii) it set 2-log *Cryptosporidium* removal requirements for systems that filter; iii) it lowered filtered water turbidity requirements; and iv) it included disinfection benchmark provisions to assure continued levels of

microbial protection while facilities take the necessary steps to comply with new DBP standards.

Stage 1 Disinfectants and Disinfection Byproducts Rule (Stage 1 DBPR): The final Stage 1 DBPR was promulgated in December 1998 and made effective in February 1999 (USEPA, 1999). It applies to community water systems and non-transient non-community systems, including those serving fewer than 10,000 persons, that add a disinfectant to the drinking water during any part of the treatment process. The final Stage 1 Disinfectants and Disinfection Byproducts Rule included the following key provisions: i) it set maximum residual disinfectant level (MRDLs) for three disinfectants (chlorine [4.0 mg/L], chloramines [4.0 mg/L], and chlorine dioxide [0.8 mg/L]); and ii) it lowered maximum contaminant level (MCLs) for total trihalomethanes to 0.080 mg/L, haloacetic acids (HAA5) to 0.060 mg/L, and set two inorganic disinfection byproducts (chlorite (1.0 mg/L) and bromate (0.010 mg/L)).

Long Term 1 Enhanced Surface Water Treatment Rule (LT1ESWTR): The Rule was promulgated in January 2002 and made effective in January 2005 (USEPA, 2002). The purpose of the LT1ESWTR is to improve the control of microbiological pathogens such as *Cryptosporidium* in public drinking water systems serving fewer than 10,000 persons. It also protects the public against increases in risk from such pathogens in cases where systems alter their disinfection practices to meet new disinfection byproduct standards promulgated under the Stage 1 Disinfectants and Disinfection Byproducts Rule (DBPR). The rule was developed based on the IESWTR, but has been modified to reduce the burden on small systems.

Long Term 2 Enhanced Surface Water Treatment Rule (LT2 ESWTR): The LT2 ESWTR was promulgated in January, 2006 and made effective in March, 2006 (USEPA, 2006a). The purpose of the LT2 ESWTR is to reduce disease incidence

associated with *Cryptosporidium* and other pathogenic microorganisms in drinking water. The rule applies to all public water systems that use surface water or ground water that is under the direct influence of surface water. The LT2 ESWTR classified filtered water systems into one of four treatment categories (bins) based on actual monitoring results. Systems classified in higher bins must provide additional water treatment to further reduce *Cryptosporidium* levels by 90% to 99.7% (1.0 to 2.5-log), depending on the bin. All unfiltered water systems must provide at least 99% or 99.9% (2 or 3-log) inactivation of *Cryptosporidium*, depending on monitoring results. The LT2 ESWTR introduced *Cryptosporidium* log inactivation CT tables for ozone disinfection treatment. The CT values for *Cryptosporidium* inactivation credits are 15 to 25 times higher than for *Giardia*. Therefore, a larger ozone dose is needed to meet *Cryptosporidium* inactivation credit. Consequently, the LT2 ESWTR will increase operating costs, and may increase ozone disinfection by-product formation (Rakness, 2005). The USEPA also published the draft LT2ESWTR Implementation Guidance Manual and Draft LT2 ESWTR Toolbox Guidance Manual (USEPA, 2003), which included alternative inactivation credit calculation methods to assist with design and operation of full-scale ozone disinfection systems.

Stage 2 Disinfectants and Disinfection Byproducts Rule (Stage 2 DBPR): The Stage 2 DBPR was proposed in August 2003 and promulgated on December 15, 2005 (USEPA, 2006b). The Stage 2 DBP rule focuses on public health protection by limiting exposure to DBPs, specifically total trihalomethanes (TTHM) and five haloacetic acids (HAA5), which can form in water through disinfectants used to control microbial pathogens. This rule applies to all community water systems and nontransient noncommunity water systems that add a primary or residual disinfectant other than ultraviolet (UV) light or deliver water that has been disinfected by a primary or residual disinfectant other than UV.

2.1.2 Regulations in Canada

In Canada, drinking water regulations are developed through a federal-provincial-territorial consultative process. The drinking water guidelines are established by health Canada (Health Canada, 2006). However, each province adopts fully or partially the guidelines set forth by Health Canada and enforces them legally. The current Guidelines outline a standard for total coliforms and *E. Coli* of zero per 100 mL, however no numerical guidelines exist to monitor and control the concentrations of viruses and resistant protozoa such as *Giardia* and *Cryptosporidium parvum*. Viruses and protozoa are under review for potential regulations in the next revision of the guidelines (Health Canada, 2006). However, the Guidelines state: "If the presence of viable, human-infectious cysts or oocysts is known or suspected in source waters, or if *Giardia* or *Cryptosporidium* has been responsible for past waterborne outbreaks in a community, a treatment and distribution regime and a watershed or wellhead protection plan (where feasible) or other measures known to reduce the risk of illness should be implemented. Treatment technologies in place should achieve at least a 3-log reduction in and/or inactivation of cysts and oocysts, unless source water quality requires a greater log reduction and/or inactivation". The guidance suggests the use of CT concept to design drinking water disinfection systems, however does not provide CT tables for different disinfectants. Some water treatment plants are voluntarily using the USEPA's SWTR approach to ensure that the treated water is microbiologically safe for drinking purposes by minimizing the waterborne concentration of viruses and *Guardia lamblia* (Bdantyne, 1999). For disinfection by-products, the Guidelines specify an interim maximum acceptable concentration (IMAC) of 0.100 mg/L for TTHMs and an IMAC of 0.01 mg/L for Bromate (Health Canada, 2006).

The detailed disinfection requirements are given in many Canadian provincial regulations. For example, the Ontario Ministry of Environment (MOE) requires that

drinking water systems that obtain water from a raw water supply which is surface water or ground water under the direct influence of surface water must achieve a minimum a 2-log (99%) removal or inactivation of *Cryptosporidium oocysts*, a 3-log (99.9%) removal or inactivation of *Giardia cysts* and a 4-log (99.99%) removal or inactivation of viruses before the water is delivered to the first consumer. At least 0.5-log removal or inactivation of Giardia cysts and 2-log removal or inactivation of viruses must be provided through the disinfection portion of the overall water treatment process. In "Procedure for Disinfection of Drinking Water in Ontario" (MOE, 2006), the CT tables for inactivation of *Cryptosporidium oocysts*, *Giardia cysts* and viruses by different chemical disinfectants have been provided. It also stated that "The treatment processes must be designed and always operated to achieve the required removal or inactivation of pathogens as a priority with the minimization of disinfection by products formation as a secondary objective".

Generally, American regulations are more stringent than those in Canada. However, it is expected that Canadian regulations will follow a similar path to those stipulated in the United States. It is therefore necessary to consider American regulations when designing new treatment plants or when altering disinfection practices at existing treatment plants in order to ensure that new treatment processes meet forecasted future Canadian regulations (Bdantyne, 1999).

2.1.3 Effects of Current Regulations on Application of Ozone Disinfection Treatment

The American and Canadian drinking water regulations have been and will continue to be more and more stringent to ensure that drinking water is microbiologically safe and at the same time minimize health risks resulting from disinfection by-products. The stricter requirements for removal/inactivation of pathogenic microorganisms especially

Cryptosporidium and the lower limits for chlorinated disinfection by-products are major drive forces for many water utilities to choose ozone as a primary disinfectant. Ozone has been proven to be an excellent alternative disinfectant in many cases: i) to enhance *Cryptosporidium* and *Giardia* inactivation treatment; ii) to partially replace chlorine to reduce the formation of the chlorinated DBPs such as TTHM and HAA5; and iii) to be used in treatment plants without filtration systems meeting disinfection requirement by ozone alone (Rakness, 2005). Therefore, it is expected that the application of ozonation will continue to grow in the water industry.

However, ozone disinfection is currently a more expensive technique than chlorination and ultraviolet (UV) disinfection. In addition, ozonation of waters containing bromide can produce other types of DBPs (including bromate, aldehydes, and carboxylic acids) above regulated levels, leading to tradeoffs between microbial and chemical risks (Amy et al., 2000; Bellamy et. al., 1998). In efforts to meet increasingly stringent drinking water regulations and to be cost-effective, water suppliers are required to optimize ozone dosage. The purpose of this study is to develop computational fluid dynamics (CFD) models to fully describe ozone disinfection systems and to use CFD as an effective tool to balance between the microbial inactivation requirements and DBP-related health risks.

2.2 Aqueous Chemistry of Ozone

2.2.1 Reactions of Ozone in Water

Ozone is a gas of limited solubility that must first be dissolved into water to be effective against microorganisms（Langlais et al., 1991; Bryant et al., 1992; Singer and Hull, 2000). Once dissolved, aqueous ozone engages in complex chemistry that includes

auto-decomposition and reaction with various constituents of the water, in addition to reaction with microorganisms (Langlais et al., 1991).

Aqueous ozone may react with various species via two pathways: direct reaction by molecular ozone and/or indirect reaction by the radical species that are formed when ozone decomposes in water (Langlais et al., 1991). Depending on the treatment objectives, either pathway may be relevant. In the case of disinfection, the direct reaction pathway of molecular ozone is relevant because the reaction of molecular ozone with different constituents of natural water sources is relatively slow and selective (Langlais et al., 1991), whereas OH radicals react rapidly with many types of dissolved species and are therefore scavenged before they encounter particles such as microorganisms. This has been demonstrated experimentally using *Giardia muris cysts* (Labatiuk et al., 1994, as cited by Urfer et al., 1999). The evidence that is available also suggests that ozone achieves disinfection largely through oxidation reactions that damage and destroy critical components of micro-organisms (Finch et al., 2001; Bryant et al., 1992). For the oxidation of certain micropollutants in the waters, the kinetics of the direct reaction of molecular ozone is too slow, and therefore the reaction of OH radicals with such components is of importance (Urfer et al., 1999).

The mechanism of ozone reaction and decomposition has been the subject of numerous studies (e.g. Langlais et al., 1991; Singer and Hull, 2000). The two most widely accepted mechanisms for decomposition of the ozone in water are shown in Table 2.1.

Table 2.1 Mechanisms of ozone decomposition in water

Steps	Hoigne, Staeholin and Bader mechanisms (Langlais *et al*, 1991)	Gordan, Tomiyasn and Fukuton mechanisms (Langlais *et al*, 1991)
Initiation Step	(1) $O_3 + OH^- \xrightarrow{k_1} HO_2 + O_2^-$	(9) $O_3 + OH^- \xrightarrow{k_9} HO_2^- + O_2$
	(1') $HO_2 \xrightarrow{k_1'} O_2^- + H^+$	(10) $HO_2^- + O_3 \xrightarrow{k_{10}} O_3^- + HO_2$
		(11) $HO_2 + OH^- \xrightarrow{k_a} O_2^- + H_2O$
Propagation/ termination step	(2) $O_3 + O_2^- \xrightarrow{k_2} O_3^- + O_2$	(2) $O_3 + O_2^- \xrightarrow{k2} O_3^- + O_2$
	(3) $O_3^- + H^+ \xrightarrow{k_3} HO_3$	(12) $O_3^- + H_2O \xrightarrow{k_{12}} OH + O_2 + HO^-$
	(4) $HO_3 \xrightarrow{k_4} OH + O_2$	(13) $OH + O_3^- \xrightarrow{k_{13}} O_2^- + HO_2$
	(5) $OH + O_3 \xrightarrow{k_5} HO_4$	(14) $OH + O_3^- \xrightarrow{k_{14}} O_3 + HO^-$
	(6) $HO_4 \xrightarrow{k_6} HO_2 + O_2$	(15) $OH + O_3 \xrightarrow{k_{15}} HO_2 + O_2$
	(7) $HO_4 + HO_4 \rightarrow H_2O_2 + 2O_3$	(16) $OH + CO_3^{2-} \xrightarrow{k_{16}} OH^- + CO_3^-$
	(8) $HO_4 + HO_3 \rightarrow H_2O_2 + O_3 + O_2$	(17) $CO_3^- + O_3 \rightarrow products (CO_2 + O_2^- + O_2)$

In natural water, the reaction and decomposition of ozone are strongly dependent on water quality. Some species may induce the formation of a superoxide ion (O_2^-) from an ozone molecule, which then initiate the ozone chain reaction. These species are called initiators. Some other species may react with the hydroxyl radical (OH·) and regenerate the superoxide anion (O_2^- or HO_2^-), these species promote ozone decomposition, and are called promoters. There are also some species that are capable of consuming hydroxyl radical but do not generate the superoxide ions. These species provide a stabilizing effect on the ozone molecule in the water, and are called inhibitors.

Aqueous ozone chemistry is still the subject of research. Some researchers have tried to develop kinetic-based mechanistic models to predict ozone reactions (Yuteri and Gurol, 1988; Chelkowska et al., 1992; Westerhoff et al., 1996). But the precise description of

ozone reactions is still difficult at the present time because of the complexity of ozone reactions and limited information on kinetic constants.

2.2.2 Pathways and Reactions of the DBP Formation

Bromate (BrO_3^-) is the main ozone disinfection byproduct of human health concern. Drinking water regulations in the U.S. have specified a maximum contaminant level (MCL) of 10 μg/l for the bromate ion (USEPA et al., 1998). Future regulations for bromate may be lowered since 10 μg/L currently represents a 10^{-4} excess cancer risk level and is higher than the normal regulatory level of 10^{-6} (Westerhoff, 2002).

Bromate can form through both a molecular ozone pathway and a hydroxyl radical pathway, depending on the dissolved organic carbon (DOC) concentration, Br^- content, and pH of the source water (Siddiqui et al., 1998). In the molecular ozone pathway, Br^- is first oxidized by dissolved ozone to form the hypobromite ion (OBr^-) which is then further oxidized to BrO_3^- as shown below.

$$Br^- \xrightarrow{O_3} BrO^- \xrightarrow{O_3} BrO_2^- \xrightarrow{O_3} BrO_3^-$$

Via the hydroxyl radical pathway, the dissolved ozone plays an indirect role by decomposing ozone to produce hydroxyl radicals, which further react with bromine species to produce BrO_3^-.

Figure 2.1 shows the possible chain reactions for bromate formation during ozonation treatment. Molecular ozone, OH radical reactions, and reactions of intermediate species with some water matrix components are shown in this figure.

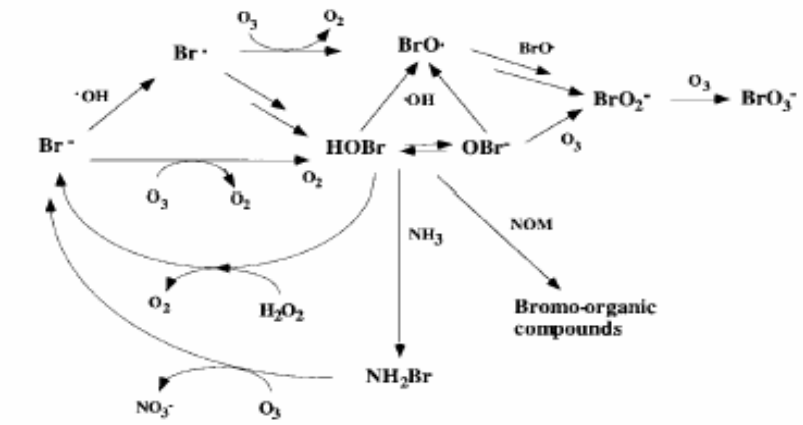

Figure 2.1 Bromate formation pathways (von Gunten and Pinkernell, 2000)

Previous research (Hofmann and Andrews, 2001) indicated that, the rate constants of the ozone molecular pathway reactions are much lower than those for the hydroxyl radical pathway reactions. Therefore, the ratio of the O_3/OH will have great influence on the reactions of bromate formation. In other word, the rate of ozone decomposition may greatly affect bromate formation.

2.2.3 Effects of Water Quality on Ozone Decay and DBP Formation

Many aqueous species can function as the initiators, promoters, or inhibitors of the reactions of ozone decomposition and bromate formation. Therefore, the ozonation process highly depends on water quality parameters, including pH, alkalinity, natural organic matter (NOM), and temperature etc.

Temperature

Temperature influences the solubility of the ozone as well as its chemical reaction-rate coefficients. The Henry's Law coefficient increases in the temperature range typical for

water treatment by about 5% /˚C. Also, activation energies for the reactions of ozone with specified reactants at ambient temperature typically are in the range 35 to 50 kJ/mol. The decomposition of ozone in natural water, however occurs by chain reactions and their temperature effects vary for different types of waters (Hoigne, 1994).

Since the concentration of hydroxyl radicals increases with increasing temperature, bromate formation will be accelerated at higher temperatures, though some researchers agree that temperature has a relatively small effect on bromate formation relative to pH and ammonia concentration (von Gunten and Pinkernell, 2000).

pH

OH^- is the main initiator of the chain reaction for ozone decomposition. Therefore, an increase in pH will promote ozone decomposition and influence the oxidation reactions of ozone with other species. It was reported that when ozone dissolves in aqueous solutions at pH levels below 7, it does not react with water and is present as molecular O_3. As the pH is elevated, however, spontaneous decomposition of ozone occurs to ultimately produce a variety of very reactive free radials, such as the hydroxyl radical ($OH\cdot$) (Gorden, 1995).

pH also has great influence on the bromate formation (von Gunten and Pinkernell, 2000). Decreasing pH can change the bromate formation in two ways:

(1) Shift of $HOBr/OBr^-$ equilibrium to HOBr to prevent further oxidation by ozone.

(2) Decrease of the rate of OH radical formation from ozone decomposition which results in a decrease of the rate of the oxidation of HOBr.

Therefore, bromate formation in ozonation processes may be controlled by the method of pH depression.

Alkalinity

Carbonate and bicarbonate ions can scavenge the hydroxyl radicals formed during the ozone decomposition, which otherwise would act as chain carriers in the radical-type reactions decomposing ozone in water. As a result, alkalinity species may reduce the decomposition rate of the dissolved ozone and inhibit the hydroxyl radical pathway of bromate formation or other ozone consumption reactions. This means that a water with high alkalinity may have better disinfection performance and lower DBP formation (Fabian, 1995).

In addition, in waters with low dissolved organic matter (DOC), bicarbonate and carbonate may become the dominant scavengers for OH radicals and thereby protect micropollutants from being oxidized. Above pH 8.5, the effect of alkalinity becomes pH dependent because carbonate ions scavenge OH radicals with rate constant much larger than that of bicarbonate ion (Hoigne, 1994).

Ammonia

Ammonia (NH_3) reacts with ozone very slowly, and does not significantly affect ozone decomposition due to its slow reaction with ozone and $OH\cdot$. However, in the presence of the bromide ion, ammonia can mask the hypobromate ion formed during ozonation and thereby delay the formation of bromate, bromoform and further bromo-organic compounds (Langlais et al., 1991). As a result, the formation of bromate can be inhibited in ammonia-containing water.

Addition of ammonia may be used as a bromate control method. However, bromate removal by ammonia addition is not efficient for waters that have a low pH and/or already contain high ammonia levels (Westerhoff, 2002).

Natural organic matter (NOM)

The stability of ozone largely depends on the type and content of natural organic matter (NOM). NOM can affect the ozone stability in two ways: (a) directly through reacting with ozone; (b) indirectly by scavenging of OH radicals (OH·) and leading to an accelerated ozone decomposition.

NOM is involved in bromate formation in several ways by (1) influencing ozone demand and rate of ozone decay, (2) affecting OH· concentrations, (3) reacting with HOBr/OBr and (4) potentially reacting with brominated radicals.

Generally, the presence of the NOM in water will lower the stability of ozone through direct reaction with molecular ozone and consumption of OH radicals. The presence of NOM inhibits the formation of bromate especially at the initial period of ozonation (Song, 1996).

Summary of the effects of water parameters

The effects of the above water quality parameters on ozone decomposition and bromate formation are summarized in Table 2.2 (adapted from Westerhoff, 2002).

Table 2.2 Effects of water quality parameters on ozonation

Parameters	Disinfection efficiency	Decomposition rate	Bromate formation rate
Temperature +	+	+	+
pH+	–	+	+
Bromide +	–	+	+
Alkalinity +	+	–	–
NOM +	–	+	–
Ammonia +	unchanged	unchanged	–

("+": increasing concentration or value; "–": decreasing concentration or value)

2.3 Overview of the Ozone Disinfection Process

2.3.1 Process Description

In drinking water treatment, ozone is produced by an ozone generator. The feed gas can be either air or pure oxygen. A high voltage (6-20 KV) is applied to two electrodes and the high voltage produces an arc. In the arc, part of the O_2 is converted into O_3. Ozone is very unstable and reverts back to O_2 within minutes. Therefore ozone must be generated on-site and cannot be shipped to water treatment plants.

For the ozone to perform disinfection and oxidation it must be brought into the water and dispersed as finely as possible. This is accomplished generally through fine bubble diffusers located in baffle chambers, or in a turbine type contactor. Figure 2.2 shows the typical arrangement for three types of ozone contactor.

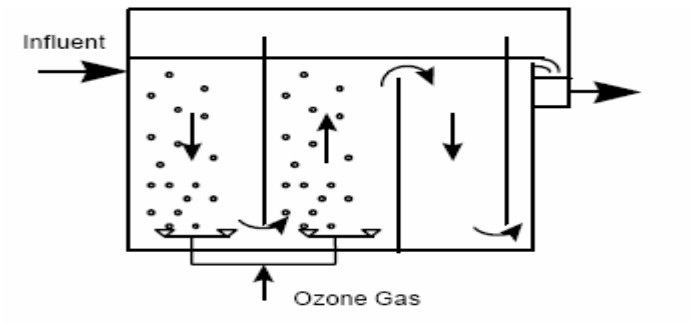

(a) Baffled chamber

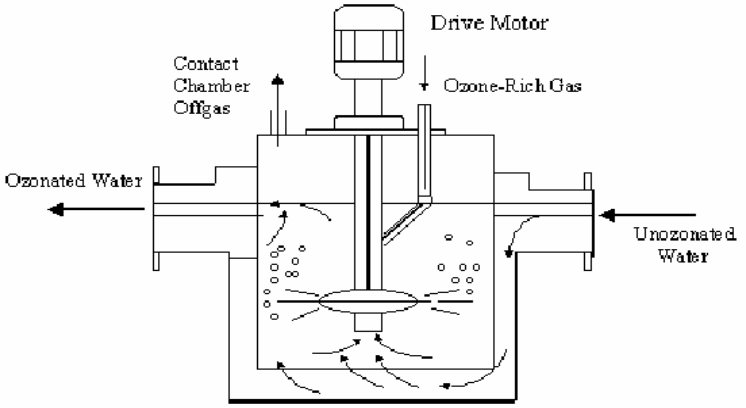

(b) Turbine Diffuser

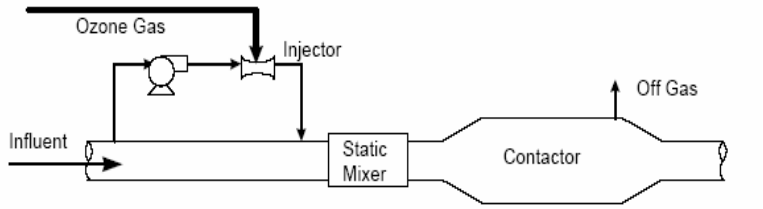

(c) Side-stream ozone system

Figure 2.2 Three typical types of ozone contactors (adapted from USEPA, 1999)

Baffled chamber diffusers seem to be most prevalent because of its multiple advantages, such as: no moving parts, effective ozone transfer, low hydraulic headloss, and operational simplicity (USEPA, 1999). The number of chambers, their geometry, the diffuser systems, and their operation differ from plant to plant and are subject to the experience of the design engineers. A typical ozone contactor usually has several compartments in series with bubble diffusers at the bottom. The chambers are covered to prevent the escape of ozone and to increase the partial pressure of the ozone in the contactor. Additional chambers follow to guarantee a contact time between the ozone and the water. Each of the chambers has sampling ports so that the ozone concentration in each chamber can be determined. This is needed to calculate the product of concentration and detention time to get the required CT value.

Research has shown that the following design and operational variables may have a significant impact on the ozone contactor performance (Bellamy, 1995; Singer and Hull, 2000):

- Geometry of the ozone contactor (configuration, cell numbers, inlet/outlet arrangement)
- Mode of contacting, e.g., cocurrent, countercurrent, and turbine (completely mixed)
- Placement, shape, and number of baffles
- Diffuser placement
- Range in water flow rates
- Gas/liquid flow ratio (dose and feed gas concentration)

All of these factors relate to the disinfection objective. The relationship between these factors and the efficiency of disinfection, however still has not been defined (Bellamy, 1995). To date, no single model (either mathematical or empirical) or approach has been developed to account for all above factors in the design and operation of ozone processes.

2.3.2 Factors Affecting Ozone Disinfection Performance

The efficiency of the ozone disinfection process is governed by several key components including contactor hydraulics, ozone mass transfer, ozone chemistry, microbial inactivation kinetics, and DBP formation kinetics (Bellamy, 1995).

2.3.2.1 Ozone Contactor Hydraulics

Contactor hydrodynamic conditions are of primary importance in ozonation systems since mixing conditions significantly affect the observed gas and liquid concentration profiles, and can greatly affect disinfection efficiency (Bellamy, 1995). Ozone contactors should be designed to provide adequate residence time for the microbial inactivation.

Tracer studies have long been used to determine mixing in disinfection contactors. The residence time distribution (RTD) is measured by applying a conservative tracer to the inlet of an ozone contactor and measuring the effluent concentration as a function of time. Two types of tracer studies are typically performed, pulse tracer tests or step tracer tests. The pulse tracer test involves the injection of a mass of tracer solute instantaneously into the reactor influent, while the step tracer test is performed via a step changes in concentrations of a tracer added to the influent of the reactor. The effluent tracer concentration as a function of time is recorded during the tracer testing

and the residence time distribution curve can be obtained from tracer test data (Levenspiel, 1999; USEPA, 1991).

Modelling of the ozone contactor hydrodynamics has been well addressed in some previous studies (Bellamy, 1998; Cheng, 1999; Kim, 2002). The most commonly used models are Plug Flow with Dispersion model (PFD), the Continuous Stirred Tank Reactor model (n-CSTR), the Axial Dispersion model or a combination of one or more of these models. Due to the complexity of ozone contactor mixing, these models are questionable to be used for accurately prediction of hydraulic performance. Application of these models is not feasible under varying operational conditions, such as change of gas/liquid flow rates and water level.

Ozone Mass Transfer

Since ozone gas has limited solubility and it must first be dissolved into water to be effective against microorganisms, the transfer of ozone from gas phase to the liquid phase is of central importance in the study of ozonation systems applied for drinking water treatment.

According to the two-film theory developed by Lewis and Whitman (1924) as cited by Singer and Hull (2000), ozone mass transfer occurs across the gas and liquid films. For relatively insoluble gases such as ozone, the gas-phase resistance becomes negligible compared with the liquid-phase resistance. The rate of ozone mass transfer according to the two-film model is given by the following equation:

$$\frac{dC_l}{dt} = K_l\, a(C_l^{*} - C_l) \qquad (2.1)$$

where

C_l = liquid phase ozone concentration g O_3/m^3

K_l = liquid-phase ozone transfer coefficient, m/min

a = interfacial area per unit volume, m^2/m^3

C_l^* = saturation liquid phase ozone concentration, g O_3/m^3

t = time, min

For a gas-liquid ozone system, the reactions in liquid phase (water) are quite fast. It is therefore important to consider if the liquid film reactions can increase the concentration gradient in the film to enhance mass transfer (Singer and Hull, 2000). A dimensionless Hatta number can be used to calculate the enhancement factor. The Hatta number (Ha) is expressed as:

$$Ha = (k_l \cdot D_{O_3})^{1/2} / K_l \qquad (2.2)$$

where, k_l is the first-order rate constant with ozone (min^{-1}); D_{O_3} is the diffusion coefficient of ozone in water (m^2/min); and K_l is the liquid phase mass transfer coefficient (m/min).

For significant reactions in the liquid phase to produce enhanced mass transfer, the Hatta number must be greater than 0.3 (Singer and Hull, 2000). Several studies (Yurteri, 1988; Zhou and Smith, 1995; Singer and Hull, 2000) have demonstrated that the Hatta number is much less than 0.3 at different ozone reaction conditions, even at high pH values where ozone decomposition is rapid. Therefore the enhancement of mass transfer by liquid film reactions is negligible, and it is an acceptable approach to model mass transfer and ozone reactions as separate processes.

As ozone is a sparingly soluble gas, its transfer efficiency is mainly controlled by such physical parameters as temperature, gaseous flow rate, water quality and type of diffusers (Zhou and Smith, 1995; Marinas, 1999; Wu and Masten, 2001; Beltran, 2005). In this study, the mass transfer coefficient was estimated from literature correlations. Additional details of the empirical model selection for mass transfer coefficient will be discussed in Chapter 4.

The Decomposition Kinetics of Ozone

Once dissolved in water ozone becomes very unstable. Previous ozonation studies have showed that for water containing natural organic matter there is a rapid initial consumption of ozone followed by a slower period of decay (Zhou and Smith, 1995; Marinas, 1999; Singer and Hull, 2000; Wu and Masten, 2001; Beltran, 2005). Figure 2.3 shows a conceptual ozone decomposition curve plotting log concentration versus time.

The difference between the applied ozone dose and the initial ozone residual is termed as the immediate ozone demand (IOD), and can be expressed as:

$$IOD = C_{in} - C_0 \tag{2.3}$$

where, C_{in} is the applied ozone dosage (mg/L) and C_0 is the initial ozone residual (mg/L).

For a specific water, the IOD is usually a function of ozone dosage (El-Baz, 2002). However, the experimental results of Kim (2002) show that the IOD is almost constant at different dosages. Therefore, the IOD value is strongly water quality dependent and should be determined for site-specific conditions.

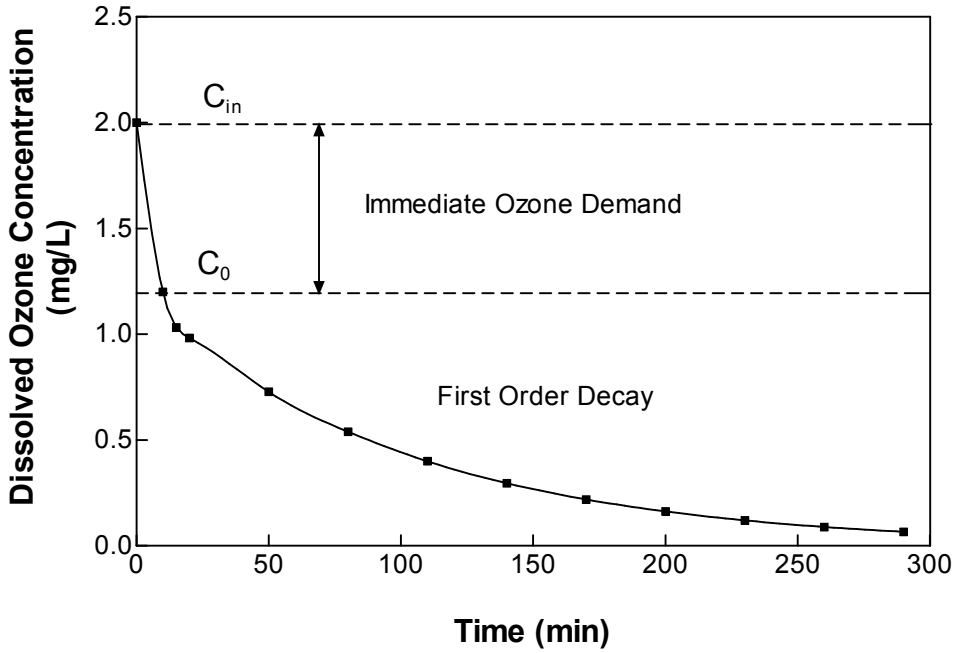

Figure 2.3 A typical ozone decomposition curve

Following the fast initial demand period, the slower decay period of ozone residual can typically be characterized with a pseudo first-order kinetics model as follows (Langlais et al., 1991):

$$\frac{dC_l}{dt} = -k_d C_l \tag{2.4}$$

where k_d = water quality dependent decay rate constant (min^{-1}) and C_l is dissolved ozone concentration (mg/L), t = time (min)

The decomposition of ozone is also highly dependent on water quality parameters. Previous studies have been conducted to develop models for predicting the effects of water quality factors on ozone decay kinetics (Chen et al., 1999; Chelkowska et al., 1992; Westerhoff et al., 1996; Yuteri and Gurol, 1988; Siddiqui et al., 1998; Urfer et al.,

1999). Two types of models have been employed, one is a numerical model, and the other is an empirical model.

The numerical models were based on ozone chemistry. Such models can be more widely used under varying water quality conditions. This approach includes many intermediate reactions and detailed information on the reaction kinetics is currently still limited. Different numerical models have resulted in completely different predicted results (Chelkowska et al., 1992; Westerhoff et al., 1996; Yuteri and Gurol, 1988).

Empirical decomposition models have used data from bench or full scale experiments (Chen et al., 1999; Siddiqui et al., 1998; Urfer et al., 1999). Since most current empirical models are obtained for limited numbers of synthetic waters or natural waters, these models are site-specific. Hoigne (1995) indicated that, for a given water, the sensitivity of ozone decomposition with respect to small changes in chemical composition can be estimated from empirical correlation, however, correlation including varying types of waters is highly uncertain. Therefore, empirical models are site-specific, unless a model is validated with a wide range of water sources.

Microbial Inactivation Kinetics

Numerous studies have been performed to describe the kinetics of microbial inactivation by ozone for batch systems (Finch et al., 2001). Table 2.3 summarizes reported models.

Table 2.3 Summary of microbial inactivation kinetic model of ozone

Model	Survival ratio
Chick-Watson	$-kC^nT$
Hom	$-kC^nT^m$
Rational	$\frac{-1}{x-1}\ln[1+N_0{}^{x-1}(x-1)kC^nT]$
Hom-power law	$\frac{-1}{x-1}\ln[1+N_0{}^{x-1}(x-1)kC^nT^m]$
Multiple target	$\ln[1-(1-e^{-kCT})^{n_c}]$
Series-event	$\frac{-kCT+\ln[\sum_{\kappa=0}^{l-1}\frac{(kCT)^\kappa}{\kappa!}]}{x-1}$

(Source: Adapted from Finch et al., 2001)

The Chick-Watson model is a pseudo first order rate model that predicts a linear log survival plot. However, ozone disinfection systems rarely display first order kinetics. Typical log survival plots exhibit “shoulders” or “tailing”. The presence of a “shoulder” has been attributed to inadequate mixing, delays in diffusion of the disinfectant to target sites on microorganisms, or the condition of multiple target sites required for microbial inactivation. “Tailing” has been attributed to the presence of distinct sub-populations with varying resistance to a disinfectant or a distributed inactivation resistance within one population (Gyurek, 1998).

The Hom model accounts for derivations from the Chick-Watson model. The intrinsic kinetics aer assumed to be pseudo first-order. The Hom model, however predicts derivations from first-order kinetic behaviour due to non-ideal conditions in a batch reactor. For m=1, the disinfection kinetics follow a pseudo-first order relationship

(Chick-Watson model). For m>1, the presence of "shoulders" is predicted; for m<1, "tailing" is predicted.

The Rational model employs the power law to describe disinfection kinetics. Similar to the Hom model, the rational model can predict "shoulders" and "tailings" for x>1 and x<1, respectively.

The Multiple target model states that each microorganism possesses multiple "target sites", all of which must be contacted by the disinfectant to inactivate individual or grouped microorganisms. Multiple target models are thought to be unsuitable to accurately describe disinfection kinetics because microorganism clumps are of unequal size and consequently it is unlikely that cell damage will be randomly distributed across the microbial community.

The Series event model considers that an organism has an infinite number of targets, and that a finite number of lethal events are required for inactivation. Series event models assume that each lethal event is first-order with respect to disinfectant concentration. Since this assumption is not valid for most ozone disinfection systems, series event models are generally thought to be unsuitable to describe ozone disinfection behaviour. Furthermore, series-event models are not well suited to predict "tailing" behaviour.

Finch et al. (1992) performed *Giardia* inactivation studies using ozone and found that the Chick-Watson model was not appropriate in describing the inactivation of *Giardia muris cysts* since ozone competing reactions and demands significantly affected the residual concentration thereby increasing the survival of *Giardia cysts*. In a later study, Finch et al. (1994) reconfirmed that the Hom-type kinetic model more accurately represented the ozone inactivation of parasite cysts and oocysts, including *Giardia* and

Cryptosporidium, than other models. Thus, the Hom model has been more commonly used for ozone disinfection processes in recent ozone studies (Finch et al., 1994; Gyurek, 1998; Bellamy et al., 1998; Carlson et al., 2001; Kim, 2002).

Bromate Formation Kinetics

Bromate formation is also highly dependent on water quality parameters and some operational conditions such as ozone dosage and residence time. Similar to the ozone decomposition kinetics, bromate formation kinetics also have two types of models: empirical models and kinetic based models.

Most of the empirical bromate formation models permit predictions based on water quality conditions (DOC, [Br^-], pH, alkalinity, and temperature) and on treatment conditions reflected by transferred ozone dose and contact time (Song et al., 1996; Ozekin and Amy, 1997; Siddiqui et al., 1994). Transferred ozone dose is defined as the amount of aqueous ozone consumed by the water matrix (Buffle, 2005). These models are based on true-batch ozonation experiments using synthetic waters or raw waters containing bromide.

Carlson recommended using the models developed by Amy and coworkers (Carlson et al., 2001) to predict bromate formation. The equations are as follows:

When NH_3 is not present in the source water:

$$[BrO_3^-] = 1.55 \times 10^{-6} \times (DOC)^{-1.26} (pH)^{5.82} (O_3 dose)^{1.57} (Br^-)^{0.73} (t)^{0.28} \quad (2.5)$$

When NH_3 is present in the source water:

$$[BrO_3^-] = 1.63 \times 10^{-6} \times (DOC)^{-1.3} (pH)^{5.79} (O_3 dose)^{1.59} (Br^-)^{0.73} (t)^{0.27} (NH_3 - N)^{-0.033} \quad (2.6)$$

Amy also gave the following equations to adjust for the effect of the temperature on bromate formation.

$$[BrO_3^-]_{@temp\ T} = [BrO_3^-]_{@temp\ 20^oC}\,(1.035)^{(T-20)} \quad (2.7)$$

where $[BrO_3^-]_{@temp\ T}$ = bromate concentration at temperature T.

More recently, several researchers have reported that, in some cases, the formation of bromate tends to increase linearly with ozone exposure for various synthetic and natural waters under conditions relevant to drinking water disinfection (Kim, 2002; Manassis and Constantinos, 2003; Tyrovola and Diamadopoulos, 2005; Tang et al., 2005). Accordingly, the following empirical expression could be used:

$$C_B = k_B \int_0^t C_l\,dt = k_B CT \quad (2.8)$$

in which C_B is the bromate concentration (mg/L) and C_l is the dissolved ozone concentration (mg/L), and k_B is the rate constant for bromate formation (min^{-1}) which is water quality dependent (e.g., pH and alkalinity). For a constant water quality condition, k_B is constant and can be obtained by linear regression analysis of bromate data obtained from batch experiments plotted against the corresponding CT values (Tang et al., 2005).

As an alternative approach, the kinetic-based bromate formation model incorporates the reaction kinetics of the main reactions involved (Siddiqui et al., 1994). To set up a kinetic based model, the detailed reactions and accurate kinetic constants must be known and validated. If natural organic matter (NOM) or other species are involved in the reaction, the model will be more complex. These factors will greatly affect the accuracy and feasibility of the models.

2.3.3 CT Concept

The current commonly used approach for estimation of ozone disinfection performance involves application of a CT concept. C is defined as average ozone residual concentration at the outlet of a contactor chamber evaluated by direct measurement through contactor sampling ports or estimated from Table 2.4. T is the residence time which is usually prescribed as T_{10}, the residence time of the earliest ten percent of microorganisms to travel from the contactor inlet to outlet, as determined from a tracer residence time distribution (RTD) (USEPA, 1991; Greene, 2002). The USEPA employs this conservative T_{10} value to ensure a minimum exposure time for ninety percent of the water and microorganisms entering a disinfection contactor to disinfectants (Chen, 1998). Table 2.5 presents the CT values required by US EPA used to determine *Cryptosporidium* log inactivation credit for ozone or chlorine dioxide at different water temperature (USEPA, 2006).

Table 2.4 Guidelines for prediction of ozone residual concentration based on chamber inlet and outlet ozone concentrations (USEPA, 1991; USEPA, 2003)

Type of Chamber	Concentration C for CT product
First Dissolution	Not applicable for *Cryptosporidium*, but certain inactivation credit can be granted for *Giardia* and virus provided that the ozone residual at the outlet of the first contact chamber met minimum concentration levels
Reactive	C_{eff}
Co-Current Dissolution	Max (C_{eff} , $[\frac{C_{\inf} + C_{eff}}{2}]$)
Counter-Current Dissolution	$\frac{C_{eff}}{2}$

Table 2.5 USEPA recommended CT (mg/L min) values for inactivation of *Cryptosporidium parvum oocyst* (USEPA, 2006)

Log credit	Temperature °C										
	≤0.5	1	2	3	5	7	10	15	20	25	30
0.25	6.0	5.8	5.2	4.8	4.0	3.3	2.5	1.6	1.0	0.6	0.39
0.5	12	12	10	9.5	7.9	6.5	4.9	3.1	2.0	1.2	0.78
1.0	24	23	21	19	16	13	9.9	6.2	3.9	2.5	1.6
1.5	36	35	31	29	24	20	15	9.3	5.9	3.7	2.4
2.0	48	46	42	38	32	26	20	12	7.8	4.9	3.1
2.5	60	58	52	48	40	33	25	16	9.8	6.2	3.9
3.0	72	69	63	57	47	39	30	19	12	7.4	4.7

The CT approach is the simplest way to evaluate disinfection treatment efficiency, but it has some significant drawbacks:

The CT approach uses the ozone residual concentrations measured at certain ports to represent the average ozone concentration in whole chamber. However the ozone system is a gas/liquid system with complex mixing condition and reactions, and the ozone concentrations may vary very significantly in space. A previous study by Bellamy (1995) demonstrated the variability of ozone concentrations in dissolution cells. Carlson et al. (2001) found that the measured ozone residual concentrations differed four-fold from one sampling port to another, and for the same sampling port, the variations in the operational conditions induced a three-fold variation in ozone concentration. Thus, using a single ozone residual concentration value to calculate the inactivation ratio of a whole chamber could over or under estimate ozone disinfection efficiency.

The effect of ozone contactor hydraulics is also described by a single parameter, T_{10}. Such a simple parameter is over conservative and can not reveal all the underlying

factors governing hydrodynamic behaviours (Greene, 2002). In addition, T_{10} values are usually obtained from tracer tests, which are time-consuming and expensive to perform for existing full-scale reactors.

The current CT approach ignores the details of other important components which may affect the design of ozone disinfection systems, including ozone mass transfer, ozone demand and decay, microbial inactivation, and bromate formation kinetics. Previous research has demonstrated that application of the CT approach may result in inaccurate estimation of ozone disinfection efficiency (Bellamy et al., 1998).

Therefore, there is a need to develop a robust and flexible tool to fully describe ozone disinfection processes and contribute to their design.

2.4 Existing Models for Simulation of Non-ideal Ozone Reactor Performance

2.4.1 Integrated Disinfection Design Framework (IDDF)

The Integrated Disinfection Design Framework (IDDF) is another approach for designing ozonation processes (Bellamy et al., 1998). It is a completely segregated fluid model which assumes that molecules are grouped together in aggregates of a larger number of molecules. The IDDF approach incorporates three components in one model, including a contactor hydraulic module, disinfectant decay kinetics module, and a pathogen inactivation module. It utilizes mathematical relationships for each of the three disinfection components. Through this approach, the integrated model can be solved with the complex integral shown in Figure 2.4, in which *C(t)* is the disinfectant

concentration, *Co* is the initial disinfectant concentration, *k** is the first-order disinfectant decay constant, *N* is the number of viable microorganisms per unit volume, *No* is the initial number of viable microorganisms per unit volume, *K* is the microbial inactivation rate constant, *m* and *n* are constants for Hom inactivation kinetics model, *No* is the initial number of viable microorganisms per unit volume, θ is the ratio of residence time to mean residence time (T_{10}/T), and d is the dispersion coefficient. Carlson et al. (2001) further developed the IDDF approach by introducing an IDDF spreadsheet method, which allows the use of the RTD data determined from tracer tests directly as an input to the hydraulics module.

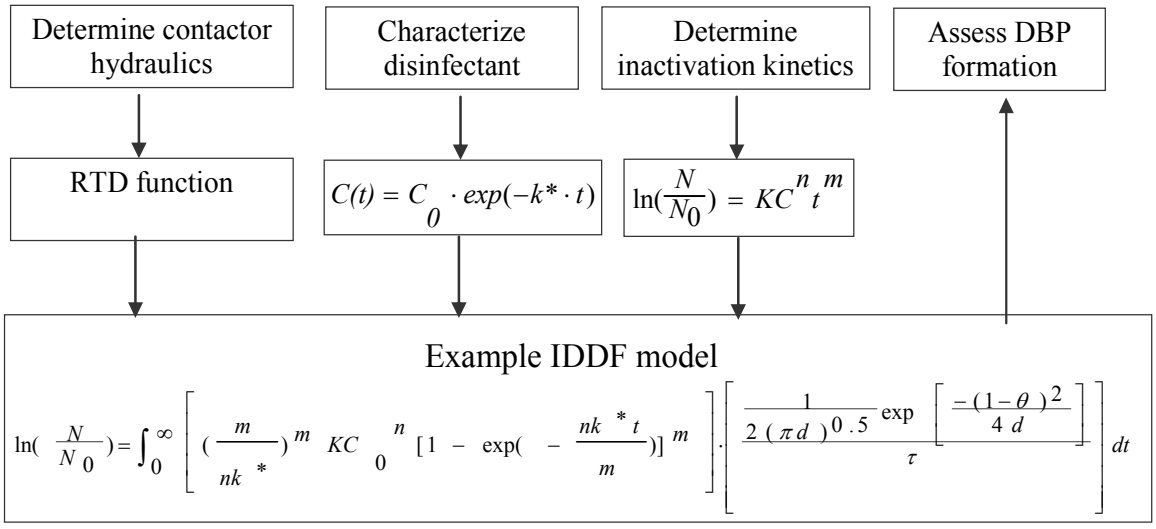

Figure 2.4 Flowchart for development of mathematical models for Integrated Disinfection Design Framework (Source: Bellamy 1998)

It has been shown that the IDDF method is more accurate than the CT method in predicting ozone disinfection efficiency (Bellamy 1998; Carlson et al., 2001). However, the IDDF model makes the assumption that fluids in the disinfection reactor are completely segregated which is not true for real fluids (Greene, 2002). It ignores the

detailed hydrodynamic characteristics that affect process efficiency. This assumption may result in an over estimation of ozone disinfection efficiency (Craik, 2005).

2.4.2 Complete Micro-Mixing Models

The perfectly micro-mixed model assumes that complete mixing and exchange of reacting material occurs between adjacent elements of a fluid on a molecular scale as they travel through the reactor. A method for determining conversion for the case of complete micro-mixing based on the concept of life expectancy of an element of fluid within the reactor,λ, was proposed by Zwietering (1959). The general equation for the complete micro-mixing model is:

$$\frac{dc}{d\lambda} = -r(C) + (C - C_{in})\frac{E(\lambda)}{1 - F(\lambda)} \tag{2.9}$$

where C_{in} is the reactant concentration at the inlet of the reactor, C is the local concentration within the reactor, $r(C)$ is the local rate of reaction at reactant concentration C, λ is the residence time, $E(\lambda)$ is the life expectancy density distribution function and $F(\lambda)$ is the life expectancy cumulative distribution function. $E(\lambda)$ and $F(\lambda)$ are related to the tracer resident time distribution $E(t)$ and are determined from tracer information (Craik, 2005). The concentration at the outlet of the reactor, C_{out}, can be determined by solving the differential equation with boundary conditions of $\lambda = 0$ at the outlet and $\lambda = 1$ at the inlet.

A mathematical description of a completely micromixed reactor was derived by substituting ozone concentration, live parasite concentration, and the respective rate expressions for ozone decay and inactivation kinetics, into the general equation for complete micro-mixing to yield the following two differential equations (Craik, 2005):

$$\frac{dc}{d\lambda} = -k_d C + (C - C_{in}) \frac{E(\lambda)}{1 - F(\lambda)} \tag{2.10}$$

and

$$\frac{dN}{d\lambda} = -kCN + (N - N_0) \frac{E(\lambda)}{1 - F(\lambda)} \tag{2.11}$$

The above equations can be solved simultaneously to determine dissolved ozone concentration and the live parasite concentration at different positions in the reactor from inlet to outlet.

According to the modeling results of Craik (2005), calculations of inactivation based on the assumption of complete micro-mixing may tend to underestimate microbial inactivation. In addition, computations for micro-mixed analysis are somewhat more complex than those required for segregated flow analysis. Therefore this approach has seldom been used by previous researchers and in real engineering design.

2.4.3 Axial Dispersion Model (ADM)

The axial dispersion flow model (ADM) is a common modeling approach for prediction of bubble column ozone reactors. An application of the axial dispersion flow model concept for modeling two phase ozone reactors usually assumes that the liquid phase is in axial dispersion and the gas phase is in plug flow. The ADM model expressions representing the steady-state dissolved and gas-phase ozone concentrations in a bubble column contactor are as follows (Kim, 2002):

$$d\frac{d^2 C_L}{dz^2} \pm \frac{dC_L}{dz} + N_L\left(\frac{C_G}{m} - C_L\right) - N_G C_L = 0 \tag{2.12}$$

$$\frac{d(\frac{C_G}{m})}{dz} - \frac{N_L}{S}(\frac{C_G}{m} - C_L) = 0 \tag{2.13}$$

in which C_L is the liquid phase ozone concentrations; C_G is the gas phase ozone concentrations; z is the normalized downward distance from the top of the contactor in the axial direction; d is the dispersion number; N_L is the Stanton number; N_D is the Damköhler number; S is the stripping factor; m is the Henry's law constant.

The axial dispersion model was applied by Marinas et al. (1993), Zhou et al., (1994), and Singer and Hull (2000) to predict hydrodynamics and ozone residual profiles in bubble diffuser contactors. Chen (1998) and Kim (2002) extended the ADM model by integrating microbial inactivation kinetics models for prediction of the profiles of microorganisms in ozone bubble columns. Their modelling results were validated by pilot experimental data. As concluded by Chen (1998), the ADM model appears to be a good approach for representing the distribution of dissolved ozone concentration and the disinfection efficiency in bubble-diffuser ozone columns.

The advantages of the ADM models are their simplicity and hence ease of solving. However, they do rely on empirical input, such as axial dispersion coefficients (Chen, 1998; Kim, 2002). The empirical inputs of the axial dispersion model are case dependent and cannot be extrapolated to other geometries, scales, and operating conditions (Cockx et al., 1997). Marinas et al. (1993) developed an empirical model to describe axial dispersion coefficient for a pilot ozone bubble diffuser contactor. The effects of operating conditions on dispersion efficiency were considered. However, such a model can only be used for bubble columns with similar geometry (Kim, 2002). Thus, this modelling approach is difficult to apply for prediction of full scale ozone contactor performance. Such a shortcoming can be overcome by the use of computational fluid dynamics (CFD) as discussed in following section.

2.5 CFD Modeling of the Ozonation Process

2.5.1 Computational Fluid dynamics

Computational Fluid Dynamics (CFD) is the science of predicting fluid flow, heat transfer, mass transfer, chemical reactions and related phenomena by solving the mathematic equations that governing these processes using numerical algorithms (Versteeg et al., 1995). The fluid hydrodynamics governing equations are known as the Navier-Stokes (N-S) equations. These are partial differential equations which were derived in the early nineteenth century. They have no known general analytical solution but can be discretized and solved numerically.

CFD has increased in popularity during recent years due to the development of advanced commercial CFD codes and the increasing power of computational resources. There are many advantages to using CFD including low cost and quick solutions. One of the main advantages of CFD is its ability to test a large number of variables at a much lower cost than with experimental models (Hossain, 2005). Another advantage of the CFD approach is its efficiency to simulate both small scale (laboratory pilots) and large scale (full-scale) facilities without the use of particular scale-up laws. Thus, CFD can be used to obtain more accurate information about the performance of water treatment processes and find rapid design solutions for improvement (Do-Quang et al., 1999).

Applications of CFD are common in industries as diverse as the auto industry, the aerospace industry, and in the medical/biological/chemical research field. It also has been used somewhat sporadically in the drinking water field for the past decade or so; including the study of mixing in reservoirs, design of clearwells and contact tanks, and

optimization of design parameters for flocculation and sedimentation tanks (Grayman et al., 2003). The potential for CFD is clearly being recognized by the water industry.

2.5.2 Fundamentals of Multiphase CFD Modelling

For multiphase flow, two main CFD approaches can be applied. While most models compute the flow field of the continuous phase using the Navier-Stokes equations, the dispersed phases can either be calculated as semi-continuous phases where all phases are regarded as interpenetrating continua (Eulerian–Eulerian approach) or as discrete entities (bubbles, particles or clusters) in the eulerian-Lagrangian approach (Schugerl and Bellgardt, 2001; Lakehal, 2002; Michele, 2002; Ansys, 2005).

The Eulerian–Eulerian approach

The Eulerian–Eulerian approach is commonly adopted for the prediction of interpenetrating media situations, including gas–liquid mixtures such as bubbly flows. This approach can be employed in two distinctive forms: the one-fluid formulation and the two-fluid approach. In the one-fluid formulation, the particle concentrations are assumed to be a continuous phase. In the two-fluid formulation, also known as the six equation model approach, the phases are treated as two interpenetrating continua evolving within a single system: each point in the mixture is occupied simultaneously (in variable proportions) by both phases. Each phase is then governed by its own conservation and constitutive equations; these are then coupled through interphase interaction properties. Eulerian/Eulerian methods are suitable for large phase density ratios and if body forces are important (Hossian, 2005).

Eulerian-Lagrangian approach

In the Eulerian-Lagrangian approach (also known as the particle tracking approach), individual particles or clouds of particles are treated in a discrete way. The fluid phase is treated as a continuum by solving the time-averaged Navier-stokes equations, while the dispersed phase is solved by tracking a large number of particles, bubbles or droplets through the calculated flow field. The dispersed phase can exchange momentum, mass and energy with the fluid phase (Hossain, 2005). This model is usually suitable when the dispersed phase occupies a low volume fraction. The particle trajectories are computed individually at specified intervals during the fluid phase calculation. (Greene, 2002; Lakehal, 2002; Ansys, 2005; Hossain, 2005). Treating particles via the Lagrangian approach is in essence natural because their motion is tracked as they move through the flow field, which preserves their actual non-continuum behaviour and accounts for their historical effects in a natural way (Schugerl and Bellgardt, 2001; Lakehal, 2002). However, the most important disadvantage of a Eulerian-Lagrangian model is its relatively high computational load .

The Eulerian-Eulerian approach for simulating turbulent dispersion has its own advantages as compared to Eulerian-Lagrangian methods. For flow laden with a large number of particles the quantitative description of the variation in particle concentration is much simpler by means of the Eulerian-Eulerian method since, for the same purpose, statistical sampling is required with the Eulerian-Lagrangian description. In addition, the Eulerian-Eulerian approach allows both phases to be computed over a single grid, whereas the Eulerian-Lagrangian methods require the interpolation of quantities between the fixed grid nodes (Lakehal, 2002).

When overall information about the particulate phase is required, rather than the individual behavior of distinct particles or bubbles, the flows are more effictively

modelled using the Eulerian-Eulerain multiphase model (Delnoij et al., 1997). For the studies of the large-scale industrial flow structures, the Eulerian-Eulerian approach shows more significant benefit in its computational efficiencies. Therefore, in this research, the Eulerian-Eulerian approach was selected to model gas-liquid flow behaviour, the dissolution and reactions of ozone, chemical tracer tests, and bromate formation in ozone contactors.

Because micro-organisms are physically unlike a molecular ozone or chemical tracer, but rather are discrete, a Lagrangian approach to determining disinfection is more intuitive (Lyn and Blatchley, 2005). Many previous studies in modeling drinking water UV disinfection reactor employed the Lagrangian approach (Chiu et al. 1999; Lyn and Blatchley 2005; Ducoste 2005). However, the Eulerian-Eulerian approach has also been successfully used in predicting microbial inactivation of UV, chlorine, and ozone disinfection systems (Do-Quang et al, 1999; Green 2002; Lyn and Blatchley 2005; Ducoste 2005). Lyn et al. (1999) and Lyn and Blatchley (2005) conducted numerical studies using both Eulerian and Lagrangian approaches to predict UV disinfection efficiency. Consistent results were obtained showing that the disinfection efficiency predicted by the Lagrangian approach is slightly lower than that by the Eulerian approach but the results of the predictions were close. Therefore, Lyn and Blatchley (2005) suggest that both approaches could be applied for UV disinfection.

However, to date, no study has been reported using the Lagrangian approach for simulating microbial inactivation of ozone contactors. In the present research, both the Eulerian-Eulerian and Eulerian-Larangian approaches were implemented in the CFD modeling of ozone processes and the results from the two approaches were compared.

2.5.3 CFD Software Packages

In recent years, there have been many commercial CFD packages available that may be applied to solve complex multiphase and multi dimensionality flow problems, such as ozone contactors. A sample of such packages is provided in Table 2.6.

Table 2.6 Example of commercial CFD packages

CFD package	Company	Website
Fluent & Fidap	FLUENT, Inc.	www.fluent.com
CFX	ANSYS, Inc.	www.ansys.com/cfx/
Phonics	CHAM	www.cham.co.uk
Star-CD	The CD adapco Group	www.cd-adapco.com
Flow-3D	Flow Science, Inc	www.flow3d.com
Estet Astrid	Simulog Technologies	www.simulog.fr
Disinfex	British Hydromechanics Research Group	www.bhrgroup.co.uk

CFX is one of the most powerful commercial CFD codes. It has a wide range of physical models available for solving industrial problems. Both Eulerian-Eulerian and Eulerian-Lagrangian multiphase are supported in CFX. Multiple phases (fluids) can be solved simultaneously with the coupled solver in a robust and efficient manner, which provides substantial stability and run-time benefits. Therefore, the CFX code was chosen for this study.

2.5.4 Example Studies in the Literature

The CFD modelling approach has been applied to simulate various disinfection processes including chlorination, ozonation, and UV irradiation.

CFD modelling of chlorination processes has been conducted by numerous researchers (Do-Quang et al, 1999; Greene, 2002; Ducoste, 2001; Crozes et al., 1998). The main efforts of their research were to investigate the contactor hydraulics. Peplinski et al. (2002) and Crozes et al. (1998) studied the sensitivity/uncertainty of the CFD modelling. Greene (2002) set up a more comprehensive three dimensional (3D) CFD model to address all major components of chlorine disinfection processes in continuous flow systems (flow structure, mass transport, chlorine decay, and microbial inactivation). Such a model was found to be more accurate for predicting disinfection performance than the traditional CT approach and IDDF approach.

CFD application for UV disinfection has also drawn the focus of many researchers in recent years, mainly because the disinfection performance of full-scale UV systems is hard to be empirically validated. Lyn et al. (1999) and Chiu et al. (1999) developed two-dimensional (2D) Eulerian-Eulerian disinfection models for UV reactors. In contrast to chlorine disinfection processes, the disinfectant field in a UV reactor has fixed position and intensity gradient independent of the flow field. The Chiu et al. (1999) model accurately predicted experimental inactivation levels over a range of UV dose levels, in contrast the Eulerian-Eulerian model of Lyn et al. (1999) which exhibited poor correlation at high UV doses for the same data set. The improved performance of the Chiu et al. model over the Lyn et al. model was attributed to differences in the flow sub-models (Laser Doppler Velocimetry measurement versus numerical simulation) rather than the inactivation model algorithms. Downey et al. (1998) utilized an Eulerian-Lagrangian approach to simulate microbial transport in a UV reactor. The

reactor flow field was established by numerical simulation with an Eulerian model; microbial transport was then simulated with a Newtonian particle model. Particle travel times were estimated for a pulse input of 100 particles at the reactor inlet, and plotted to develop reactor RTD curves. Simulation RTDs correlated with experimentally derived tracer curves.

CFD modelling of ozonation processes is more complicated than modelling of chlorination and UV processes, because the ozonation process includes more complicated problems, such as interphase mass transfer, multiphase, reactions, etc.. Several researchers (Murrer et al., 1995; Peltier et al., 2001; Huang et al. 2002) tried to simplify the problem by developing mono-phase CFD models to simulate the ozone contactors and apply their models to optimize the ozone contactor hydraulics. These models did not consider the effects of the gas phase on contactor hydraulics, so they are not capable of predicting the effects of gas flow rate, gas concentration, and gas injection locations on the contactor flow patterns.

Henry and Freeman (1995) provided a two-phase 2D CFD model to track ozone bubble trajectories and their influence on the velocity and pressure distribution of the mean flow field. A tracer test simulation was conducted using a transient advection-diffusion analysis and the simulation results were validated by tracer tests. The effects of the gas/liquid ratio and addition of vanes, corner fillets and wall foils were analyzed to optimize the contactor design. Ta and Hague (2004) used similar approach in a 3D CFD modelling of full-scale contactor. The focus of their study was only on contactor hydraulics. No attempt was performed to simulate ozone profile and pathogen inactivation performance.

Kamimura et al. (2002) developed a mono-phase CFD model for an O_3/UV reactor based on CFD analysis. The mono-phase fluid dynamics model is combined with a

complex radical reaction model. This radical model consists mainly of two processes, i.e., the photochemical reaction process and the O_3/UV reaction process. The validity of the radical reaction model was evaluated by comparing the simulated concentrations of total organic carbon (TOC), H_2O_2, and dissolved ozone with experimental data obtained from a bench-scale CSTR. Once the radical reaction model was validated, CFD simulation was executed to obtain the distribution of the concentration of TOC, ozone, $OH^{\cdot}$ and other substances in the reactor. The CFD model was used for optimizing the reactor configuration and operational conditions, to reduce the ozone demand required for decomposing TOC. The weaknesses of this model include that it is a single phase model and the model relies on details of very complex ozone reaction kinetics. Such information is difficult to obtain at site-specific conditions.

Do-Quang et al. (1999) formulated an ozone disinfection model for a two-phase ozone disinfection system. Water velocity and ozone gas hold-up fields were numerically estimated from a two phase, Eulerian flow sub-model. Ozone concentrations in the water phase were then predicted by solution of coupled mass transfer and first-order ozone decay expressions. It was reported that predicted reactor ozone concentrations correlated well with experimental results. However, the model did not consider the effects of water quality on model parameters and no attempt was performed to use Lagriangian approach to simulate pathogen inactivation.

As discussed above, previous researchers have demonstrated the capabilities of CFD, however the focus of its application has been largely on modelling the hydraulic behaviour of contactors, which is only one of the components of the system design. There are few studies considering the effects of water quality on CFD model and there is limited information on applying CFD model to optimize the operation of ozone contactors at varying operational conditions. No model has been reported to compare the Eulerian and Lagrangian approaches for predicting ozone disinfection efficiency.

No reported studies have compared the CFD approach with two commonly used disinfection design approaches: CT_{10} and Integrated Disinfection Design Framework (IDDF).

2.6 Summary

In this chapter, the factors affecting ozone disinfection performance, the different approaches for modeling of ozonation process, and the status of using a computational fluid dynamics (CFD) technique for describing ozonation systems were reviewed. A number of areas were identified herein that would require further research. These included:

- The CT_{10}, IDDF and other common modeling approaches may overestimate or underestimate ozone disinfection efficiency. Therefore, a more accurate modeling method should be developed which can fully integrate contactor hydraulics, ozone mass transfer, ozone reactions and microbial inactivation within the model

- Most of previous CFD studies applied two dimensional or single phase CFD models to describe ozone contactors. Because of the complex of ozonation process, these models are not capable of accurately predicting contactor performance. It is needed to develop a three dimensional multiphase model for improving the design and operation of ozonation systems. It is also required to fully validate the CFD model by full-scale experimental data.

- No previous researchers compared the Eulerian-Eulerian approach with the Eulerian-Langrangian modeling approach in predicting disinfection efficiency of

ozone systems. Since the two approaches have fundamental differences, there is a strong need to compare them and find a better approach for predicting ozone disinfection efficiency.

- Many water quality factors can significantly affect ozone disinfection efficiency. Previous studies focused on investigating the effects of individual factors or parameters based on bench-scale experimental studies. There is a research need to select more appropriate parameters and utilize CFD modeling to quickly evaluate the effects of water quality on ozone disinfection performance.

- No previous CFD modelling studies have been done to investigate the effects of ozone monitoring points and tracer test methods on ozone disinfection efficiency calculation. To accurately determine ozone dosage and predict CT values, it would be important to optimize ozone monitoring points and tracer test strategies

- No previous research works have ever compared the CT_{10}, IDDF and CFD approaches for full-scale ozonation systems. It would be very necessary to conduct such a comparison study to determine the best approach for the design and operation of full-scale ozone disinfection processes.

CHAPTER 3 EXPERIMENTAL METHODS

The objective for conducting the experiments as described in this chapter is to provide model inputs for the computational fluid dynamics (CFD) modelling of ozone contactors and to validate the modelling results. A series of lab-scale and full-scale experimental studies were undertaken for two full-scale ozone contactors, one was at the Mannheim Water Treatment Plant (WTP) located at Kitchener, Ontario, Canada; and another was at Desbaillets Water Treatment Plant located at Montréal, Quebec, Canada. The lab-scale ozone decay kinetics experiments and full-scale ozone profile testing for the Mannheim WTP ozone contactors were conducted at the University of Waterloo by the author. Other experimental data were kindly provided by the Regional Municipality of Waterloo and the École Polytechnique de Montréal. A summary of the experimental methodologies for the two case studies are presented in this chapter.

3.1 Two Case Studies

3.1.1 Mannheim Water Treatment Plant Ozone Contactors

The Mannheim Water Treatment Plant (WTP) is operated by the Regional Municipality of Waterloo in Ontario, Canada. It was designed to treat Grand River source water at a nominal production capacity of 72 millions liters per day (MLD). There are two parallel ozone contactors in this plant. The three-dimensional schematic drawing of one of the contactors is shown in Figure 3.1. The ozonated gas is injected into each contactor by fine bubble diffusers in the first two cells, and dissolved ozone further

reacts in the following four cells. The 13 year old Mannheim ozone system has recently been modified to include new liquid oxygen fed ozone generators in order to enhance operational flexibility and remove some diffusers from the system.

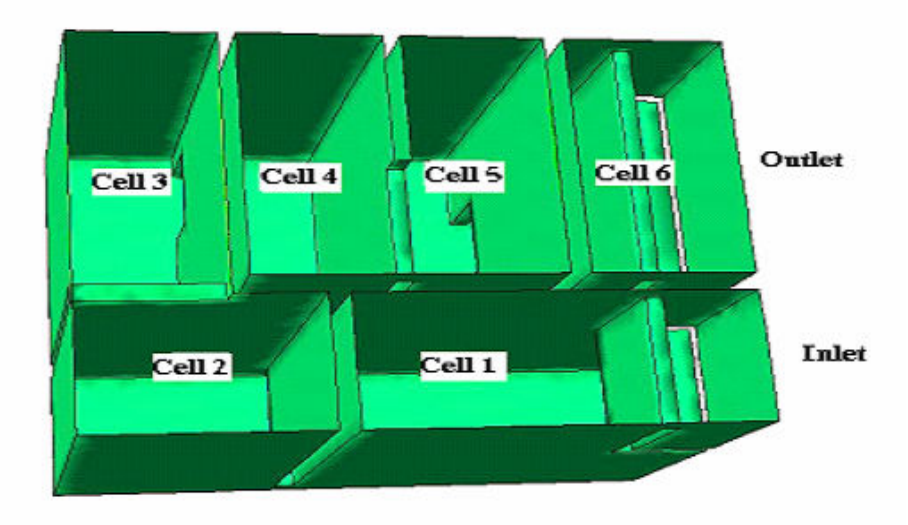

Figure 3.1 Three dimensional schematic drawing of Mannheim WTP ozone contactor

3.1.2 Desbaillets Water Treatment Plant Ozone Contactors

The DesBaillets Water Treatment Plant (WTP) is the largest facility in the province of Quebec, Canada. This plant has a capacity of 1,136 million litres per day (249.92 million imperial gallons per day (MIGD) or 300.13 million gallons per day (MGD)), and treats the St. Lawrence River's water, which is of good quality. The treatment process is composed of a direct sand filtration (5 meter/hour (m/h)) without pre-coagulation, post-ozonation followed by a final chlorination. The DesBaillets WTP has six parallel ozone contactors each with 2 cells and ozone gas is fed in the first cell of each contactor through 126 porous fine bubble diffusers. Figure 3.2 shows the geometry

of a DesBaillets WTP ozone contactor. The cell 1 of the contactor is operated in the counter-current mode, while the cell 2 is run at co-current mode.

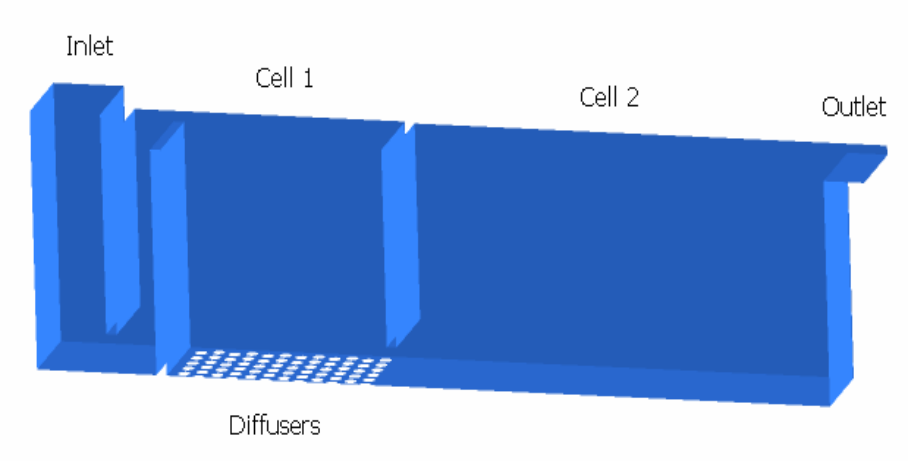

Figure 3.2 Three dimensional schematic drawing of DesBaillets WTP ozone contactor

3.2 Determination of Ozone Demand and Decay Kinetics

The experimental approaches for investigating ozone demand and decay kinetics of Mannheim WTP ozone system are described in this section.

Ozone Production

Ozone gas was generated from pure oxygen by a water cooled laboratory scale ozone generator (Hankin Atlas Ozone Systems Ltd., OzoneTM type S model 2), and then was bubbled through a small gas washing bottle (volume of 1 L) containing deionized (DI) distilled water (Milli-Q, Millipore Corp, Bedford, Ma) to produce ozone stock solution.

The ozone generation experimental apparatus is shown in Figure 3.3. A fritted glass diffuser was used to generate fine bubbles within the gas washing bottle. To obtain higher dissolved ozone concentration, the bottle was immersed in an ice bath. Milli-Q water was ozonated in semi-batch model for about 1 to 1.5 hours to obtaining a typical ozone concentration in stock solution of 20 to 30 mg/L. The stock solution was then kept in amber bottle with ice bath and used within 2 hour. Before conducting each decay kinetics test, the ozone concentration in this ozone stock solution was measured on a UV spectrophotometer (HP8453, Hewlett-Pakard, Polo Alto, CA) by setting the absorbance at the wavelength of 258 nm (Bader and Hiogne, 1981).

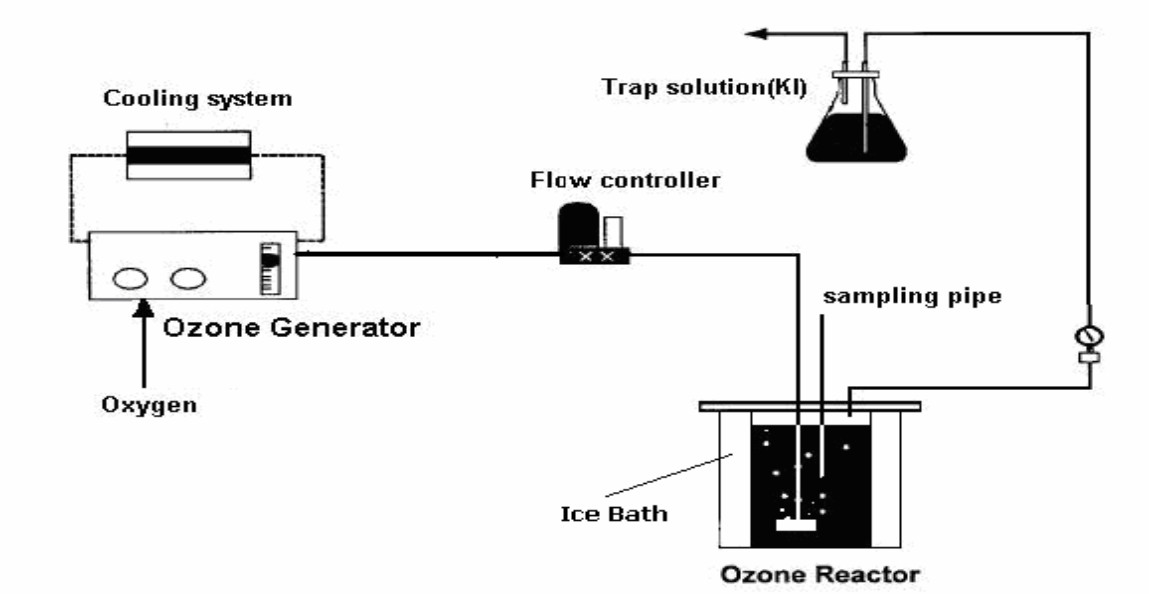

Figure 3.3 Experimental setup for ozone generation

Ozone Demand and Decay Tests

A bench scale ozone reactor was used to study ozone demand and decay kinetics of the source water of the Mannheim ozone system. Figure 3.4 shows the experimental setup. The reactor was made of a 2 L beaker, covered by a floating plate to make the reactor headspace free. The floating plate was wrapped with Teflon tape. Mixing of the reactor was accomplished by using a magnetic stir bar. The experimental temperature was controlled to be the same as the onsite temperature at the Mannheim WTP by immersing the batch reactor in a large glass water container. The water in the container was circulated from a water bath. All glassware was made ozone-demand free before experiments by adding high concentration ozonated DI water and allowing sufficient contacting time between ozone and potential contaminants on glassware.

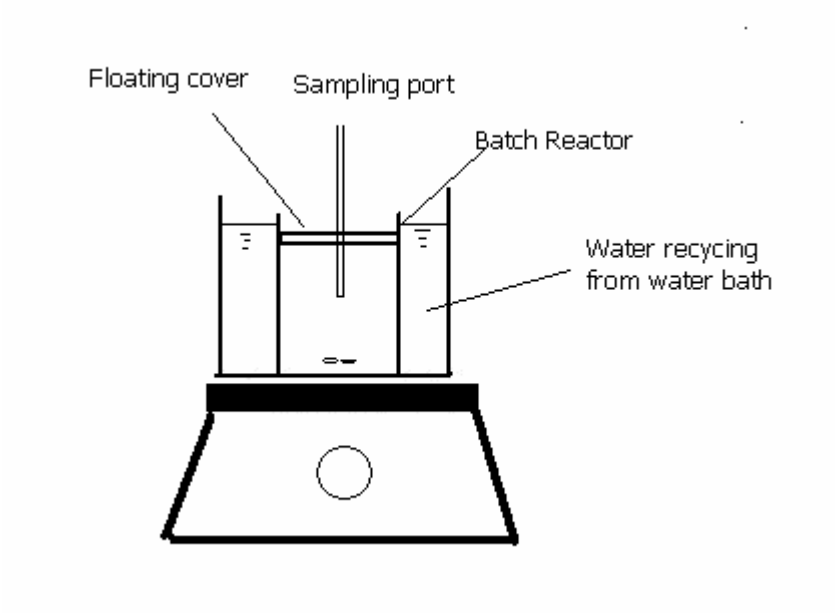

Figure 3.4 Bench scale experimental ozone system

The water samples were taken from a Mannheim WTP sampling port located between the sedimentation tank and ozone contactor. The ozone demands and decay testing was accomplished in the above batch mode. Before starting a test, the reactor was charged with known volumes of water samples and ozone stock solution based on the desired ozone dosage. When the ozone stock solution was added, the time was set as zero. Samples were then withdrawn from the sampling port of the reactor using a 50 mL O_3 demand free glass syringe at predetermined time intervals (Kim, 2002). Samples were collected in 50 mL beakers and immediately reacted with the indigo reagent contained in the Hach accuvac vials. After having taken all the samples, the ozone residuals of the samples were detected by a Hach DR/2400 spectrophotometer.

By measuring the ozone residual at various time intervals until no dissolved ozone was detectable, an ozone decay curve for the relation between ozone residual and the reaction time can be generated. The rate of dissolved ozone decomposition in water can be expressed as:

$$-\frac{d[O_3]}{dt} = k[O_3]^m \tag{3.1}$$

where, k = decomposition rate constant; and m = reaction order of ozone decomposition. The values of k can be calculated by integrating the above differential equation and plotting a semi-log line from the experimental data of dissolved ozone versus time (Wu, 2001).

The immediate ozone demand was calculated by determining the intercept of the first-order regression line extended to time zero. The intercept is the natural logarithm of the initial ozone concentration. The immediate ozone demand equals the ozone dose minus the initial concentration (Kim, 2002a).

Ozone demand and decay testing for the Desbaillets WTP ozone contactors was done by the École Polytechnique de Montréal and the experimental method could be found in El-Baz (2002) and Barbeau et al. (2003).

3.3 Tracer Test Methodology

In this study, the tracer test results were used to validate the CFD model. Tracer data for the Desbaillets WTP ozone contactors was kindly provided by the École Polytechnique de Montréal (El-Baz, 2002). Tracer test data of the Mannheim WTP ozone contactors before system modification was kindly provided by the Regional Municipality of Waterloo. Shown in this section are tracer test methodologies used in the two case studies.

DesBaillets WTP Ozone Contactors

Tracer tests at the Desbaillets WTP were conducted using a step injection of hydrofluorosilic acid (El-Baz, 2002; Barbeau et al., 2003). Figure 3.5 shows the tracer injection and monitoring locations.

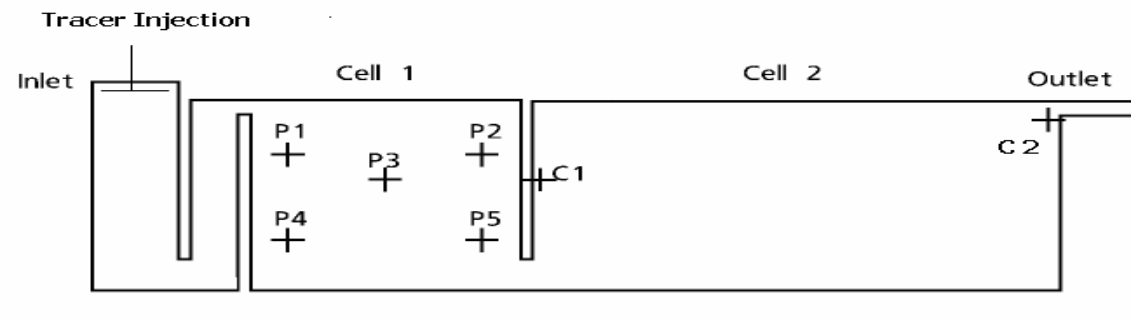

Figure 3.5 Tracer injection and monitoring points for the DesBaillets WTP ozone contactor (El-Baz, 2002)

The stock tracer solution was made by mixing 79% of hydrofluorosilic acid (purity 24% by weight) and 21% of water. The dosage of tracer was set as 2 mg/L during the tests. Since such a dosage led to effluent fluoride concentration above the regulated level (1.5 mg/L), the ozone contactor effluent was blended with the water in storage tanks to meet the regulation requirement (El-Baz, 2002). Tracer tests were performed at three flow rates (1.47, 2.16 and 3.24 m^3/s) to characterize the hydrodynamics of the contactor. The stock tracer solutions was pumped into the contactor through a spray nozzle system and uniformly distributed through the spray nozzles. The concentrations of tracer were continuously detected using an automatic fluorometer (Hach Company) at the location C1 and C2 respectively, as shown in Figure 3.5. Tracer data were entered into an EXCEL spreadsheet for analysis. T_{10}/T value and normalized tracer residence time distribution (RTD) curves were generated from this spreadsheet. The results were used to validate the CFD model.

Mannheim WTP Ozone Contactors:

Tracer tests at the Mannheim WTP ozone contactors before system modification were conducted by Dillon Consulting Limited (Ontario, Canada). A pulse injection method was employed and hydrofluosilic acid (HFS) was utilized since it was readily available in the plant. The tests were run at three flow rates (0.19, 0.29, and 0.38 m^3/s). The T_{10}/T values for each test were provided by the Regional Municipality of Waterloo (Ontario, Canada) and used for CFD model validation.

3.4 Ozone Residual Profile Testing

Mannheim WTP Ozone Contactor

Water samples were taken from ozone concentration monitoring points located at the outlet of each cell of the Mannheim ozone contactors to obtain full-scale ozone residual profiles. The indigo trisulfonate method, with AccuVac ampoules (Hach Co., Loveland, Colo.), was utilized to determine ozone concentrations and the samples were measured onsite. Since ozone in water is generally not very stable, all the analysis was performed soon after sampling. Duplicate samples were collected and detected for each sampling point. If the residual difference between the duplicate samples was greater than 0.05 mg/L, a third sample was taken to repeat the test.

When conducting ozone residual profile testing, the operational parameters including ozone dose, gas/liquid flow rates, gas concentration and water temperature were also recorded. These parameters were used as the CFD model inputs. The ozone residual profile data were used for validation of the CFD simulation results and for the study of optimizing ozone-sampling point with the CFD approach.

DesBaillets WTP Ozone Contactor

The Desbaillets ozone contactor has five sampling points taps (P1 to P5) installed in the first cell and two sampling points (C1 and C2) located at the outlet of cell 1 and cell 2. The locations of these sampling points are shown in Figure 3.5. The ozone residuals were measured using the indigo colometric method (Method 4500-O_3, B), as described in standard methods (APHA et al., 2001). The flow rates of the sampling lines were adjusted at 3 litres per minutes and overflowed in a 250 mL beaker. Duplicated samples were collected from the beakers using a syringe and slowly injected into the

indigo reagent for measurement. The tests were performed at different operational conditions to capture the effects of temperature, water flow rates and applied dosage.

3.5 Biodosimetry Test using Indigenous Aerobic Spore Formers

The purpose of the biodosimetry tests was to use indigenous aerobic spore formers (ASFs) as indicators of disinfection efficiency and to validate the various approaches (CT_{10}, CT-IDDF, and CFD) for prediction of ozone disinfection efficiency. The biodosimetry tests for the DesBaillets WTP ozone contactors were conducted by the École Polytechnique de Montréal (Broséusa et al., 2005).

ASFs have the advantage of being fairly abundant in surface waters. They are also highly resistant to ozone (Nieminski et al., 2000; Facile et al., 2000; Craik et al., 2002) and typically exhibit a linear inactivation with respect to CT. It is therefore suggested that ASF may be a potential way to validate the disinfection efficiencies of full-scale ozone contactors (Benoit, 1997; Broséusa et al., 2005).

Before conducting each full-scale validation test, pilot scale biodosimetry tests were performed onsite to create reference curves for the corresponding source waters. These reference curves provided the relationships between the effective CT and disinfection efficiencies of ASF by ozone. They were used to calculate the corresponding Biodosimetric CT for full-scale ozone contactors. This process is similar to what is currently being done to validate UV reactors, using reference curves developed with MS2 phages (USEPA 2003). The details of pilot scale testing were described by Broséusa et al. (2005).

Full-scale validation tests were performed the day following the pilot test for biodosimetric reference curves. Each of the full-scale validations was performed by

applying four increasing ozone doses and maintaining a constant flow rate. During the tests, influent and ozonated waters were sampled in one-liter sterile bottles (analysis done in triplicate) and ten liter carboys (analysis done in duplicate) containing sodium thiosulfate (final concentration, 0.01%) respectively. ASF measurement in ozonated water was performed using a larger water sample volume because of the lower concentration of surviving ASF (Broséusa et al., 2005). The data obtained from full-scale testing was used for the comparison of CT_{10}, IDDF based CT, CFD based CT and Biodosimetric CT, which will be further described in Chapter 7.

3.6 Analytical Methods

Dissolved Ozone Concentration Measurement

The Hach ozone method (Hach Company, Loveland CO) used for ozone residual testing is based on the indigo methods (Bader and Hiogne, 1981). A previous study by Coffey et al. (1995) has shown good agreement between the Hach method and the standard indigo method (Method 4500-O_3) by APHA et al. (2001). The concentrations of the ozone stock solutions were measured on a UV spectrophotometer (HP8453, Hewlett-Pakard, Polo Alto, CA) by setting the absorbance at the wavelength of 258 nm. The ozone concentration was calculated by:

$$[O_3] = 48{,}000 \times \frac{A_{258}}{M_o} \qquad (3.2)$$

where, A_{258} was the sample absorbance at 258nm, and M_o was the molar absorptivity of gaseous ozone which was set as 2900 M^{-1} CM^{-1} in this study to convert absorbance to mg O_3/L (Bader and Hiogne, 1981).

Analysis of Indigenous Aerobic Spore-formers (ASF)

For influent water samples, spore measurements were done following the method developed by Barbeau et al. (1997). 1 liter (L) of influent water samples from the ozonation process were filtered through 0.45 µm filters (HAWG047S1, Millipore, USA), placed on pads (AP10047S1, Millipore), saturated with 1.5 mL of Trypticase Soy Broth (TSB), pasteurized at 75°C for 15 minutes, and then incubated at 35°C for 22-24h. Due to the relatively low concentrations expected in ozonated waters, a different technique was developed using the approach proposed by Hijnen et al. (2000). In order to improve the method detection limit, large volumes of water (10 L) were filtered through large diameter (142 mm) 0.45 µm filters (HAWP 14250, Millipore) using a pressure filter holder (YY30 14236, Millipore) and a peristaltic pump (Model 7521-40, Masterflex). Filters were then placed in Petri dishes containing 25 ml of Trypticase Soy Agar (TSA), pasteurized at 75°C for 15 minutes and incubated at 35°C for 22-24 h. The filter holder was autoclaved at 121°C during 15 minutes before all experiments and disinfected between each type of water to be filtered. Filtering 1 L of influent water (N_0) and 10 L of ozonated water (N) eliminated the potential effect of the filtration cake on the ASF count. Preliminary assays indicated that ASF recovery in large volumes of water was statistically equivalent to ASF enumeration in a large number of 100 mL samples (Broséusa et al., 2006).

CHAPTER 4 DEVELOPMENT, VALIDATION, AND APPLICATION OF A MULTIPHASE CFD MODEL FOR OZONE DISINFECTION PROCESSES

4.1 Introduction

Ozone treatment of drinking water has been used for decades and is currently considered one of the most effective microbial disinfection technologies. However, the application of ozonation processes has been limited due to high capital, operating and maintenance costs, as well as the potential formation of bromate in waters containing appreciable levels of bromide. For water treatment plants with ozonation treatment processes or those planning to use such processes, it is of special interest to optimize ozone dosage levels to balance disinfection requirements and costs, as well as the formation of ozone disinfection by products (DBPs), such as bromate.

Parts of this chapter have been published in: Chemical Water and Wastewater Treatment VIII, IWA Publishing, London, ISBN 1 84339 068X; 2004 International Ozone Association-Pan American Group Conference, International Ozone Association; 2005 AWWA Water Quality Technology Conference and Exposition, American Water Work Association; Proceedings of 12th Canadian National Conference and 3rd Policy Forum on Drinking Water, Canadian Water and Wastewater Association. A manuscript related to this chapter has also been submitted to the Journal of Ozone: Science & Engineering.

The commonly used approach for calculating ozone disinfection efficiency and ozone dosage involves application of the CT concept. In this approach, it is usually assumed that the average concentration is equal to the contactor-effluent concentration C (ozone residual) although in some cases an integrated CT is calculated which takes into account ozone decay. T is usually represented by T_{10}, which is the detention time at which 10% of the water has passed through the contactor (USEPA, 1991). The CT concept is conservative because the average ozone concentration is actually higher than the residual and the residence time of 90% of the water is longer than T_{10}. Furthermore, the current CT concept gives little consideration to the effects of water qualities (other than temperature and pH) and operational parameters (e.g. ozone dose, gas/liquid flow rates, gas concentration, etc.) on ozone disinfection efficiency; therefore it is not flexible for optimizing system performance under changing water quality conditions. In an effort to meet increasingly stringent drinking water regulations and to be cost-effective, there is a need to develop a robust tool to describe ozonation processes and contribute to their design and operation.

The more recently developed Integrated Disinfection Design Framework (IDDF) is a somewhat more sophisticated approach for designing ozonation processes (Bellamy et al., 1998). The IDDF approach incorporates four components in one model, including a contactor hydraulic module, a disinfectant decay kinetics module, a pathogen inactivation module and a DBP formation module. It has been shown that the IDDF method is more accurate than the CT method in predicting ozone disinfection efficiency (Carlson et al., 2001). The IDDF approach employs the tracer residence time distribution (RTD) together with a disinfectant decay kinetic model to predict disinfection efficiency in a chemical disinfection process. However, the use of the RTD ignores the complex three dimensional (3D) flow behaviour within a contactor. Additionally, the IDDF approach uses the assumption that fluids in the disinfection contactor are completely segregated. This assumption may over or under-estimate

disinfection efficiency (Greene, 2002). Therefore, there is a need to develop a more accurate approach to contribute to the design and operation of ozone disinfection processes.

Other literature reported studies concentrated on modeling the hydrodynamics and disinfection performance using reactor theory models, such as continuously stirred tank reactor (CSTR), plug flow reactor (PFR), CSTR cascade, axial dispersion reactor, back-flow cell, and various combinations of these models (Zhou and Smith, 1994; Reddy et al., 1997; Chen, 1998; Roustan et al., 1999; Kim, 2002). The advantages of these models are their simplicity and hence ease of solving. However, they do rely on empirical input, such as axial dispersion coefficients (Chen, 1998; Kim, 2002). These empirical inputs are case dependent and cannot be extrapolated to other geometries, scales, and operating conditions (Cockx et al., 1997). However, such a shortcoming can be overcome by the use of computational fluid dynamics (CFD).

Computational fluid dynamics (CFD) is the science of predicting fluid flow, mass transfer, chemical reactions and related phenomena by solving the mathematic equations governing these processes using numerical algorithms (Versteeg et al., 1995). The main advantage of the CFD approach is its ability to catch small-scale phenomena and its efficiency to simulate both small-scale (laboratory pilots) and large-scale (full-scale reactor) facilities without the use of particular scale-up laws. Thus, the predictions of the CFD tool can be used to obtain more accurate information about the performances of the industrial plant; and find, if necessary, rapid design solutions to improve it (Do-Quang et al., 1999). CFD has gained large popularity during the last two decades due to the development of advanced commercial CFD codes and increasing power of computational sources. Applications of CFD are common in industries as diverse as the auto industry, the aerospace industry, and in the medical, biological, and chemical research field. It also has been used somewhat sporadically in the drinking

water field for the past decade or so, including study of mixing in reservoirs, design of clearwells and contact tanks, and optimization of design parameters for flocculator and sedimentation tank (Grayman et al., 2003). CFD has come into use recently for evaluating disinfection systems, including chlorination, ultraviolet (UV), and ozonation processes (Lyn et al. 1999; Greene, 2002; Do-Quang et al., 1999). However the focus of its previous application in drinking water disinfection treatment has been largely on modeling the hydraulic behaviour of contactors, which is only one component of system design (Greene, 2002).

The preliminary objective of this research was to develop a CFD based integrated disinfection design approach for full-scale ozone disinfection processes. This new approach employed a three-dimensional multiphase CFD model to address all the major components of ozone disinfection processes: ozone mass transfer, ozone decay, microbial inactivation, and disinfection by-product formation kinetics. The second injective was to validate and apply the CFD approach to optimize the hydraulics and disinfection performance of full-scale ozone contactors in the Desbaillets Water Treatment Plants (WTP) in Montreal, Quebec and the Manheim Water Treatment Plant in Kitchener, Ontario.

4.2 The Multiphase CFD Model For Ozone Disinfection Processes

Bubble-diffuser ozone contactors are commonly used in drinking water and wastewater treatment processes (Rakness, 2005). Figure 4.1 shows a typical over-under baffled ozone contactor. Chambers in which ozone is added through porous medium diffusers are usually called dissolution chambers. Chambers in which no ozone is added to but ozone residual is present are called reaction chambers (Langlais et al., 1991; Rakness, 2005).

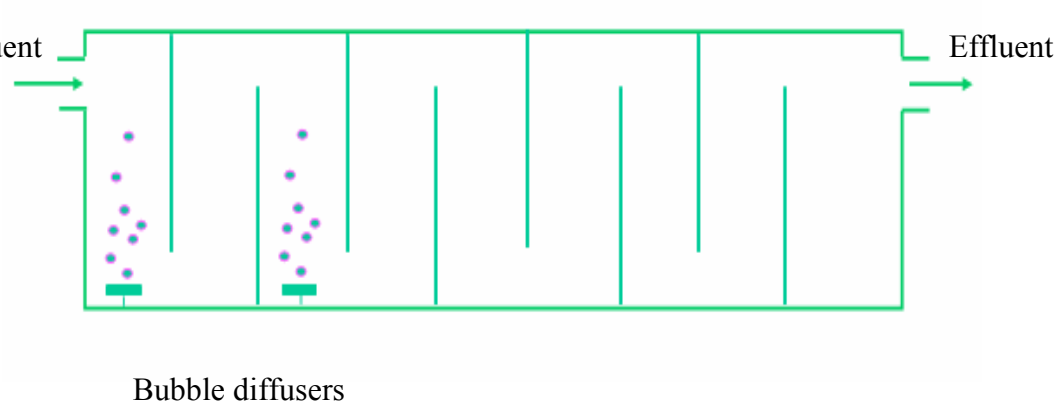

Figure 4.1 A typical bubble diffuser ozone contactor

Ozone disinfection system involves multi-component transport and reactions within two phases. As the ozonated air or oxygen is transported through the system, ozone diffuses into the liquid phase (water) where it reacts with contaminants or decomposes until leaving the system. The system has four principle components: water, air, ozone and pathogens. Typically, ozone and pathogen concentrations in the liquid water and air are sufficiently small that their effects on the bulk macroscopic properties of the liquid and air are negligible.

The computational fluid dynamics models have been developed for simulation of the multiphase ozone disinfection process. The numerical models are capable of predicting fluid fields, tracer residence time distribution (RTD), ozone mass transfer, ozone demand and decay reactions, and microbial inactivation efficiencies in full-scale bubble diffuser ozone contactors. The numerical simulation models are described in detail in this section.

4.2.1 Governing Equations

Eulerian–Eulerian and Eulerian–Lagrangian methods have been extensively used to simulate multiphase problems (Lakehal, 2002; Green, 2002; Lyn, 2005). A comparison of Eulerian-Eulerian and Eulerian –Lagrangian approaches was described in Chapter 2. In the present work an Eulerian-Eulerian approach (Lakehal, 2002) was used to model the turbulent hydrodynamics of the liquid phase (continuous phase) and gas phase (dispersed phase). The two phases were treated as interpenetrating continua coexisting in the flow domain. The share of the flow domain each phase occupies was given by the volume fraction. Each phase had its own velocity, temperature, and physical properties. The flow was considered to be isothermal in this work so the energy equation was ignored. The multiphase CFD model for ozone disinfection process included mass conservation, momentum conservation and volume conservation equations (Michele, 2002) as described below.

Mass Conservation Equations

The transport equations representing mass conservation for liquid and gas phases are:

$$\frac{\partial}{\partial t}(\rho_l r_l) + \frac{\partial}{\partial x_i}(\rho_l r_l u_{l,i}) = 0 \tag{4.1}$$

$$\frac{\partial}{\partial t}(\rho_g r_g) + \frac{\partial}{\partial x_i}(\rho_g r_g u_{g,i}) = 0 \tag{4.2}$$

where, subscript g denotes the gas phase, subscript l denotes the liquid phase. For a given phase α, ρ_α is its density, r_α is its volume fraction, and $u_{\alpha,i}$ is its flow velocity in the i-direction.

For ozone systems, the amount of ozone mass transfer between air and water is sufficiently small compared with the bulk masses of the air and water phases, thus the mass that is carried from one phase into another is negligible. Additionally, the ozone concentrations in water and air are also small enough that the effects of ozone transfer on the bulk macroscopic properties of the liquid and air are also negligible. Therefore, mass transfer and source terms were not included in mass conservation equations in this study.

Momentum Conservation Equations

The momentum balances in multiphase formation for gas and liquid phases are:

$$\frac{\partial}{\partial t}(\rho_g r_g u_{g,i}) + \frac{\partial}{\partial x_j}(\rho_g r_g u_{g,i} u_{g,j}) = -r_g \frac{\partial p}{\partial x_i} + \frac{\partial}{\partial x_i} r_g \mu_g (\frac{\partial u_{g,i}}{\partial x_j} + \frac{\partial u_{g,j}}{\partial x_i}) + M_{gl,i} \qquad (4.3)$$

$$\frac{\partial}{\partial t}(\rho_l r_l u_{l,i}) + \frac{\partial}{\partial x_j}(\rho_l r_l u_{l,i} u_{l,j}) = -r_l \frac{\partial p}{\partial x_i} + \frac{\partial}{\partial x_i} r_l \mu_l (\frac{\partial u_{l,i}}{\partial x_j} + \frac{\partial u_{l,j}}{\partial x_i}) + M_{\mathrm{lg},i} \qquad (4.4)$$

where p is pressure and it is assumed that the gas and liquid phase have a shared pressure field (Lo, 2000). $M_{\alpha\beta,i}$ represents the interfacial force in the i-direction acting on phase α due to the presence of phase β.

The total interfacial force acting between two phases (α and β phases) may arise from several independent physical effects.

$$M_{\alpha,\beta} = M^{D}_{\alpha,\beta} + M^{L}_{\alpha\beta} + M^{LUB}_{\alpha\beta} + M^{VM}_{\alpha\beta} + M^{TD}_{\alpha\beta} \qquad (4.5)$$

The terms indicated in the right hand side of above equation represent the interphase drag force, lift force, wall lubrication force, virtual mass force, and turbulence dispersion force, respectively (Vesvikar and Al-Dahhan, 2005; Do-Quang et al., 1999). The interphase drag force, $M_{\alpha\beta}^{D}$, accounts for force experienced by the dispersed phase due to the relative motion of the continuous phase. The lift force, $M_{\alpha\beta}^{L}$, accounts for the force acting perpendicularly on the direction of the rising dispersed phase due to vorticity or shear in the continuous phase nonuniform flow field. The wall lubrication force, $M_{\alpha\beta}^{LUB}$, accounts for the force when the dispersed phase is moving in the vicinity of the wall. The virtual mass force, $M_{\alpha\beta}^{VM}$, appears when a dispersed phase accelerates relative to the continuous phase; some part of the surrounding continuous phase is also accelerated with the dispersed phase—this extra acceleration of the continuous phase has the effect of added inertia or ‘‘virtual mass.’’ The turbulent dispersion force, $M_{\alpha\beta}^{TD}$, considers the additional dispersion of phases from high volume fraction regions to low volume fraction regions due to turbulent fluctuations (Vesvikar and Al-Dahhan, 2005).

Note that the interfacial forces between two phases are equal and opposite. Hence, the net interfacial forces sums to zero:

$$M_{\alpha\beta} = -M_{\beta\alpha} \tag{4.6}$$

Appropriate models were required to account for these forces (Kuipers and Swaaij, 1998; Rafique et al., 2004; Ranade, 2002; Sokolichin and Eigenberger, 1994, Sokolichin et al., 2004). Only the interphase drag force and turbulence dispersion force were considered in the present model, because the effects of other non-drag forces became less significant in large gas-liquid phase columns (Vesvikar and Al-Dahhan, 2005; Lo, 2000; ANSYS, 2004).

The interphase drag force, $M_{\alpha\beta}^{D}$, was modeled with the Grace Drag model (Clift et al.,1978). This model was developed using air–water data and hence produces better results for air–water systems (Vesvikar and Al-Dahhan, 2005), therefore it was appropriate for modelling ozone disinfection processes which consisted of air and water phases. The Grace Drag model is expressed as:

$$M_{g,l}^{D} = \frac{3}{4}\rho_l \frac{r_g}{d_g} C_D (u_g - u_l)\left|u_g - u_l\right| \tag{4.7}$$

where, d_g is the gas bubble diameter, u_g and u_l are the gas and liquid velocities, and C_D is the drag coefficient given by:

$$C_D = r_l^P C_{D\infty} \tag{4.8}$$

where $C_{D\infty}$ is the single bubble Grace drag coefficient, P is a correction factor for dense bubble effects (or bubble swarm effect). Previous studies done by Lo (2000) and Gobby (2004) showed that dense bubble effects can be represented by P = 4 in the above equation.

$C_{D\infty}$ is determined by:

$$C_{D\infty} = \max(C_D(sphere), C_D(distorted)) \tag{4.9}$$

where $C_D(sphere)$ is the drag coefficient in the spherical cap regime, which is well approximated by:

$$C_D(sphere) = \frac{8}{3} \tag{4.10}$$

$C_D(distorted)$ is the drag coefficient in the distorted particle regime given by:

$$C_D(distorted) = \frac{4}{3}\frac{gd_g}{U_T^2}\frac{\Delta\rho}{\rho_l} \tag{4.11}$$

where the terminal velocity U_T is given by:

$$U_T = \frac{\mu_l}{\rho_l d_g} M^{-0.149}(J - 0.857) \tag{4.12}$$

M is Morton number and is defined as:

$$M = \frac{\mu_g^4 g\Delta\rho}{\rho_c^2 \sigma^3} \tag{4.13}$$

and J is given by:

$$J = \begin{cases} 0.94H^{0.751} & if \quad 2 < H \le 59.3 \\ 3.42H^{0.441} & if \quad H > 59.3 \end{cases} \tag{4.14}$$

$$H = \frac{4}{3} EoM^{-0.149}\left(\frac{\mu_l}{\mu_{ref}}\right)^{-0.14} \tag{4.15}$$

$$Eo = \frac{g\Delta\rho d_g^2}{\sigma} = Eotvos \quad number \tag{4.16}$$

in which, Eo is the Eotvos number, μ_{ref} = 0.0009 kgm^{-1} s^{-1} is the reference molecular viscosity of water (Lo, 2000), g is the gravitational acceleration, $\Delta\rho$ is the density difference between the phases, σ is the surface tension coefficient and d_g is the diameter of the bubble.

The bubble size in ozone contactors is variable in full-scale ozone contactors and is difficult to determine experimentally. However, previous studies (Langlais et al., 1991; Wu, 2001) have shown that the average bubble size in ozone contactors is in a narrow range between 2 mm and 5 mm. Vesvikar and Al-Dahhan (2005) conducted gas-liquid simulations with different bubble diameters ranging from 2–12 mm, and found that the change in diameter did not affect the results significantly. The same observation was made by van Baten et al. (2003) and Sokolichin et al. (2004). Thus, an average bubble diameter of 3 mm was used in the present simulations. Bubble coalescence and break-up were not taken into account to simplify the simulation.

The turbulent dispersion force, $M_{\alpha\beta}^{TD}$, considers the additional dispersion of phases from high volume fraction regions to low volume fraction regions due to turbulent fluctuations. The model of Lopez de Bertodano (1991) was used in this study for describing the turbulent dispersion force:

$$M_l^{TD} = M_g^{TD} = -c_{TD}\rho_l k_l \nabla r_l \qquad (4.17)$$

where c_{TD} is the dispersion coefficient, for which values of 0.1 - 0.5 have been used successfully for bubbly flow with bubble diameters in the order of a few millimetres. The dispersion coefficient was taken as 0.1 in this study which is suitable for the bubble size range utilized (Gobby, 2004); k_l is the turbulent kinetic energy of liquid phase which is described below.

Volume Conservation Equation

The volume fractions of all phases sum to unity:

$$\sum_{\alpha=1}^{N_P} r_\alpha = 1 \tag{4.18}$$

4.2.2 Turbulence Model

Fluid flows in full-scale ozone contactors are turbulent because the turbulence Reynold numbers in these contactors are usually higher than 10^4. Therefore, turbulence modeling is of crucial importance for the correct description of multiphase flows in ozonation systems. In this study, the impact of turbulence on the hydrodynamics was modeled in both phases by the Boussinesq Eddy Viscosity model which assumes that the effective viscosity is the sum of the molecular and turbulent viscosities, and diffusion of momentum in phase α is governed by an effective viscosity:

$$\mu_{eff,\alpha} = \mu_\alpha + \mu_{t,\alpha} \tag{4.19}$$

Liquid Phase Turbulence Model

For the liquid phase, the standard k-ε model (Launder & Spalding, 1974) was used to simulate the turbulent eddy viscosity μ_t. At this point of time the k-ε model is the most commonly used turbulence model for solving engineering CFD problems (Schugerl and Bellgardt, 2001; Michele, 2002). Using this model, the value of eddy viscosity $\mu_{t,l}$ in

liquid phase was set by the following equation based on two scales of turbulences: the turbulent kinetic energy k_l, and the turbulent energy dissipation rate ε_l:

$$\mu_{t,l} = \rho_l C_\mu \frac{k_l^{\,2}}{\varepsilon_l} \tag{4.20}$$

where C_μ = 0.09 is the model coefficient, and ρ_l is the density of liquid flow.

k_l and ε_l. were calculated using additional equations representing their production, destruction, and transport (Wright and Hargreaves, 2001):

$$\frac{\partial(r_l \rho_l k_l)}{\partial t} + \nabla \bullet (r_l(\rho_l u_{l,i} k_l - (\mu + \frac{\mu_{tl}}{\sigma_k})\nabla k_l)) = r_l(P_{k,l} - \rho_l) \tag{4.21}$$

$$\frac{\partial(r_l \rho_l \varepsilon_l)}{\partial t} + \nabla \bullet (r_l \rho_l u_{l,i} \varepsilon_l - (\mu + \frac{\mu_{tl}}{\sigma_\varepsilon})\nabla \varepsilon_l) = r_l \frac{\varepsilon_l}{k_l}(C_{\varepsilon 1} P_{k,l} - C_{\varepsilon 2} \rho_l \varepsilon_l) \tag{4.22}$$

where $C_{\varepsilon 1}$, $C_{\varepsilon 2}$, σ_κ and σ_ε are constants (standard values of 1.44, 1.92, 1, and 1.3 were applied). $P_{k,l}$ is the turbulence production due to shear and buoyancy forces.

Gas Phase Turbulence Model:

For the dispersed gas phase, a Dispersed Phase Zero Equation model was used. The Dispersed Phase Zero Equation model is a simple extension of the standard k-epsilon (k-ε) model and is easy to implement. The turbulent scales from the liquid phase, k_l and ε_l, were assumed to apply to the dispersed gas phase. There is no need to solve additional turbulence equations for the dispersed phase. This is the recommended

algebraic model for a dispersed phase (Vesvikar and Al-Dahhan, 2005; ANSYS, 2005). With this model the eddy viscosity of the gas phase, $\mu_{t,g}$, is expressed as:

$$\mu_{t,g} = \frac{\rho_g}{\rho_l}\frac{\mu_{t,l}}{\sigma} \tag{4.23}$$

The parameter σ is a turbulent Prandtl number relating the dispersed phase kinematic eddy viscosity $\mu_{t,g}$ to the continuous phase kinematic eddy viscosity $\mu_{t,l}$. The Prandtl Number is specified to be 1 which is appropriate for bubble flows (Lo, 2000).

Turbulence Enhancement Model

In flows with a dispersed phase, large particles in the dispersed phase tend to increase turbulence in the continuous phase due to the presence of wakes behind the particles. This is known as Particle Induced Turbulence. The Sato Enhanced Eddy Viscosity model was used to model this effect in this study. In this model, turbulence enhancement by air bubbles was modeled using an enhanced continuous phase eddy viscosity (Sato and Sekoguchi, 1975):

$$\mu'_{t,l} = \mu_{t,l} + \mu_{te,g} \tag{4.24}$$

where $\mu'_{t,l}$ is the total liquid phase turbulence eddy viscosity; $\mu_{t,l}$ is the usual Shear Induced Eddy Viscosity; and $\mu_{te,g}$ is an additional Particle Induced Eddy Viscosity:

$$\mu_{te,g} = C_{\mu,g}\rho_l r_g d_g \left|u_g - u_l\right| \tag{4.25}$$

The variable $C_{\mu,g}$ has a value of 0.6 (Lo, 2000).

The total effective viscosity of the liquid phases is:

$$\mu_{eff,l} = \mu_l + \mu_{t,l} + \mu_{te,g} \tag{4.26}$$

Scalable Wall-Function Model:

As fluid flow approaches a wall, rapid changes in velocity occur in a thin sublayer in which the flow is influenced by molecular viscous effects and does not depend on free stream parameters (Versteeg and Malalasekera, 1995; Wright and Hargreaves, 2001). The sublayer has a substantial influence upon the near wall flow. An adequate numerical resolution of the solution in the sub-layer requires a very fine mesh because of the sub-layer thinness and the high gradients in this region. Therefore, such a model is computationally intensive and often not suitable for industrial applications (Versteeg and Malalasekera, 1995; Wright and Hargreaves, 2000; Utyuzhnikov, 2005). To avoid this, the scalable wall-function approach (Grotjans and Menter, 1998) was used for near wall treatment in this study. This approach is a modified form of the standard wall function approach (Versteeg and Malalasekera, 1995).

In the wall-function approach, the viscosity affected sublayer region is bridged by employing empirical formulas to provide near-wall boundary conditions for the mean flow and turbulence transport equations. The near wall velocity scale u^* is related to the wall-shear-stress, τ_ω, by means of following relations (Grotjans and Menter, 1998):

$$\tau_\omega = \rho u^* u_\tau \tag{4.27}$$

$$u^* = C_\mu^{1/4} k_l^{1/2} \tag{4.28}$$

$$u_\tau = \frac{U_t}{\frac{1}{\kappa}\ln(y^*) + C} \tag{4.29}$$

$$y^* = (\rho u^* \Delta y)/\mu \tag{4.30}$$

where, u_τ is the friction velocity scale; τ_ω represents the wall shear stress; u^* is the near wall velocity scale; U_t is the known velocity tangent to the wall at a distance of Δy from the wall, κ is the von Karman constant and C is a log-layer constant depending on wall roughness (natural logarithms are used).

The scalable wall-function approach limits the y^* value by $\tilde{y}^* = \max(y^*, 11.06)$. The value of 11.06 is the intersection between the logarithmic and the linear near wall profile. The computed $\tilde{y}^*$ is therefore not allowed to fall below this limit. This eliminates fine grid inconsistencies of standard wall functions. The scalable wall functions thus allow solution on arbitrarily fine near wall grids, which is a significant improvement over standard wall functions (Grotjans and Menter, 1998).

4.2.3 Sub-Models for Ozone Mass Transfer, Reactions and Microbial Inactivation

The water entering the system contains natural organic matter (NOM) and pathogens. As the water flows pass through the ozone contactor, ozone diffuses from the gas phase into the liquid phase where it reacts with the NOM and pathogens as it decays naturally

in the water. One undesired consequence of the ozone reactions is the formation of ozone disinfection by-products, such as bromate, which are transported in the liquid phase and discharged from the system. In this section, complete transport models of the gas phase ozone, liquid phase ozone, natural organic matter, pathogens, and bromate transport and reactions are given.

Regulatory agencies and operators are interested in estimating various system performance indicators, including: effective ozone exposure CT and tracer residence times. Models equations for estimating these indicators are also presented here.

General Species Transport Equation

When a species ϕ exists in phase α, the corresponding field variable is denoted ϕ_α, the transport of this additional variable ϕ_α is expressed as:

$$\frac{\partial}{\partial t}(r_\alpha \rho_\alpha \phi_\alpha) + \nabla \bullet (r_\alpha u_\alpha \rho_\alpha \phi_\alpha) - \nabla (r_\alpha (\rho_\alpha D_\alpha^{(\phi)} + \frac{\mu_{t\alpha}}{Sc_{t\alpha}}) \nabla \phi_\alpha) = S_\alpha^{(\Phi)} + T_\alpha^{(\Phi)} \qquad (4.31)$$

where r_α is the volume fraction of the phase, u_α is the flow velocity, ρ is the density of flow, ϕ_α is the conserved quantity per unit mass of phase α, $D_\alpha^{(\phi)}$ is the kinematic diffusivity for the scalar in phase α, $Sc_{t\alpha}$ is the turbulent Schmidt number, $S_\alpha^{(\Phi)}$ is the external volumetric source term, with units of conserved quantity per unit volume per unit time; $T_\alpha^{(\Phi)}$ represents the total source to ϕ_α due to inter-phase transfer across interfaces with other phases (ANSYS, 2004).

In this study, ozone concentrations in gas/liquid phases, natural organic matter (NOM), microorganisms, and bromate concentration were all treated as transported scalars

(additional variables) and obtained by solving transport equations. Individual transport balances were distinguished by their respective source processes as described below.

Ozone Mass Transfer

Ozone must be dissolved into the liquid phase before reacting with contaminants (including pathogens) in water. Based on the well known two film theory (Danckwerts, 1970), the transfer of ozone from gas phase to liquid phase through the phase interface is due to a concentration gradient, which is caused by a resistance to the mass transfer developed in each phase. Since ozone is sparingly soluble in water (Beltran, 2005), the gas phase resistance is usually considered negligible and the concentration gradient on liquid phase film controls the ozone mass transfer rate in the bulk fluid (Langlais et al., 1991). Thus, the source term for the interfacial transfer of ozone between gas and the water can be modeled as follows (Singer and Hull, 2000):

$$S_{tr} = k_{l,tr} a [C_l^* - C_l] \tag{4.32}$$

$$a = \frac{6}{d_g} * r_g \tag{4.33}$$

where the source term S_{tr} represents the rate of interfacial ozone mass transfer between the two phases; C_l^* is the saturation concentration of ozone in water; C_l is the local ozone residual concentration; $k_{l,tr}$ is the liquid phase mass transfer coefficient; a is the volumetric interfacial area (1/m); r_g is the local gas phase fraction; and d_g is bubble size.

The saturation concentration of ozone in water C_l^* can be calculated according to Henry's law (Singer and Hull, 2000):

$$C_l^* = C_g / H \tag{4.34}$$

where H is the Henry's law constant. In this study, an empirical ozone Henry's law constant equation, which was reported by Perry (1973), is used. This equation has also used by other researchers in modeling ozone systems (Marinas et al., 1991; Kim et al., 2002). The effect of pressure on Henry law constant was not considered in this study. The formula of the empirical equation is:

$$\log H = \begin{cases} 3.25 - \dfrac{840}{T} & when \quad 278K \le T \le 288K \\ 6.20 - \dfrac{1687}{T} & when \quad 288K \le T \le 303K \end{cases} \tag{4.35}$$

The liquid phase mass transfer coefficient of ozone k_L can be determined by batch-scale experiments (Beltran, 2005) or estimated using some empirical equations proposed by Higbie (1935), Van Hughmark (1967), and Calderbank (1959). The Higbie model has been widely used to simulate mass transfer in ozonation system (Cockx et al., 1999; Masscheleain, 1982; Langlais et al., 1985) and other gas-liquid systems (Rahimi et al., 2006):

$$k_L = 2\sqrt{\frac{D_{O3} V_B^*}{\pi d_g}} \tag{4.36}$$

where D_{O3} is the molecular diffusivity of ozone in water; V_B^* is the gas slip velocity, $V_B^* = \left| u_g - u_l \right|$, which can be estimated from the gas superficial velocity V_s and gas hold-up fraction r_g.

$$V_B^* = \frac{V_s}{r_g} \tag{4.37}$$

The Higbie model was used in this study to estimate liquid phase mass transfer coefficient. It can also be expresses as (Masscheleain, 1982; Langlais et al., 1985; Chen, 1999):

$$k_L = 1.13\sqrt{\frac{D_{O3}V_B^*}{d_g}} \tag{4.38}$$

Ozone Decomposition Reactions

Once dissolved in water ozone becomes very unstable. Langlais et al. (1991) and Kim et al. (2002a) indicated that the decomposition of ozone includes two stages:

The first stage is called the initial ozone fast-demand period. In this stage, the reaction of ozone usually occurs in a few seconds dependent on water quality (Cho et al., 2003). This is due to the presence of substances (mainly natural organic matter (NOM)) that radically react with ozone through direct reactions.

The rate of the reaction between dissolved ozone and the fast reacting NOM is usually too fast to be measurable via batch reactor experiments when source water contains high concentrations of fast reacting NOM (Kim et al., 2002b,c). To characterize this phenomenon in the first stage, a concept called instantaneous ozone demand (IOD) is often used (Bellamy, 1995; Singer et al., 2000), which can be measured as the transferred ozone dose minus the initial ozone residual. It represents the ozone concentration that is immediately consumed by ozone demanding substances in water.

Based on this definition, IOD represents the initial concentration of fast reacting NOM ([NOM_f]), and IOD is only exerted if [NOM_f] is greater than zero.

The IOD concept assumes that the first stage has an infinite reaction kinetic constant. However, for modelling purposes, second order reaction kinetics can be applied. Several studies (Lev and Regli, 1992; Chen, 1998; and Kim et al., 2002) applied second order reaction kinetic models to describe this fast reaction period. Therefore, the source term corresponding to the reaction in the first stage is:

$$S_{demand} = k_{NOM_f}[NOM_f]C_l \tag{4.39}$$

in which source term S_{demand} represents the ozone consumption rate during the first stage which equals the reaction rate of $[NOM_f]$; $[NOM_f]$ is the concentration of fast reacting natural organic matter, in unit of [kg[O_3]/m^3]; k_{NOM_f} is a second-order rate constant (m^3/kg s); and C_l represents the liquid ozone concentration (kg/m^3).

Since the reaction of NOM and ozone is too fast, measurement of k_{NOM_f} is often difficult (Kim, 2002). For the modelling purpose, the reaction rate k_{NOM_f} used in this study was set at 3.20 (L/mg s), based on a study by Hunt and Marinas (1999). Tang et al. (2005) and Kim et al. (2002) applied the same value in their Axial Dispersion Reactor Models for modelling of ozone column. This rate constant was acceptable for modelling purposes because it resulted in 90% completion of the second-order reaction in seconds, which is consistent with the experimental observations in this study and previous studies by others (Hunt and Marinas, 1999; Tang et al., 2005; Kim, 2002).

The second stage of ozone decomposition is a period of moderate decay consumption, in which ozone decays more slowly due to reactions with the remaining substances in water. This second stage is more important for microbial disinfection performance.

The decay rate of ozone during this slower decay stage is commonly expressed by a pseudo first-order kinetic equation as follows (Langlais et al., 1991):

$$S_{decay} = -k_d C_l \tag{4.40}$$

where S_{decay} is the source term for the decay process, C_l is the dissolved ozone concentration, and k_d is the water quality dependent decay rate constant determined by laboratory-scale experiments.

Microbial Inactivation

Although pathogens also contribute to ozone demand and decay reactions, the amount of ozone they consume is negligible due to the extremely low mass concentrations of pathogens in water. Therefore, the effects of pathogens on ozone reactions were not considered, and the pathogen inactivation process was modelled separately in this study,

Several classic disinfection kinetics models are commonly used for evaluating disinfection efficiency of chemical disinfectants, including the Chick's law model, the Check-Watson model, the Rennecker-Marinas model, and the Hom-Haas model (MWH, 2005). The Hom-Haas model was found to be more robust than other models (Haas and Karra, 1984).

$$\ln(\frac{N}{N_0}) = -k_p C_l^{\,n} t^m \tag{4.41}$$

The Hom-Haas model can also be rearranged to express the kinetics without time (t) as an independent variable (Haas et al., 1995):

$$S_N = \frac{dN}{dt} = -mN \cdot (k_p C_l^n)^{\frac{1}{m}} [-\ln(N/N_0)]^{(1-\frac{1}{m})} \quad (4.42)$$

where S_N is the source term for microbial inactivation processes, N is the number of viable microorganisms per unit volume, N_0 is the initial number of viable microorganisms per unit volume, C_l is the dissolved ozone concentration, k_p is a disinfection kinetic constant depending on the types of pathogens, t is the exposure time (or residence time) of pathogens in ozonated water, and m and n are constants. Table 4.1 lists some literature reported constants of various pathogens. These constant however may change with the change of water quality conditions (Finch et al., 2001).

Table 4.1 Some reported Hom-Haas model constants for ozone disinfection

Microorganism	K_p (min^{-1})	n	m	Source
Cryptosporidium parvum oocysts	$0.68 \times \theta^{temp-22}$, $\theta = 1.080$	0.71	0.73	Gyurek et al. (1999) Li et al. (2001)
Giardia	$2.35 \times \exp(0.0723 \times temp)$	1	1	Carlson et al. (2001)
Viruses	$4.90 \times \exp(0.07 \times temp)$	1	1	Carlson et al. (2001)

Disinfection By-Product (Bromate) Formation

Various ozone disinfection models have been discussed in Chapter 2. However, most models are in complex forms and are not feasible to be integrated within the CFD model. A simplified linear empirical bromate formation proposed by von Gunten (1994) has been confirmed by many other researchers in recent years (Tang et al., 2005; Kim, 2002). Such a linear relationship between CT and bromate concentration was applied to describe bromate formation. The source term for its transport equation is:

$$S_B = \frac{dC_B}{dt} = -k_B C_l \tag{4.43}$$

where S_B is the source term for bromate formation process; C_B is the bromate concentration in water; C_l is the dissolved ozone concentration; and k_B is the water quality dependent bromate formation kinetic constant.

As discussed above, the ozone mass transfer, reaction and microbial inactivation processes are highly related to each other. Figure 4.2 shows the kinetics involved in these complex processes.

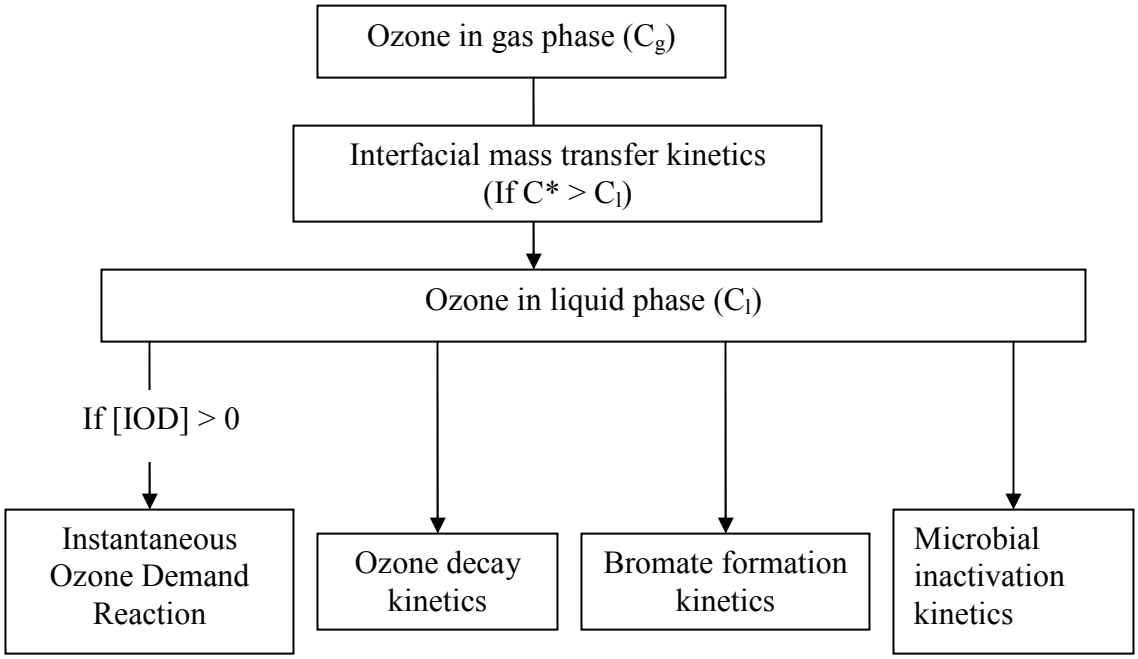

Figure 4.2 Modelling scheme for simulating ozone mass transfer and reactions

Tracer Residence Time Simulation

Ozone contactor hydraulic performance can be assessed quantitatively by tracer residence time distribution (RTD). Two approaches were used for modelling tracer residence time.

One approach was to model steady state "water age" using the transport equation 4.31, and a source term of 1 [s s^{-1}] was used for calculating the residence time at any locations within the contactor.

Another approach was a transient solution to simulate the tracer residence time distribution curve. The tracer simulation was run as a pulse injection test as in a full-

scale tracer study. First, a steady state CFD simulation was performed for calculating the fluid velocity fields. Then the tracer scalar was defined as an additional variable. The flow field obtained from the simulation was used as the initial condition and was frozen when conducting unsteady state simulations to solve the tracer scalar transport equations. The tracer residence time distributions were obtained by monitoring the tracer concentration at the outlets of the ozone contactors.

CFD-Based CT

Since the current USEPA and most Canadian provincial drinking water disinfection regulations (e.g. Ontario and Quebec) employ a CT concept and use CT tables to calculate disinfection efficiency (MOE, 2006; MENV, 2002), a CFD-based CT was also developed using an additional variable transport equation. The source term of the transport equation for CT is derived as follows:

When a parcel of liquid fluid flows from the inlet to the outlet of a contactor, a cumulative ozone exposure as a function of time is defined as:

$$CT \equiv \int_{t_{inlet}}^{t_{outlet}} C_{l,parcel}\, dt \tag{4.44}$$

Then it follows that

$$\frac{D(CT)}{Dt} \equiv C_l \tag{4.45}$$

At any instance in the time of the parcel's travel from inlet to outlet, the total derivative $\frac{D(CT)}{Dt}$ is defined as:

$$\frac{D(CT)}{Dt} = \frac{\partial}{\partial t} CT + u_i \frac{\partial}{\partial x_i} CT \tag{4.46}$$

Combining the above two equations and multiplying the result by the liquid phase volume fraction r_l gives the transport equation for ozone exposure (CT). As with other additional variable equations, the effects of turbulent diffusion should also be included, thus the final form of the CT transport equation is:

$$\frac{\partial}{\partial t}(r_l CT) + \nabla \bullet (r_l U_l CT) - \nabla(r_l (D_l^{(CT)} + \frac{\mu_{tl}}{\rho_l Sc_{tl}})\nabla CT) = r_l C_l \tag{4.47}$$

Thus, the source term for CT is defined as:

$$S_{CT} = r_l C_l \tag{4.48}$$

where r_l is volume fraction of water.

Overall Source Process

The CFD model developed in this study included transport equations for all the important chemical or biological components of an ozone disinfection system including the fast reacting natural organic matter (NOM_f), ozone concentration in gas/liquid phases (C_g and C_l), bromate concentration (C_B), ozone exposure (CT), and pathogen concentration (N). The source terms for these components are shown in Table 4.2.

Table 4.2 Kinetics and source terms of transport equations for modelling ozone processes

Component (species)	Processes	Source or sink terms for transport equations
Gas phase ozone concentration (C_g)	Mass transfer: $\frac{dC_l}{dt} = k_l a(C^* - C_l)$ $C^* = C_g / H$ $a = \frac{6}{d_g} * r_g$	$S_{tr} = -k_l a(C^* - C_l)$
Dissolved ozone concentration (C_l)	Mass transfer: $\frac{dC_l}{dt} = k_l a(C^* - C_l)$ Ozone decay: $\frac{dC_l}{dt} = -k_d C_l$ Ozone demand (When $[IOD] > 0$): $-\frac{d[IOD]}{dt} = -k_{NOM_f}[NOM_f]C$	$S_l = \begin{cases} k_l a(C^* - C_l) - k_d C_l & if \quad [IOD] \le 0 \\ k_l a(C^* - C_l) - k_d C_l - k_{NOM_f}[NOM_f]C_l & if \quad [IOD] > 0 \end{cases}$
Instantaneous ozone demand (IOD)	When $[IOD]$ >0 and C_l>0: $\frac{d[IOD]}{dt} = -k_{NOM_f}[NOM_f]C_l$ When $[IOD]$>0 and $C_l \le 0$ $\frac{d[IOD]}{dt} = -k_l a C^*$ Otherwise: $-\frac{d[IOD]}{dt} = 0$	$S_{[IOD]} = \begin{cases} -k_{NOM_f}[NOM_f]C_l & if \quad [IOD] > 0 \quad and \quad C_l > 0 \\ -k_l a C^* & if \quad [IOD] > 0 \quad and \quad C_l \le 0 \\ 0 & if \quad [IOD] \le 0 \end{cases}$
CT	$\frac{D(CT)}{Dt} \equiv C_l$	$S_{CT} = C_l$
Pathogens (N)	$\ln(\frac{N}{N_0}) = -k_m C_l^{\,n} t^m$	$S_N = \frac{dN}{dt} = -mN \cdot (k_m C_l^{\,n})^{\frac{1}{m}} \left[-\ln\left(N/N_0 \right) \right]^{(1-\frac{1}{m})}$
Bromate (C_B)	$\frac{dC_B}{dt} = k_B C_l$	$S_B = k_B C_l$
Tracer	$\frac{dC_{tracer}}{dt} = 0$	0

4.3 Full-Scale Case Studies

Using the three-dimensional multiphase computational fluid dynamics (CFD) model described in Section 4.2, all the major processes within an ozone disinfection system (ozone mass transfer, ozone decay, microbial inactivation, and disinfection by-product formation) can be predicted. The main focuses of this study were to use the CFD model to investigate ozone contactor hydraulics, mass transfer and reactions. The CFD-based CT was also simulated and used as an indicator for describing the microbial inactivation and disinfection by-product formation processes, since no site-specific models of these two processes were available during the period of this study. This is a reasonable approach because, as described in Section 4.2, the CT has strong correlation with the above two processes in ozone systems.

Prior to applying the model, it was essential to test the sensitivity of the results to various aspects of the CFD algorithm, including mesh density, discretisation scheme, and turbulence model selection. By doing this, it could be certain that the results were realistic rather than the product of a numerical artefact (Wright and Hargreaves, 2001). In addition, the CFD model was validated using experimental data obtained from the ozone disinfection systems of the DesBaillets Water Treatment Plant (WTP) in Montreal, Quebec and the Mannheim Water Treatment Plant in Kitchener, Ontario, so that the same closure and CFD sub-models could be used to simulate other geometries and operating conditions with a suitable level of confidence (Vesvikar and Al-dahhan, 2005).

4.3.1 The DesBaillets Water Treatment Plant ozone contactor

The DesBaillets Water Treatment Plant (WTP) in Montreal, Quebec is the second largest drinking water filtration plant in Canada. The plant was built in 1979 and has a

capacity of 1,200 million litres per day (MLD). Raw St. Lawrence River is treated by filtration and ozonation, followed by chlorination before being discharged into the distribution system. The DesBaillets WTP has six parallel ozone contactors, each with two cells, and ozone gas is fed in the first cell of each contactor through 126 porous fine bubble diffusers. The total length, width, and height of each contactor are 23.8 m, 5.50 m and 7.16 m respectively.

Meshing

Three dimensional CFD modelling is computationally expensive. Since the DesBaillets WTP ozone contactor has a symmetric geometric structure, only half of the contactor was modelled. Thus, the number of meshes and computational time were significantly reduced. The geometry of the ozone contactor was built by commercial CAD software: Solidworks™ and Ansys Design Modeler™. The geometry model then was imported into CFX-mesh to generate a mesh. Figure 4.3 shows the geometry and mesh of half of DesBaillets ozone contactor used in the CFD modeling. Unstructured tetrahedral grids were used for the CFD modeling and were refined at areas close to the gas diffusers and baffles. The total element number was about 420,000.

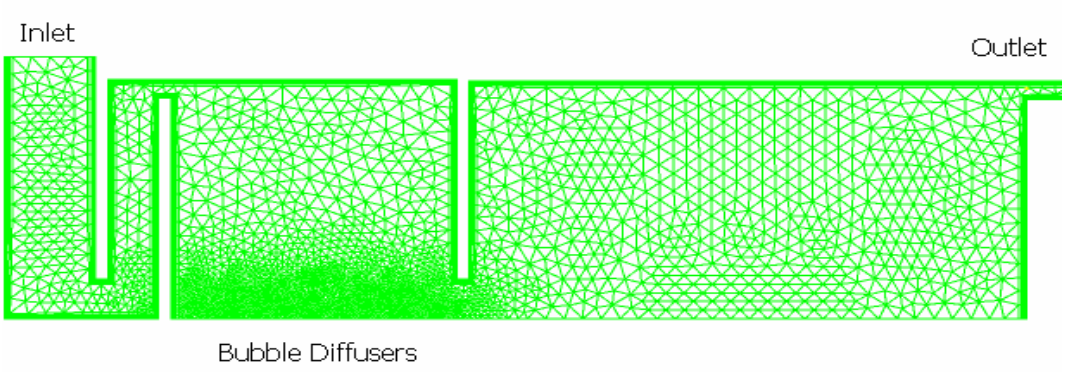

Figure 4.3 Schematic drawing and mesh of a DesBaillets WTP ozone contactor

Boundary conditions

The boundary condition of water and gas inlets were provided by specifying uniform velocities calculated from water and gas flow rates. For water inlet, the velocity was in the range of 0.1 to 0.3 m/s and the volume fraction of water was 1. For gas inlets, the velocity varied from 0.01 to 0.03 m/s and the volume fraction of air was 1. The outlet was set as a zero pressure gradient boundary condition and the reference pressure was set as 0 atmosphere (atm). A non-slip boundary condition was used for water at all the wall boundaries and a free-slip boundary condition was applied for gas phase at the walls. The free water surface was set as a degassing outlet which assumed that the surface was flat, frictionless and impervious to liquid to simplify the simulation, however, gas was allowed to leave at the rate at which it arrived at the surface. Such a degassing free surface boundary condition has been applied by other researchers (Zhang, 2000; Vesvikar and Al-dahhan, 2005). Since only half of the geometry was modelled, a symmetric boundary was given for the symmetric plane which was located in the middle of real ozone contactor.

4.3.2 The Mannheim Water Treatment Plant Ozone Contactor

The Mannheim Water Treatment Plant (WTP) is operated by the Regional Municipality of Waterloo, Ontario, Canada. It was designed to treat Grand River source water at a normal production capacity of 72 millions liters per day (MLD). The Grand River water, which is affected by both agricultural and municipal use, is moderate to high in hardness and alkalinity and averages an organic carbon concentration of 5 to 7 mg/L. There are two parallel baffled ozone contactors in the plant. The ozonated gas is injected into each contactor by fine bubble diffusers in the first two cells, and dissolved ozone further reacts in the following four cells. The ten year old ozone system has been modified to include new liquid oxygen (LOX) ozone generators to increase ozone gas

concentration and remove some diffusers from the system. The research efforts of the present study were focused on investigating the change of contactor performance before and after system modification.

Geometry and Meshing

Figure 4.4 is the three dimensional schematic drawing of one contactor. The geometry of the ozone contactor consisted of 6 cells with a total volume of 370.5 m^3. The height and width of the contactor were respectively 10.3 m and 8.3 m. Before system modification, there were 44 fine bubble diffusers in the first cell and 22 bubble diffusers in the second cell. Each of the diffusers was 800 mm (length)×100 mm (diameter). During modification, 34 diffusers were removed from the contactor, and the remaining diffusers were changed to be 200 mm (length)×100 mm (diameter).

The unstructured tetrahedral 3-D mesh was used and mesh was refined at areas closing to the gas diffusers and baffles. Total element number of the mesh was about 680,000, which was determined based on the mesh sensitivity study, which will be described in Section 4.5.1.1.

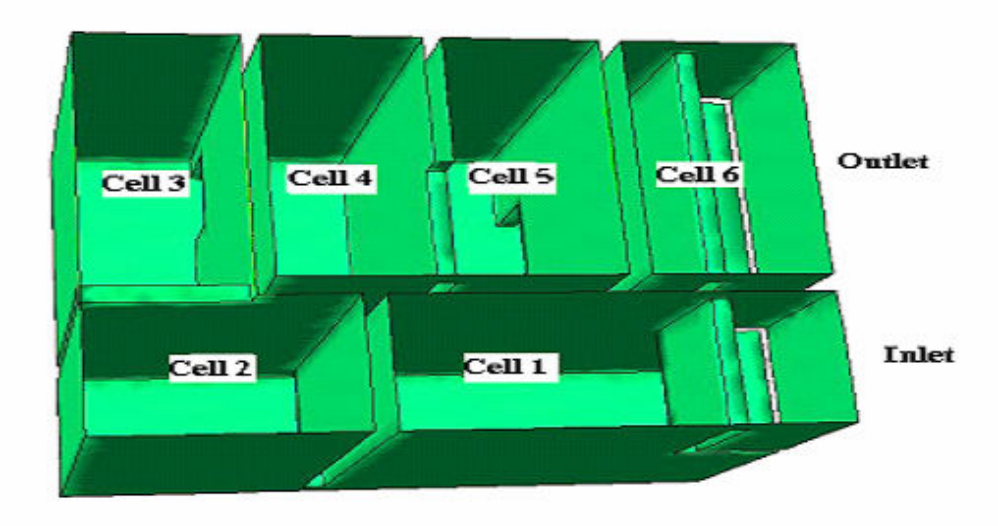

Figure 4.4 Schematic drawing of the Mannheim WTP ozone contactor

Boundary conditions

The velocity at water inlet was in the range of 0.45 m/s and the volume fraction of water was 1. For gas inlets, the velocity varied from 0.022 m/s and the volume fraction of air was 1. Other boundary conditions were same as those used in the modelling of DesBaillets ozone contactor.

4.3.3 Numerical Method

The numerical solution of the CFD modeling was carried out with a finite-volume based program CFX10 (Ansys, 2005). CFX employs an unstructured control volume mesh. The governing equations for fluid flow, mass transport and decay are discretized in the computational domain by a finite volume method. Discretization of the non-linear differential equations yields a system of linear algebraic equations that are solved

iteratively. In this study, a second order high-resolution differencing scheme was applied to all equations. The time step used varied in range between 100s and 0.001s from the start to the end of a run. For each run, the hydrodynamics was solved first in a transient manner until steady state was reached. Steady state was indicated by a state when all the key variables (e.g. local velocities of the two phases and the volume fraction of the gas phase) remained constant. All the simulations were done on a Pentium 4 PC with 3.0 GHz CPU and 2G memory. The computational times for obtaining the converged solutions usually were between 1 days to 4 days. Figure 4.5 shows the procedures for CFD modelling of ozone disinfection processes.

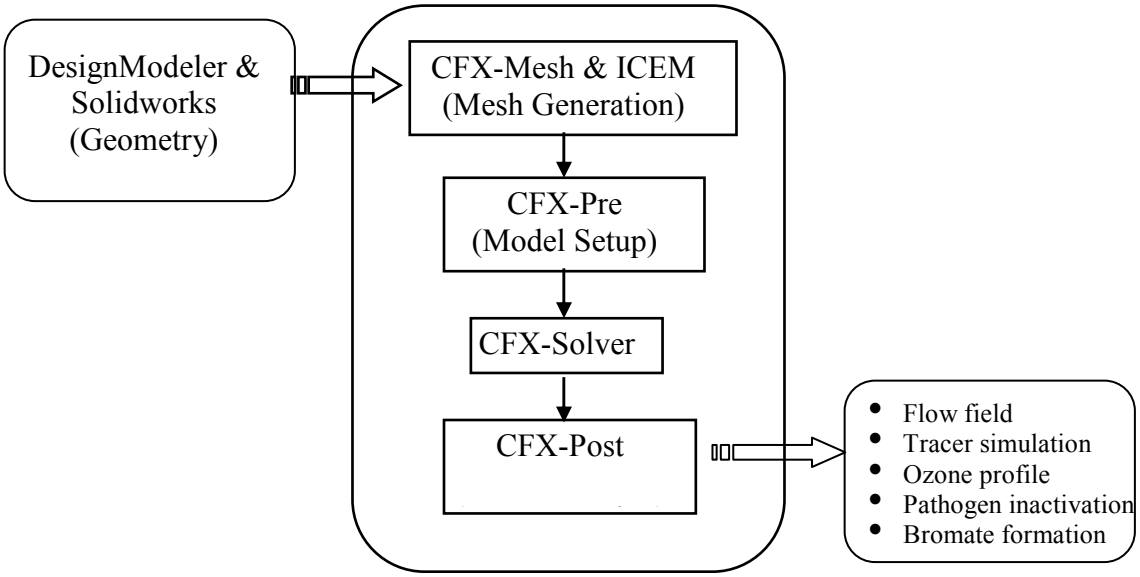

Figure 4.5 Procedures for CFD modelling of ozone disinfection processes

4.4 Results and Discussions

4.4.1 DesBaillets Water Treatment Plant Ozone Contactor Study

4.4.1.1 Model Sensitivity Study

Sensitivity to Mesh Density

As the mesh is refined a more accurate solution can be expected, however, the finer the mesh, the more time is needed for computations. Therefore, the mesh density should be selected such that an acceptable accurate solution is obtained within a reasonable simulation time. At the same time, it is necessary that the solution obtained is mesh-independent (Vesvikar and Al-dahhan, 2005). In this study, the effect of mesh density on the accuracy of CFD modelling was evaluated by performing a series of tracer residence time distribution simulations at three different mesh density conditions. The number of elements for the three meshes were 320,803, 370,982, and 424,891 respectively. Figure 4.6 presents the comparison result which suggests that there was only a slight difference in tracer RTD prediction under the three mesh density conditions. One possible reason for such a difference is that uniform flow rates were defined for gas and water inlet boundary conditions. However, in real situation, the flow rates may vary across the inlet surfaces. Further reduction of mesh size did not significantly improve the accuracy of modelling. Therefore, the mesh size of 424,891 was selected for the rest of studies.

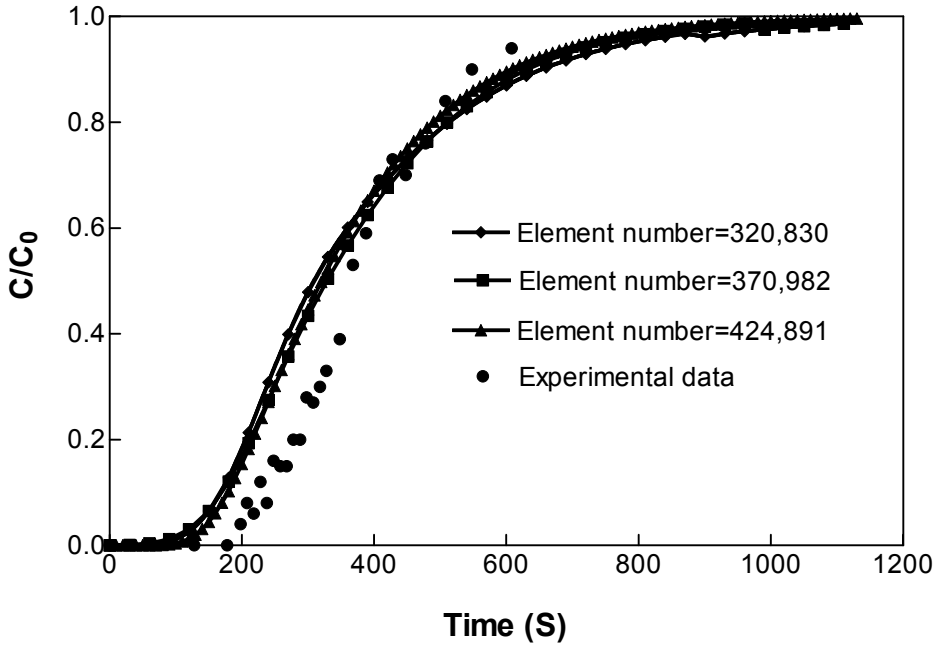

Figure 4.6 Sensitivity of the mesh density on the simulation of tracer residence time distribution

Sensitivity to Choice of Turbulent Model

The effect of the turbulence model on the tracer RTD was also studied. In addition to the standard k–ε model, three other commonly used turbulence models including the RNG k–ε model (Yakhot and Orzag, 1986), the shear stress transport (SST) turbulence model (Mentor, 2003) and the Speziale-Sarkar-Gatski (SSG) model (Speziale et al., 1991) were used for comparison purpose. Figure 4.7 shows tracer RTD simulation results for the different models. In all four cases the tracer curves varied slightly and the standard k-ε model fit best with the experimental result. This suggested that the k–ε model was most appropriate and it was deemed sufficiently accurate for the study

undertaken here. In addition, the RNG k-ε, SST, and SSG models usually require much longer computational times. Therefore, the k–ε model was selected for this study.

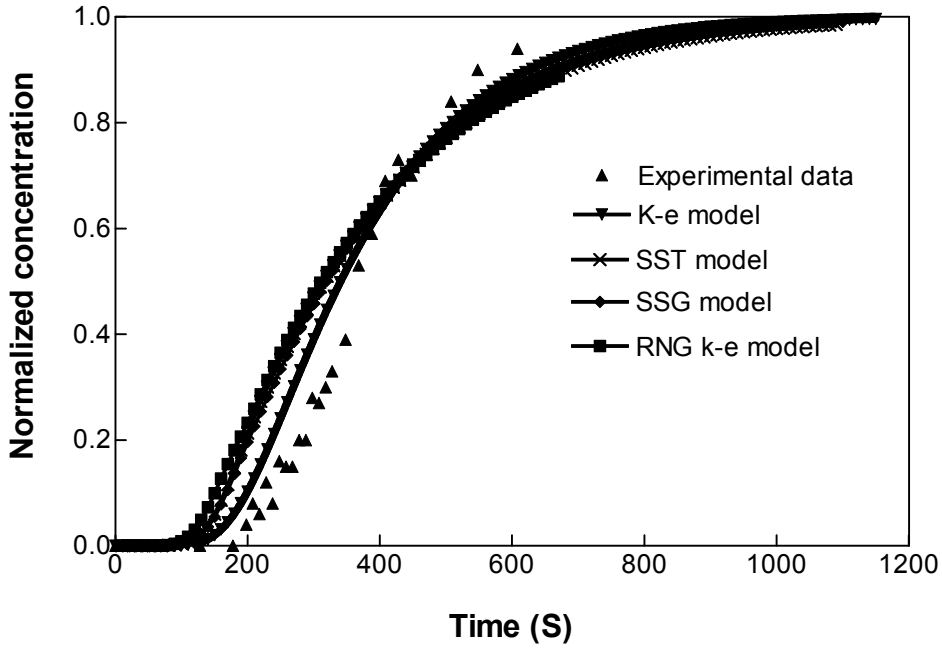

Figure 4.7 Sensitivity of the turbulence model on the simulation of tracer residence time distribution

Sensitivity to the Selection of Air Bubble Size

As discussed previously, previous literature studies (Langlais et al., 1991; Wu, 2001) have shown that the average bubble size in ozone contactors is in a narrow range between 2 mm and 5 mm. To simplify the simulation, a constant bubble size was used in this study. The sensitivity of the bubble size on the modelling was studied to determine if this is a reasonable assumption. The modelling was run at different bubble sizes from 2mm to 5mm. The simulated air volume fraction and dissolved ozone concentrations were compared as presented in Figures 4.8 and 4.9. The results showed that, in the modelled bubble size range, the volume fractions and dissolved ozone

concentration at the 7 monitoring points inside the ozone contactors were not significantly affected by bubble size selection. This was consistent with the results of Vesvikar and Al-Dahhan (2005) on the CFD modelling of an anaerobic digester. They found that, when bubble diameters in the range of 2–12 mm, the change in diameter did not affect the results significantly. The same observation was made by van Baten et al. (2003) and Sokolichin et al. (2004). Thus, an average bubble diameter of 3 mm was used in the present simulations.

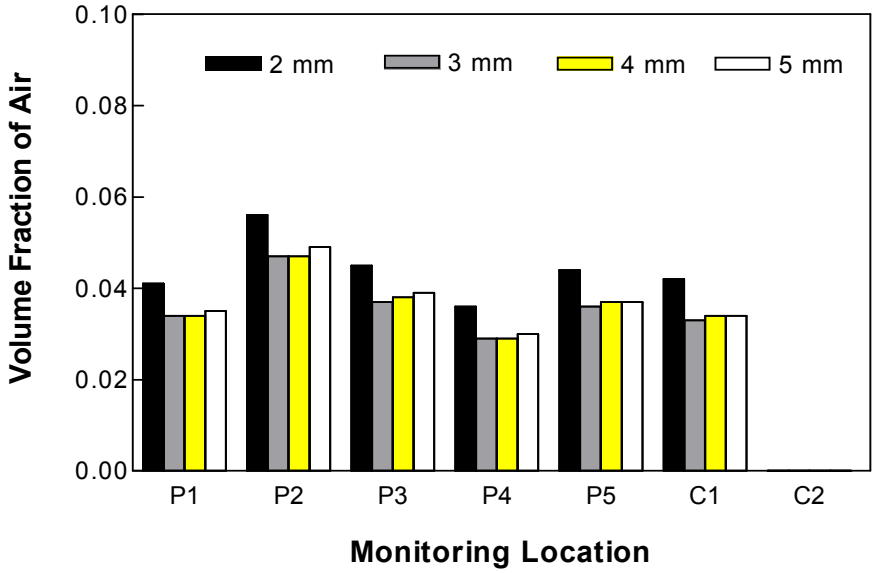

Figure 4.8 The simulated air volume fraction at different bubble sizes

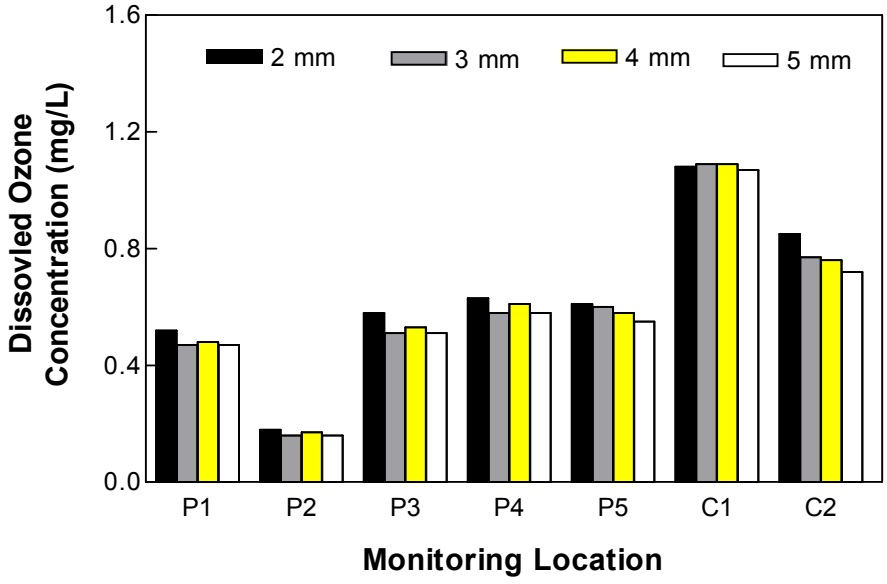

Figure 4.9 The simulated dissolved ozone concentration at different bubble sizes

4.4.1.2 Model Validation

The CFD model was validated by comparison of the simulated tracer residence time distribution (RTD) with field tracer test data (El-Baz, 2002) obtained at the DesBaillets WTP ozone disinfection system at two different flow rates. Figure 4.10 showed the comparison results at the flow rate of 2.16 m^3/s for two monitoring points C1 and C2. The locations of the two points are shown in Appendix A. Good agreement was observed between the CFD modelling and experimental tracer test results. The simulated and measured T_{10}/T ratios at flow rates of 2.16 m^3/s were 0.51 and 0.55 respectively; and the simulated and measured T_{10}/T ratios at flow rates of 1.47 m^3/s were 0.50 and 0.51 respectively.

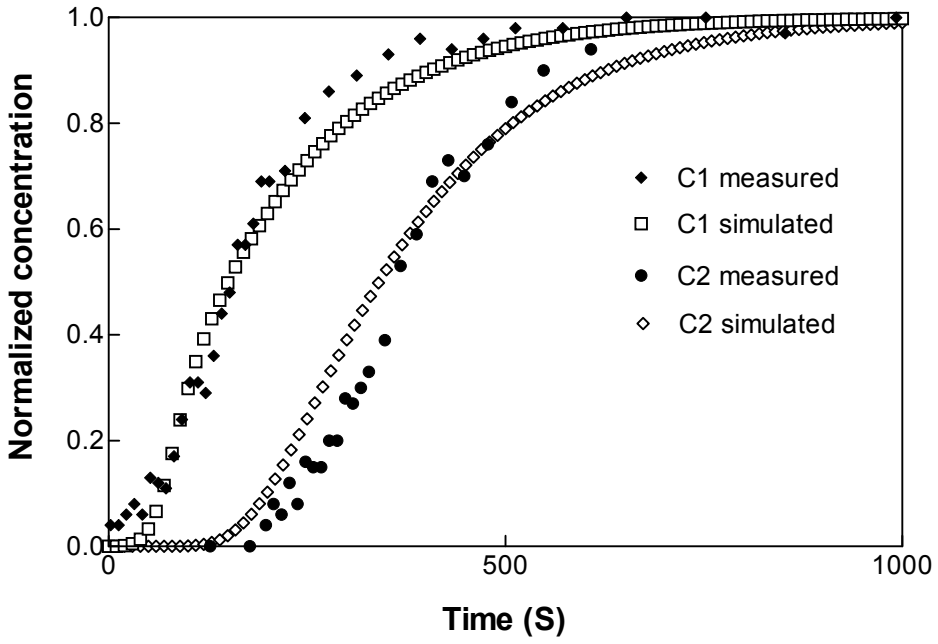

Figure 4.10 Comparison of simulated and experimental tracer curves

In addition, local ozone residual concentrations were obtained by solving transport equations for ozone mass transfer and reactions. The ozone demand and decay kinetics parametes used were determined by experimental study done by the École Polytechnique de Montréal (El-Baz, 2002).

Figure 4.11 CFD shows the predicted CFD ozone residual distribution and the locations of the monitoring points inside the ozone contactor. The modelling conditions include: water flow rate=2.16 m^3/s, gas flow rate = 0.25m^3/s, ozone concentration in gas = 1.4%, immediate ozone demand (IOD) =0.96 mg/L and ozone first order decay constant = 0.12 1/min. The comparison between the numerical and measured ozone concentrations at these monitoring points is given in Table 4.3. Although relatively big differences were observed at a point near the gas diffusers (P4) and a point at the edge of the short circuiting zone (P2), the predicted ozone concentrations at all other monitoring points were within 11% of the measured values. It was thus considered that the CFD modelling could sufficiently accurately predict mass transfer and reactions of ozone within the contactors.

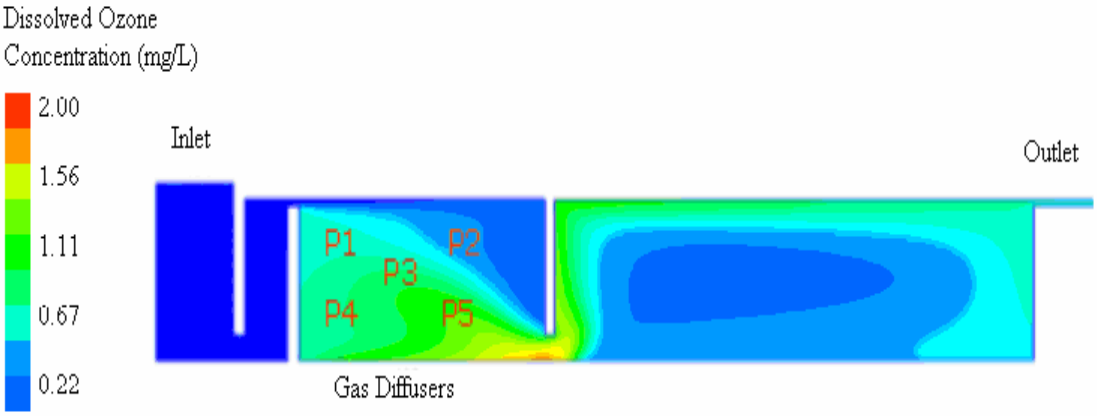

Figure 4.11 CFD predicted ozone residual distribution

Table 4.3 A Comparison between the predicted and measured ozone concentrations at 6 monitoring points

Monitoring points	P1	P2	P3	P4	P5	Outlet
Predicted ozone concentration (mg/L)	0.60	0.34	0.81	0.76	0.71	0.64
Measured ozone concentration (mg/L)	0.54	0.44	0.74	1.03	0.64	0.67
Difference (%)	11	25	10	26	11	5

4.4.1.3 Prediction of Disinfection Performance

The CFD model was applied to investigate the contactor hydraulics under various operational conditions. Figure 4.12 displays a typical flow field inside the contactor. From the velocity field, it was observed that large recirculation zones existed in the two cells and caused short-circuiting and dead zones. The existence of dead zones and short-circuiting would reduce the contacting opportunities between ozone and pathogens and make disinfection efficiency significantly less than it otherwise could be.

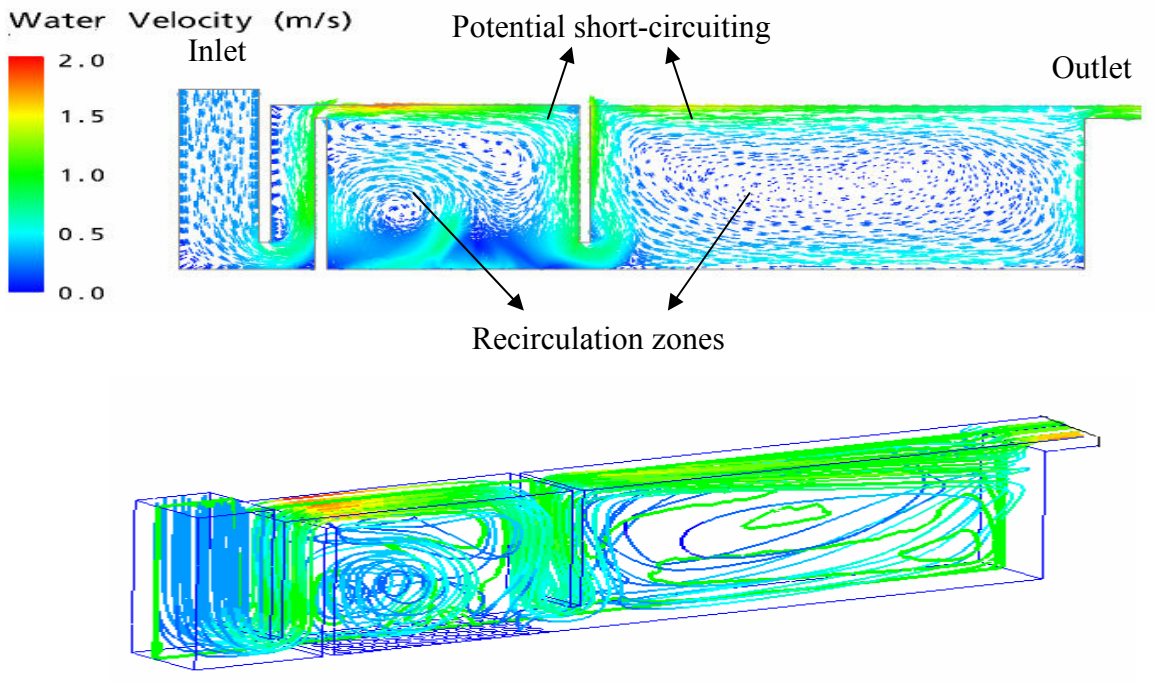

Figure 4.12 Simulated velocity vector field and streamlines of the DesBaillets WTP ozone contactor

In the present study, a CFD-based CT concept was introduced to characterize ozone disinfection performance, in which C is the local ozone residual concentration and T is the local residence time. As described in Section 4.3, this CT was calculated by solving a species transport equation using C (local ozone residual) as a source term, and it represented the accumulated CT exposure dose for pathogens that traveled from the contactor inlet to a specific internal location. The disinfection efficiency of a contactor could be evaluated by determining the CFD-based CT values at outlet locations.

Figure 4.13 shows the simulated ozone residual distribution and CT value distributions as well. CFD modeling can also predict log inactivation directly based on the pathogen inactivation kinetics model. However to be consistent with current regulations, which are based on the CT approach, only CFD simulated CT values are discussed herein. The

total disinfection efficiency of a contactor could be calculated using the CFD based CT at the outlet of the contactor.

As shown in Figure 4.13, the flow field could significantly affect the ozone residual and CT distributions. A portion of the water might experience short-circuiting phenomena (for example, at the top surface of cell 2) and had a much smaller CT than other portions of water exiting the contactor. Such phenomena may be a potential risk to safe drinking water disinfection.

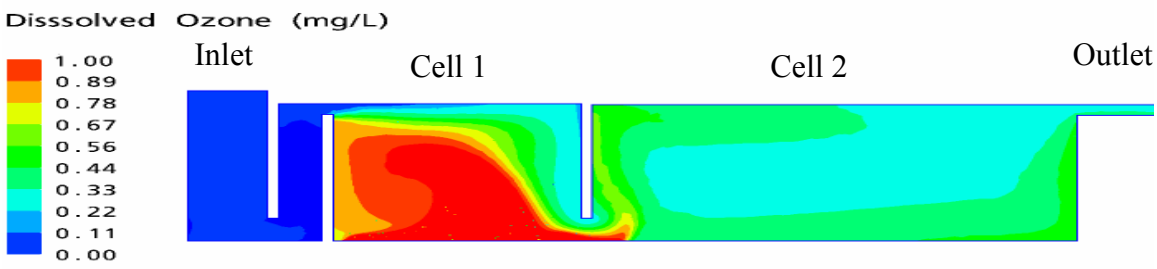

(a) Ozone residual distribution

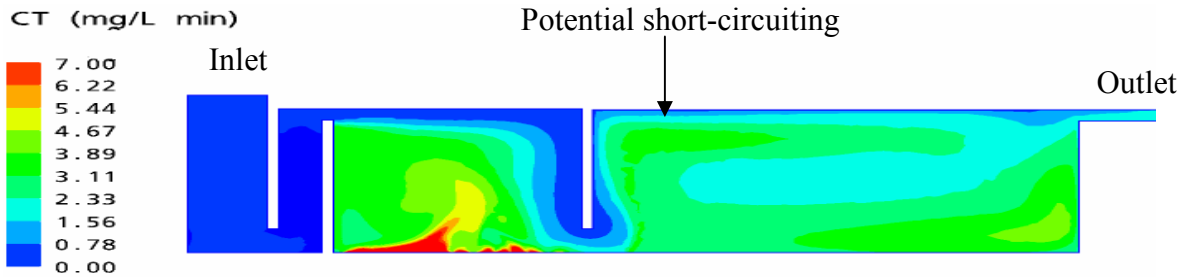

(b) CT value distribution

Figure 4.13 Simulated ozone residual and CT value profiles within the DesBaillets WTP ozone contactor

In Chapter 7 of this thesis, the CFD simulated CT value was also compared with CT calculated by the traditional CT_{10} method. The results showed that, under different modeling conditions, the CFD simulated CT value could be 80% to 140% higher than the traditionally calculated CT_{10} value. This indicated that the traditional CT_{10} method might significantly underestimate disinfection efficiency, and CFD was a better alternative for evaluating ozone disinfection treatment performance even though a safety factor should be considered to account for the uncertainty factors of the CFD modeling.

4.4.1.4 Effects of Baffling on Contactor Hydraulics and Disinfection Efficiency

To minimize the recirculation in the second cell, an alternative contactor configuration was modelled. Four additional baffles were placed into cell 2 of the contactor. Figure 4.14 presents the CFD simulated velocity fields. The results suggested that, after adding baffles in the second cell, the flow field became more uniform and the dead zones and short circuiting as described in Figure 4.12 were significantly reduced.

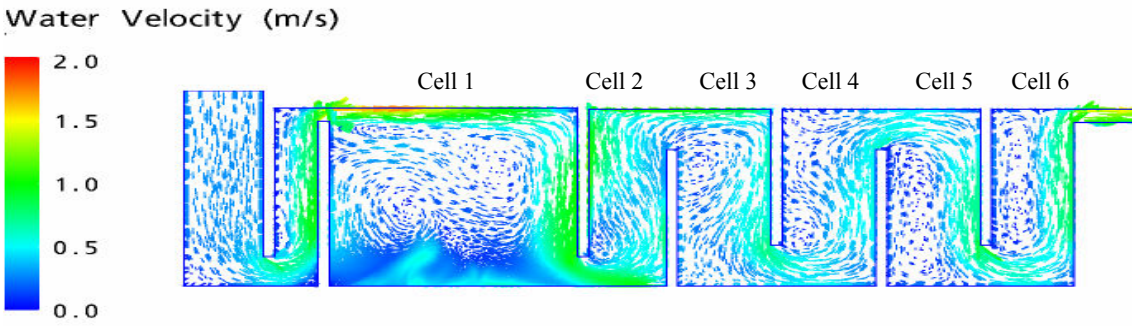

Figure 4.14 Simulated flow field after installing four baffles in a DesBaillets ozone contactor

Figure 4.15 shows the CFD simulated CT after adding baffles inside cell 2. After modifying the contactor configuration, the upstream pressure propagation from cell 2

back baffle wall changes the flow patterns in cell 1 which affects the CT distribution in cell 1. The CT values after cell 1 were uniform. No obvious surface short-circuiting occurred and therefore the treatment efficiency was improved. In fact, the average CT at the contactor outlet has been increased 64% (from 1.78 mg/L*min before adding battles to 2.79 mg/L*min after adding baffles) after adding baffles. Therefore, using the CFD-based CT concept, it was possible to quantitatively evaluate ozone disinfection efficiency and to assist with the design and operation of full-scale ozone contactors.

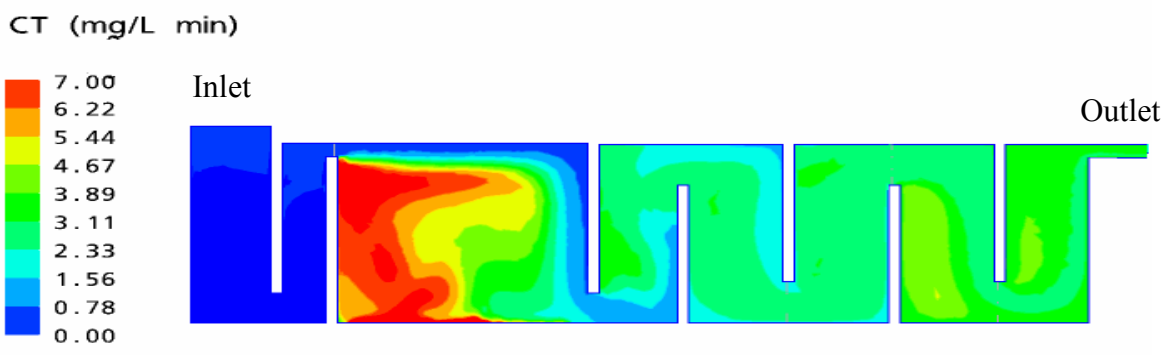

Figure 4.15 Simulated CT after installing four baffles in a DesBaillets ozone contactor

4.4.1.5 Effects of water quality on ozone contactor performance

As discussed in Chapter 2, the water quality factors, such as temperature, pH, alkalinity, natural organic matter, and ammonia, can significantly affect the ozone decomposition and disinfection performance. Previous researchers tried to model the effects of individual parameters on ozone decay and disinfection efficiency using empirical or mechanistic models (Amy et al., 2000; Kim, 2002). However, the empirical models are usually strongly site specific, and the mechanistic models are currently still not feasible due to the fact that the ozone reactions in the natural waters are too complex to be fully

described (Kim, 2002). To-date, none of these models has been used reported to be used to assist with the design and operation of full-scale ozonation systems.

However, the above water quality factors can be indirectly described by two water quality indicators: immediate ozone demand (IOD) and ozone decay kinetic constant (k_d) (Langlais et al., 1985; Chen, 1998; Finch et al., 2001). These two parameters therefore were included in the CFD modelling to characterize the effects of water quality. Experimental studies of DesBaillets WTP source water were done at different seasonal conditions, and it was found that the immediate ozone demand of DesBaillets ozone contactor source water varies from 0.4 to 1.2 mg/L and the ozone decay kinetic constant k_d changes in the range of 0.05 to 0.15 min^{-1} (El Baz, 2002) .

Figure 4.16 shows the effects of these two parameters on the effective CT predicted by CFD modelling at a constant operational condition (water flow rate = 2.16 m^3/s; gas flow rate =0.34 m^3/s). It was found that, for the DesBaillets WTP ozone system, the immediate ozone demand (IOD) had a strong influence on CT prediction. The increase of the IOD from 0.4 to 1.2 mg/L resulted in the decrease of the CFD-based CT from 4.0 to 2.3 mg/L min. Since the IOD mainly represents the level of natural organic matters in source water, this result suggested that enhancing pre-treatment for the removal of NOM was a key approach to improving the DesBaillets ozone contactor performance.

Figure 4.17 presents the effects of ozone decay kinetics constant on the CFD-based CT. It could be observed that the influence of ozone decay kinetics constant (k_d) on ozone disinfection seemed to be much smaller than the influence of immediate ozone demand. Increasing k_d from 0.05 to 0.15 min^{-1} only led to a 0.6 mg/L min decrease of CT. This

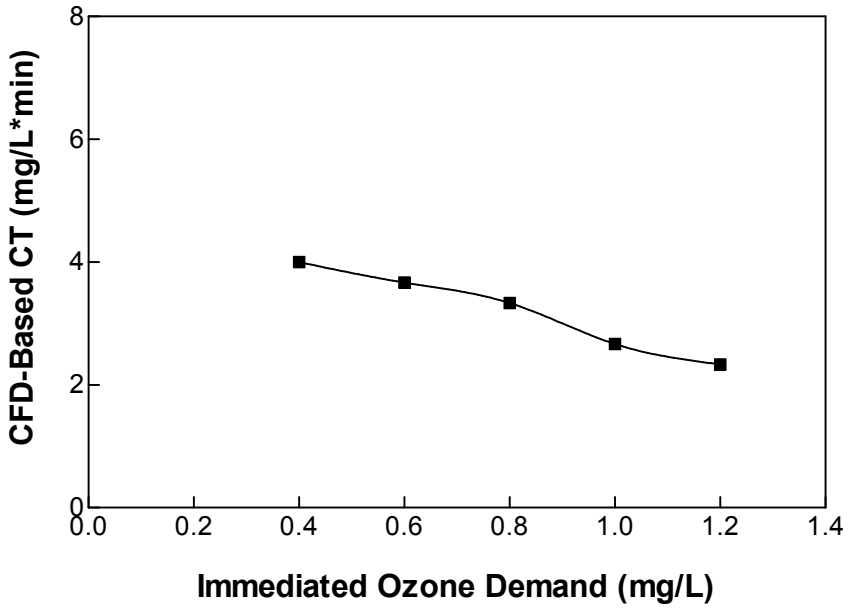

Figure 4.16 Effects of immediate ozone demand on the CT of DesBaillet ozone contactor

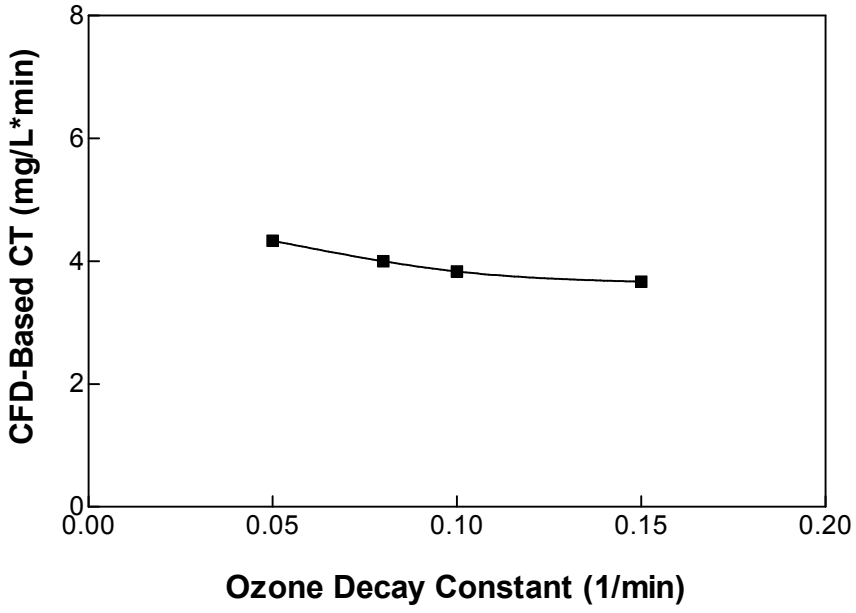

Figure 4.17 Effects of ozone decay constant on the CT of DesBaillet ozone contactor

was due to the fact that the DesBaillets ozone contactor has a short residence time (hydraulic retention time is about 5 min). Therefore, the role of ozone decay was limited compared with that of the immediate ozone demand.

Based on the above analysis, it was suggested that the treatment plant should conduct routine tests to determine the immediate ozone demand and use this information to optimize the ozone system operation.

4.4.2 Mannheim Water Treatment Plant Ozone Contactor Study

4.4.2.1 Model Validation

For the ozone contactor of the Mannheim Water Treatment Plant (WTP), in Waterloo, Ontario, Canada, the system was undertaking system modifications including installing liquid oxygen (LOX) diffuser systems and removing some diffusers during this study.

Before the system modification, The CFD hydraulic model was validated through a comparison between the CFD simulated T_{10} and the T_{10} values obtained from full-scale tracer tests results provided by the Regional Municipal of Waterloo previously performed by others. Figure 4.18 shows a CFD simulated tracer tests for the outlets of each of the 6 cells at a water flow rate of 16.93 million litres per day (3.72 MIGD or 4.47 MGD). At two different water flow rates (16.93 and 30.58 million litres per day), the simulated T_{10} values were respectively 16.3 and 11.1 minutes, which were in close agreement with experimental T_{10} values of 15.9 and 10.3 minutes. It was also observed that contactor hydraulics changed greatly with the change of flow rate. Application of

the CFD approach allows us to quantify the hydraulic changes to direct the design and operation of an ozonation process.

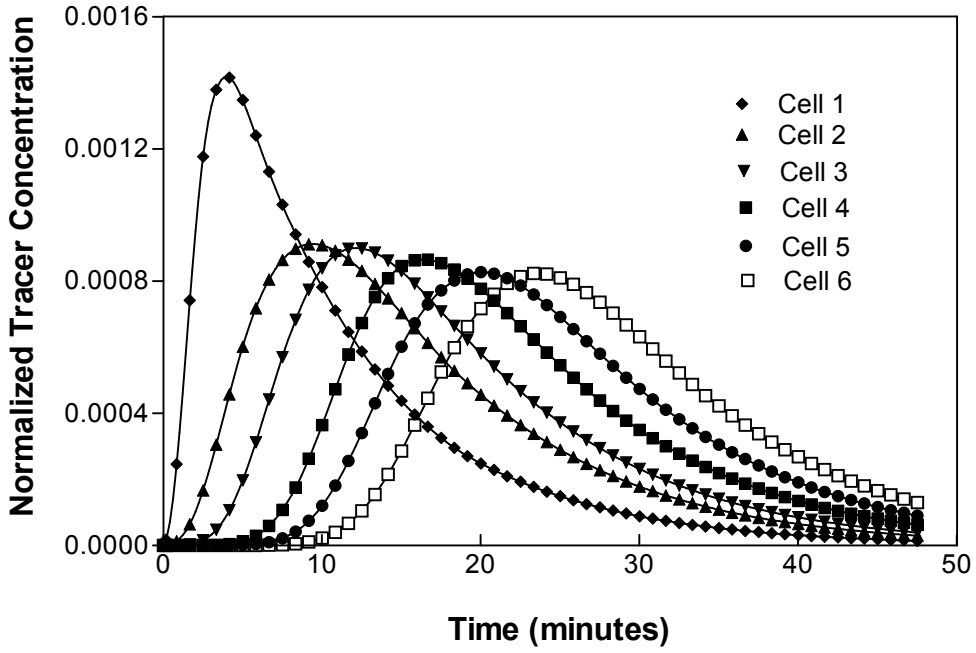

Figure 4.18 Numerical tracer RTD curves for the outlet of each cell in the Mannheim contactor

After the system modification, experimental and modeling studies were done to further validate the CFD model. The ozone profiles were simulated using the experimentally determined ozone demand and decay kinetics. The validation test was done at the following conditions: water flow rate=0.43 m^3/s, gas flow rate = 0.007 m^3/s, ozone concentration in gas = 7%, water temperature =12 °C, immediate ozone demand (IOD) =1.21 mg/L and ozone first order decay constant = 0.21 1/min. Figure 4.19 presents a comparison between the CFD predicted and the on-site tested ozone profiles along the modified ozone contactor. In general, the predicted ozone residual at most sampling

points fitted well with experimental data. The CFD predicted results at the sampling points of cell 2 and cell 3 showed a relatively larger difference (about 20%) with the measured values. One possible reason for this was that, in this study, the grab sampling locations were determined from photos provided by the Regional Municipal of Waterloo (Ontario, Canada) instead of by measurements. As what will be discussed in Chapter 5, the ozone residuals might vary significantly at the outlets of the cells (particularly the cells 2, and 3) following the ozone dissolution cell. Inaccurate determination of the monitoring locations might make residual measurements and predictions differ from their actual values.

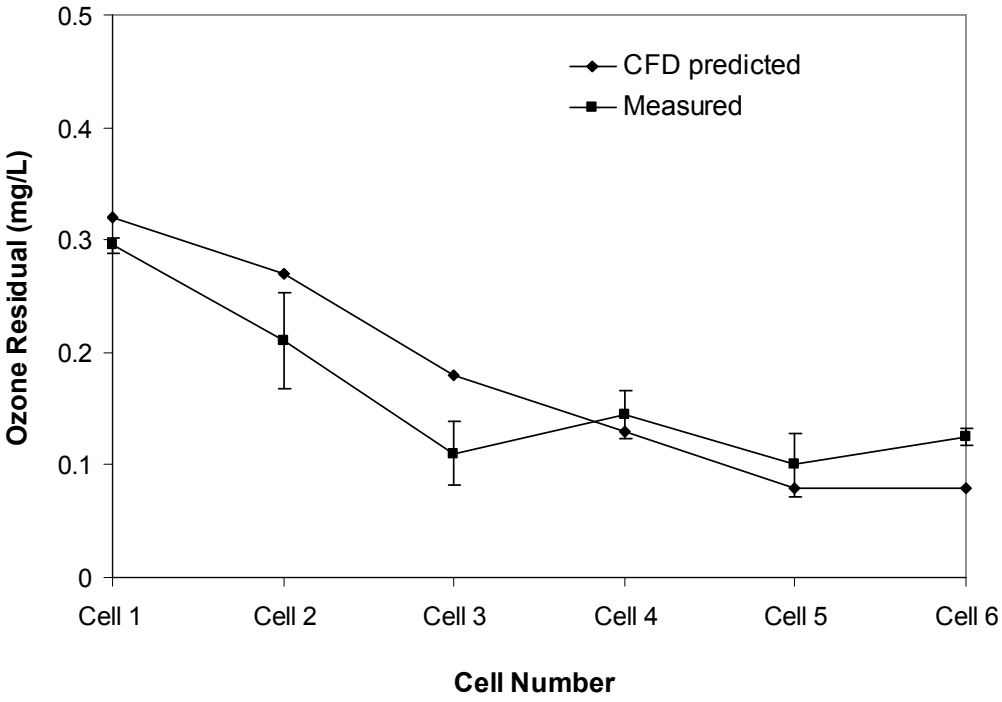

Figure 4.19 A comparison between the CFD predicted and on-site tested ozone profiles for the Mannheim WTP ozone contactor

4.4.2.2 Ozone Contactor Hydraulics Before and After Modification

This 13 year old ozone contactor system of Mannheim WTP was recently modified to include liquid oxygen (LOX) fed ozone generators to increase ozone concentration in gas from original 1-1.5 wt. % to 6-10 wt.%. Due to the significant change of ozone concentration, 28 of the original 44 diffusers in cell 1 were removed from the system. Likewise, 6 of 22 diffusers in cell 2 and all the 34 diffusers in cell 3 were also removed. The comparison of the numerical tracer RTD of the ozone contactor before and after modification is presented in Figure 4.20. The results predict that reducing the number of diffusers in the contactor and increasing the ozone concentration in the gas has led to an increase in residence time of the water. Therefore, it was suggested that the Mannheim WTP should conduct tracer tests for the modified ozone contactor and adjust the T_{10}/T ratio used for disinfection credit calculation to operate the system more economically.

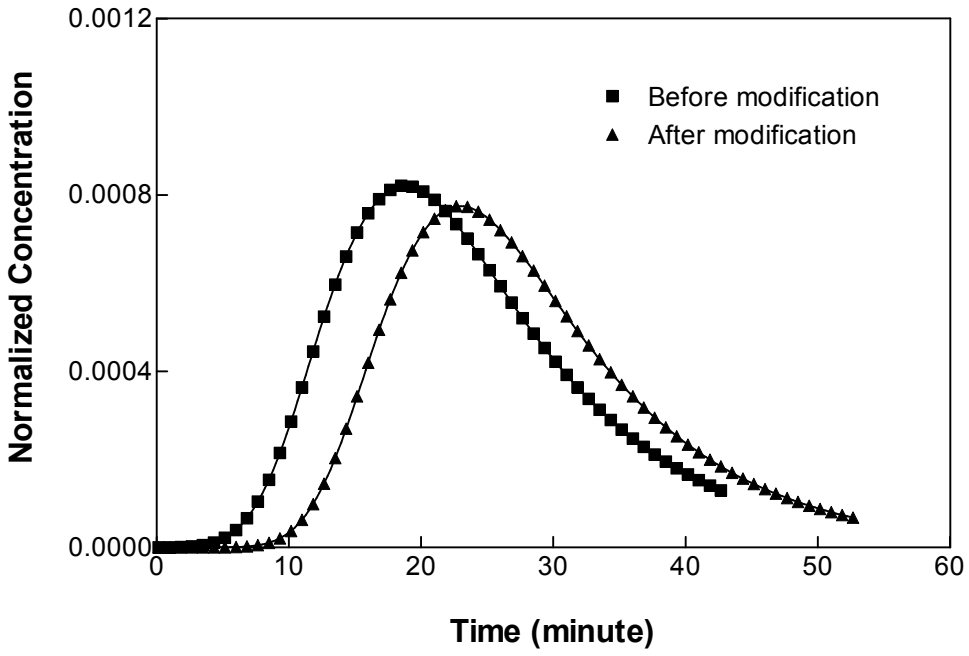

Figure 4.20 Predicted contactor hydraulics before and after system modification

4.5 Conclusions

A three-dimensional multiphase CFD model in the Eulerian-Eulerian framework was developed to fully describe ozone disinfection processes. The model employed all the major components of ozone disinfection processes: contactor hydraulics, mass transfer, ozone decomposition, microbial inactivation and bromate formation. The sensitivities of mesh density, turbulence model selection, and bubble size selection were studied. The results showed that k-ε model was appropriate for this study. Changing the bubble size in the rage of 2 to 5 mm did not significantly affect the modelling results, therefore a constant bubble size 3mm was selected for the modelling.

The CFD model was validated by tracer test data and ozone residual profiles. Numerical solutions agreed well with the field test data obtained from the Desbaillets and Mannheim ozone contactors. The results suggested that dead zones and short-circuiting existed in the investigated contactors and might significantly reduce disinfection efficiency. Installing additional baffles in the second cell of the DesBaillets contactors could improve contactor hydraulics and therefore ozone disinfection efficiency. The effects of water quality on ozone disinfection were also investigated. The results of DesBaillets case study indicated that immediate ozone demand (IOD) had more significant influence on disinfection efficiency compared with the ozone decay constant did. It was therefore suggested that the IOD should be tested routinely to improve the ozone dosage determination.

This study demonstrated the power of CFD for predicting the performance of full-scale ozone disinfection processes. The model developed in this study could be used for ozone contactor design, evaluation, and troubleshooting. It could also be used as a virtual experimental tool to optimize ozone contactor behaviour under varying water quality and operational conditions.

CHAPTER 5 IMPROVING OZONE RESIDUAL MONITORING AND TRACER TESTING STRATEGIES FOR FULL-SCALE OZONE CONTACTORS BASED ON CFD MODELING

5.1 Introduction

The USEPA Surface Water Treatment Rule (SWTR) Guidance Manual (USEPA, 1991) recommended that the microbial inactivation credit of an ozone contactor can be evaluated by a "CT" concept which is defined as the product of ozone concentration ("C") in a cell and disinfectant contact time or exposure time ("T"). CT tables relating *Giardia* and virus log inactivations with associated ozone CT values were given in the SWTR Guidance Manual (USEPA, 1991). In the recently released Long Term 2 Enhanced Surface Water Treatment Rule (LT2ESTR), an additional CT table was provided to calculate the log inactivation rate of *Cryptosporidium parvum* by ozone (USEPA, 2006). Depending on temperature, *Cryptosporidium* CT values are 15 to

---

Parts of this chapter have been published in: 2006 AWWA Water Quality Technology Conference and Exposition, American Water Work Association; Proceedings of 12th Canadian National Conference and 3rd Policy Forum on Drinking Water, Canadian Water and Wastewater Association.

25 times higher than CT values for equivalent *Giardia* and virus log-inactivation credit. Similar CT tables have been adopted by some Canadian provincial regulations such as the Procedure for Disinfection of Drinking Water in Ontario (MOE, 2006). The direct effect of this new CT table is that ozone dose needed for *Cryptosporidium parvum* inactivation will be much greater than the dose for *Giardia* and virus inactivation. Therefore, to minimize ozone dosage to reduce operational costs and at the same time to decrease disinfection by-product formation, water suppliers have to accurately determine CT values.

The ozone residual value, C, can be obtained from on-line ozone residual analyzers or measured from grab samples (USEPA, 2006). Accurate ozone residual data will allow the calculation of correct log-inactivation values and allow optimized performance to be maintained. However, based on previous pilot and full-scale studies, the ozone residual profile in a contactor may vary significantly depending on the method of operation, water quality and water flow conditions (Chen, 1998; Bellamy, 1995). The potential variation of ozone concentration at sampling locations may greatly affect the ozone concentration monitoring results. One potential efficient way to determine the optimal sampling locations is through numerical modeling. However, to-date no modelling studies have been reported to determine the variation of ozone residuals in ozone contactors and to optimize ozone residual monitoring strategy.

The disinfectant contact time T_{10} is usually determined through conducting step-input or pulse input tracer studies. The accuracy of the tracer test results can be affected by multiple factors including the stability of water/gas flow, tracer injection method, sampling location, and tracer detection method. It is therefore not unusual to see significant differences between two tracer curves obtained under the same testing conditions. In addition, tracer testing is costly and time-consuming. Thus, there is also

a need to optimize tracer test strategies to be used for accurate determination of contactor hydraulics.

Therefore, the primary objective of this study was to apply a computational fluid dymanics (CFD) modelling approach to investigate the ozone concentration variation in ozone cells and to optimize the locations of ozone residual monitoring points. The second objective was to study the effects of tracer injection methods and tracer monitoring points on tracer test results and to optimize tracer test strategy.

5.2 CFD Model Description

A multiphase model was developed and validated by comparing with full-scale tracer test data and ozone profiles obtained from the Desbaillet Water Treatment Plant ozone contactors (Zhang et al., 2005; Zhang et al., 2006). The Eulerian-Eulerian approach was used for simulating bubbles dispersed in water during ozonation processes (Lakehal, 2002; Versteeg and Malalasekera, 1995; Zhang et al., 2005). The interfacial transfer of ozone between gas and liquid systems were modeled based on the well known two film theory (Danckwerts, 1970; Singer and Hull, 2000). The ozone reactions were modeled as two stage reactions: the first stage was instantaneous ozone demand (IOD); the second stage was ozone decomposition described by a pseudo first-order kinetic equation (Langlais et al., 1991). All the species were modelled by solving species transport equations with appropriate source terms as described in Chapter 4 and Zhang et al. (2006).

Ozone contactor hydraulic performance could be assessed from tracer residence time distribution (RTD) curves. Step or pulse additions of a tracer could be made resulting in so-called F and E RTD curves (Levenspiel, 1999). Numerical simulation of tracer tests was conducted in two steps. First the steady state fluid flow was established. In a second step, the steady state flow field solution was applied as an initial condition. A tracer was introduced at a source point in the inlet to the tank, and the concentration at the outlet was tracked by solving the transient tracer scalar transport equation. Simulations with both step and pulse injections were produced. T_{10} values were then directly obtained from the tracer F curve as described by Teefy (1996).

5.3 Case Study

The CFD model was applied to simulate the ozone disinfection system at the DesBaillets Water Treatment Plant (WTP) (1,200 million liters per day/317 million gallons per day) in Montreal, Canada. The DesBaillets WTP has six parallel ozone contactors, and each contactor has two cells. Ozone gas is fed in the first cell of each contactor through 126 porous fine bubble diffusers. The total length, width, and height of each contactor are 23.8 m, 5.50 m and 7.16 m, respectively. Figure 5.1 shows the ozone residual monitoring points inside a DesBaillets ozone contactor. The system initially used two sampling points for measuring ozone residuals: C1 for cell 1 and C2 for cell 2. To improve the accuracy of ozone residual monitoring in cell 1, five additional sampling ports (P1 to P5) were installed. The average ozone residual from these five monitoring points are used for CT calculation instead of using the residual at a single point C1. The contactor hydraulics was previously evaluated using a step injection of hydrofluorosilic acid as the tracer chemical (El Baz, 2002). As shown in Figure 5.2, a distribution pipe was installed on the inlet surface to provide uniform

injection of the tracer chemicals uniformly across the width of the contactor during the tracer tests.

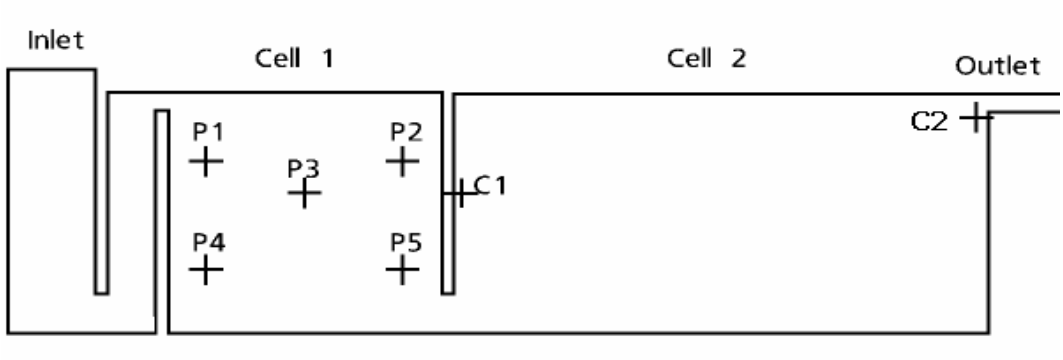

Figure 5.1 Ozone residual sampling ports in a DesBaillets WTP ozone contactor

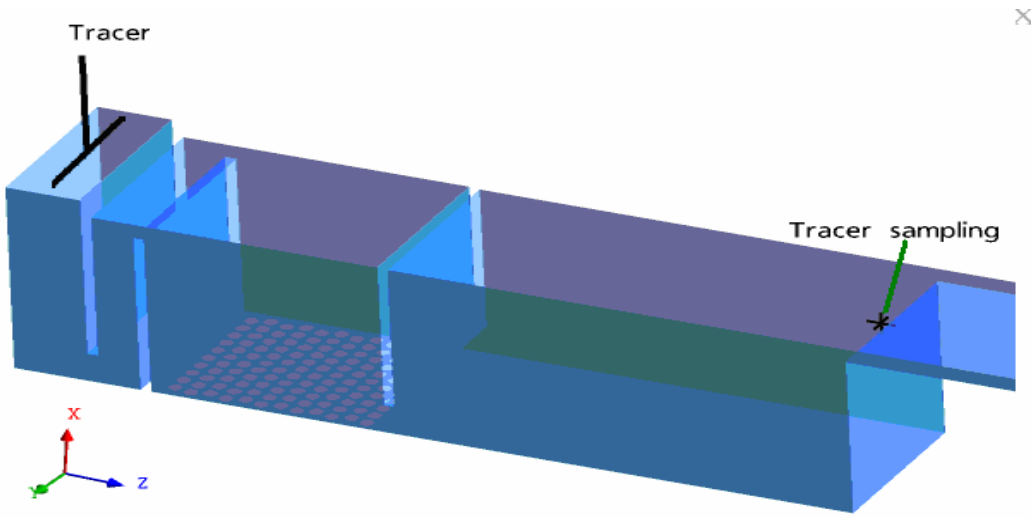

Figure 5.2 Tracer injection pipe and sampling point in a DesBaillets WTP ozone contactor

5.4 CFD Modelling Results and Discussion

5.4.1 Distribution of Dissolved Ozone Concentration at the Outlet of the Cells

When the effluent CT method is used for microbial inactivation credit calculation, the dissolved ozone concentration should be measured at the outlet of each cell (USEPA, 1991). However, current regulations do not provide a clear guidance on how to locate these ozone monitoring points. It is therefore important to investigate the sensitivity of the sensor locations on ozone residual monitoring to assist with ozone contactor design and operation.

Figure 5.3 presents the CFD simulated ozone profiles at different planes at the outlet area of cell 1. As shown in Figure 5.2, the Y axis represents distance along the width of the contactor from the central symmetric plane and X axis represents the vertical distance from the bottom of the contactor. It can be observed that the ozone concentration varied widely at the outlet. The residuals were above 1.0 mg/L at the centre area of the outlet planes and decreased to 0.2 mg/L at the locations close to the side walls. The maximum value could be more than one order of magnitude higher than the average value. The modelling results also indicated that ozone residuals were more sensitive to the sampling locations at the outlet area of cell 1. Measuring ozone residual at the upstream or downstream of the baffle may lead to under or over estimation of outlet ozone concentrations. Under the current regulation framework (MENV, 2002; USEPA, 2006), C represents the outlet concentration of a cell Therefore, the present work suggests that the ozone sensor or sampling port should be located within the plane under the baffle wall.

Based on the drinking water regulations of the province of Quebec, Canada (MENV 2002), the CT value of the first cell was calculated based on the residence time T_{10} of the cell multiplied by half of the ozone residual at the outlet of the cell. The above result indicated that the selection of inappropriate monitoring points would lead to incorrect calculation of CT values for log inactivation evaluation.

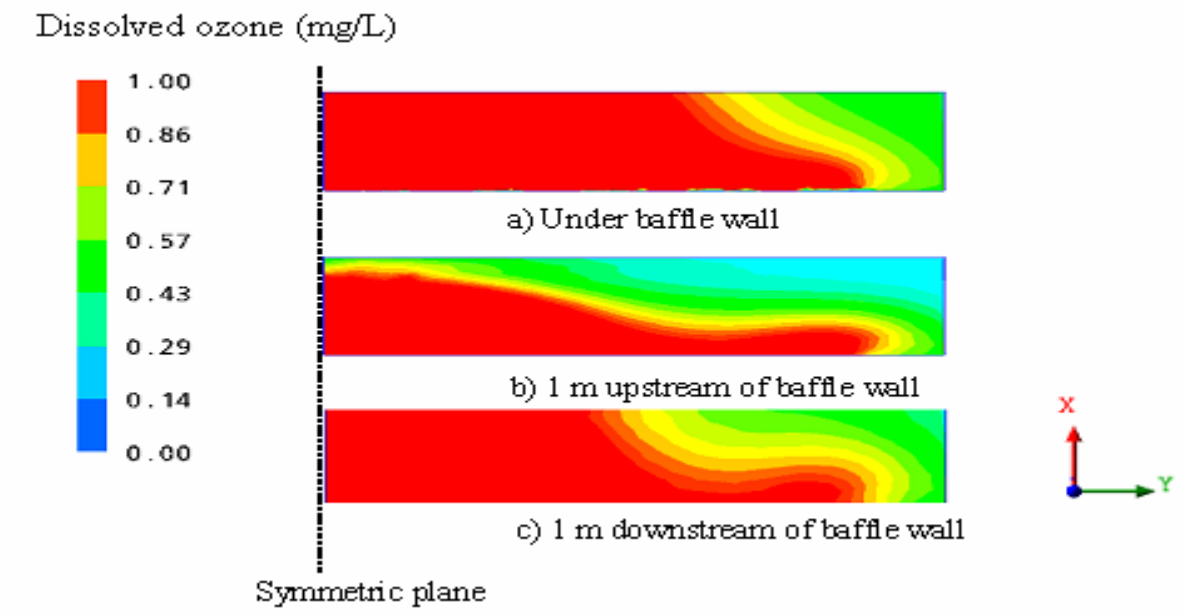

Figure 5.3 Simulated ozone residual distributions around the outlet of cell 1 in the DesBaillets WTP ozone contactor (only half of the outlet is shown)

Using the CFD modeling approach, it is possible to locate the potential "optimal" location for ozone residual monitoring under a specific operational condition. The shaded region in Figure 5.4 shows the area at the outlet of a cell where calculated ozone concentrations were within ± 20 % of the average outlet ozone concentration calculated through CFD modeling. The 20% value is chosen as a reasonable one for purpose of illustration.

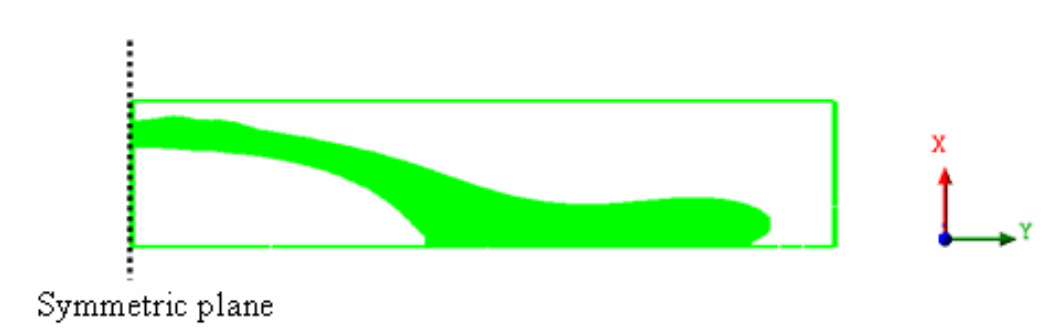

Figure 5.4 The area at the outlet of cell 1 where ozone concentrations are within ± 20 % of the average value (water flow rate =3.22 m^3/s; gas flow rate=0.21m^3/s; ozone dose=2.2 mg/L)

It would be expected that more representative monitoring results could be obtained when ozone sampling ports or online sensors were installed within or close to the shaded area shown in Figure 5.4. However, the ozone residual distributions at the outlet of cell 1 were strongly affected by the operational parameters.

Figure 5.5 shows the variation of the "optimal" ozone sampling zones at two different water and air flow rates. Since the shape of the optimal zones changed significantly at different conditions, it would be difficult to determine a universal optimal point which could always represent the average ozone residual.

Previous studies showed that other factors, such as ozone dosage and water quality, might also affect the dissolved ozone concentration distribution (Bellamy, 1995). It was therefore suggested that multiple ozone monitoring points should be provided at the outlet of cell 1 to obtain a more representative ozone residual, if possible.

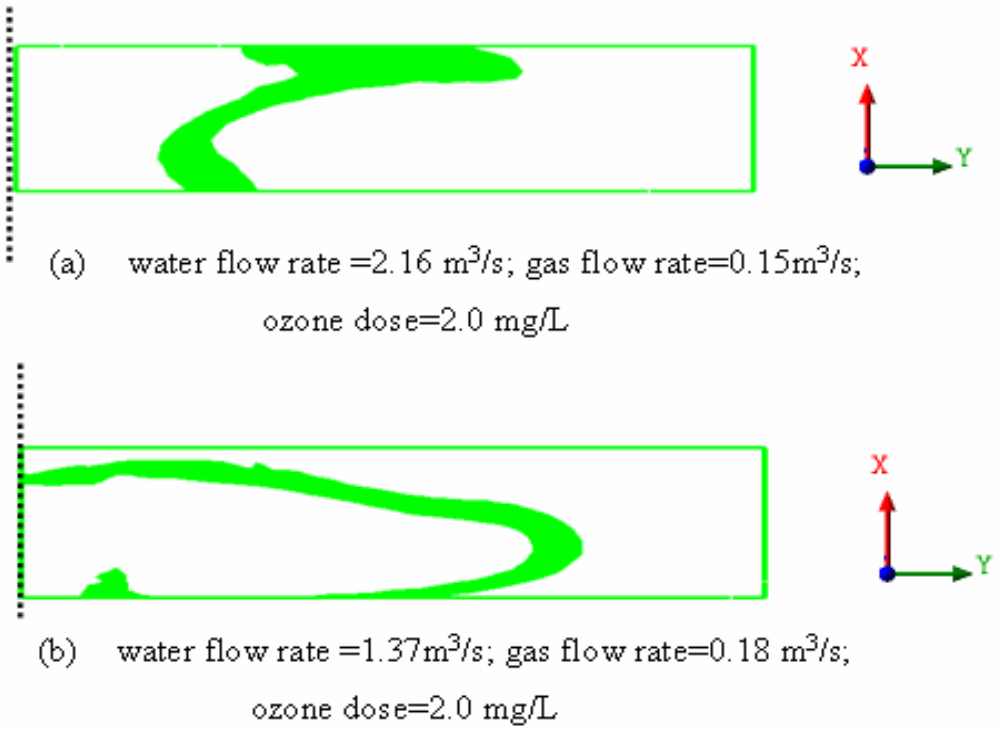

Figure 5.5 The area at the outlet of cell 1 where ozone concentrations are within ± 20 % of the average value

Figure 5.6 shows an example of installing three monitoring points (S1 to S3) at the cell 1 outlet. Table 5.1 presents a comparison of the mass flow averaged calculated ozone concentration, residual at point C1 (shown in Figure 5.1), and the average ozone residual calculated from three points. It could be observed that, the residuals at point C1 were higher than the outlet average residuals at the current modeling conditions. The three point averaged ozone residual agreed reasonably well with the averaged residual at the outlet of cell 1. Using this multiple points monitoring strategy, one could obtain a more representative ozone residual for the cell 1 outlet concentrations.

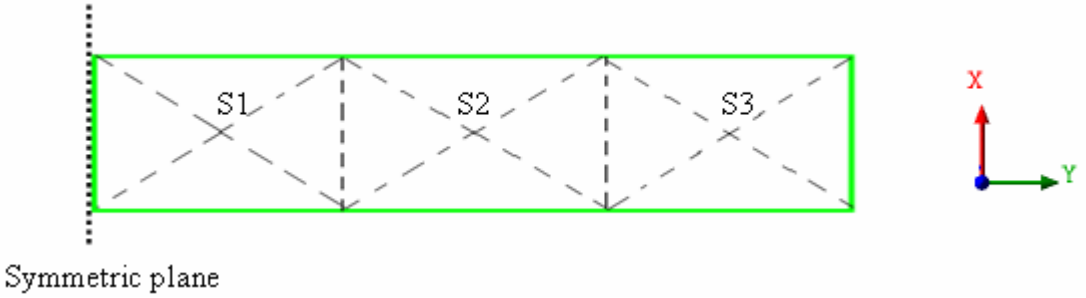

Figure 5.6 The location of 3 sampling points at the outlet of cell 1

Table 5.1 A comparison of the mass flow averaged ozone concentration and the arithmetic average residual calculated from three points at outlet of cell 1

Modeling conditions	Ozone Residual at Cell 1 (mg/L)		
	Outlet Average	Residual at point C 1	Three points (S1 to S3) Average*
Water flow rate: 3.22 m^3/s Gas flow rate: 0.21 m^3/s Ozone concentration in air: 0.015 kg/m^3 Ozone demand:0.60 mg/L Ozone decay constant:0.10 min^{-1}	1.09	1.45	1.07
Water flow rate: 2.16 m^3/s Gas flow rate: 0.15 m^3/s Ozone concentration in air: 0.0167 kg/m^3 Ozone demand:0.53 mg/L Ozone decay constant: 0.12 min^{-1}	0.85	1.25	0.94
Water flow rate: 1.37 m^3/s Gas flow rate: 0.18 m^3/s Ozone concentration in air: 0.016 kg/m^3 Ozone demand: 0.69 mg/L Ozone decay constant: 0.10 min^{-1}	0.98	1.01	0.97

* Arithmetic average

5.4.2 Spatial Distribution of Dissolved Ozone Concentration within Ozone Contactors

As discussed above, the DesBaillets WTP initially used point C 1 (see Figure 5.1) as the only monitoring point for the CT calculation. This monitoring point is located behind the baffle wall and in the region of short-circuiting caused by buoyancy flow. Therefore it usually over-estimates the ozone residual of Cell 1, and is not appropriate to be used for CT calculation. To improve the accuracy in monitoring ozone residuals, five additional monitoring points have been installed in Cell 1 of the DesBaillets ozone contactor to obtain the average ozone residual in this cell for CT calculation.

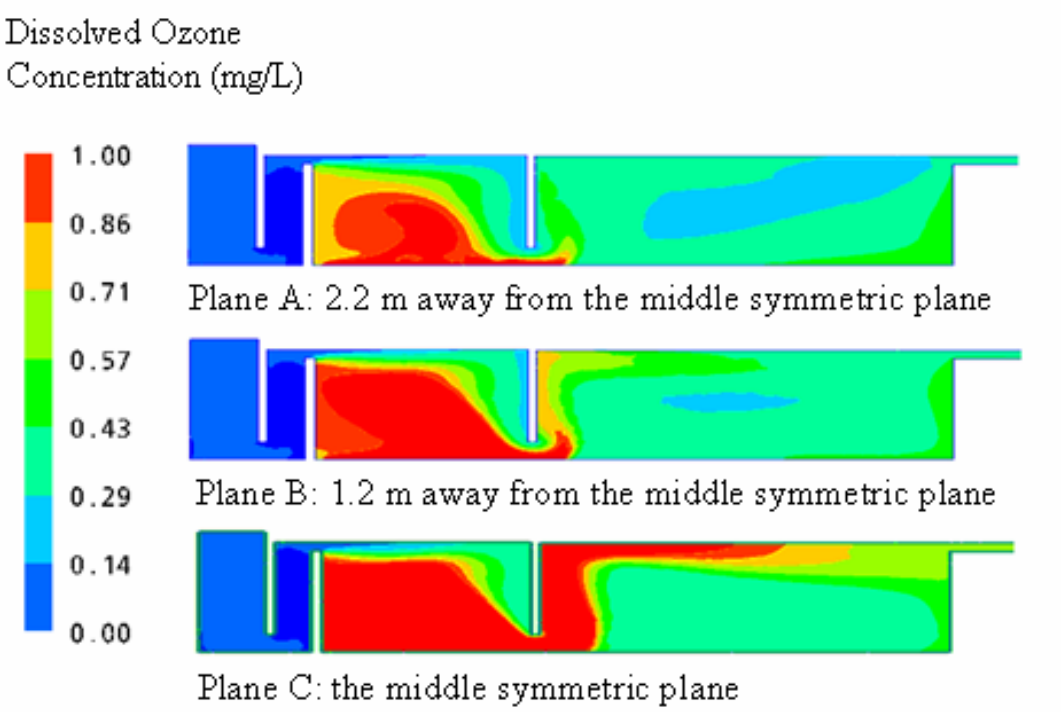

Figure 5.7 Spatial ozone residual distributions along the horizontal profile of the DesBaillets WTP ozone contactor.

Figure 5.7 shows the spatial variation of the ozone residual profile at a water flow rate of 3.25 m3/s, gas flow rate of 0.27 m3/s, and ozone dosage of 2.20 mg/L. The CFD simulated results suggested that ozone concentrations at the plane closest to the side wall (Plane A) were much smaller than those at other two locations (Planes B and C). Therefore installing sampling ports close to, or flush with, the walls should be avoided to prevent under-estimation of average ozone concentration. It could also be observed that the dissolved ozone concentrations varied significantly along the contactor which was caused by the existence of short-circuiting and recirculation zones within the contactor.

Table 5.2 shows a comparison of the volume averaged residual and average residual calculated from five points at different planes. The volume averaged residual was calculated as the integral of ozone concentration in cell 1 divided by the total volume of cell 1. It could be found that installing the five monitoring points on the middle plane (plane C) might over-estimate the volume averaged ozone residual, while putting monitoring points on the plane closest to the wall (Plane A) may under-estimate ozone residuals. A better prediction of the averaged ozone residual could be done by installing the monitoring points on the plane 1.2 m away from the middle plane.

Table 5.2 A comparison of the volume averaged residual and arithmetic average residuals calculated from 5 points at different planes

Modeling conditions	Ozone Residual at Cell 1 (mg/L)			
	Volume average	5 points average* in plane A	5 points average* in plane B	5 points Average* in plane C
Water flow rate: 0.28 m^3/s Gas flow rate: 0.02 m^3/s Ozone concentration in air:0.015 kg/m^3 Ozone demand:0.60 mg/L Ozone Decay constant:0.10 min^{-1}	0.99	0.69	0.93	1.27
Water flow rate: 0.186 m^3/s Gas flow rate: 0.011 m^3/s Ozone concentration in air:0.017 kg/m^3 Ozone demand:0.53 mg/L Ozone Decay constant: 0.12 min^{-1}	0.69	0.46	0.73	0.86
Water flow rate: 0.127 m^3/s Gas flow rate: 0.013 m^3/s Ozone concentration in air: 0.016 Ozone demand: 0.69 mg/L Ozone Decay constant: 0.10 min^{-1}	0.82	0.53	0.76	0.94

5.4.3 Ozone residual distribution in the contactor after installing additional baffles

To improve the contactor hydraulics in the second cell, an alternative contactor configuration was modelled. Four additional baffles were placed into cell 2 of the contactor. Figure 5.8 shows CFD predicted averaged ozone residuals at the outlet of each cell after installing four additional baffles in the contactor.

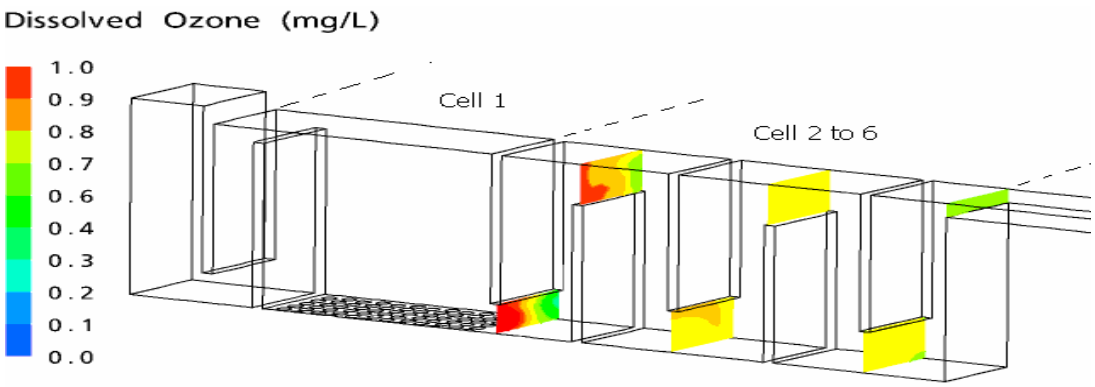

Figure 5.8 CFD predicted ozone residuals at the outlet of each cell after installing additional baffles

Figure 5.9 presents a comparison of the volume averaged residual and outlet average residual for each contactor cell. It could be observed that the volume averaged residuals were significantly higher than the outlet average residuals in the first two cells. For other cells, the differences became negligible. The maximum and minimum concentration values at the outlets of each cell are also shown in Figure 5.9. The large variations of the ozone concentrations at the outlets of cell 1 to 3 suggested that the residuals would be very sensitive to the monitoring locations in these cell outlet areas. At the outlets of cell 1 and cell 2, the maximum residuals could be one order of magnitude higher than the minimum values.

Therefore, the monitoring points should be determined very carefully to be more representative. It was also suggested that multiple monitoring points at the outlet of certain cells should used instead of just one point to provide more accurate indicators to system operators.

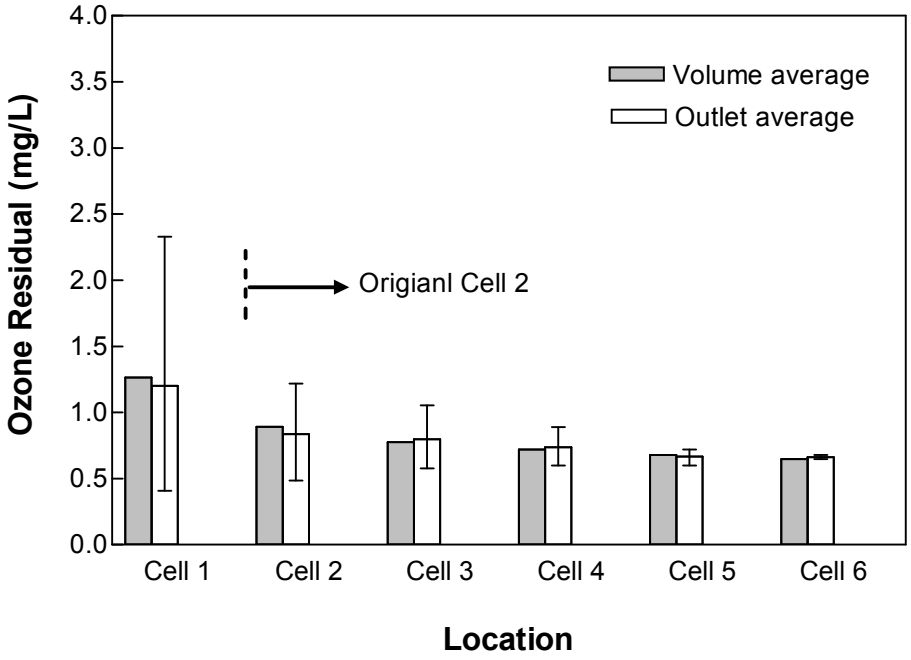

Figure 5.9 Simulated ozone residuals of each cell after installing additional baffles

5.4.4 Effects of Tracer Injection Points on RTD and T_{10}

The CFD model was also used to study factors affecting tracer residence time distribution (RTD). Numerical tracer tests were performed by pulse-injecting a pre-determined amount tracer in a very short time from the inlet of the contactor and monitoring the tracer concentration at the outlet of the contactor. Figure 5.10 shows the simulated tracer residence time distribution curves (E curves) obtained through four different tracer injections: 1) "tracer 1" was injected at an inlet point close to side wall; 2) "tracer 2" was injected at an inlet point between the side wall and middle symmetric plane; 3) "tracer 3" was injected at an inlet point on the middle symmetric plane, and

4) “tracer inlet” was injected uniformly over the cross-section of the contactor inlet. These tracer curves were the modelling results at a water flow rate of 3.25 m^3/s, gas flow rate of 0.27 m^3/s, and ozone dosage of 2.20 mg/L. For this specific case, the tracer injection method only slightly influenced tracer RTDs. Tracer 1 has a maximum T_{10} (164 seconds) and Tracer 3 has a minimum T_{10} (155 seconds). Only very small difference (<6%) was observed for different injection points, which might be because the Desbaillets WTP contactor has two small cells before cell 1. These two cells allowed the tracer chemicals to be mixed and uniformly distributed before the tracer entered cell 1.

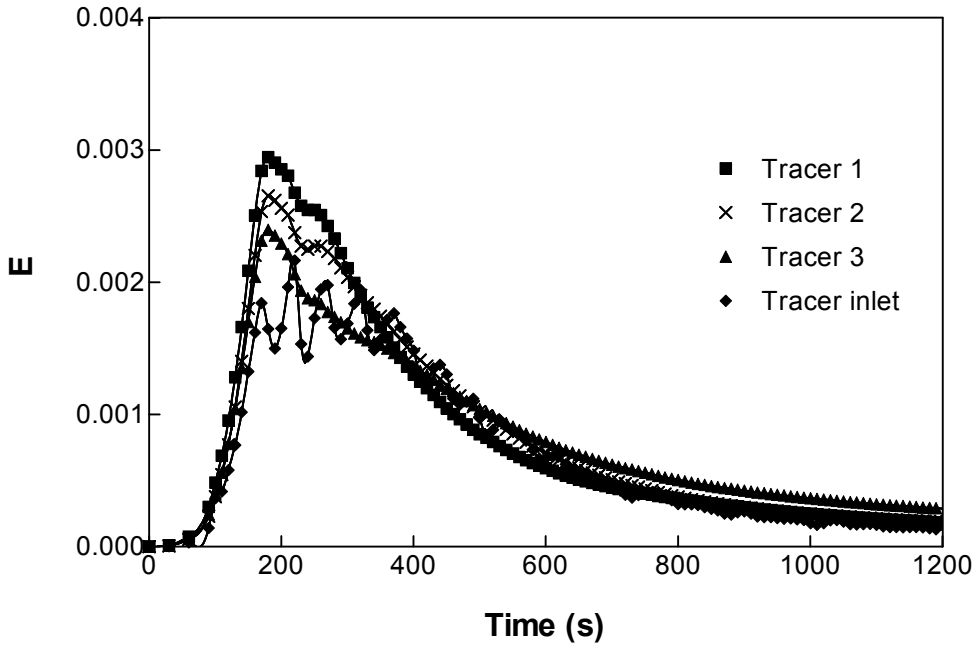

Figure 5.10 Effects of tracer injection location on tracer residence time distribution

5.4.5 Effects of Tracer Monitoring Point Selection on RTD and T_{10}

The effects of tracer monitoring points on tracer RTD tests were also studied. The concentration of chemical tracer was monitored at three points located at the contactor outlet. Figure 5.11 shows the location of the three monitoring points: Point 1 is 0.5m away from the side wall; point 3 is on the middle symmetric plane; and point 2 is located between points 1 and 2. Figure 5.12 presents the simulated tracer RTD curves for the three points. The RTD curve obtained from the numerical monitoring of mass flow averaged chemical tracer concentrations at the contactor outlet is also shown for comparison purposes. Significant differences in the tracer RTDs were observed at the three different tracer monitoring points. The T_{10} calculated from these RTD curves differed by more than

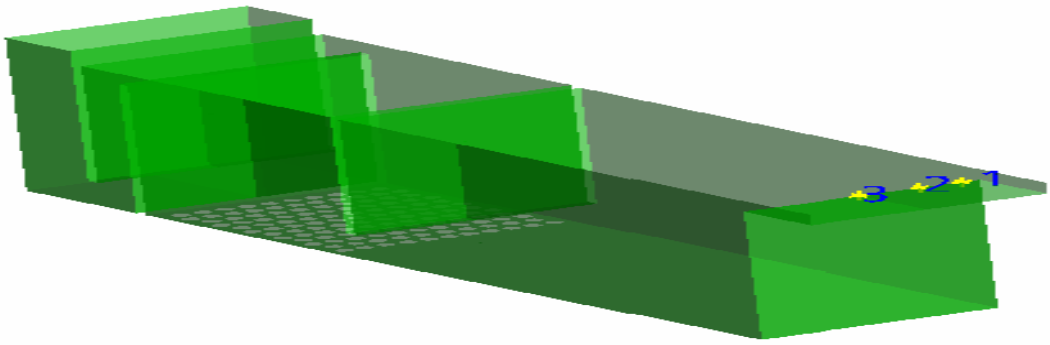

Figure 5.11 Three monitoring points for simulation of tracer residence time distribution

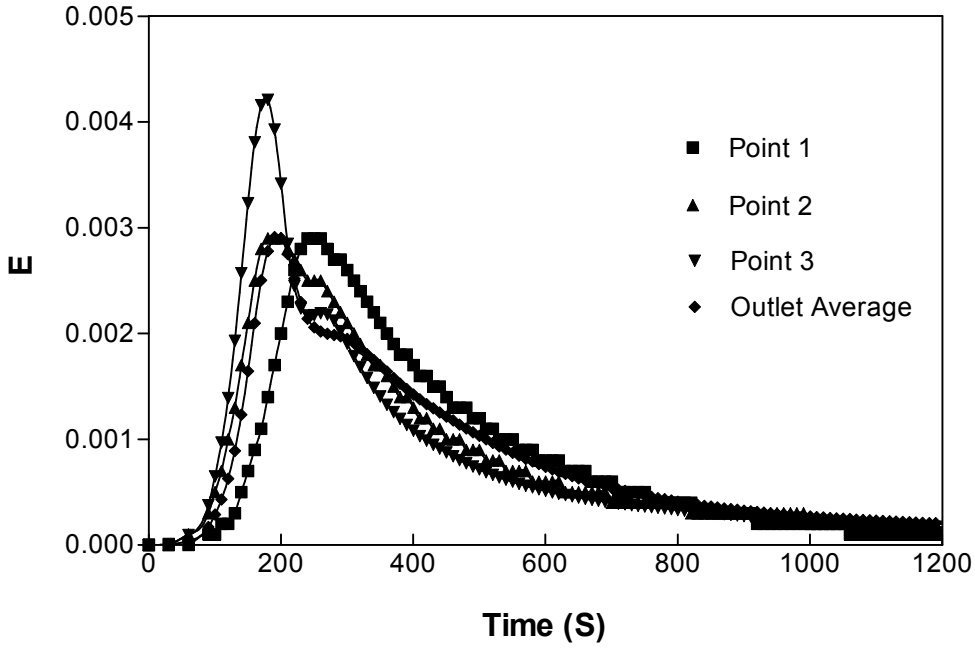

Figure 5.12 Effects of tracer monitoring points on residence time distribution

20% (T_{10} values of points 1, 2, 3 and outlet average were 145, 160, 172, 185 seconds respectively). Since the tracer RTD of monitoring point 2 was close to the average RTD curve, it might be more appropriate for the contactors studied. This result also suggested that more accurate tracer RTD and T_{10} information could be obtained if multiple monitoring points were used and the tracer RTD were calculated by averaging the measured tracer concentrations at different monitoring points.

5.5 Conclusions

This work evaluated a computional fluid dynamics (CFD) modeling approach for determination of CT values of full-scale ozone contactors. The most significant

contribution of this work was that, for the first time, a CFD model was applied to illustrate and improve an ozone residual monitoring strategy. For the DesBaillets ozone contactors, the CFD modelling results showed that ozone residuals in the cross section of the outlet of each cell differed by an order of magnitude. The variation of residuals was affected by multiple factors, including water/gas flow rate, temperature, baffling conditions, etc (Bellamy, 1995). Therefore, it was suggested that multiple ozone residual sampling points should be installed at the outlet of some ozone contactor chambers to provide more accurate indicators to system operators. Optimum locations and numbers of ozone sensors could be determined based on CFD modelling and experimental study. Ultimately, a guideline document could be developed for various basic contactor designs. The results also suggested that installing five monitoring points on the middle plane of certain cells (e.g. cell 1) or on a plane close to the side wall might over- or under-estimate the volume average ozone residual. A better prediction of the volume average residual could be obtained when the monitoring points are installed on a plane located 1.2 m away from middle plane. It is suggested that full-scale experimental studies should be done in future through the measurement of spatial distribution of ozone residuals inside ozone contactors to further validate the results of this study.

The CFD model was also used to study the factors affecting the residence time distribution (RTD). The results suggested that the selection of tracer injection locations as well as tracer sampling locations could affect the RTD prediction or measurement. The T_{10} values calculated from the CFD predicted that RTD curves at different outlet locations varied by more than 20% variation. It is therefore recommended that multiple sampling points be employed during tracer tests. In summary, the CFD approach is an efficient tool for improving measurement or prediction of CT values, and it can be used in various ways for operating and designing full-scale ozone disinfection systems.

CHAPTER 6 A COMPARISON OF EULERIAN AND PARTICLE TRACKING APPROACHES FOR PREDICTION OF OZONE CONTACTOR PERFORMANCE

6.1 Introduction

The use of an advanced modelling tool, computational fluid dynamics (CFD), to simulate the flow and reactions in drinking water disinfection reactor processes has attracted much attention in recent years (Greene, 2002). CFD modeling has been applied for the simulation of various disinfection processes, including chlorination, UV radiation and ozonation (Lyn et al., 1999; Do-Quang et al., 1999; Greene, 2002; Ta et al., 2004; Zhang et al., 2005). With a CFD modelling approach, the velocity field, residence time distribution (RTD), disinfectant profiles can be obtained by numerical solution of the Reynolds-averaged, Navier-Stokes and species transport equations (Greene, 2002; Zhang, 2005).

Some researchers (Do-Quang et al., 2002; Greene, 2002; Mofidi et al., 2004; Ducoste et al., 2005) also tried to use CFD modelling to predict the disinfection efficiencies. In general, two approaches were used to model microbial inactivation processes: one is the Eulerian approach and another is the Lagrangian approach (also called particle tracking approach). In the Eulerian approach, the spatial distribution of viable microorganisms in a reactor is viewed as a continuous field, similar to that of a

dissolved species (Greene, 2002). The concentration of microorganisms inside the reactor is expressed as a function of spatial coordinates and simulated by solving the species advection-diffusion transport equations with appropriate source terms (Lyn et al., 1999; Do-Quang et al., 1999). In a Lagrangian approach, microorganisms are viewed as discrete particles and the motion of individual microorganisms is independent of each other. The trajectory of each particle is calculated by solving the particles equations of motion, assuming a known turbulent fluid velocity field. The inactivation efficiencies of microorganisms are then determined by incorporating the particle trajectories with microbial inactivation kinetics information through the reactor (Downey et al., 1998; Chiu et al., 1999).

Several studies had been done to compare the Eulerian and Lagrangian approaches, in simulating UV dose for UV disinfection systems. Chiu et al. (1999), Do-Quang et al. (2002), and Mofidi et al. (2004) used an Eulerian approach to model UV reactors and their results show that the Eulerian approach slightly overpredicted the inactivation level. In contrast, the Lagrangian approach was applied by other researchers (Downey et al., 1998; Ducoste et al., 2005) and the results fit well with experimental data.

However, to-date, no studies have been reported to compare the two different approaches for modelling ozone disinfection systems. In this study, both the particle tracking and Eulerian approaches were used to evaluate ozone disinfection performance. The objective was to compare these two CFD approaches for modeling the tracer residence time distribution (RTD) and characterizing ozone disinfection performance.

6.2 CFD Modelling Methodology

6.2.1 Flow Equations

A two phase three dimensional CFD model has been developed to describe ozonation processes (Zhang et al., 2005). The hydrodynamics of ozone contactors were based on continuity and momentum balance equations for the two-phases: water and ozonated gas. The impact of turbulence on ozone contactor hydrodynamics was modeled in both phases. For the liquid phase, the standard k-ε model was used (Launder & Spalding 1974). The turbulence of the dispersed gas phase was modeled using a Dispersed Phase Zero Equation model and bubble induced turbulence was taken into account as per Sato and Sekogochi (1975).

To model ozone transport and associated reactions, ozone decomposition kinetics and mass transfer kinetics submodels were included in the form of species transport equations. The details of the species transport equations and the sink terms used to describe ozone decomposition and ozone transfer can be found in Chapter 4 and Zhang et al. (2005). The model was based on the following assumptions:

- Mass transfer resistance for ozone absorption was limited by the liquid side and was not enhanced by ozone reactions in the liquid phase (Singer and Hull, 2000)

- Henry's law applied (Beltran, 2004)

- The ozone decay rate in the liquid phase was pseudo first order, whereas it was negligible in the gas phase (Zhou et al., 1995)

-

- Bubble size was set as a constant (3 mm) based on literature reported ranges (Langlais et al., 1991; Wu, 2001)

- The free water surface of the contactor was treated as a free slip surface, which had been demonstrated to be reasonable by other researchers (Greene, 2002)

6.2.2 CFD-based CT

A common approach for determining ozone disinfection efficiency involves the application of a C×T concept (C is the ozone residual concentration in the contactor at time (T)) (USEPA, 1991). The CT concept for ozone systems is similar to the UV dose (intensity × residence time) concept currently used for evaluating UV disinfection performance (MWH, 2005)

When the CT concept is used to estimate full-scale ozone contactor disinfection performance, C is usually defined as the ozone residual concentration at the outlet of a chamber and T is the residence time of microorganisms in the chamber. For T, the USEPA employs a conservative residence time T_{10} which is the residence time of the earliest 10% of the microorganisms to travel from the contactor inlet to outlet, to ensure a minimum exposure time for 90% of the water and microorganisms entering a disinfection contactor (Chen, 1998; US EPA, 1991; Greene, 2002). Because of the existence of dead zones and short circuiting in full-scale ozone contactors, the microorganisms that enter the contactor at the same time may encounter significantly different pathways in the contactor. Therefore, using a single residence time T_{10} may result in inaccurate prediction of contactor hydraulic performance. In addition, ozone residuals may also vary substantially in a contactor, suggesting that a single ozone residual value will not be able to characterize ozone distribution within a given contactor. To accurately predict ozone disinfection efficiency, a CFD-based CT concept

was introduced in this study which was defined as the accumulated ozone exposure ($\int Cdt$) for all pathogens passing through an ozone reactor. This concept considerd three dimensional variations of ozone profiles inside ozone contactors and the differences in residence time of the microorganisms. Such a CFD-based CT value could be modelled by the Eulerian or Lagrangian approaches.

6.2.2.1 Eulerian Modelling Approach

With the Eulerian approach, ozone contactor hydraulic performance (represented by tracer residence time distribution) and disinfection efficiency (represented by CT) can be modelled by solving species transport equations:

$$\frac{\partial}{\partial t}(r_\alpha \rho_\alpha \phi_\alpha) + \nabla \bullet (r_\alpha U_\alpha \rho_\alpha \phi_\alpha) - \nabla (r_\alpha (\rho_\alpha D_\alpha^{(\phi)} + \frac{\mu_{t\alpha}}{Sc_{t\alpha}}) \nabla \phi_\alpha) = S_\alpha^{(\Phi)} \qquad (6.1)$$

where ϕ_α is the concentration of a species; r_α is the volume fraction of each phase; U_α is the flow velocity; ρ is the density of flow; ϕ_α is the conserved quantity per unit mass of phase α; $D_\alpha^{(\phi)}$ is the kinematic diffusivity for the species in phase α; $Sc_{t\alpha}$ is the turbulent Schmidt number; $S_\alpha^{(\Phi)}$ is the source term for a species transport equation.

To model a tracer residence time distribution (RTD) curve, the tracer was defined as a nonreacting species and a transient simulation was conducted. First, a steady state CFD simulation was performed to calculate the fluid velocity fields. The flow field obtained from the above simulation was then used as the initial condition when conducting unsteady state simulations to solve the tracer species transport equation. Since the tracer was non-reacting during transport, the source term of the species transport equation was

set as zero. The tracer residence time distributions were obtained by monitoring the average tracer concentration at outlets of ozone contactors.

A CFD-based CT was also predicted using an additional variable transport equation. The source term of the transport equation for CT is derived as follows:

When a parcel of liquid fluid flows from the inlet to the outlet of a contactor, a cumulative ozone exposure as a function of time is defined as:

$$CT \equiv \int_{t_{inlet}}^{t_{outlet}} C_{l,\,parcel}\, dt \tag{6.2}$$

It then follows that

$$\frac{D(CT)}{Dt} \equiv C_{l,parcel} \tag{6.3}$$

At any instance in the time of the parcel's travel from inlet to outlet, the total derivative $\frac{D(CT)}{Dt}$ is defined as:

$$\frac{D(CT)}{Dt} = \frac{\partial}{\partial t} CT + u_i \frac{\partial}{\partial x_i} CT \tag{6.4}$$

Combining the above two equations, multiplying the result by the liquid phase volume fraction r_l gives the transport equation for ozone exposure (CT). As with other additional variable equations, the effects of turbulent diffusion should also be included, thus the final form of the CT transport equation is given as:

$$\frac{\partial}{\partial t}(r_l CT) + \nabla \bullet (r_l U_l CT) - \nabla(r_l(\frac{\mu_{tl}}{\rho_l Sc})\nabla CT) = r_l C_l \quad (6.5)$$

As such, the source term for CT was defined as:

$$S_{CT} = r_l C_l \quad (6.6)$$

where r_l is the volume fraction of water. In most cases, r_l is close to 1, therefore:

$$S_{CT} = C_l \quad (6.7)$$

For a continuous flow system, the mass flow rate weighted average CT value at the outlet of a contactor was determined by:

$$\overline{CT}_{outlet} = \frac{\int CTdm}{\int dm} \quad (6.8)$$

where *m* is the local mass flow at the outlet of the contactor.

6.2.2.2 Particle Tracking Modelling Approach

In the Lagrangian approach, micro-organisms are treated as discrete particles where their trajectories are predicted by integrating the force balance on the particles. The trajectory of a single particle is calculated by solving particle equations of motion, assuming a known turbulent fluid velocity field. Particle concentration is estimated from the statistics of a large number of trajectories. This approach is applicable when the volume fraction of the dispersed phase (gas phase in this study) is small (James et al., 2003). The conservation equations of the model include:

Equations for calculating positions of particles:

$$x_i^n = x_i^o + v_{pi}^o \sigma t \tag{6.9}$$

$$v_p = v_f + (v_p^o - v_f)\exp(-\frac{\sigma t}{\tau})) + \tau F_{all}(1 - \exp(-\frac{\sigma t}{\tau})) \tag{6.10}$$

where the superscripts *o* and *n* refer to old and new values respectively, x_i is the position of a particle, σt is the time step and v_{pi} is the particle velocity.

Momentum transfer:

$$m_p \frac{dv_p}{dt} = F_D \tag{6.11}$$

In the above equation, F_D is the drag force acting on the particle. The drag force between flow and particles need to be considered in particle transport equations:

$$F_D = \frac{1}{2}\rho C_D A_F |U_s| U_s \tag{6.12}$$

where ρ is the density in the continuum, A_F is the effective particle cross section area, U_s is the slip velocity between the particle and the surrounding fluid and C_D is a drag coefficient.

C_D is defined by the Schiller Naumann Drag model (Schiller and Naumann, 1933):

$$C_D = \max(\frac{24}{\mathrm{Re}}(1 + 0.15\,\mathrm{Re}^{0.687}), 0.44) \tag{6.13}$$

The particle Reynolds number Re is defined by

$$\mathrm{Re} = \frac{\rho |U_s| d}{\mu} \tag{6.14}$$

where d is the particle diameter and μ is viscosity in the continuum.

In fluids, the random motion of fluid elements (eddies) imparts a continuous random motion to suspended particles. Repeated eddy interactions cause the particles to disperse over time. Therefore, the effect of turbulent dispersion should be included in the particle tracking model. The present work adopted the a classical stochastic approach of Gosman and Ioannides (1981) for the estimation of fluid velocities. It is assumed that a particle is always within a single turbulent eddy before entering another eddy. Each eddy has a characteristic fluctuating velocity $v_f^{'}$. When a particle enters an eddy, the fluctuating velocity for that eddy is added to the local mean fluid velocity to obtain the instantaneous fluid velocity used in Equations 6.10 and 6.11. The particle will stay in the eddy as long as the particle/eddy interaction time is less than the eddy lifetime τ_e and the displacement of the particle relative to the eddy is less than the eddy length l_e. Otherwise, the particle is assumed to be entering a new eddy with new characteristic $v_f^{'}$, τ_e, and l_e.

The characteristic fluctuating velocity $v_f^{'}$, the eddy lifetime τ_e and the eddy length l_e are calculated based on the following equations (James et al., 2003):

$$v_f^{'} = \Gamma (2k / 3)^{1/2} \tag{6.15}$$

$$l_e = \frac{C_\mu^{3/4} k^{3/2}}{\varepsilon} \tag{6.16}$$

$$\tau_e = l_e / (2k/3)^{1/2} \tag{6.17}$$

where k and ε are the local turbulent kinetic energy and dissipation, and C_μ is a turbulence constant. The variable Γ is a normally distributed random number which accounts for the randomness of turbulence about a mean value. A random number generator creates this distribution. Because of this randomness, each component of the fluctuating velocity may have a different value in each eddy.

The sizes of these neutrally discrete particles used in this study were between 1 μm and 100 μm, which were within the range of sizes of pathogenic protozoa in water (MWH, 2005). These particles were uniformly injected into the contactor from the inlet in a very short period time, 0.1 second. A statistically significant number of particles (10,000 in this study) were used to produce a particle-concentration independent particle tracking results (Ducoste et al., 2005). The residence time distribution curve could then be determined from data produced for the particles that leave through the outlet. The particle trajectories were obtained through a transient particle tracking solution. The ozone profile and particle tracking time of particle trajectories were then exported to a Microsoft Excel® file to calculate average CT value at the contactor outlet.

Since the particles were injected simulateously from the contactor inlet but exited the contactor outlet at different time and at different particle number rates, therefore the average CT was determined based on the particle residence time distribution curve. First, the CT on each particle trajectory was calculated by integration of ozone concentration and particle tracking times along the particle trajectory. Then, the average CT value at the outlet of a contactor was determined by the following equation:

$$\overline{CT}_{outlet} = \frac{\sum (CT)_i E_{pi} \Delta t}{\sum E_{pi} \Delta t} \qquad (6.18)$$

where $(CT)_i$ is the accumulated CT of *i*th particle trajectory, E_{pi} is the number rate of the particles that receive the ozone dose $(CT)_i$, Δt is the time period over which these particles exit the contactor outlet.

The procedures for calculating CT via Eulerian and Particle tracking approaches are summarized in Figure 6.1.

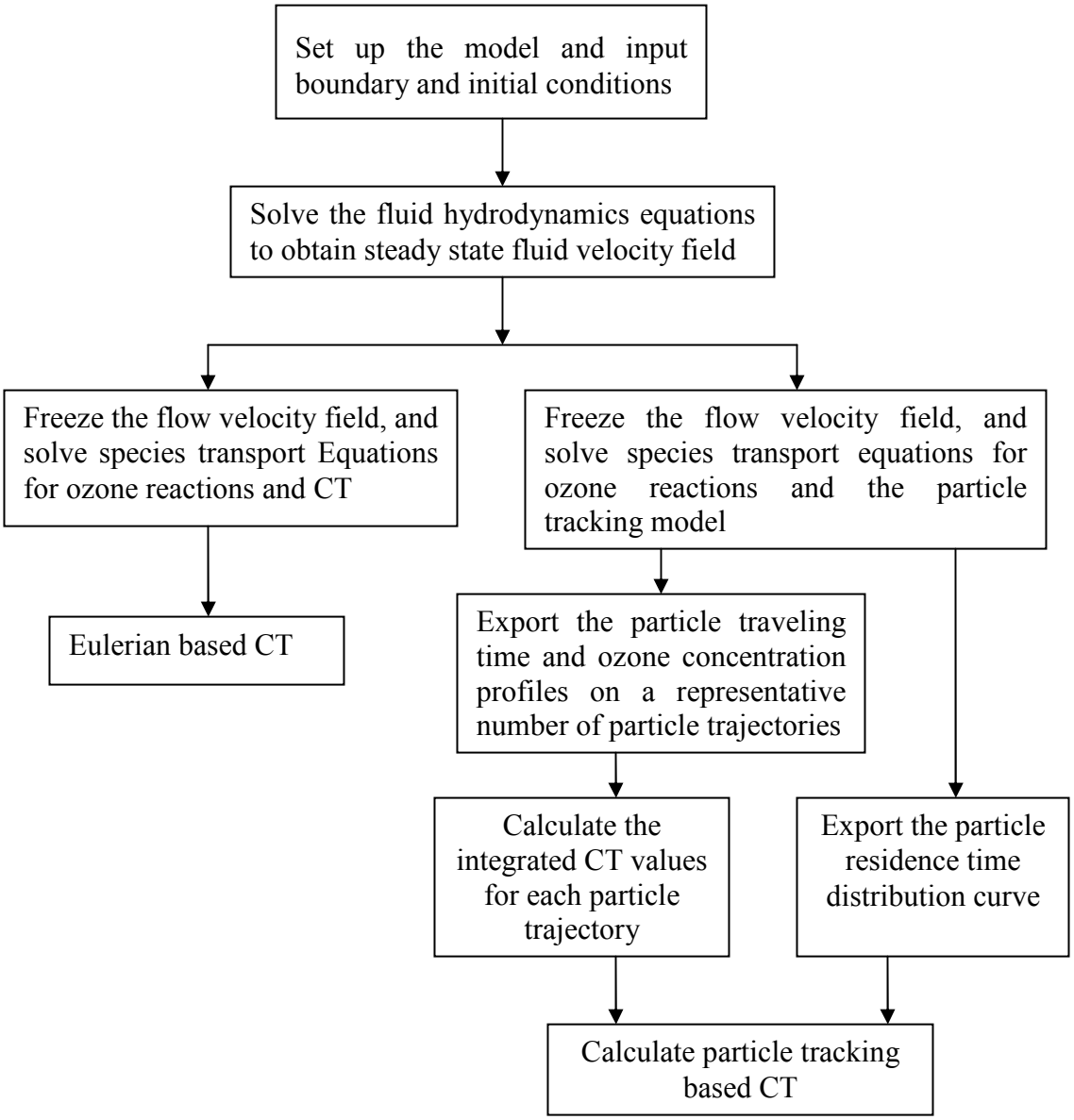

Figure 6.1 Procedures for predicting CT through Eulerian and Particle tracking approaches

A finite volume commercial CFD code CFX 10 (Ansys, 2005) was used. Presented in Table 6.1 is a summary of the comparisons between the Eulerian and Langragian approaches used in this study.

Table 6.1 A comparison of Eulerian approach *vs.* Lagrangian approach

Components	Eulerian Approach	Lagrangian Approach	Note
Model Description	The CT of an ozone contactor is obtained by solving species advection-diffusion model.	The CT is calculated based on particle trajectories, which are obtained by solving the particles equations of motion and momentum transfer	The Eulerian approach predict continuous fields of species, and Particle tracking model gives discrete solutions
Slip Velocity	0	$\neq 0$ unless the C_D is very big (∞)	
Turbulence Dispersion or Diffusion Model	Turbulent diffusion is based on concentration gradient with the turbulence time and length scales: $\tau_t \propto \frac{k}{\varepsilon}$ $l_t \propto \frac{k^{3/2}}{\varepsilon}$	Turbulent dispersion is based on stochastic approach. The turbulence time and length scales are: $\tau_e \propto \frac{k}{\varepsilon}$ $l_e \propto \frac{k^{3/2}}{\varepsilon}$	The turbulent time scales and length scales are in the same order.
Numeric Solutions	Second-order high resolution scheme (HRS) from control volume node to face	Second order pathline integration	Second order discretization schemes are used in both approaches
Average CT at contactor outlet	Mass flow rate weighted	Particle mass weighted	

6.3 Case Studies

6.3.1 Verification Case Study

Two hypothetical ozone reactors were used to examine the difference between the two CFD modelling approaches: Eulerian and particle tracking. Figure 6.2 presents the geometries of two reactors designed to emphasize differences and do not necessarily represent a particular type of ozone reactor. The tetrahedral-based mesh was adopted for CFD modelling and prism layers were applied to wall surfaces to resolve the effects of boundary layers. To reduce the computation time, a two dimensional (2D) simulation was done for the verification case study. The meshes were generated on one fine layer of the reactor geometries in the Z direction, and both sides of the layer were defined as the symmetric boundary conditions. All meshes were generated with a commercial meshing tool: CFX-Mesh (Ansys, 2005). The numbers of the mesh elements of the two reactors were 10,564 and 19,376 respectively. To simplify the analysis, the systems were assumed to be single phase reactors. Both dissolved ozone and influent water were assumed to enter into the systems from the reactor inlets. The inlet velocity of the water was set to be 0.186 m/s and the influent dissolved ozone was assumed to be 2 mg/L. The instantaneous ozone demand of influent water and ozone decay kinetics constant were set as 0 mg/L and 0.05 min^{-1}. These are reasonable values for ozone systems, and the overall conclusions would not be expected to be sensitive to the values chosen.

For the Eulerian approach, the flow conservation equations were solved under steady state conditions. The obtained flow fields were then “frozen” and the species transport equations corresponding to the dissolved ozone, chemical tracer, and CT were solved under transient conditions. In all the simulations, second-order discretization of the governing equations was applied and the simulations were considered to be converged

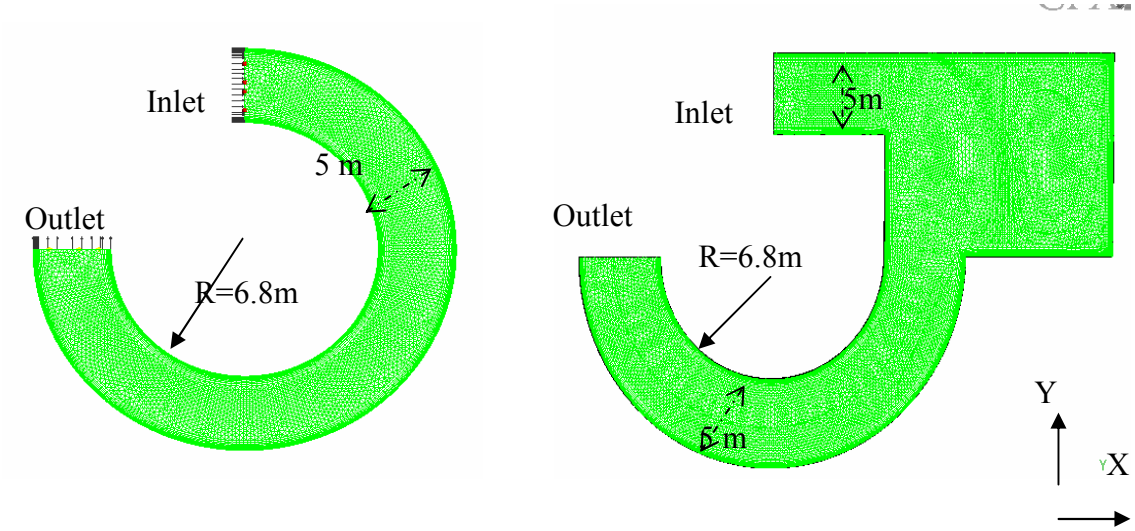

a) Ozone reactor 1 b) Ozone reactor 2

Figure 6.2 Geometries of two hypothetical ozone reactors

when the root mean square normalised residuals for all the equations were less than 10^{-4} and the global imbalance of each species was less than 0.1%.

For the particle tracking model, three different sizes of particles (1, 10, and 100 μm) were injected individually from the reactor inlets during a period of 0.1 second. By trial and error, the number of each type of injected particles was set as 10000. Further increase in the population of particles led to computational difficulties due to time or computer memory limitations. Although the model has the capacity to handle liquid, gas or solid phase "particles", the particles were defined as solid particles because the pathogens are solid. The particle tracking model was solved under transient conditions using a pre-determined fixed flow field. The data was then exported to an Excel® file to calculate CT values as described in Section 6.2.2.

6.3.2 Full-scale Ozone Contactor Study

A full-scale case study was performed for ozone contactors located at the DesBaillets Water Treatment Plant (WTP) in Montreal, Canada. The DesBaillets WTP has a capacity of 1,200 million litres per day (317 million gallons per day). The St. Lawrence River is used as source water. The raw water is treated by filtration and ozonation, followed by chlorination before entering the distribution system. The DesBaillets WTP has six parallel ozone contactors each with 2 cells and ozone gas is fed in the first cell of each contactor through 126 porous fine bubble diffusers. The total length, width, and height of each contactor are 23.8 m, 5.50 m and 7.16 m respectively. A three dimensional (3D) CFD model was developed. Figure 6.3 shows the geometry and mesh of a DesBaillets ozone contactor used in CFD modeling. Unstructured tetrahedral grids were used for the CFD modelling and were refined at areas close to the gas diffusers and baffles. The total element number was about 420,000.

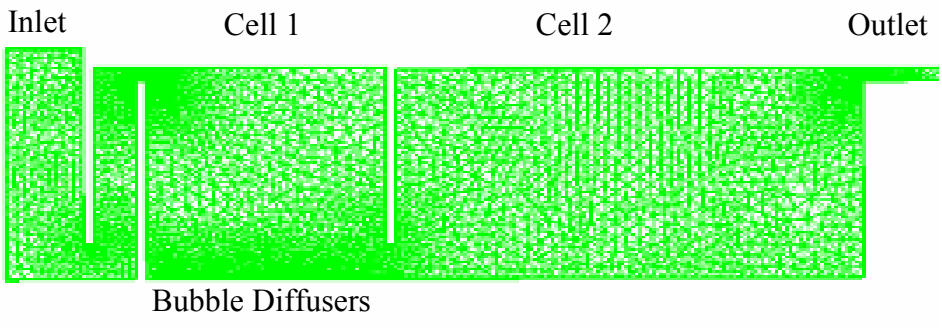

Figure 6.3 Mesh used for modelling of a DesBaillets WTP ozone contactor

The system was considered as a multiphase reactor. Based on the common range of the ozone system operational parameters in DesBaillet WTP, the inlet velocity of the water at the inlet was 0.186 m/s and the velocity of the gas at the diffuser surfaces was set at 0.022 m/s. The concentration of ozone in the gas by weight was 1.4 %. For both Eulerian and particle tracking approaches, the tracer residence time distributions and CT values of the ozone contactor were modeled using the same procedures as for modeling the hypothetical ozone reactors.

6.4 Results and Discussion

6.4.1 Results of Verification Case Study

A CFD model was applied to investigate the hydraulics of the two hypothetical ozone reactors. Figure 6.4 displays the velocity fields inside the two reactors. As expected, flow in reactor 1 was essentially uniform throughout the whole domain, while significant short-circuiting existed in reactor 2. A substantial dead zone could be observed in the rectangular segment of the reactor 2, which indicated that most of this rectangular segment can not provide effective contact time for microorganisms and disinfectant.

Similar phenomena were displayed by the particle tracking results shown in Figure 6.5. For reactor 1, particles passed smoothly from inlet to outlet without recirculation and shortcircuiting. For reactor 2, only a very small portion of the particles went into the "dead zone" and most particles passed through a short "passageway" as shown in the figure. Thus, reactor 1 was considered to be close to an ideal plug flow system, and reactor 2 represented a non-ideal system in which flow mixing was more complex, as in most full-scale ozone contactors.

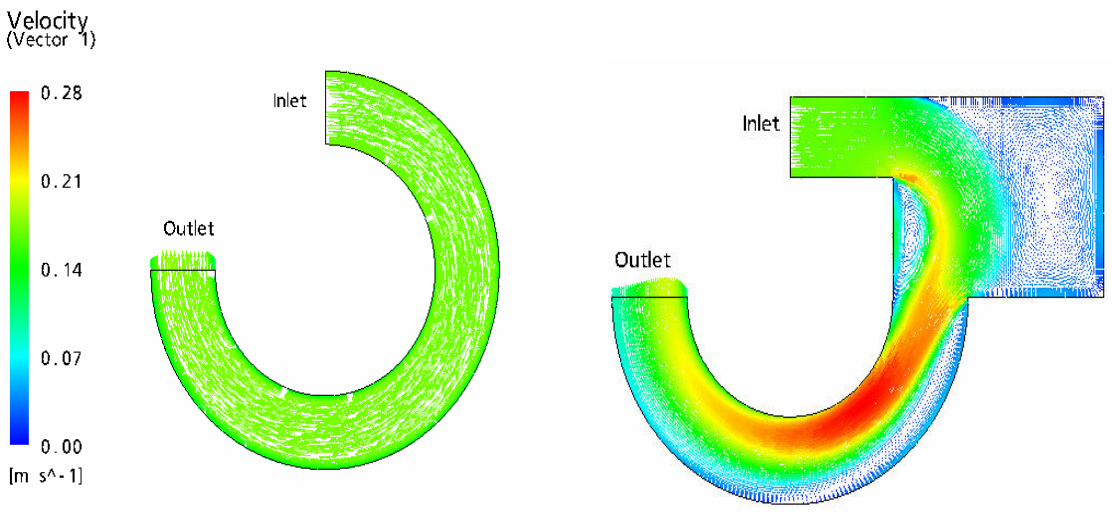

Figure 6.4 Flow velocity distributions in reactor 1 (left) and reactor 2 (right)

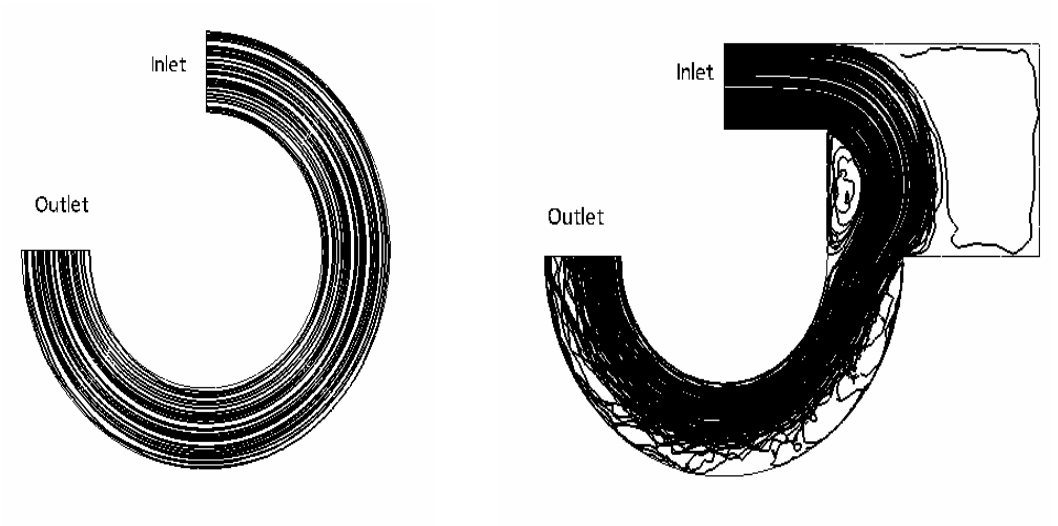

Figure 6.5 Particle trajectories in reactor 1 (left) and reactor 2 (right)

Using the methodologies described in Section 6.2, the CT value can be obtained either by solving a species transport equation (Eulerian approach) directly or by calculating it from particle tracking modeling results. Figure 6.6 shows the CFD simulated CT value distributions based on the Eulerian approach. Obviously, the flow field could significantly affect CT distributions. In reactor 1, CT increased smoothly from inlet to outlet. However, in reactor 2, much higher CT values were observed in the dead zone area compared with those in the short-circuiting zone, which was caused by the high residence time in the dead zone.

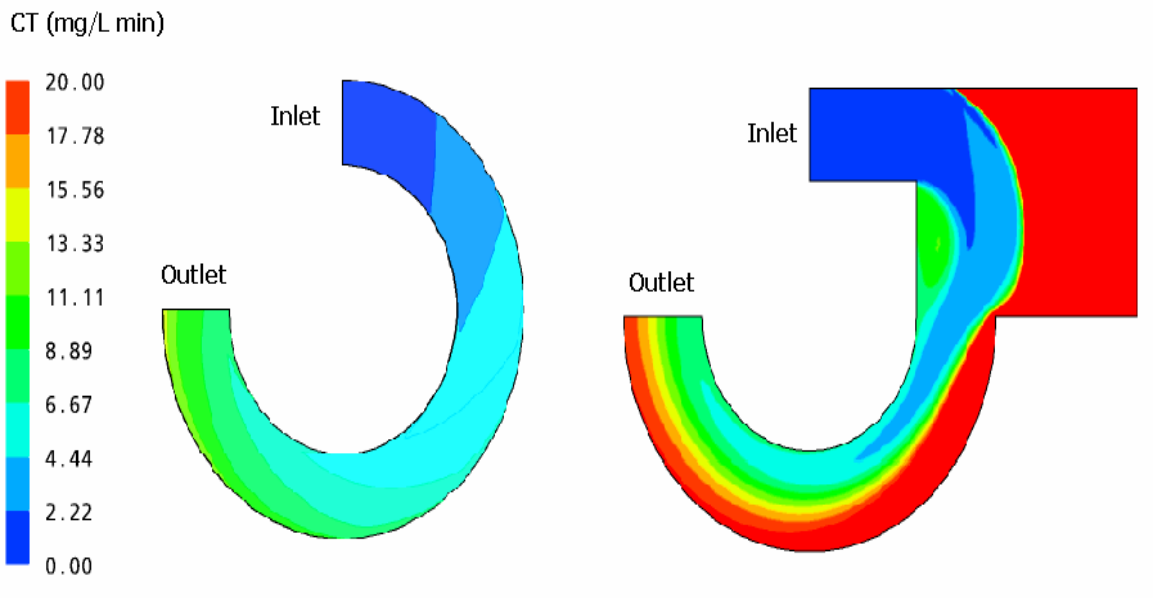

Figure 6.6 Eulerian CT distribution in reactor 1 (left) and reactor 2(right)

Figure 6.7 shows the velocity and Eulerian-based CT value profiles along the outlets of the Reactor 1 and 2. It can be observed that both the velocity and CT values were more uniformly distributed at the outlet of the reactor 1. However, they varied greatly from one to the other side at the outlet of the reactor 2 which was due to the existence of strong short-circuiting inside the reactor.

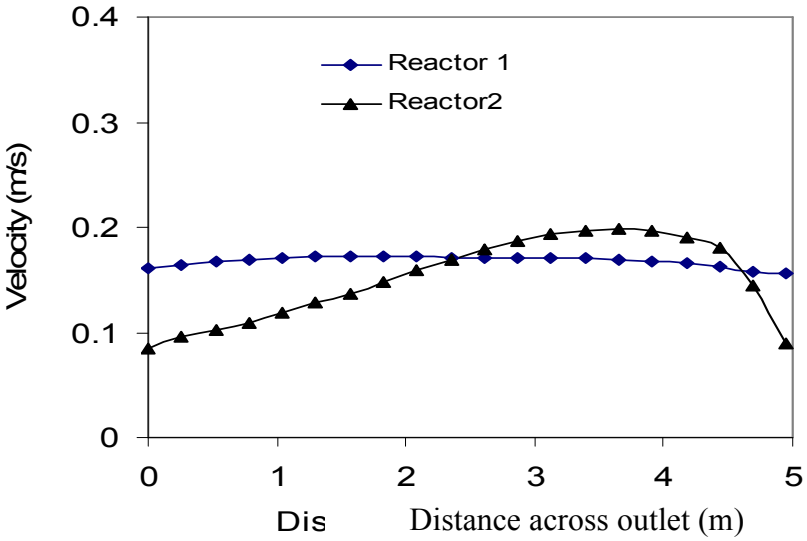

(a) Velocity distribution at outlets of reactors

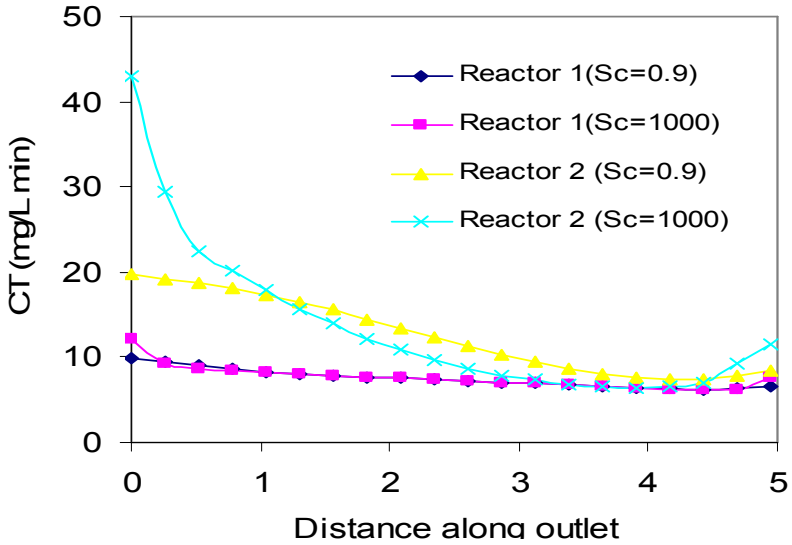

(b)

Figure 6.7 Distribution of velocity and Eulerian based CT at the outlet of the reactors 1 and 2 (*Sc* : Schmidt number)

Table 6.2 compares the results of CFD simulated CT values determined using the Eulerian and particle tracking approaches. It can be observed that the effects of the particle size (1, 10, and 100 μm) on CT prediction were negligible for both approaches. Since the size of the main target pathogens (*Cryptosporidium* and *Giardia*) for ozone disinfection treatment fell within the range of the simulated range (MWH, 2005), the above result suggests that an arbitrary particle size in the range of 1 to 100 μm could be chosen when the particle tracking model was used to simulate ozone disinfection performance.

Table 6.2 Comparison of CT values: Eulerian vs particle tracking

Case Study	Particle diameter (μm)	CT at outlet simulated by particle tracking (mg/L min)	CT at outlet simulated by Eulerian approach (mg/L min)	
			Sc =0.9	*Sc* =1000
Reactor 1	1	7.78	7.82	7.80
	10	7.76		
	100	7.76		
Reactor 2	1	10.84	11.67	11.33
	10	10.68		
	100	10.83		

The most important finding from the results in Table 6.2 was that, the CT values predicted by the two different approaches were very close for reactor 1 but differed slightly for reactor 2. The reason for the negligible difference for reactor 1 was due to the fact that the reactor 1 exhibited more ideal plug flow behavior and there was no short-circuiting or dead zones within the system. Therefore, the residence time (T) and ozone profiles (C) on particle trajectories can better represent those values in the main flow. Therefore both approaches could equally characterize the performance of this reactor.

For the reactor 2, the Eulerian approach based ozone exposure CT was slightly higher than the particle tracking based CT. The possible reasons for this might include: 1) in the particle tracking model, only limited number of particles (10,000) could be released from the reactor inlet due to the limitation of the computer power. Therefore, these particles might not be able to completely represent the particle trajectories of all the pathogens within the reactor 2; 2) only a relatively small number of particle trajectories (30 to 50) were used for calculation of CT due to the complexity of the data process procedures and limitation of computer power. These limited numbers of particles may not be sufficient to fully represent all the particles. For instance, the selected particle trajectories as shown in Figure 6.5 might not be able to represent the particles that could travel through the dead zone, and thus lead to underestimation of the CT values. It was expected that better CT prediction could be obtained using more particle trajectories for calculation.

Table 6.2 presents the effect of the Turbulent Schmidt number (Sc) on the Eulerian approach. The Schmidt number is a measure of the relative strength of turbulent viscosity and turbulent diffusion (Launder & Spalding, 1974). In most of the environmental flow, both turbulent viscosity and turbulent diffusion are important, therefore it usually should be close to 1 (Lakehal, 2002). As shown in Equation 6.5, when the Schmidt number is much lower than 1, the turbulent diffusion may be dominant during the CT transport process. When the Schmidt number Sc is much higher than 1, it means that turbulent diffusion is not important. In this study, the CT transport equation was simulated at two different Schmidt numbers: one was the default value 0.9 and another was 1000. The purpose of modeling CT at a larger Schmidt number (1000) was to "turn off" the turbulent diffusion term and therefore to investigate the effect of turbulent diffusion on the CT value prediction. Table 6.2 shows the modeling results at the two different different Schmidt numbers. It was found that the Schmidt number had a negligible effect on reactor 1 performance but did affect CT

predictions for reactor 2, although the impact was less than 10% over the range simulated. For reactor 2, even with a very high Schmidt number (1000), the Eulerian-based CT values were still slightly larger than the particle tracking-based CT values. Similar phenomena were observed by Chiu et al. (1999), Do-Quang et al. (2002), and Mofidi et al. (2004) in their UV disinfection modelling studies. Ducoste et al. (2005) explained that the main reason for the difference between the two approaches was that the pathogens in UV system were actually inactivated instead of being completely "killed" during the UV disinfection process. The Eulerian approach assumes that the particle concentrations are reduced after the pathogens are inactivated, thus, as Ducoste discussed, will result in a bigger concentration gradient in the diffusion term and may over-estimate disinfection efficiency. Based on their study, Ducoste et al.(2005) suggest that "turning off" the diffusion term may make the Eulerian approach fit better with the Lagrangian approach. However, this conclusion is doubtful, because: 1) the pathogens inside non-ideal reactors always exhibit a certain level of concentration gradient due to the existence of short-circuiting or dead zones. Therefore, it is inappropriate to completely shut off the diffusion term in the Eulerian approach; 2) it is also questionable to turn off the diffusion term in the Eulerian approach but use the dispersion model in the Lagrangian approach.

The results of this study however suggested that the main reason for the differences of the Eulerian and Particle tracking models was due to the limitations of the injected particle numbers and the particle tracking data processing procedures. It was expected that the particle tracking modeling results could fit better with Eulerian approach if sufficiently large number of particles were tracked and used for CT predictions.

6.4.2 Full-scale Ozone Contactor Study

The two CFD modeling approaches were also applied to simulate the hydraulics and CT of the ozone contactors in the Desbaillets Water Treatment Plant. Figure 6.8 displays typical particle trajectories inside the contactor. It was observed that large recirculation zones existed in the two cells and caused short-circuiting and dead zones. The existence of dead zones and short-circuiting might reduce the contacting opportunities between ozone and pathogens and make disinfection efficiency significantly less than it otherwise could be.

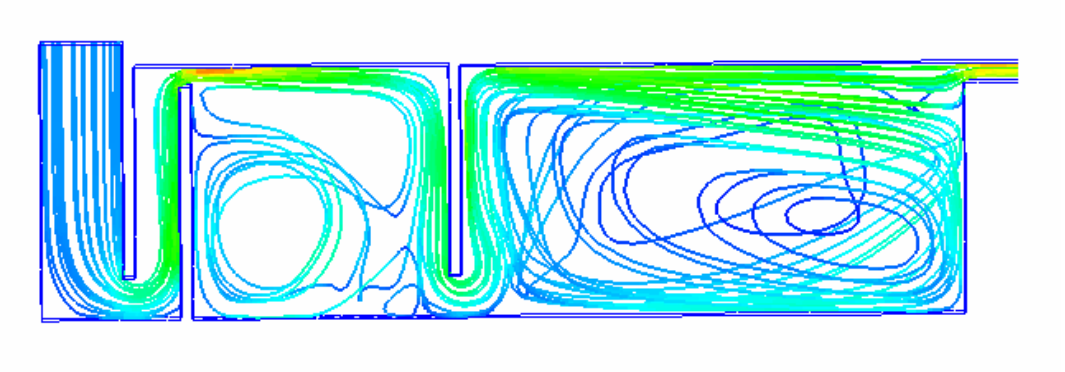

Figure 6.8 Particle trajectories of the Desbaillets ozone contactor

The effects of particle size on the prediction of flow hydraulics, represented by particle residence time distributions (RTDs), were studied for three particle sizes (1, 10, and 100 μm). Figure 6.9 shows that the effect of particle size was negligible with respect to particle RTD prediction.

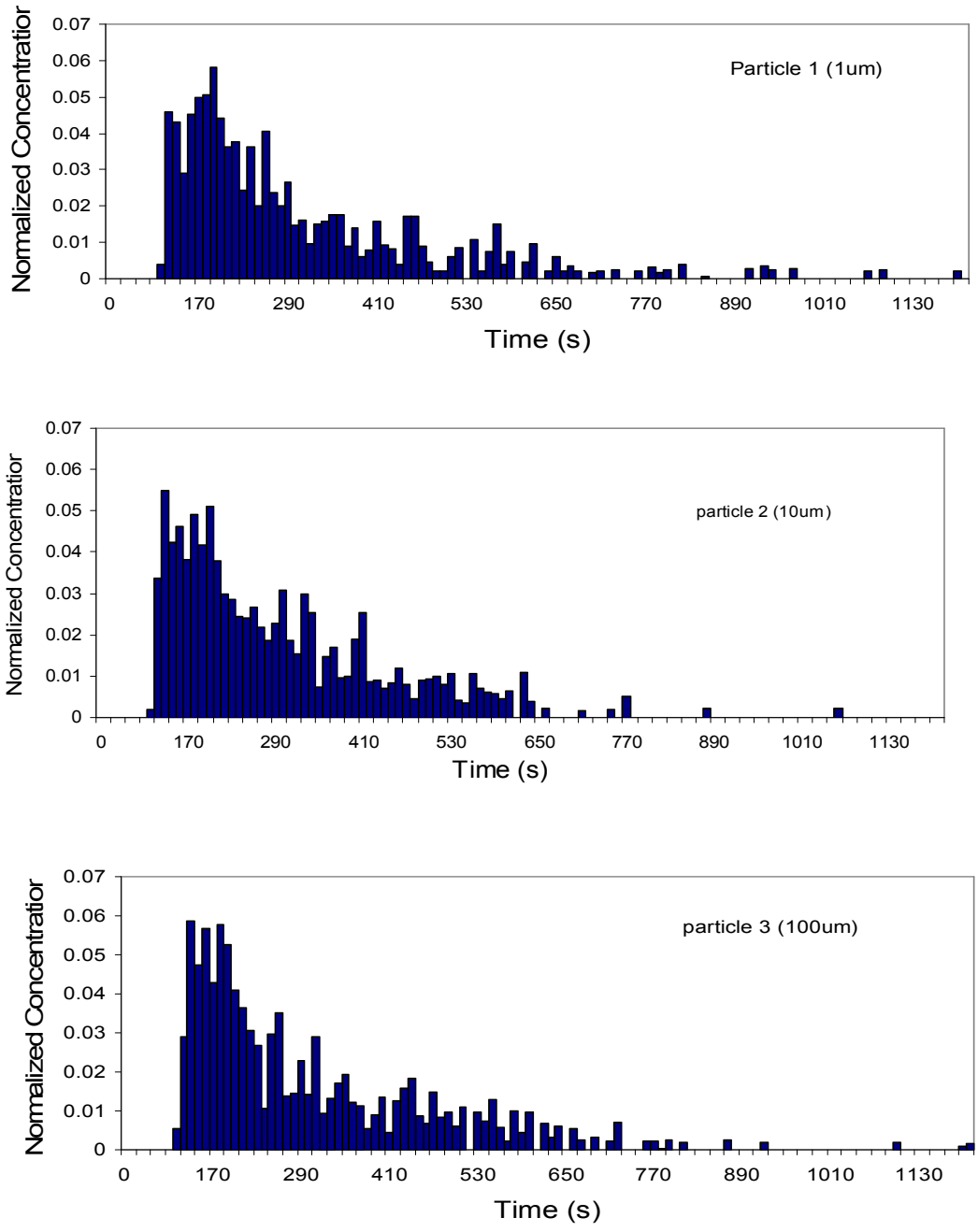

Figure 6.9 Effect of particle size on particle tracer residence time distribution

Figure 6.10 presents a comparison of the tracer RTD curves simulated by the Eulerian and particle tracking approaches. The Eulerian approach-based RTD results fit better with experimental data while the particle tracking method provided shorter residence time than the experimental values. The different tracer RTD predictions were also mainly caused by the limited numbers of particles used in particle tracking modelling. Since the particles passed the contactor in a discrete way, the particle tracking method might miss some important residence time distribution information, leading to an underestimation of the residence time. In the contrast, the Eulerian approach provided continuous tracer residence time information. The Eulerian approach also assumed that the tracer was a dissolved chemical species, which was usually the case for full-scale contactor hydraulics studies. It was therefore suggested that the Eulerian approach might be a better method for prediction of the chemical tracer residence time distribution and T_{10} values.

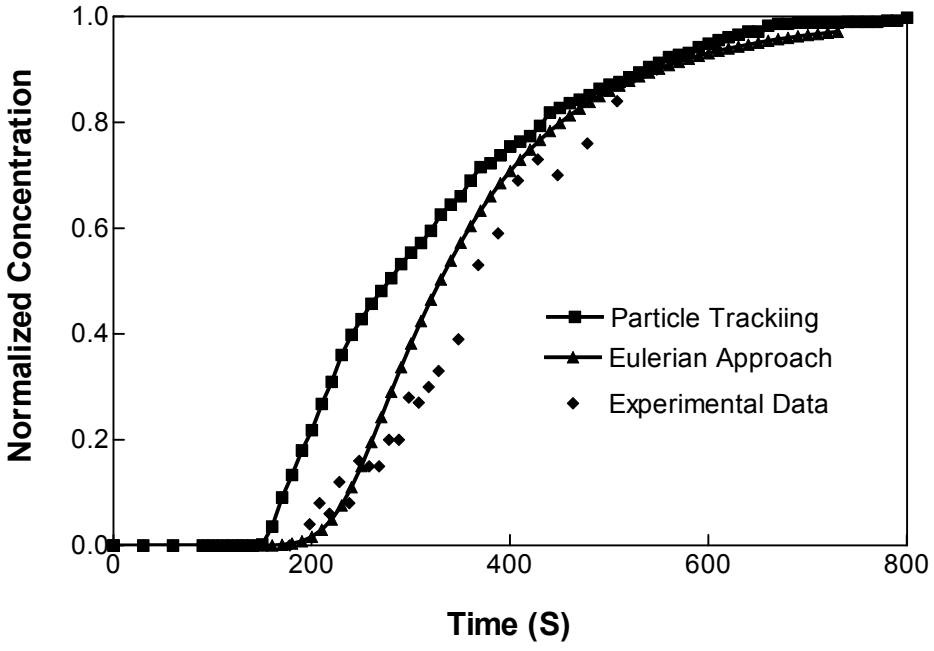

Figure 6.10 Comparison of tracer curves: particle tracking *vs*. Eulerian approach

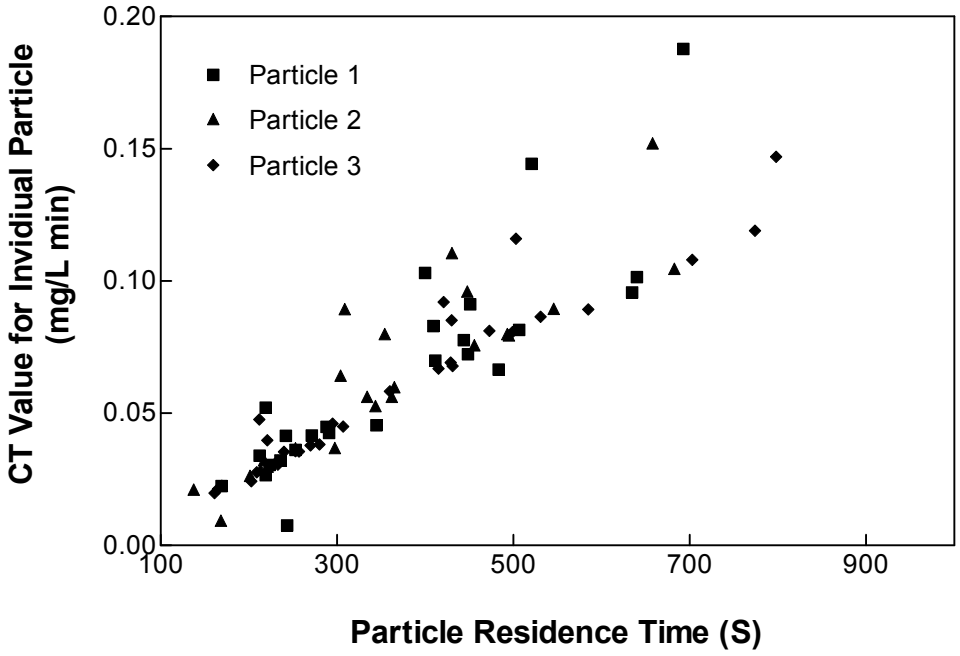

Figure 6.11 Particle tracking-based CT vs. particle residence time for the ozone contactor

Figure 6.11 presents the relationship between the particle tracking time and particle tracking based CT for individual particles in the ozone contactor. Generally, the two parameters had a linear relationship but with some variations. This was due to the existence of the strong recirculation zones inside the contactor, and particles might be exposed to different dosage even though when their particle tracking time is the same.

The CFD model was also used to estimate the CT values for the Desbailets WTP ozone contactor. Table 6.3 shows the average CT value at the contactor outlet calculated by the Eulerian and particle tracking approaches. Again it could be seen that the particle size had negligible effects on the particle tracking-based CT. The results also showed that the Eulerian approach-based CT was slightly higher than the particle tracking-based CT. This was consistent with the results of the verification case studies.

Table 6.3 also shows the Eulerian based CT values simulated at two different Schmidt numbers (0.9 and 1000). As with the comparison done for reactor 2, the Eulerian-based CT value was smaller at higher Schmidt numbers. However, even when the Schmidt number was set at an unreasonably high value of 1000 (when turbulent diffusion is negligible), the Eulerian-based CT value was still larger than particle tracking-based CT values.

Since the full-scale ozone contactors are non-ideal reactors, particles may have much more complex trajectories compared to that in an ideal reactor. Therefore, more accurate CT prediction results should be able to be obtained through particle tracking model using more powerful computers and tracking more particles.

Table 6.3 Comparison of CT values: Eulerian vs particle tracking

Case study	Particle diameter (μm)	CT at contactor outlet simulated by particle tracking (mg/L min)	CT at contactor outlet simulated by the Eulerian approach (mg/L min)	
			$Sc = 0.9$	$Sc = 1000$
BesBaillets WTP Ozone Contactor	1	0.92.		
	10	0.97	1.07	1.02
	100	0.88		

* Sc : Schmidt number

6.5 Conclusions

In the present study, the disinfection performance of two hypothetical ozone reactors and a full-scale contactor has been simulated using a computational fluid dynamics model. For the first time, the Eulerian and particle tracking approaches, two commonly utilized methods for study of the ozone disinfection process, have been compared. Several important conclusions can be drawn from the current results:

- For ozone reactors with plug flow characteristics, either approach could be used to evaluate contactor hydraulics and disinfection efficiency (CT value).

- For reactors with non-ideal hydraulic performance, the particle tracking model predicted slightly smaller CT than the Eulerian approach does. This was mainly due to the complex particle trajectories in the non-ideal reactors. To further improve the accuracy of the particle tracking modelling, it was suggested to use more powerful computers which allow tracking a larger number of the particles.

- For the full scale contactor investigated, the tracer residence time distribution curve predicted by the Euerlian approach provided a better fit to the experimental results, which indicated that the Eulerian approach might be more suitable for the simulation of chemical tracer performance.

- The effect of particle size (1 μm to 100 μm) used in this study on the particle tracking method was negligible.

- The results of this work provide important insight in understanding the complex performance of multiphase ozonation systems and may play an important role in further improving CFD modelling approaches for full-scale ozone disinfection

systems. Further investigation should be done to study the effects of model inputs on the two modelling approaches and to compare the two approaches for full-scale ozone contactors with different flow patterns.

CHAPTER 7 A COMPARISON BETWEEN CT_{10}, IDDF-BASED CT, AND CFD-BASED CT FOR EVALUATION OF DRINKING WATER OZONE DISINFECTION PERFORMANCE

7.1 Introduction

The concept of regulating disinfection treatment through CT, the product of the residual disinfectant concentration (C) and a characteristic time of pathogen exposure to the disinfectant (T), was introduced by the U.S. Environmental Protection Agency (USEPA) in the Surface Water Treatment Rule (SWTR) (USEPA, 1991). Using an appropriate CT calculation method to determine ozone dosage is important since low ozone dosages may not be able to provide sufficient credit for inactivation of pathogens and high dosages can lead to increased concentration of disinfection byproducts. The U.S. Environmental Protection Agency (EPA) published the Long-Term 2 Enhanced Surface Water Treatment Rule (LT2ESWTR) in January 2006 which included a new CT table for evaluation of log inactivation credit of Cryptosporidium by ozone (USEPA, 2006). These CT values are one order of magnitude higher than the values required for Giardia inactivation (Rakness, 2005). Therefore, it becomes more important to accurately calculate the CT of ozone systems to reduce capital and operating costs and minimize

the concentrations and therefore the associated risk of disinfection by-product in finished water.

Various methods have been proposed for calculation of the CT of ozone systems. The most commonly used is the CT_{10} methodology (USEPA, 1991), in which C is ozone residual concentration and the T_{10} is the length of time at which 90% of the water passing through the unit is retained within the basin or treatment unit (USEPA, 1991). This method is a simple way to evaluate disinfection efficiency. However, it has been well documented that the CT_{10} approach may result in under-estimation of the disinfection efficiency (Bellamy et al., 1998; Greene, 2002; Carlson et al. 2001; Zhang et al., 2005).

Alternatively, the Integrated Disinfection Design Framework (IDDF) (Bellamy, 2000) and computational fluid dynamics (CFD) approaches (Murrer et al., 1995; Do-Quang et al., 1999; Huang, 2002; Zhang et al., 2005) have been studied for evaluating full-scale ozone disinfection systems. Both approaches incorporate all the major components of ozone disinfection processes within the models although the two approaches have fundamental differences.

Limited studies had been previously done to compare the different CT approaches. Barbeau et al. (2003) compared the IDDF approach with the CT_{10} method and found that the CT values calculated by the IDDF are usually about 2 times higher than those determined by the traditional CT_{10} method. Greene et al. (2004) performed a study to compare the IDDF approach with a CFD modelling approach in predicting disinfection efficiencies of a pilot scale chlorination reactor consisting of long channels. Their results show that the CFD-predicted disinfection efficiencies fit better with experimental results. However, to date, no studies have been reported to compare the

CFD design approaches with CT_{10} and IDDF methods for either pilot-scale or full-scale ozonation systems.

The objective of this study was to perform a full-scale assessment to compare the above three disinfection design approaches. To be consistent with the current CT-table based regulations (USEPA, 2006), the three approaches were compared based on their prediction of CT values which are used to represent the disinfection efficiencies of ozone disinfection processes. The comparison was done based on the study of a full-scale ozone contactor at the DesBaillet Water Treatment Plant (WTP) in Montreal, Canada. In addition, the CT values obtained by three approaches were compared with bioassay test results conducted by Broséus et al. (2005) to determine the most appropriate method for design and operation of full-scale ozone systems.

7.2 Case Study

The DesBaillets Water Treatment Plant (WTP) has a capacity of 1,136 million litres per day (MLD) and it is the largest facility in the province of Quebec and the second largest water treatment plant in Canada. The St. Lawrence River is used as a source for the production of drinking water. Due to good raw water quality of the source water, a relatively simple treatment is used, including direct sand filtration without coagulant, post-ozonation, and chlorination.

The WTP ozonation process has six parallel ozone contactors. The total length and depth of each contactor are 11 m and 6.5 m respectively. Each contactor consists of two large cells in series. The first cell is operated in the counter-current mode, and the second cell is co-current. Ozone gas (1-2% by weight in air) is injected through porous media bubble diffusers located at the bottom of the first cell (Broséus et al., 2005). All the contactors have the same geometry and operational characteristic parameters

therefore, only one was studied. Figure 7.1 shows the schematic drawing of the contactor.

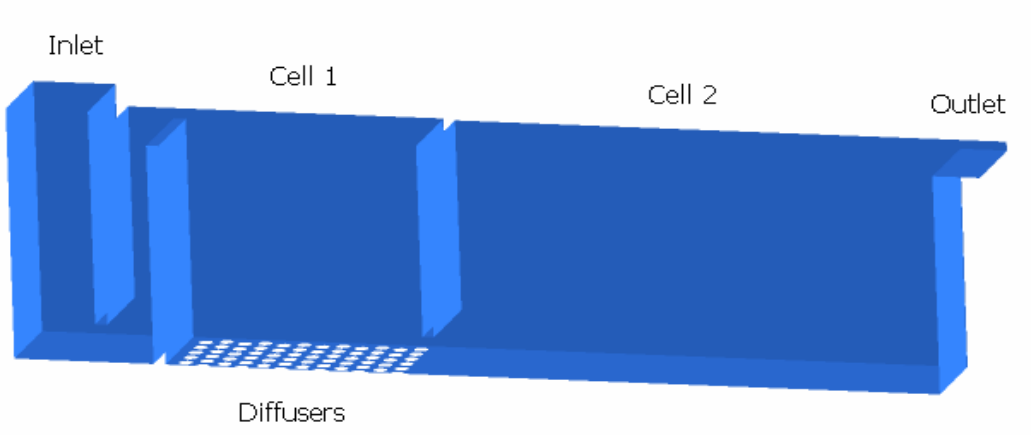

Figure 7.1 Schematic drawing of a DesBaillets WTP ozone contactor

7.3 Theoretical Background and Methodologies

The CT concept was originally based on the assumption that the inactivation kinetics of pathogens follows the Chick-Watson model (MWH, 2005). For ozone systems, this model can be expressed as:

$$\frac{d[N]}{dt} = -k_p[N]\cdot[O_3] \qquad (7.1)$$

where *[N]* is the pathogen concentration, $[O_3]$ is ozone residual concentration and k_p is the pathogen inactivation rate constant.

Equation 7.1 can be integrated to the following form:

$$\log \frac{[N]}{[N_0]} = -0.4343 \times k_p \int [O_3] dt \tag{7.2}$$

Equation 7.2 indicates that the log inactivation is determined by the inactivation rate constant, the ozone concentration, and the pathogen inactivation reaction time.

The term $\int [O_3] dt$ in Equation 7.2 is often called the ozone-exposure, or ozone *CT* value, as it is the integral form of the ozone residual concentration times time:

$$\log \frac{[N]}{[N_0]} = -0.4343 \times k_p \times CT \tag{7.3}$$

The CT tables published by USEPA for various pathogens were based on the model shown in Equation 7.3 and the CT requirements in the table were determined by performing a statistical analysis of literature data related to pathogen inactivation by the disinfectants under various conditions (Crozes, 1999). Since most of the literature data were based on completely mixed batch reactor studies in which the ozone residuals and residence times are constant, the CT table can accurately relate CT to the log inactivation ratio of pathogens. For full-scale ozone contactors, however, estimation of the CT value can be accomplished in different ways. Three different CT calculation methods for the characterization of the ozone contactor performance are discussed in this thesis as follows.

7.3.1 CT_{10}

For multiple chamber ozone contactors, an integrated CT_{10} approach is commonly adopted to calculate the CT_{10} values (Rakness, 2005). The total CT of the ozone contactor is determined by summing up the CT values of all individual chambers using the following equation:

$$CT_{10} = \sum C_i T_{10i} \tag{7.4}$$

where i is the number of ozone cells (or chambers), T_{10i} is derived from tracer tests. C_i is the ozone residual concentration at the outlet of each cell (mg/L). The ozone residual (''*C*'' in the CT product) is the ozone concentration at the exit of a chamber.

The DesBaillets contactor consists of two cells. All the diffusers are located at the bottom of cell 1, therefore cell 1 is called the dissolution cell and cell 2 is called the reactive cell. Based on the drinking water regulations in the province of Quebec, Canada (MENV 2002, Broséus et al. 2005), the following expression is used for calculation of the CT_{10} for porous diffuser ozone contactors with counter-current dissolution:

$$CT_{10} = \frac{C_{res}}{2} \times \frac{T_{10}}{T} \times T_1 + \sum_i C_{res\ i} \times \frac{T_{10}}{T} \times T_i \tag{7.5}$$

where C_{res} is the ozone residual in the first cell, T_{10} is the time of 10% of a tracer to have appeared in the effluent and T is the total theoretical retention time in the contactor, T_i is the theoretical retention time of the cell i, and $C_{res\ i}$ is the ozone residual of cell i.

7.3.2 IDDF-based CT

The Integrated Disinfection Design Framework (IDDF) is an alternative approach for designing ozonation processes (Bellamy et al., 1998; Carlson et al., 2000). The IDDF approach assumes that the flows in ozone contactors are segregated. Each discrete element of incoming fluid is assumed to take a different route and a different length of time to pass through the vessel. The IDDF approach incorporates four components in one model, including a contactor hydraulic module, disinfectant decay kinetics module, pathogen inactivation module and a DBP formation module (Bellamy et al. 1998; Carlson et al. 2001; Ducoste et al. 2001; Rakness 2001). The original IDDF approach utilizes mathematical relationships for each of the components (Bellamy et al. 1998). The integrated model can be solved with a complex integral (Bellamy, 2000). Carlson et al. (2001) further developed the IDDF approach by introducing an IDDF spreadsheet method, which allows the use of a tracer-test RTD directly as an input to the hydraulics module.

The purpose of the present study was to compare the IDDF approach with other CT calculation methods. Therefore, the pathogen inactivation module were not integrated in the CT calculation. CTs were calculated by incorporating a tracer E curve, obtained from tracer tests or CFD simulation, and the ozone residual profile calculated based on the first-order decay kinetic model.

$$CT_i = \sum_{j=0}^{\infty} E_j C_j \Delta t_j = \sum_{j=0}^{\infty} E_j \Delta t_j [C_o \exp(-k_d t_j)] \tag{7.6}$$

where, i is the number of the cell of contactor, j is the integration step number; C_o is the influent disinfectant concentration, C_j is the residual ozone concentration calculated by assuming that ozone decay follows first-order kinetics as discussed in Chapter 4, k_d is

the ozone decay kinetic constant, Δt_j is the time step, E_j is the normalized tracer concentration at time step *j* on a tracer E curve (Levenspiel 1999).

As described above, the DesBaillets WTP ozone contactor has two cells. In this study, the IDDF-based CT of each cell was predicted through integration of tracer residence time distribution curves and ozone profiles along the cell. The tracer RTD curves were obtained from CFD modelling. The ozone profile was determined by the ozone decay kinetics obtained from an experimental study done by the École Polytechnique de Montréal. It was assumed that, ozone residuals in cell 1 increased linearly until reaching the average concentration at the outlet of cell 1, and the ozone profiles in cell 2 were simulated based on a first-order decay kinetics (Benbeau et al., 2003; Broséus et al., 2005). All the calculations were performed using a Microsoft Excel tabular format. A similar IDDF-based CT calculation method was used by Benbue et al. (2003).

7.3.3 CFD-based CT

A two phase, three dimensional, CFD model has been developed to describe ozonation processes (Chapter 4 of this thesis and Zhang et al., 2005). The hydrodynamic behaviour of ozone contactors was modelled based on continuity and momentum balance equations for the two-phases: water and ozonated gas (Versteeg and Malalasekera, 1995; Podowski, 2003). For the liquid phase, the standard k-ε model was used (Launder and Spalding 1974). The turbulence of the dispersed gas phase was modeled using a Dispersed Phase Zero Equation model. Bubble induced turbulence was taken into account as per Sato and Sekogochi (1975). To model ozone transport and associated reactions, ozone decomposition kinetics and mass transfer kinetics sub-models were included in the form of species transport equations. The details of the species transport equations and the sink terms used to describe ozone decomposition and ozone transfer can be found in Chapter 4.

The results in Chapter 6 of this thesis showed that both the Eulerian and particle tracking approaches could be used for quantification of microbial disinfection efficiency of full-scale ozone contactors. Since the Eulerian approach is easier to implement and is computationally economic, it was used in this study for predicting CFD-based CT. A finite volume commercial CFD code CFX 10 (Ansys, 2005) was used. The additional variable transport equation for solving the CFD-based CT is as follows:

$$\frac{\partial}{\partial t}(r_l CT) + \nabla \bullet (r_l U_l CT) - \nabla(r_l(\frac{\mu_{tl}}{\rho_l Sc_{tl}})\nabla CT) = S_{CT} \tag{7.7}$$

where r_l is volume fraction of water, u_l is the water flow velocity; ρ_l is the density of flow; $Sc_{t\alpha}$ is the turbulent Schmidt number.

The source term S_{CT} was defined as:

$$S_{CT} = r_l C_l \tag{7.8}$$

where C_l is the dissolved ozone concentration

7.3.4 Bioassy-based CT

To validate the CT calculation methods and determine the best approach for predicting ozone contactor disinfection performance, bioassays were conducted by the Ecole Polytechnique de Montréal (Broséus et al., 2005) using indigenous aerobic spore-formers as a biodosimetric tracer. Indigenous aerobic spore formers (ASF) are usually abundant in surface waters and resistant to ozone (Nieminski et al. 2000; Facile et al.

2000; Craik et al. 2002). They also typically exhibit a linear inactivation with respect to CT. Therefore, it is possible to use the ASF to validate the CT of full-scale ozone contactors (Broséus et al., 2005).

The bioassay-based CT was obtained by conducting pilot-scale and full-scale tests. First, experiments were performed on a continuous-flow ozone pilot system to obtain the correlation between the microbial inactivation and effective CT. The ASF was injected into the inlet of the pilot ozone contactor at different ozone dosages. At each dosage condition, the ASF concentrations at inlet and outlet, ozone concentration profiles and the residence times were measured. Thus a reference CT curve could be generated for describing the inactivation ratio and effective CT. Second, the ASF concentrations at the full-scale ozone contactor inlet and outlet at the DesBaillets WTP were measured. By measuring the ASF inactivation ratio during full-scale validations, it was possible to link it to the CT measured in the pilot contactor (Broséus et al., 2005). The detailed experimental method can be found in Broséus et al. (2005). This validation process is similar to the bioassay tests for validation of UV reactors using reference curves developed with MS2 phages (USEPA 2003).

7.4 Results

In Chapter 4, the CFD model was validated using tracer experimental data and monitored ozone profiles. In this Chapter, CFD-based CT values under varying conditions, as shown in Table 7.1, were simulated using the validated model. These modelling conditions are the same as the operational conditions for the bioassay tests conducted by the Ecole Polytechnique de Montréal (Broséus et al., 2005)

7.4.1 Comparison of CT_{10}, IDDF-based CT, CFD-based CT and Bioassy-based CT

The CT values at the above four operational conditions (see Table 7.1) were modelled

Table 7.1 Summary of the modeling conditions for comparison of different CT calculation methods

	Gas flow rate (Nm^3/s)	Ozone dose (mg/L)	Immediate O_3 demand (mg/L)	O_3 decay kinetic constant (min^{-1})	O_3/air (% by wt)
Run 1	0.15	0.98	0.45	0.11	1.16
Run 2	0.20	1.46	0.67	0.08	1.30
Run 3	0.25	1.83	0.84	0.06	1.30
Run 4	0.30	2.03	0.94	0.05	1.22

using the CFD, CT_{10}, and IDDF approaches and also compared with the bioassay-based CT. Figure 7.2 presents the comparison results of the four CT prediction methods under various operating conditions. The results showed that, among the three CT prediction methods, the CFD-based CT values fitted best with the bioassay-based CT values obtained from bioassay experiments.

Figure 7.2 also showed that the CT_{10} method gave the lowest prediction of CT. In all the conditions, the CT_{10} values were lower than the bioassay-based CT values. At higher ozone dose conditions, the bioassay-based CT values could be 1.0 to 1.5 times higher than the CT_{10} values. This indicated that the traditional CT_{10} method may

significantly underestimate disinfection efficiency which may lead to over-dosing of ozone and an excessive production of disinfection by-products, such as bromate.

It was also found that, at current modelling conditions, the IDDF-based CT values were higher than the CFD-based CT values and the bioassay-based CT values. This suggested that the IDDF-based CT may over-estimate the CT for the Desbaillet ozone contactors and the CFD approach may be a better option for evaluating Desbaillet WTP ozone disinfection treatment performance.

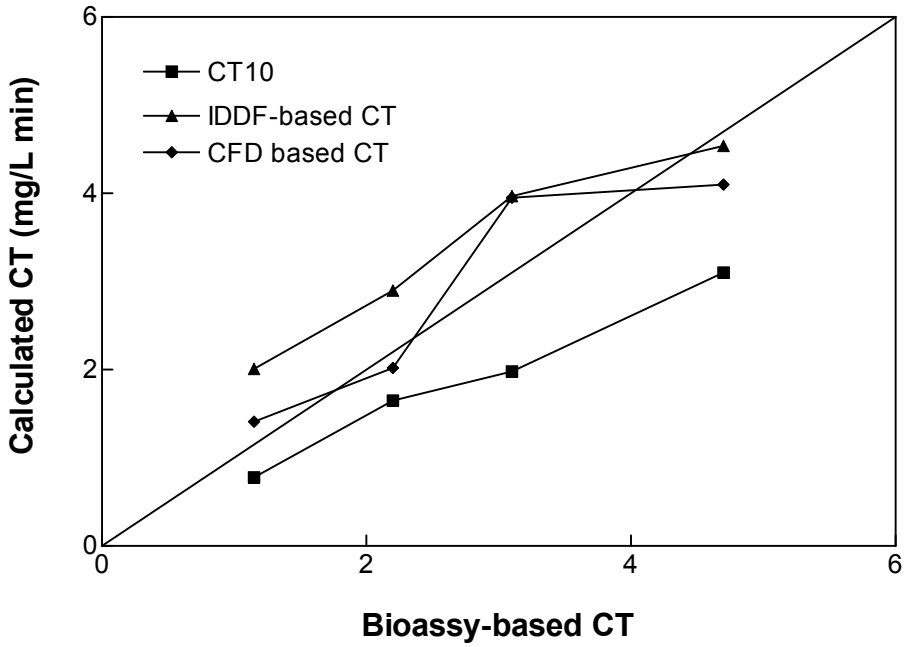

Figure 7.2 Comparison of the four CT prediction methods under various operating conditions

7.4.2 Comparison of Three Approaches for Alternative Contactor Configurations

Considering the fact that the DesBaillets WTP ozone contactor had only two chambers which exhibited relatively poor mixing behaviours, two additional comparisons were conducted at alternative contactor configurations as shown in Figure 7.3. The case 1 configuration included 4 additional baffles in the cell 1 of the original ozone contactor and the case 2 configuration had 6 additional chambers in the contactor. The purpose of modelling these two additional cases was to study the effect of contactor hydraulics on the different CT methods.

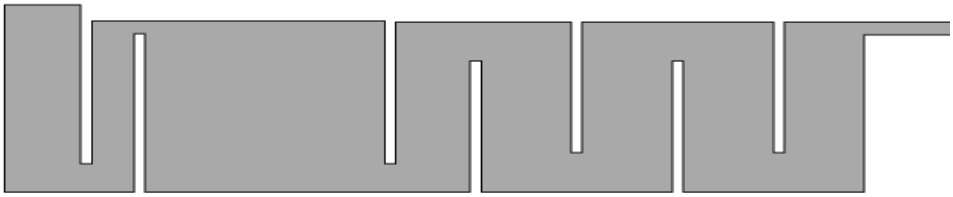

(a) Alternative contactor configuration: Case 1

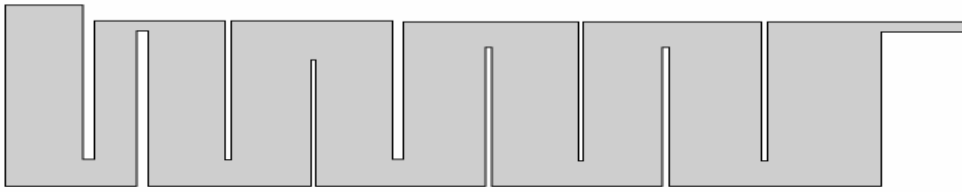

(b) Alternative contactor configuration: Case 2

Figure 7.3 Two alternative contactor configurations for studying the CT approaches

Figure 7.4 and Figure 7.5 present the comparison of the flow fields and the tracer residence time (RTD) curves inside the contactor configurations. Obviously, the case 2 scenario provided best mixing performance. In contrast to the strong recirculation and shot-circuiting existed in the original contactor, the case 2 contactor had the most uniform flow field and minimum short-circuiting and dead zones. It was therefore closer to plug flow. The T_{10}/T ratio of the original contactor and cases 1 and 2 were 0.55, 0.78, and 0.82, respectively.

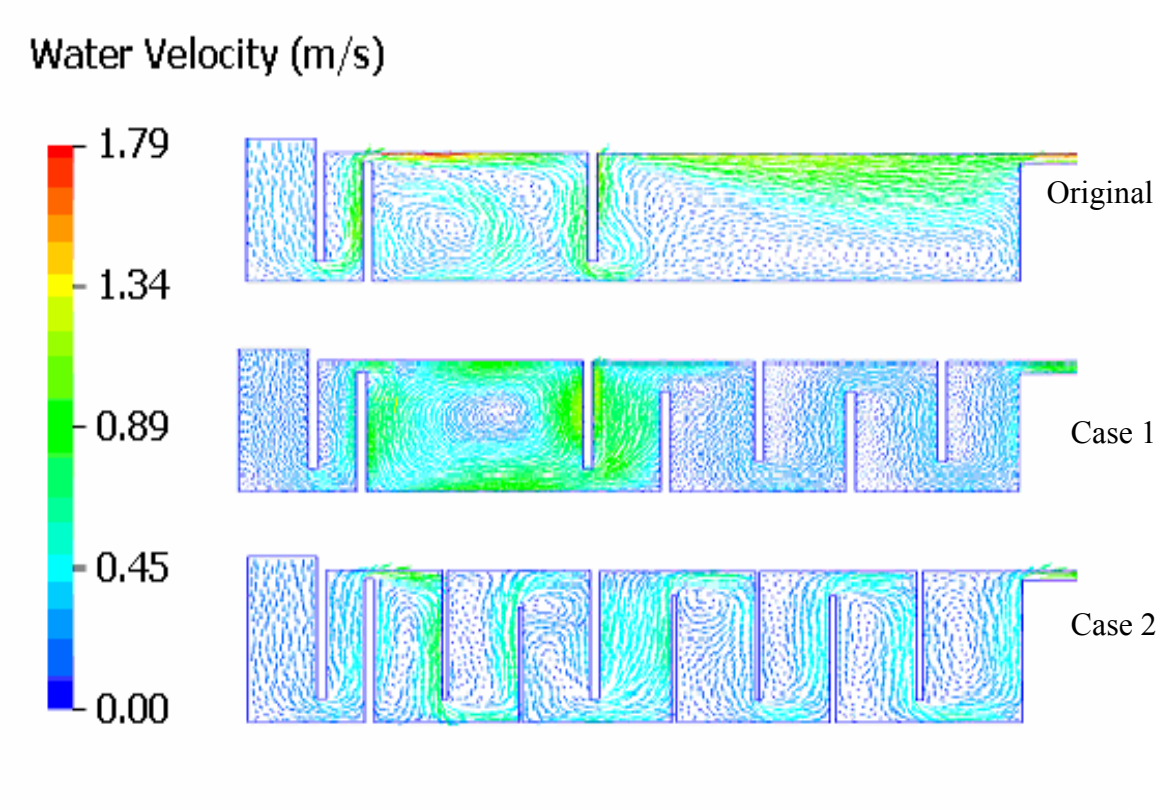

Figure 7.4 Comparison of the flow velocity fields (m/s) at different contactor configurations

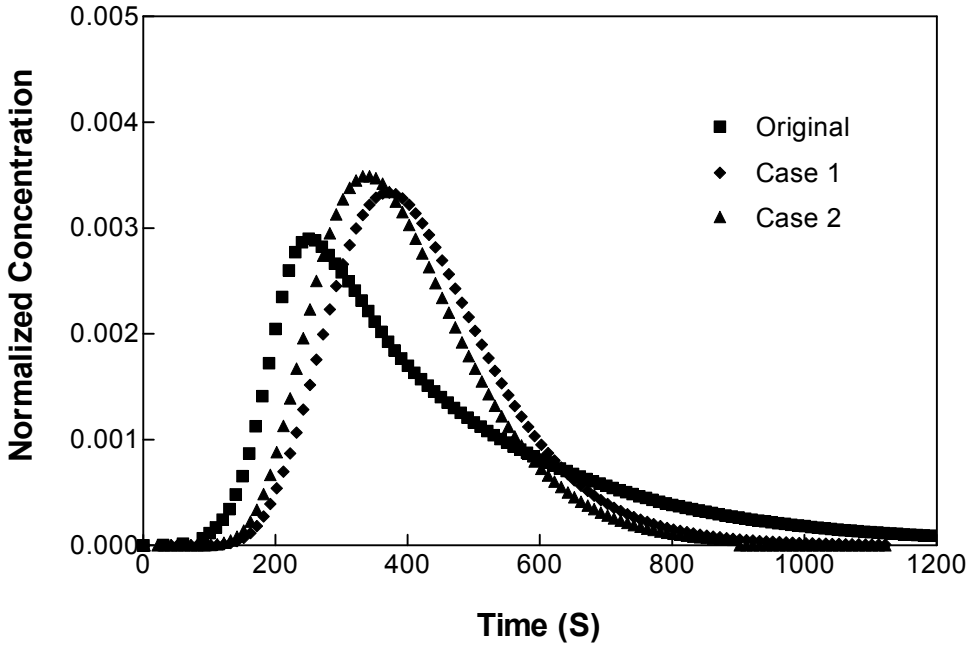

Figure 7.5 Comparison of the predicted tracer residence time distributions at different contactor configurations

Figure 7.6 provides a comparison of the CT values of three alternative contactors using different calculation methods: CT_{10}, IDDF-based CT and CFD-based CT. As with previous results, the CT_{10} values were smaller than the CT values predicted by the two other approaches, and the CFD-based CT was smaller than IDDF-based CT. However, the difference between CFD and IDDF approaches became smaller from the original case to case 1 and then case 2. This indicated that the degree of the difference among the IDDF and CFD approaches was sensitive to the contactor configuration. Smaller difference could be obtained in larger T_{10}/T systems. One possible reason for this observation is that, at higher T_{10}/T conditions, the flows were more segregated (Greene, 2002). The IDDF concept, which assumes that the flow is completely segregated, is therefore acceptable at such conditions for prediction of disinfection performance. On the contrary, at lower T_{10}/T conditions, the effects of micromixing become stronger and

the IDDF may over-estimate system performance. The CFD model developed in this study does not employ an assumption of mixing state and thus it may provide better description of disinfection efficiency for any types of full-scale ozone contactors.

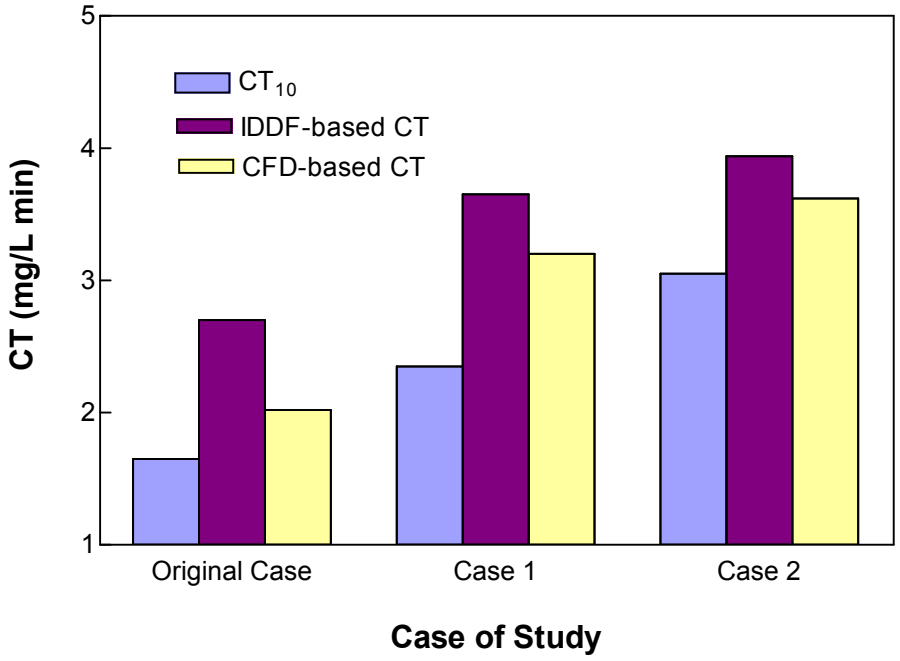

Figure 7.6 Comparison of CT calculation methods at different contactor configuration conditions

7.5 Discussion

In the above study, it was found that CT_{10}–based CT values were usually much less than the CT simulated by the two other modelling approaches and were lower than the real dose as described by the bioassay-based CT. This demonstrated that the traditional CT_{10} method might significantly underestimate disinfection efficiency. The potential

reasons or this included: 1) the CT_{10} approach used a very conservative residence time T_{10} to represent the residence time of all pathogens; 2) this approach essentially assumed that all the reactive chambers were CSTR reactors, in which the effluent concentration is used to represent the concentrations inside the contactor. However, the ozone concentration varied significantly in most chambers, especially when there were few chambers and mixing was poor.

It was also observed that the IDDF-based CT was higher than the calculated CT_{10}. This was due to the fact that the IDDF approach integrates the tracer residence time distribution curves with the ozone profiles along the ozone contactor. However, in all the results, the IDDF-based CT over-estimated the performance represented by the biodosimetric CT. The potential reasons for this were that the IDDF assumes that the fluid in the contactor is completely segregated, which means that the fluid mixing occurs on a macroscopic level (Greene et al. 2004; Craik, 2005). Under this assumption, molecules move in groups, and molecules in one group do not interact with molecules in another group. The IDDF approach does not take into account micro-mixing effects or molecular interactions. However, real fluids in contactors are usually partially segregated fluids in which microscopic level mixing may significantly affect the macroscopic level mixing. In addition, the IDDF uses a tracer residence time distribution curve to represent the contactor hydraulics. However, residence time distribution alone does not precisely characterize the degree of separation, and different reactor geometries may exhibit a similar residence time distribution (Levenspiel 1999). Therefore, the IDDF approach may lead to over- or under-estimation of disinfection performance. The CFD modelling approach, however, does not rely on assumptions of fluid mixing levels. Given accurate modelling conditions, the CFD-based CT can be obtained based on detailed information for ozone concentrations and residence times of all micro-organisms, thus it is possible to provide better prediction of ozone disinfection performance in either small or large scale ozone disinfection systems.

Table 7.2 Key differences of CT_{10}, IDDF and CFD methodologies

Major components in the models	CT_{10}	IDDF-based CT	CFD-based CT
Contactor Hydraulics	Each contactor chamber is assumed to be a CSTR reactor. A very conservative parameter T_{10} is used to represent the contactor hydraulics	Assumes the flows are segregated. Tracer Residence Time Distribution (RTD) is used to represent contactor hydraulics.	Predicted by Navier-stokes equation based fluid equations
Ozone mass transfer	Not included	Not included	The two-film interfacial mass transfer model used and implemented by solving species transport equations
Ozone demand and decay	Not available. The ozone concentrations are monitored at the outlet of the ozone chambers and used as representative parameters for a whole chamber	The ozone profiles are simulated based on site-specific ozone decay kinetics.	The ozone concentrations at any location in the contactor are simulated based on site-specific ozone demand and decay kinetics by solving species transport equations
Microbial inactivation kinetics	Not available	The site-specific microbial inactivation kinetics can be integrated into the model	The site-specific microbial inactivation kinetics can be integrated into the model by solving species transport equations

The simulation results also suggested that the differences between the IDDF and CFD approaches were sensitive to contactor mixing performance. When a contactor shows poor mixing performance and has substantial dead zones or short-circuiting, the CFD modelling approach is a better option for predicting CT values. However, when contactor hydraulics is close to plug flow, the IDDF and CFD may provide similar CT prediction results.

The key differences between the three CT prediction methods are summarized in Table 7.2.

7.6 Conclusions

The CT of ozone disinfection processes was studied using different CT prediction methods: CT_{10}, IDDF-based CT, and CFD-based CT. The following conclusions can be drawn from the comparison studies:

- The CT_{10} approach uses only two simplified, overly conservative parameters (ozone residual C and residence time T_{10}) to describe the ozone disinfection performance. Therefore, it may underestimate ozone disinfection efficiency and result in over-dosing of ozone.

- The IDDF approach uses the assumption that fluids in the contactors are completely segregated. It ignores the effects of micro-scale mixing of fluids. Based on the comparison results presented in this chapter, this approach is questionable in situations when the contactors have substantial short-circuiting and dead zones. However, it may be suitable for use when ozone contactors have high T_{10}/T ratios because the flows were more segregated at such conditions and the IDDF concept, which assumes that the flow is completely segregated, is therefore more acceptable.

- The CFD approach employs a three-dimensional multiphase CFD model to address all the major components of ozone disinfection processes. Current results showed that, for various modelling conditions, the predicted CFD-based CT values fitted well with the bioassay-based CT values. Since the CFD approach does not rely on knowledge of the contactor mixing state, it can be effectively used for predicting disinfection performance in various types of full-scale or pilot-scale ozone contactors.

- The accuracy of CFD modelling can be affected by some uncertainty factors including geometry information, mesh quality, boundary conditions, flow regimes (e.g. laminar or turbulent; steady or unsteady), and numerical description of the flow field. Therefore, appropriate safety factors should be included in the CFD based design. In the future, CFD validation studies should be done for ozone contactors with different geometries under varying water quality and operational conditions. Ultimately, a guideline of safety factors could be developed for various ozone contactor designs.

CHAPTER 8 CONCLUSIONS AND RECOMMENDATIONS

This thesis has described the development of a comprehensive three dimensional (3D) multiphase computational fluid dynamics (CFD) model to predict components of ozone disinfection processes: contactor hydraulics, ozone mass transfer, ozone demand and decay, and microbial inactivation. The model has been validated using full-scale experimental data, including tracer test results, ozone profiles, and bioassay tests from full-scale ozone contactors in two Canadian drinking water treatment plants (WTPs): the DesBaillets WTP in Montréal, Quebec and the Mannheim WTP in Kitchener, Ontario. In addition, the Eulerian and particle tracking (or Lagriangian) approaches have been compared for prediction of microbial inactivation efficiency (represented by the effective CT) of ozone contactors; the CFD model has been used to improve ozone monitoring and tracer test strategies to assist with ozone contactor operation and ozone disinfection efficiency prediction; and the different CT prediction approaches have been compared for evaluation of ozone disinfection performance based on full-scale investigations.

8.1 Conclusions

The following conclusions can be drawn regarding the development and validation of a multiphase computational fluid dynamics (CFD) model for ozone processes:

- An Eulerian-Eulerian multiphase model had been developed to model the hydrodynamics of complex gas-liquid ozone contacting systems. Using the CFD model, flow structures in two full-scale ozone contactors were simulated. A mesh density dependence study was conducted. The sensitivity of modelling to the turbulence models was also investigated and the k-ε model was found to be more appropriate for the modelling. Good agreement was observed between the numerical tracer simulation and experimental tracer test data from ozone contactors at the DesBaillets WTP in Montreal, Quebec and the Mannheim WTP in Kitchner, Ontario. This suggested that the Eulerian-Eulerian modelling approach developed in this study was capable of predicting multiphase ozone contactor hydraulic performance with a fair degree of accuracy.

- All the main components of ozone disinfection processes, including ozone mass transfer between two phases, ozone demand and decay kinetics, tracer transport, microbial inactivation kinetics, and bromate formation kinetics, were integrated within the CFD model through the use of species transport equations with appropriate source terms. The simulated dissolved ozone concentration profiles agreed well with the monitored ozone profiles of the ozone contactors at the DesBaillets and Mannheim WTPs. This further validated the CFD model for predicting the performance of full-scale ozone disinfection processes. The results of this study revealed that by combining the CFD hydrodynamics model with the transport models, the ozone mass transfer and reactions could be predicted reasonably well without any pre-assumption about flow characteristics (e.g. continuous stirred tank reactor (CSTR) or plug flow reactor (PFR)) or dispersion level).

- The CFD model was applied to investigate ozone contactor performance at the DesBaillets WTP. The CFD-predicted flow fields showed that recirculation zones

and short circuiting existed in the DesBaillets contactors. The simulation results suggested that the installation of additional baffles would increase the residence time and improve disinfection efficiency. The CFD model was also applied to simulate ozone contactor performance at the Mannheim Water Treatment Plant before and after the installation of new liquid oxygen (LOX) ozone generators to increase the ozone gas concentration and removal of some diffusers from the system. The modelling results suggested that such changes led to an increase in effective residence time and adjusting operational parameters was required after system modification.

- The effects of bubble size on the CFD modelling were studied. The results suggested that changing bubble size from 2 mm to 5 mm, which was the typical range of the bubble size in full-scale bubble diffuser ozone contactors, did not significantly affect the prediction of gas hold-up and dissolved ozone residuals.

The developed CFD model is expected to provide an efficient tool to balance microbial inactivation and bromate formation in full-scale ozone bubble diffuser contactors. Once the site-specific model inputs (kinetics of ozone decomposition, microbial inactivation and bromate formation) are determined by bench-scale experiments, the CFD model can be used to predict optimal ozone dosage in order to reduce the concentrations of disinfection by-products and therefore the associated risk, and to be cost effective.

Conclusions from the comparison between the Eulerian and particle tracking approaches for the prediction of microbial inactivation efficiency of ozone contactors are the following:

- To the author's knowledge, for the first time, the Eulerian and particle tracking approaches, two commonly utilized methods for predicting microbial inactivation

efficiency, have been compared for the study of ozone disinfection processes. The modelling results of two hypothetical ozone reactors suggested that, for ozone reactors with plug flow characteristics, either approach could be used to evaluate contactor hydraulics and disinfection efficiency (CT value). For reactors with non-ideal hydraulic performance, the particle tracking model predicts slightly smaller CT than the Eulerian approach does. This was mainly due to the complex particle trajectories in the non-ideal reactors. To further improve the accuracy of the particle tracking modelling, it is suggested to use more powerful computers which allow tracking larger amounts of the particles.

- For the full scale contactor investigated, the particle tracking-based CT values are slightly lower than the CT values predicted by the Eulerian approach, but the difference between the two approaches are within 10%. It was also observed that the tracer residence time distribution curve predicted by the Euerlian approach provided a better fit to the experimental results. It was suggested that the Eulerian approach may be more suitable for the simulation of chemical tracer performance due to the facts that: 1) it more closely reflects the actual physical behaviour of the chemical tracers; and 2) it was much more computationally economical than the particle tracking approach.

- It was also found that the effect of particle size (1 μm to 100 μm) used in this study on particle tracking method was negligible.

- The results of this work is useful in understanding the complex performance of multiphase ozonation systems and may play an important rule in further refining CFD modelling approaches for full-scale ozone disinfection systems.

The important findings and conclusions from using the CFD modelling to improve ozone monitoring and tracer test strategies include the following:

- The most significant contribution of this part of the work was that a CFD model was applied to illustrate and improve an ozone residual monitoring strategy. For the DesBaillets ozone contactors, the CFD modelling results showed that ozone residuals in the cross section of the outlets of some cells differed by an order of magnitude. The variation of residuals was affected by multiple factors, including water/gas flow rate, temperature, and baffling conditions etc. Therefore, it was suggested that multiple ozone residual sampling points should be installed at the outlets of certain cells to provide more accurate indicators to system operators.

- The CFD model was also used to study the factors affecting the residence time distribution (RTD). The results suggested that the selection of tracer injection locations as well as tracer sampling locations could affect the RTD prediction or measurement. The CFD calculated T_{10} values predicted that RTD curves at different outlet locations varied by more than 10%. It was therefore recommended that multiple sampling points be employed during tracer tests.

In addition, the investigation regarding the comparison of different CT prediction approaches lead to the following conclusions:

- The CT_{10} approach use only two simplified, overly conservative parameters (ozone residual C and residence time T_{10}) to describe ozone disinfection performance. Therefore, it may underestimate ozone disinfection efficiency and result in over-dosing of ozone.

- The IDDF approach uses the assumption that fluids in the contactors are completely segregated. It ignores the effects of micro-scale mixing of fluids. Based on the

comparison results presented in Chapter 7, this approach is questionable in situations when the contactors have strong short-circuiting and dead zones. However, it may be suitable for use when the ozone contactors have high T_{10}/T ratios and exhibiting behaviour close to plug flow reactors.

- The CFD approach employs a three-dimensional multiphase CFD model to address all the major components of ozone disinfection processes. Current results showed that, at various modelling conditions, the predicted CFD-based CT values fit well with the bioassay-based CT values. Since the CFD approach does not rely on the assumption of the contactor mixing state, it can be effectively used for predicting disinfection performance in various types of full-scale or pilot-scale ozone contactors.

8.2 Recommendations for Future Research

- The main focus of this study was to develop and apply a computational fluid dynamics (CFD) modelling approach to predict the disinfection performance of the ozonation processes in drinking water treatment systems. In the drinking water industry, ozone is also widely used as a powerful oxidizing agent for the removals of colour, taste and odour. In addition, ozone can also be used in conjunction with other oxidizing agents, such as hydrogen peroxide (H_2O_2) and high energy light (ultraviolet), to improve the removal of some pollutants. In such advanced oxidation processes (AOP), the chemical reactions are more complex and faster. In the future, it would be valuable to use the developed CFD model to investigate and optimize the ozonation performance for these alternative ozone applications.

- To further improve the CFD modelling of full-scale ozone bubble diffuser contactors, the effects of bubble size distribution, bubble break-up and bubble coalescence need to be experimentally verified and included into the CFD model to provide more accurate prediction of mass transfer between the continuous and dispersed phases.

- The factors affecting the Eulerian and particle tracking approaches for the prediction of disinfection efficiency should be further investigated. The main factors may include: different turbulence diffusion/dispersion model selection, operational parameters, microbial inactivation kinetics, and contactor geometry.

- The current CFD model sets the water surfaces of the ozone contactors as a rigid wall for water and a degassing free-slip wall for air. In reality, the water surface may move dynamically, especially when the water passes the outlet weirs and the baffle walls. It is suggested that the two-phase free surface modelling method for modelling of water surfaces be investigated to better characterize ozone contactor performance.

- The strategies for improving ozone monitoring and tracer test for the DesBaillets water treatment plant were investigated in this thesis. It is suggested that more CFD modelling and experimental studies should be done for different types of ozone contactors to develop technical guidance on determining ozone residual monitoring points and tracer test method. It is also recommended that such guidance should be considered in future drinking water regulations.

- Research on the development of experimental protocols for quickly determining site-specific ozone reaction and microbial inactivation kinetics is required to provide more accurate inputs for CFD modelling. It is expected that such research

along with the development of more advanced computer technology will allow the use of CFD to assist with the real-time control of ozone disinfection processes in the future.

- The accuracy of CFD modelling can be affected by the uncertainties of model inputs including inadequately defined geometry, inadequately defined boundary conditions, lack of knowledge of the flow regimes (which may be laminar, turbulent, steady, or unsteady), and inappropriate numerical description of the flow field. Therefore, appropriate safety factors should be included in the CFD based design. In the future, CFD validation studies should be done for ozone contactors with different geometries under varying water quality and operational conditions. Ultimately, a guideline of safety factors could be developed for various ozone contactor designs.

REFERENCES

American Public Health Association (APHA), American Water Works Association (AWWA), Water Environment Federation (WEF). (2001). Standard methods for examination of water and wastewater, 20th Edition, Washington.

Amy, G., Douville, C, Daw, B., Sohn, J., Galey, C., Gatel, D. and Cavard, J. (2000). Bromate formation under ozonation conditions to inactive *Cryptosporidium*. Water Science & Technology, 41(7):61-66.

ANSYS. (2005). CFX 10 user manual. ANSYS, Inc. USA.

Bader, H. and Hoigne, J. (1981). Determination of ozone in water by indigo method. Water Research, 15:449.

Barbeau, B., Boulos, L., Desjardins, R., Coallier, J., Prévost, M., and Duchesne, D. (1997). A Modified Method for the Enumeration of Aerobic Spore-Forming Bacteria. Can. J. Microbiol., 43:976-980.

Barbeau, B., El-Baz, G., Sarrazin, V., Desjardins, R. (2003). Application of the Integrated Disinfection Design Framework (IDDF) for Disinfection Contactors Performance Evaluation. American Water Works Association Water Quality Technology Conference (WQTC), Philadelphia, Pennsylvania. CD-ROM.

Baxter, C.W., Stanley, S.J., Zhang, Q. and Smith, D.W. (2002). Developing Artificial Neural Network models of drinking water treatment processes: a guide for utilities. Journal of Environmental Engineering and Science, 1(3):201-211.

Bdantyne L. (1999). Modelling chlorine dioxides inactivatlon of microbial inadicators and disinfection by-product formation. M.A.Sc. Thesis, University of Toronto, Canada

Bellamy, W. D. (1995). Full-scale ozone contactor study. American Water works Association Research Foundation, Denver, CO., U.S.A.

Bellamy, W.D., Finch, G.R. and Haas, C.N. (1998). Integrated Disinfection Design Framework. American Water Works Association Research Foundation, Dever, Co., U.S.A.

Bellamy, W., Carlson, K., Ducoste, J. and Carlson, M. (2000). Determining disinfection needs. Journal of American Water Works Association, 92(5):44-52.

Beltran, F.J., 2004. Ozone Reaction Kinetics for Water and Wastewater Systems. Lewis Publishers, Boca Raton, Florida

Broséusa, R., Barbeaua, B. And Bouchardb, C. (2006). Validation of full-scale ozone contactor performance using biodosimetry. To be published on Journal of Water Research.

Bryant, E.A., Fulton, G.P. and Budd, G.C. (1992). Disinfection alternatives for safe drinking water. Van Nostrand Reinhold.

Bin, A.K., Duczmal, B. and Machniewski, P. (2001). Hydrodynamics and ozone mass transfer in a tall bubble column. Chemical Engineering Science, 56:6233-6240.

Calderbank, P. H. (1959). Physical Rate Processes in Industrial Fermentation. Part 11: Mixing Transfer Coefficient in Gas-Liquid Contactingwith and Without Mechanical Agitation. Trans. Instn Chem. Engrs, 37:173-182.

Carlson, K., Bellamy, W. and Ducoste, J. (2001). Implementation of the Integrated Disinfection Design Framework, AWWA Research Foundation and AWWA.

Cho, M., Kim, H., Cho, S. H. and Yoon, J. (2003). Investigation of ozone reaction in river waters causing instantaneous ozone demand. Ozone: Science & Engineering, 25(4):251-259.

Chelkowska, K., Grasso, D., Fabian, I. and Gordon, G. (1992). Numerical simulation of aqueous ozone decomposition. Ozone: Science & Engineering, 23:259-284.

Chen, C.M. (1998). Modeling drinking water disinfection in ozone bubble diffuser contactors. Ph.D. Dissertation, Purdue University, West Lafayette, Ind.

Chen Y. H., Chang C. Y., Chiu C. Y., Huang W. H., Yu Y. H., Chiang P. C., Ku Y., and Chen J. N. (2002). Dynamic Model of Ozone Contacting Process with Oxygen Mass Transfer in Bubble Columns. Journal of Environmental Engineering, 128(11):1036-1045

Chiu, K., D., Lyn, A., Savoye, P. and Blatchley, E.B. (1999). Integrated UV disinfection model based on particle tracking. Journal of Environmental Engineering-ASCE, 125(1):7-16.

Clift, R., Grace J.R. and Weber M.E. (1978). Bubbles, drops and particles. Academic Press.

Cockx, A., Line, A., Roustan, M., DoQuang, Z. and Lazarova, V. (1997). Numerical simulation and physical modeling of the hydrodynamics in an air-lift internal loop reactor. Chemical Engineering Science, 52(21-22):3787-3793.

Cockx, A., Do-quang, Z., Line, A. and Roustan, M. (1999). Use of computational fluid dynamics for simulating hydrodynamics and mass transfer in industrial ozonation towers. Chemical Engineering Science, 54:5085-5090.

Coffey, B. M., Graff, K. G., Mofidi, A. and Gramith, J. T. (1995). On-line monitoring of ozone disinfection effectiveness within and over/under baffled contactors. Proceeding, American Water Works Association National Conference. Anaheim, California. 77-132.

Craik, S.A., Smith, D.W. and Chandrakanth, M. (2000). Reaction engineering analysis of *Cryptosporidium Parvum* Inactivation in a laboratory-scale static mixer ozonation system, Proceedings of 2000 American Water Works Association, Water Quality Technology Conference.

Craik, S. A., Finch, G., Leparc, J. and Chandrakanth, M. S. (2002a). The effect of ozone gas-liquid contacting conditions in a static mixer on microorganism reduction. Ozone-Science & Engineering, 24(2):91-103.

Craik, S.A., Smith, D. W., Belosevic, M. and Chandrakanth, M. (2002b). Use of *Bacillus subtilis* spores as model microorganisms for ozonation of *Cryptosporidium parvum* in drinking water treatment. Journal of Environmental Engineering and Science, 1:173-186.

Craik, S. A. (2005). Effect of micro-mixing conditions on predictions of cryptosporidium inactivation in an ozone contactor. Ozone: Science and Engineering, 27(6):487–494.

Crozes, G., Hagstrom, J. and White, P. (1997). Approach to design of ozone facilities for *Cryptosporidium* inactivation on Lake Michigan. Proceedings of 1997 American Water Works Association, Water Quality Technology Conference.

Crozes, G., Hagstrom, J. P., Clark, M. M., Ducoste, J. and Burns, C. (1998). Improving clearwell design for CT compliance, American Water Works Assoc. Res. Foundation, Denver.

Crozes, G., Hagstrom, J., Suffet, I. H. and Young, C. (1999). Bench-scale evaluation of adsorptive processes for taste and odors control using rapid small-scale column tests and flavor profile analysis. Water Science and Technology, 40(6):39-44.

Danckwerts, P. V. (1970). Gas-Liquid Reactions, McGraw-Hill, New York

Do-quang, Z. and Cockx, A. (1998). Innovative design of enhanced *Cryptosporidum* removal in a 60 MGD WTP: use of a CFD modelling and full scale data. Proceedings of 1998 American Water Works Association, Water Quality Technology Conference.

Do-Quang, Z., Cockx, A., Line, A. and Roustan, M. (1999). Computational fluid dynamics applied to water and wastewater treatment facility modeling. Environmental Engineering and policy, 1:137-147.

Do-Quang, Z., Ramirez, C. C. and Roustan, M. (2000a). Influence of geometrical characteristics and operating conditions on the effectiveness of ozone contacting in fine-bubbles conventional diffusion reactors. Ozone: Science & Engineering, 22(4): 369-378.

Do-Quang, Z., Roustan, M. and Duguet, J. P. (2000b). Mathematical modeling of theoretical Cryptosporidium inactivation in full-scale ozonation reactors. Ozone: Science & Engineering, 22(1):99-111.

Do-Quang, Z., Janex, M.L., Perrin, D., 2002, Predictive tool for UV dose distribution assessment: Validation of CFD models by bioassays, Proceedings of AWWA Conference, New Orleans, LA.

Downey, D., Giles, D.K. and Delwiche, M.J. (1998). Finite element analysis of particle and liquid flow through an ultraviolet reactor. Computers and Electronics in Agriculture, 21:81-105.

Ducoste, J., Carlson, K., Bellamy, W. and Carlson, M. (1999). A systematic approach to reactor hydraulic characterisation: part 1 of the integrated disinfection design framework protocol, Proceedings of 1999 AWWA water quality technology conference, Tampa, Florida.

Ducoste, J., Carlson, K. and Bellamy, W. (2001). The integrated disinfection design framework approach to reactor hydraulics characterisation. Journal of Water Supply: Research and Technology—AQUA, 50(4):245-261.

Ducoste, J. J., Liu, D. and Linden, K. (2005a). Alternative approaches to modeling fluence distribution and microbial inactivation in ultraviolet reactors: Lagrangian versus Eulerian. Journal of Environmental Engineering-ASCE, 131(10):1393-1403.

Ducoste, J. and Linden, K. (2005b). Determination of ultraviolet sensor location for sensor set-point monitoring using computational fluid dynamics. Journal of Environmental Engineering and Science, 4:33-43.

Ducoste, J., Linden, K., Rokjer, D. and Liu, D. (2005). Assessment of reduction equivalent fluence bias using computational fluid dynamics. Environmental Engineering Science, 2(5):615-628.

El Baz, G. (2002). Développement d'un modèle de calcul de la performance des unités de désinfection. M.A.S Thesis, École Polytechnique de Montréal, Québec, Canada.

Fabian I. (1995). Mechanistic aspects of ozone decomposition in aqueous solution. Progress in Nuclear Energy, 29(8):167-174(8)

Facile, N., Barbeau, B., Prévost, M., and Koudjonou, B. (2000). Evaluating bacterial aerobic spores as a surrogate for Giardia and Cryptosporidium inactivation by ozone. Wat. Res., 34(12):3238-3246

Finch, G. R., Yuen, W. C. and Uibel, B. J. (1992). Inactivation of Escherichia-Coli Using Ozone and Ozone - Hydrogen-Peroxide. Environmental Technology, 13(6):571-578.

Finch, G. R., Black, E. k., Gÿurk, L. and Belosevic M. (1994). Ozone Disinfection of Giardia and Cryptosporidium. AWWARF, Denver, Colorado.

Finch, G. R., Hass, C.N., Oppenheimer, J.A., Gordon, G. and Turssell, R.R. (2001). Design criteria for inactivation of cryptosporidium by ozone in drinking water. Ozone Science & Engineering, 23:259-284.

Gobby, G. (2002). Experimental validation of a bubble column reactor, CFX validation report, AEA Technology.

Gobby D. (2004). Experimental validation of a bubble column reactor. Ansys CFX technical paper, www.ansys.com.

Gosman, A. D., and Ioannides E. (1981). Aspects of Computer Simulation of

Liquid-Fueled Combustors. AIAA Paper, No. 81-0323.

Gordon, G. (1995). The chemistry and reactions of ozone in our environment. Progress in Nuclear Energy, 29:89-96.

Grayman, W.M. and Arnold, C.N. (2003). Overview of CFD Methods in Analysis of Distribution System Tanks and Reservoirs. 2003 American Water Works Association Annual Conference.

Greene, D.J. (2002). Numerical simulation of chlorine disinfection process in non-ideal reactors. Ph.D. thesis, Drexel University, USA.

Greene, D. J., Farouk, B. and Haas, C. N. (2004). CFD design approach for chlorine disinfection processes. Journal American Water Works Association, 96(8):138-150.

Grotjans, H., and Menter F.R. (1998). Wall functions for general application CFD codes, In: Proceedings of the fourth ECCOMAS Computational Fluid Dynamics Conference, John Wiley & Sons, p1112–1117.

Gyurek L.L. (1999). Ozone inactivation kinetics of *Cryptosporidium* in phosphate buffer. Journal of Environmental Engineering ASCE., 125(10):913-924.

Gyurek, L.L. and Finch, G.R. (1998). Modeling water treatment chemical disinfection kinetics. Journal of Environmental Engineering ASCE., 124(9):783-793.

Haas, C. N. and Karra, S. B. (1984a). Kinetics of Microbial Inactivation by Chlorine .1. Review of Results in Demand-Free Systems. Water Research, 18(11):1443-1449.

Haas, C. N. and Karra, S. B. (1984b). Kinetics of Microbial Inactivation by Chlorine .2. Kinetics in the Presence of Chlorine Demand. Water Research, 18(11):1451-1454.

Haas C.N., Joffe, J., Heath, M., Jacangelo, J., and Anmangandla, U. (1998). Predicting disinfection performance in continuous flow systems from batch disinfection kinetics. Water Science Technology, 38(6):171-179.

Health Canada. (2006). Guidelines for Canadian Drinking Water Quality. http://www.hc-sc.gc.ca/ewh-semt/pubs/water-eau/doc_sup-appui/sum_guide-res_recom/index_e.html

Henry, D.J., and Freeman, E.M. (1995). Finite element analysis and T_{10} optimization of ozone contactor. Ozone: Science & Engineering, 17:587-606.

Higbie, R. (1935). The rate of absorption of a pure gas into a still liquid during a short time of exposure. Transactions of the American Institute of Chemical Engineers, 31: 365-389.

Hijnen, W. A. M., Van Veenendaal, D. A., Van Der Speld, W. M. H., Visser, A., Hoogenboezem, W., and Van Der Kooij, D. (2000). Enumeration of faecal indicator bacteria in large water volumes using on site membrane filtration to assess water treatment efficiency.Water Research, 34(5):1659-1665.

Hoigne, J. (1994). Characterization of Water-Quality Criteria for Ozonation Processes .1. Minimal Set of Analytical Data. Ozone-Science & Engineering, 16(2):113-120.

Hoigne, J. (1995). Kinetic Concepts to Quantify the Role of Oxidants and Photooxidants in Natural-Waters and Water-Treatment. Abstracts of Papers of the American Chemical Society 210:41-ENVR.

Hofmann, R. and Andrews, R.C. (2001). Ammoniacal Bromamines: A review of their influence of bromate formation during ozonation. Water Research, 35(3):599-604.

Hossain, A. (2005). CFD investigation for turbidity spikes in drinking water distribution networks, Institution Swinburne University of Technology, Australia.

Huang, T., and Brouckaert, C.J. (2002). A CFD and experimental study of an ozone contactor. Water Science and Technology, 46(9):87-93.

Huck, P.M., Anderson, W.B., Rowley, S.M. and Daignault, S.A. (1990). Formation and removal of selected aldehydes in a biological drinking water treatment process, J.Water SRT-Aqua, 39(5):321-333.

Hunt, N., K., Marinas, B.J. (1999). Inactivation of *Escherichia coli* with ozone: chemical and inactivation kinetics. Water Research, 33(11):2633-2641.

Kamimura, M., Furukawa, S. and Hirotsuji, J. (2002). Development of a simulator for ozone/UV reactor based on CFD analysis. Water Science and Technology, 46:13-19.

Kim J., and von Gunten U. (2001). Modeling the effects of water quality on bromate formation and cryptosporidium parvum oocyst inactivation during ozone treatment. 2001 AWWA annual conference proceedings, CD.

Kim, J.H. (2002a). Integrated optimization of cryptosporidium inactivation and bromate formation control in ozone contactor. PhD. Dissertation, University of Illinois:11-16 and 19-30.

Kim, J. H., Rennecker, J. L., Tomiak, R. B., Marinas, B. J., Miltner, R. J. and Owens, J. H. (2002b). Inactivation of Cryptosporidium oocysts in a pilot-scale ozone bubble-diffuser contactor. II: Model validation and application. Journal of Environmental Engineering-Asce, 128(6):522-532.

Kim, J. H., Tomiak, R. B. and Marinas, B. J. (2002c). Inactivation of Cryptosporidium oocysts in a pilot-scale ozone bubble-diffuser contactor. I: Model development. Journal of Environmental Engineering-Asce, 128(6):514-521.

Kosaka, K., Yamada, H., Shishida, Echigo, S., Minear, R. A. and Matsui, S. (2001). Evaluation of the treatment performance of a multistage ozone/hydrogen peroxide process by decomposition by-products. Water Research, 35(15):3587-3594.

Kuipers JAM, van Swaaij WPM. (1998). Computational fluid dynamics applied to chemical reaction engineering. Adv Chem Eng, 24:227–328.

Labatiuk, C.W., Belosevic, M., and Finch, G.R. (1994). Inactivation of Giardia muris using ozone and ozone – hydrogen peroxide. Ozone: Science and Engineering, 16(1):67–78.

Lakehal, D., 2002, Modelling of Multiphase Turbulent Flows for Environmental and Hydrodynamic Applications, Int. J. Multiphase Flow, 28(5):823-863.

Langlais, B., Reckhow, D. A., and Brink, D.R., (1991). Ozone in Water Treatment: Application and Engineering, LEWIS.

Launder, B. and Spalding, D. (1974). The numerical computation of turbulent flows. Computer Methods in Applied Mechanics and Engineering, 3:269-289.

Levenspiel, O. (1999). Chemical Reaction Engineering, John Wiley and Sons, New York

Lev, O. and Regli, S. (1992a). Evaluation of Ozone Disinfection Systems - Characteristic Time-T. Journal of Environmental Engineering-Asce, 118(2):268-285.

Lev, O. and Regli, S. (1992b). Evaluation of Ozone Disinfection Systems - Characteristic Concentration-C. Journal of Environmental Engineering-Asce, 118(4):477-494.

Lewis W. and Whitman W.G. (1924). The two film theory of gas absorption. Ind. Eng. Chem, 16:1215

Li, H. and Gyurek, L.L. (2001). Effect of temperature of ozone inactivation of *Cryptosporidium* in oxidant demand-free phosphate buffer. Journal of Environmental Engineering, 5:456-467.

Lo, M. (2000). Application of population balance to cfd modelling of gas-liquid reactors. Proceeding of conference on Trends in Numerical and Physical Modelling for Industrial Multiphase Flows Conference, Corse, France.

Lopez de Bertodano, B. (1991). Turbulent Bubbly Flow in a Triangular Duct. Ph. D. Thesis, Rensselaer Polytechnic Institute, Troy New York

Lucor, D., Xiu, D., Su C. and Karniadakis, G.E. (2003). Predictability and uncertainty in CFD, International Journal For Numerical Methods in Fluids, 43:483–505.

Lyn, D.A., Chiu K. (1999). Numerical modeling of flow and disinfection in UV disinfection channels. Journal of Environmental Engineering-ASCE, 125(1):17-26.

Lyn, D. A. and Blatchley, E. R. (2005). Numerical computational fluid dynamics-based models of ultraviolet disinfection channels. Journal of Environmental Engineering-Asce, 131(6):838-849.

Mitrakas M. and Simeonidis C. (2003) Conditions Affecting Bromate Formation During Ozonation of Bottled Water. Ozone: Science and Engineering, 25(3):167-175

Marinas, B. J., Liang, S. and Aieta, E. M. (1993). Modeling Hydrodynamics and Ozone Residual Distribution in a Pilot-Scale Ozone Bubble-Diffuser Contactor. Journal American Water Works Association, 85(3):90-99.

Marinas, B. J., Rennecker, J. L., Teefy, S. and Rice, E. W. (1999). Assessing ozone disinfection with nonbiological surrogates. Journal of American Water Works Association, 91(9):79-89.

Masschelein, W. J. (1982). Ozonization manual for water and wastewater treatment. 1st Ed., Wiley, New York.

Masschelein, W.J. (1982a). Contacting of ozone with water and contactor off-gas treatment. Handbook of ozone technology and applications, volume1 (R.G. Rice and A. Netzer, editors) (Ann arbour Sci. Publ., Ann arbour, MI).

Masschelein, W.J. (1982b). Continuous amperometric residual ozone analysis in the Tailfer (Brussels, Belgium) plant. Ozonization manual for water and wastewater treatment. John Wiley and Sons, Inc. NY, 1992.

Ministère de l'environnement du Québec (MENV). (2002). Guide de conception des installations de production d'eau potable.

Menter, F. R. (1994). Two-Equation Eddy-Viscosity Turbulence Models for Engineering Application. AIAA Journal, 32(8):1598-1605

Michele, V. (2002). CFD Modeling and Measurement of Liquid Flow Structure and Phase Holdup in Two-and Three-phase bubble columns. Ph.D. Dissertation, University of Braunchweig.

MOE (Ontario Ministry of Environment) (2006). Procedure For Disinfection Of Drinking
Water In Ontario, Canada.

Mofidi, A.A., Momtaz, S.W., Coffey, B.M. (2004). Predicting large-scale ultraviolet reactor performance using computational fluid dynamics and irradiance (CFD-i) modeling. 2004 AWWA Annual Conference; Orlando, FL., USA.

Murrer, J., Gunstead, J. and Lo, S. (1995). The development of an ozone contact tank simulation model. Ozone Science & Engineering, 17:607-617.

MWH Inc. (2005) Water Treatment Principles and Design. Montgomery, JA. John Wiley and Sons, New York New York.

Nieminski, E. C., Bellamy, W. D., and Moss, L. R. (2000). "Using surrogates to improve plant performance. J. Am. Water Works Assoc., 92(3):67-78.

Ozekin, K., Amy, G. (1997). Threshold levels for bromate formation in drinking water. Ozone Science and Engineering,19:323.

Page, M. (2000). Assessing he benefits of ozone use in chemical water treatment. MSc thesis, Imperial College of Science, Technology and Medicine, University of London.

Park, H., Hwang, T., Kang, J., Choi, H. and Oh, H. (2001). Characterization of raw water for the ozone application measuring ozone consumption rate. Water Research, 35: 2607-2614.

Peltier, S. and Galey, C. (2001). CFD modelling of full-scale ozone tank: Validation and optimization. Proceedings of 2001 American Water Works Association Water Quality Technology Conference.

Peplinski; D.K. and Ducoste, J. J. (2002). Modelling of disinfection contactor hydraulics under uncertainty, J. of Environmental Engineering, 11:1056-1067.

Perry, R. H., Green, D. W. and Maloney, J.O. (1973). Chemical Engineers handbook. New York, McGraw-Hill Professional.

Podowski, M.Z. (1999). CFD modeling of two-phase flow and heat transfer, 1999 CFX International Users Conference, Friedrichshafen.

Rafique M, Chen P, Dudukovic MP. (2004). Computational modeling of gas-liquid flow in bubble columns. Rev. Chem. Eng., 20:225–376.

Rahimi R., R. Rahimi M., Zivdar M.. (2006). Efficiencies of Sieve Tray Distillation Columns by CFD Simulation. Chemical Engineering & Technology, 29(3):326 - 335

Rakness, K., Rexing, D., Zegers, R. and Carlson, K. (2000). Optimising *Cryptosporidium* inactivation credit with ozone at Las Vegas using the integrated disinfection design framework, Proceedings of 2000 American Water Works Association Water Quality Technology Conference.

Rakness, K. L., Najm, I., Elovitz, M., Rexing, D. and Via, S. (2005). Cryptosporidium log-inactivation with ozone using effluent CT_{10}, geometric mean CT_{10}, extended integrated CT_{10} and extended CSTR calculations. Ozone: Science and Engineering, 27(5):335-350.

Rakness, K. L. (2005). Ozone in Drinking Water Treatment: Process Design, Operation and Optimization, American Water Works Association, Denver, Co.

Ranade V.V. (2002). Computational flow modeling for chemical reactor engineering. Process systems engineering 5. New York: Academic Press.

Roustan, M., J.P. Duguet, B. Brette, E. Brodard, and J. Mallevialle (1987). Mass Balance Analysis of Ozone in Conventional Bubble Contactors. Ozone Sci. Eng., 9:289–297.

Roustan, M., Kim, J.H. and Marinas, B. J. (2000). Drinking water ozone process control and optimization. International specialised symposium IOA 2000 " Fundamental and engineering concepts for ozone reactor design" proceedings. Toulouse, France.

Roustan, M., Line, A. and Wable, O. (1992). Modeling of Vertical Downward Gas-Liquid Flow for the Design of a New Contactor. Chemical Engineering Science 47(13-14):3681-3688.

Y. Sato, Sekoguchi, K. (1975). Liquid velocity distribution in two phase bubble flow. Int. J. Multiphase Flow, 2:79-87.

Schiller, L. and Naumann, A., (1933). A drag coefficient correlation. VDI Zeitschrift, 77: 318-320.

Schugerl, K. and Bellgardt, K.H. (2001). Bioreaction Engineering: Modeling and Control, Springer, Berlin, Germany.

Siddiqui, M, Amy, G., Ozekin, K. and Westerhoff, P. (1994). Empirically and theoretically –based models for predicting bromated ozonated By-products. Ozone Science & Engineering, 16:157-178.

Siddiqui, M, Amy, G., Ozekin, K. and Westerhoff, P. (1998). Modeling dissolved ozone and bromate ion formation in ozone contactors. Water, Air, and Soil Pollution, 108: 1-32.

Singer, P. C. and Hull, C.S. (2000). Modelling dissolved ozone behaviour in ozone contactors. American Water Works Association Research Foundation, Denver, CO.

Sato, Y. and Sekoguchi, K. (1975). Liquid Velocity Distribution in Two-phase Bubble Flow. Int. J. Multiphase Flow, 2:79-95.

Sokolichin A, Eigenberger G. (1994). Gas-liquid Flow in Bubble Columns and Loop Reactors. I. Detailed Modeling and Numerical Simulation. Chem. Eng. Sci. 49:5735–5746.

Sokolichin, A., Eigenberger, G. and Lapin, A. (2004). Simulation of buoyancy driven bubbly flow: Established simplifications and open questions. Aiche Journal 50(1): 24-45.

Song, R., Minear, R., Westerhoff, P. and Amy, G. (1996). Bromate formation and control during water ozonation. Environmental Technology 17(8):861-868.

Speziale, C. G., Sarkar, S. & Gatski, T. B. (1991). Modeling the Pressure-Strain Correlation of Turbulence: An Invariant Dynamical System Approach. J. Fluid Mech., 227: 245-272.

Ta, C. T. and Hague, J. (2004). A two-phase computational fluid dynamics model for ozone tank design and troubleshooting in water treatment. Ozone: Science & Engineering, 26(4):403-411.

Tang, G., Adu-Sarkodie, K., Kim, D., Kim, J. H., Teefy, S., Shukairy, H. M. and Marinas, B. J. (2005). Modeling *Cryptosporidium parvum* oocyst inactivation and bromate formation in a full-scale ozone contactor. Environmental Science & Technology, 39(23):9343-9350.

Teefy, S (1996). Tracer studies in water treatment facilities: a protocol and case studies. American Water Works Research Foundation, Denver, CO. U.S.A.

K. Tyrovola, K., and Diamadopoulos, E. (2005). Bromate formation during ozonation of groundwater in coastal areas in Greece. Desalination, 176:201–209.

Urfer, D., Huck, P.M., Gagnon, G.A., Mutti, D. and Smith, F. (1999). Modelling enhanced coagulation to improve ozone disinfection, Journal of American Water Works Association, 91(3):59-73.

USEPA. (1990). Guidance Manual For Compliance With The Filtration And Disinfection Requirements For Public Water Systems Using Surface Water Sources. U.S. Environmental Protection Agency, Washington, D.C.

USEPA (1991). Guidance manual for compliance with the filtration and disinfection requirements for public water systems using surface water sources. EPA 68-01-6989, U.S. Environmental Protection Agency, Washington, D.C.

USEPA. (1998). National Primary Drinking Water Regulations: Disinfectants and Disinfection Byproducts: Final Rule. Federal Register 63(241):69389-69476, U.S. Environmental Protection Agency, Washington, D.C.

USEPA. (1999a). EPA guidance manual: alternative disinfectants and oxidants. EPA 815-R-99-014. U.S. Environmental Protection Agency, Washington, D.C.

USEPA (1999b).Disinfection profiling and benchmarking guidance manual, United States Environmental Protection Agency, office of water, EPA815-R-99-013.

USEPA. (2001). National primary drinking water standards. EPA 816-F-01-007. U.S. Environmental Protection Agency, Washington, D.C.

USEPA (2003a) Ultraviolet disinfection guidance manual. EPA 815-D-03-007, Office of Water, Office of Science and Technology, Engineering and Analysis Division, U.S. Environmental Protection Agency, Washington, DC.

USEPA (2003b). Long term 2 enhanced surface water treatment rule-toolbox guidance manual (draft). EPA 815-F-03-005, U.S. Environmental Protection Agency, Washington, D.C.

USEPA. (2006a). Long Term 2 Enhanced Surface Water Treatment Rule: Final Rule. U.S. Environmental Protection Agency, Washington, D.C.

USEPA. (2006b). National Primary Drinking Water Regulations: Stage 2 Disinfectants and Disinfection Byproducts Rule; Final Rule. U.S. Environmental Protection Agency, Washington, D.C.

Utyuzhnikov S.V. (2005). Generalized Wall Functions and Their Application for Simulation of Turbulent Flows. International Journal for Numerical Methods in Fluids, 47(10-11):1323-1328

van Baten JM, Ellenberger J, Krishna R. (2003). Using CFD to Describe the Hydrodynamics of Internal Air-lift Reactors. Can. J. Chem. Eng., 81:660–668

Versteeg, H. K. and Malalasekera, W. (1995). An Introduction to Computational Fluid Dynamics, The Finite Volume Method, Addison-Wesley.

Vesvikar, M. S. and Al-Dahhan, M. (2005). Flow pattern visualization in a mimic anaerobic digester using CFD. Biotechnology and Bioengineering, 89(6):719-732.

von Gunten U. and Hoigné, J. (1994). Bromate formation during ozonation of bromide-containing waters: Interaction of ozone and hydroxyl radical reactions. Environmental Science and Technology, 28:1234-1242.

von Gunten U, Pinkernell U. (2000). Ozonation of bromide-containing drinking waters: a delicate balance between disinfection and bromate formation. Water Science and Technology, 41:53-59.

Westerhoff, P., Song, R., Amy, G. and Minear, R. (1996). Application of ozone decomposition models. Ozone Science and Engineering, 19(1):55-74.

Westerhoff, P., Song, R., Amy, G. and Minear, R. (1998). Numerical kinetic models for bromide oxidation to bromine and bromate. Water Research, 32:1687-1699.

Westerhoff, P. (2002). Kinetic-based models for bromate formation in natural waters, EPA report.

Williams, M.D., Coffey, B.M. and Krasner, S.W. (2003). Evaluation of pH and ammonia for controlling bromate , J. American Water Works Association, 95:82-93.

Wright, N.G. and Hargreaves, D.M. (2001). The use of CFD in the evaluation of UV treatment systems. Journal of Hydroinformatics, 3:59-70.

Wu, J. J. and Masten, S. (2001). Mass transfer of ozone in semibatch stirred reactor. Journal of Environmental Engineering, 127(12):1089-1099.

Hughmark, G.A., 1967, Holdup and mass transfer in bubble columns, Ind. Eng. Chem., Process Des Dev, 6(2): 218–220.

Yakhot V. and Orzag S. A. (1986). Renormalization group analysis of turbulence: basic theory. J. Science Comput, 1(1):1-51.

Yurteri, C. and Gurol, M. D. (1988). Ozone consumption in natural waters: effects of background organic matter, pH and carbonate species. Ozone Science & Engineering, 10:277-290.

Zhang, J., Huck P.M., and Anderson W.B. (2004a). Optimization of a Full-Scale Ozone Disinfection Process Based on Computational Fluid Dynamics Analysis. In: Chemical Water and Wastewater Treatment VIII, p325-334.

Zhang J., Huck P.M., and Anderson W.B. (2004b). Quantification and Optimization of the Performance of Full-Scale Ozone Contactors Based on CFD Modeling and On-site Testing. Proceedings, 2004 International Ozone Association-Pan American Group Conference, Windsor, Ontario, CD-ROM, Session 10, Paper 2.

Zhang J., Huck P.M., and Anderson W.B. (2004c). Quantification and Optimization of the Performance of Full-Scale Ozone Contactors. In: Water Supply and Water Quality, (Proceedings, XVIII-th National, VI-th International Scientific and Technical Conference, Poland. (2):443-451.

Zhang, J., Anderson W.B., Smith E.F., Barbeau B., Desjardins R., Huck P.M. (2005). Development, Validation and Implementation of a Multiphase CFD Model for Optimization of Full-scale Ozone Disinfection Processes. AWWA Water Quality Technology Conference and Exposition (WQTC), Quebec City, Quebec. November 6-10, 2005, paper Mon14-3.

Zhang J., Anderson W.B., Huck P.M., Stubley G.D. (2006a), A CFD Based Integrated Disinfection Design Approach for Optimization of Full-scale Ozone Contactor Performance, Submitted to Journal of Ozone Science and Engineering.

Zhang J., Stubley G.D., Huck P.M., Anderson W.B. (2006b). A comparison of Eulerian and Particle Tracking approaches for prediction of ozone contactor performance. To be submitted to Journal of Water Supply: Research and Technology-AQUA.

Zhang, J., Huck P.M., Stubley G.D., and Anderson W.B. (2006c). Improving Ozone Residual Monitoring and Tracer Testing Strategies for Full-scale Ozone Contactors Based on CFD Modeling. AWWA Water Quality Technology Conference and Exposition (WQTC), Denver, Colorado. November 5-9, 2006, in press.

Zhang, J., Huck P.M., Stubley G.D., Anderson W.B., and Barbeau B. (2006d). A Comparison between a CFD Approach and CT_{10} Method for Evaluation of Drinking Water Ozone Disinfection Performance. Proceedings, 12th Canadian National Conference and 3rd Policy Forum on Drinking Water, Saint John, New Brunswick, in press.

Zhang J., Anderson W.B., Huck P.M., Stubley G.D., Tadwalkar A. (2006e). Evaluation of a Computational Fluid Dynamics Modeling Approach for Prediction of Flocculation Mixing Performance at the Toronto R.L. Clark Filtration Plant, Proceedings, Owwa/Omwa Joint Annual Conference & Trade Show 2006, Toronto, Ontario, 21p.

Zhou, H., Smith, D. W., Stanley, S. J. (1994). Modeling of dissolved ozone concentration profiles in bubble columns. Journal of Environmental Engineering, 120(4):821-840.

Zhou H. and Smith, D. W. (1995). Evaluation of parameter estimation methods for ozone disinfection kinetics. Water Research, 29:679-686.

Zhou, H. and Smith, D. W. (2000). Ozone mass transfer in water and wastewater treatment: Experimental observations using a 2D laser particle dynamics analyzer. Water Research, 34(3):909-921.

Zhou, H. and Smith, D. W. (2001). Advanced technologies in water and wastewater treatment. Canadian Journal of Civil Engineering, 28:49-66.

Zwietering, T. N. (1959). The Degree of Mixing in Continuous Flow Systems. Chemical Engineering Science, 11(1):1-15.

Appendix A

Geometry and Sampling Points of the DesBaillets Water Treatment Plant Ozone Contactor

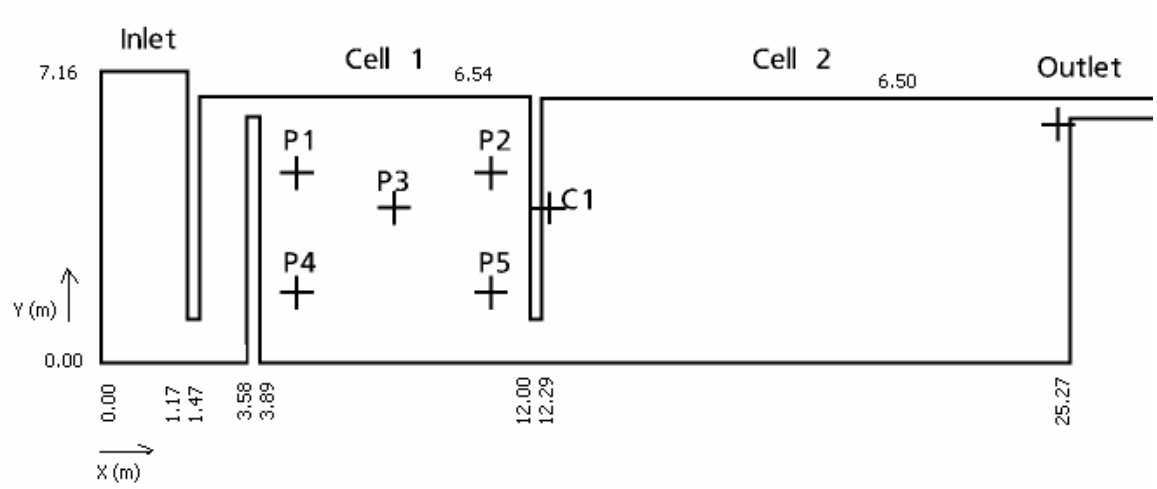

Width of the contactor (Z direction) is 5.5m

Appendix B

Arrangement of Bubble Diffusers in the Cell 1 of the DesBaillets Water Treatment Plant Ozone Contactor

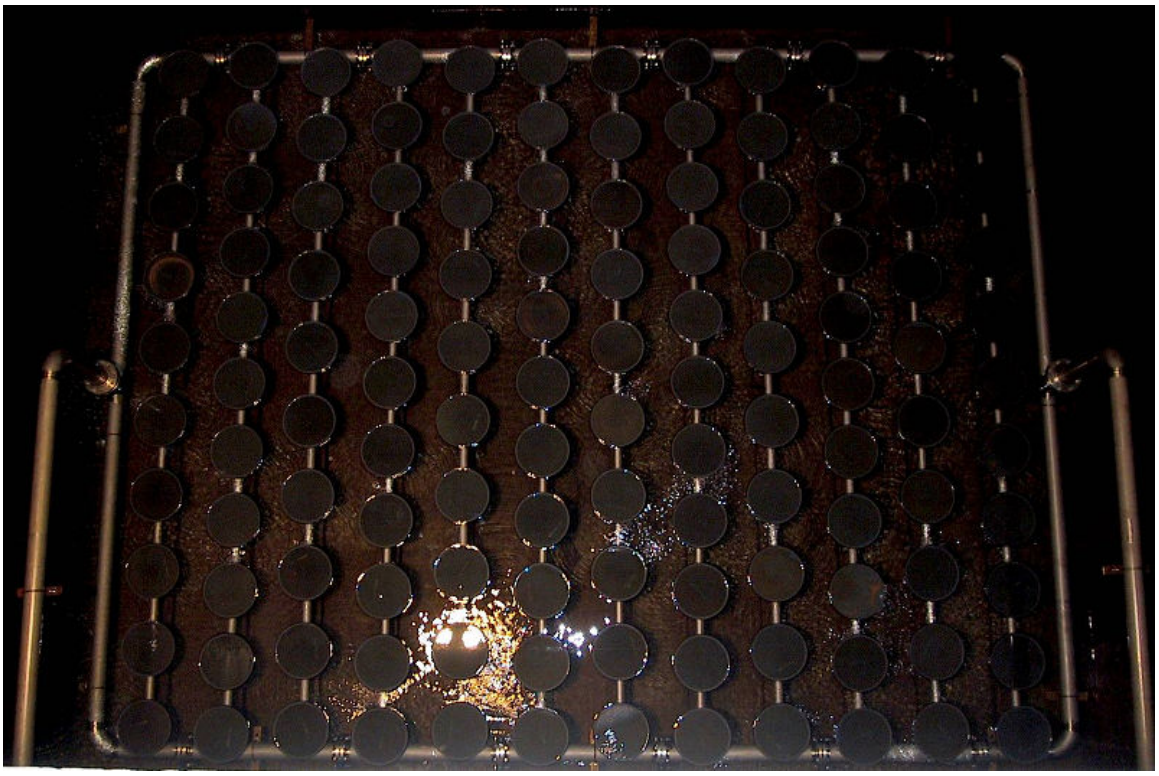

Diffuser diameter: 0.35 m

Appendix C
Geometry of the Mannheim Water Treatment Plant Ozone Contactor

1. Cell 1 and Cell 2

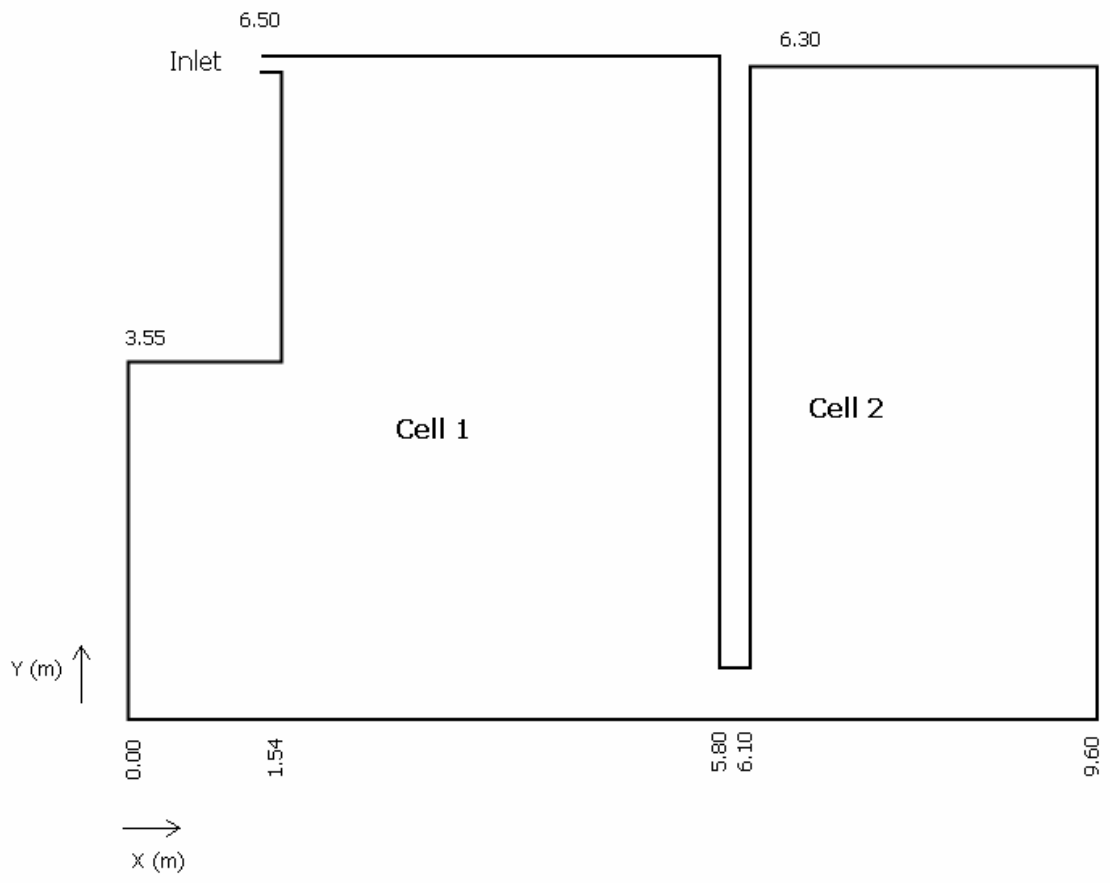

Width of Cell 1 to 2 (Z direction) is 2.40 m

2. Cells 3 to 6

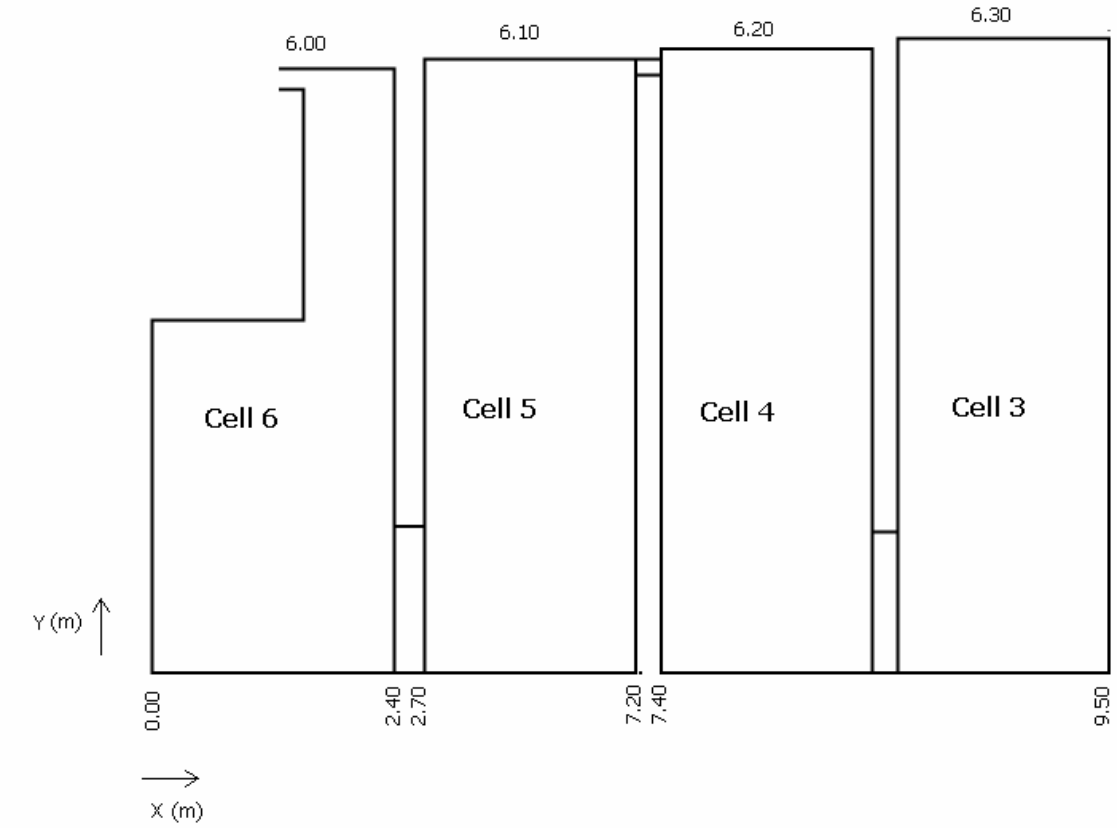

Width of Cell 3 to 6 (Z direction) is 4.50 m

Appendix D

Arrangement of Bubble Diffusers in the Cell 1 of the Mannheim Water Treatment Plant Ozone Contactor

Appendix E

Tracer Test Conditions and Results of the DesBaillets Water Treatment Plant Ozone Contactor

1. Tracer test 1

Water Flow rate (m^3/s):	2.16	Temperature (°C):	24
Gas Flow rate (m^3/s):	0.15		
Tracer dose Concentration (mg/L):	2.10		
Background Concentration (mg/L):	0.13		

Time (s)	Measured Concentration (mg/L)	Adjusted Concentration (mg/L)	C/C_0
18	0.11	-0.03	-0.01
78	0.12	-0.02	-0.01
128	0.12	-0.02	0.00
178	0.12	-0.02	0.00
188	0.11	-0.03	-0.01
198	0.22	0.08	0.04
208	0.3	0.16	0.08
218	0.25	0.11	0.06
228	0.37	0.23	0.12
238	0.29	0.15	0.08
248	0.46	0.32	0.16
258	0.44	0.3	0.15
268	0.43	0.29	0.15
278	0.52	0.38	0.2
288	0.54	0.4	0.2
298	0.69	0.55	0.28
308	0.68	0.54	0.27
318	0.73	0.59	0.3
328	0.79	0.65	0.33
348	0.91	0.77	0.39
368	1.19	1.05	0.53
388	1.32	1.18	0.59
408	1.51	1.37	0.69
428	1.59	1.45	0.73
448	1.54	1.4	0.7
478	1.64	1.5	0.76
508	1.81	1.67	0.84
548	1.94	1.8	0.9
608	2	1.86	0.94

2. Tracer test 2

Water Flow rate (m^3/s):	1.47
Gas Flow rate (m^3/s):	0.18
Temperature (°C):	24
Tracer dose concentration (mg/L):	2.10
Background Concentration (mg/L):	0.18

Time (s)	Measured Concentration (mg/L)	Adjusted Concentration (mg/L)	C/C_0
167.5	0.21	0.03	0.01
182.5	0.22	0.04	0.02
197.5	0.17	-0.01	0
212.5	0.21	0.03	0.01
232.5	0.22	0.04	0.02
252.5	0.32	0.14	0.07
272.5	0.36	0.18	0.09
292.5	0.44	0.26	0.12
312.5	0.55	0.37	0.18
342.5	0.56	0.38	0.19
372.5	0.6	0.42	0.21
402.5	0.61	0.43	0.21
432.5	0.95	0.77	0.38
462.5	1.23	1.05	0.52
492.5	1.46	1.28	0.63
522.5	1.53	1.35	0.67
552.5	1.62	1.44	0.71
582.5	1.67	1.49	0.74
612.5	1.85	1.67	0.83
652.5	1.92	1.74	0.86
702.5	1.98	1.8	0.89
762.5	2.11	1.93	0.96
822.5	2.07	1.89	0.94
882.5	2.07	1.89	0.94
942.5	2.15	1.97	0.98
1002.5	2.09	1.91	0.95
1092.5	2.16	1.98	0.98
1182.5	2.13	1.95	0.97

Appendix F

Turbulence Model Sensitivity Tests: Simulation Condition and Results

The sensitivity tests were done by simulation of the DesBaillets WTP Ozone Contactor using four different turbulence models: the standard k–ε model, the shear stress transport (SST) model, the Speziale-Sarkar-Gatski (SSG) model and the RNG k–ε model.

Simulation Conditions and Results:

Water Flow rate (m^3/s):	2.16
Gas Flow rate (m^3/s):	0.15
Temperature (°C):	24

Time (s)	Normalized Concentration			
	k-ε model	SST model	SSG model	RNG k-ε Model
0	0.00	0.00	0.00	0.00
10	0.00	0.00	0.00	0.00
20	0.00	0.00	0.00	0.00
30	0.00	0.00	0.00	0.00
40	0.00	0.00	0.00	0.00
50	0.00	0.00	0.00	0.00
60	0.00	0.00	0.00	0.00
70	0.00	0.00	0.00	0.00
80	0.00	0.00	0.00	0.00
90	0.00	0.00	0.00	0.00
100	0.00	0.00	0.00	0.01
110	0.00	0.00	0.01	0.02
120	0.00	0.01	0.01	0.03
130	0.01	0.01	0.02	0.05
140	0.01	0.02	0.04	0.07
150	0.02	0.04	0.05	0.10
160	0.03	0.06	0.08	0.13
170	0.04	0.09	0.11	0.15
180	0.06	0.12	0.14	0.18
190	0.08	0.15	0.17	0.21
200	0.10	0.18	0.20	0.23
210	0.13	0.21	0.23	0.26
220	0.15	0.24	0.25	0.29

continued

230	0.18	0.27	0.28	0.31
240	0.21	0.30	0.31	0.34
250	0.24	0.33	0.33	0.37
260	0.27	0.35	0.36	0.39
270	0.30	0.38	0.39	0.41
280	0.33	0.40	0.41	0.43
290	0.36	0.42	0.43	0.46
300	0.39	0.45	0.46	0.48
310	0.42	0.47	0.48	0.50
320	0.45	0.49	0.50	0.52
330	0.47	0.51	0.52	0.54
340	0.50	0.53	0.54	0.55
350	0.52	0.55	0.56	0.57
360	0.55	0.57	0.58	0.59
370	0.57	0.58	0.60	0.61
380	0.59	0.60	0.62	0.62
390	0.61	0.62	0.63	0.64
400	0.63	0.63	0.65	0.65
410	0.65	0.65	0.67	0.67
420	0.67	0.66	0.68	0.68
430	0.69	0.68	0.70	0.69
440	0.70	0.69	0.71	0.70
450	0.72	0.70	0.72	0.72
460	0.74	0.72	0.74	0.73
470	0.75	0.73	0.75	0.74
480	0.76	0.74	0.76	0.75
490	0.78	0.75	0.77	0.76
500	0.79	0.76	0.78	0.77
510	0.80	0.77	0.79	0.78
520	0.81	0.78	0.80	0.79
530	0.82	0.79	0.81	0.80
540	0.83	0.80	0.82	0.81
550	0.84	0.81	0.83	0.81
560	0.85	0.82	0.84	0.82
570	0.86	0.83	0.85	0.83
580	0.87	0.83	0.85	0.84
590	0.88	0.84	0.86	0.84
600	0.88	0.85	0.87	0.85
610	0.89	0.85	0.87	0.86
620	0.90	0.86	0.88	0.86
630	0.90	0.87	0.89	0.87
640	0.91	0.87	0.89	0.87
650	0.91	0.88	0.90	0.88
660	0.92	0.88	0.90	0.88
670	0.92	0.89	0.91	0.89
680	0.93	0.89	0.91	0.89
690	0.93	0.90	0.92	0.90

continued

700	0.94	0.90	0.92	0.90
710	0.94	0.91	0.92	0.91
720	0.94	0.91	0.93	0.91
730	0.95	0.92	0.93	0.92
740	0.95	0.92	0.93	0.92
750	0.95	0.92	0.94	0.92
760	0.96	0.93	0.94	0.93
770	0.96	0.93	0.94	0.93
780	0.96	0.93	0.95	0.93
790	0.96	0.94	0.95	0.94
800	0.97	0.94	0.95	0.94
810	0.97	0.94	0.95	0.94
820	0.97	0.94	0.96	0.95
830	0.97	0.95	0.96	0.95
840	0.97	0.95	0.96	0.95
850	0.97	0.95	0.96	0.95
860	0.98	0.95	0.97	0.96
870	0.98	0.96	0.97	0.96
880	0.98	0.96	0.97	0.96
890	0.98	0.96	0.97	0.96
900	0.98	0.96	0.97	0.96
910	0.98	0.96	0.97	0.97
920	0.98	0.97	0.97	0.97
930	0.98	0.97	0.98	0.97
940	0.99	0.97	0.98	0.97
950	0.99	0.97	0.98	0.97
960	0.99	0.97	0.98	0.97
970	0.99	0.97	0.98	0.98
980	0.99	0.97	0.98	0.98
990	0.99	0.98	0.98	0.98
1000	0.99	0.98	0.98	0.98
1010	0.99	0.98	0.98	0.98
1020	0.99	0.98	0.99	0.98
1030	0.99	0.98	0.99	0.98
1040	0.99	0.98	0.99	0.98
1050	0.99	0.98	0.99	0.98
1060	0.99	0.98	0.99	0.98
1070	0.99	0.98	0.99	0.98
1080	0.99	0.98	0.99	0.98
1090	0.99	0.98	0.99	0.98
1100	0.99	0.99	0.99	0.99
1110	0.99	0.99	0.99	0.99
1120	1.00	0.99	0.99	0.99
1130	1.00	0.99	0.99	0.99
1140	1.00	0.99	0.99	0.99
1150	1.00	0.99	0.99	0.99
1160	1.00	0.99	0.99	0.99

continued

1170	1.00	0.99	0.99	0.99
1180	1.00	0.99	0.99	0.99
1190	1.00	0.99	0.99	0.99
1200	1.00	0.99	0.99	0.99
1210	1.00	0.99	0.99	0.99
1220	1.00	0.99	1.00	0.99
1230	1.00	0.99	1.00	0.99
1240	1.00	0.99	1.00	0.99
1250	1.00	0.99	1.00	0.99
1260	1.00	0.99	1.00	0.99
1270	1.00	1.00	1.00	1.00

Appendix G

Mesh Density Sensitivity Tests: Simulation Condition and Results

The tests were done by simulation of the DesBaillets Water Treatment Plant ozone contactor using different mesh densities.

Contactor The simulation condition and data are as following:

Water Flow rate (m^3/s):	2.16
Gas Flow rate (m^3/s):	0.15
Temperature (°C):	24

Mesh element number: 320,803		Messh element number: 370,982		Mesh element number: 424,891
Time (s)	Normalized Concentration	Time (s)	Normalized Concentration	Normalized Concentration
0.00	0.00	0	0.00	0.00
1.00	0.00	30	0.00	0.00
10.00	0.00	60	0.00	0.00
20.00	0.00	90	0.01	0.01
30.00	0.00	120	0.03	0.03
40.00	0.00	150	0.07	0.06
50.00	0.00	180	0.12	0.13
60.00	0.00	210	0.19	0.21
70.00	0.00	240	0.27	0.31
80.00	0.00	270	0.36	0.40
90.00	0.00	300	0.43	0.48
100.00	0.00	330	0.50	0.55
110.00	0.00	360	0.57	0.60
120.00	0.01	390	0.62	0.65
130.00	0.01	420	0.68	0.69
140.00	0.02	450	0.72	0.73
150.00	0.03	480	0.76	0.77
160.00	0.04	510	0.80	0.80
170.00	0.06	540	0.83	0.82
180.00	0.08	570	0.86	0.85
190.00	0.10	600	0.88	0.87

continued

200.00	0.13	630	0.90	0.89
210.00	0.15	660	0.92	0.90
220.00	0.18	690	0.93	0.92
230.00	0.21	720	0.94	0.93
240.00	0.24	750	0.95	0.94
250.00	0.27	780	0.96	0.95
260.00	0.30	810	0.97	0.95
270.00	0.33	840	0.97	0.96
280.00	0.36	870	0.98	0.97
290.00	0.39	900	0.98	0.96
300.00	0.42	930	0.98	0.97
310.00	0.45	960	0.99	0.97
320.00	0.47	990	0.98	0.98
330.00	0.50	1020	0.98	0.98
340.00	0.52	1050	0.98	0.98
350.00	0.55	1080	0.98	0.98
360.00	0.57	1110	0.99	0.99
370.00	0.59	1140	1.00	1.00
380.00	0.61			
390.00	0.63			
400.00	0.65			
410.00	0.67			
420.00	0.69			
430.00	0.70			
440.00	0.72			
450.00	0.74			
460.00	0.75			
470.00	0.76			
480.00	0.78			
490.00	0.79			
500.00	0.80			
510.00	0.81			
520.00	0.82			
530.00	0.83			
540.00	0.84			
550.00	0.85			
560.00	0.86			
570.00	0.87			
580.00	0.88			
590.00	0.88			
600.00	0.89			
610.00	0.90			
620.00	0.90			

continued

630.00	0.91
640.00	0.91
650.00	0.92
660.00	0.92
670.00	0.93
680.00	0.93
690.00	0.94
700.00	0.94
710.00	0.94
720.00	0.95
730.00	0.95
740.00	0.95
750.00	0.96
760.00	0.96
770.00	0.96
780.00	0.96
790.00	0.97
800.00	0.97
810.00	0.97
820.00	0.97
830.00	0.97
840.00	0.97
850.00	0.98
860.00	0.98
870.00	0.98
880.00	0.98
890.00	0.98
900.00	0.98
910.00	0.98
920.00	0.98
1100.00	1.00

Appendix H

Evaluation of a CFD Modelling Approach for Prediction of Flocculation Mixing Performance at the City of Toronto's R.L. Clark Water Treatment Plant

Abstract

In this study, computational fluid dynamics (CFD) was used for evaluating flocculation treatment performance. A three-dimensional CFD model was developed to predict potential impacts of a change in equipment on flocculation mixing performance at the R.L. Clark Water Treatment Plant in Toronto. A new parameter, Local G value (velocity gradient) was introduced to quantitatively evaluate local mixing intensities. The CFD-simulated flow fields identified the locations of potential dead zones and short-circuiting that might affect flocculation efficiency. The results also indicated that local G values varied by orders of magnitude at different locations and changed significantly with impeller speed. At an impeller speed of 5 rpm, the local G values might change from 1000 s^{-1} at locations around the impellers to lower than 20 s^{-1} at locations closer to the walls. When impeller speeds increased to between 20 to 30 rpm, the local G values at most of the areas in the tank were higher than 80 s^{-1}, a typically recommended upper limit of the G value for flocculators with vertical-shaft turbines. The effects of baffling conditions on flocculation efficiency were also studied. The results to date suggested that a single baffle at the inlet location might be a better option than baffling in the middle of the tank. The indications of behaviour obtained from this modelling need to be validated by pilot- or full-scale testing.

This paper has been published in: Proceedings of 2006 OWWA/OMWA Joint Annual Conference, Ontario Water Works Association. It is attached herein to illustrate an alternative application of CFD for full-scale drinking water treatment processes.

1. Introduction

Flocculation is instrumental for the removal of particulate contaminants in conventional drinking water treatment systems. It is a physical process of agglomerating small particles into larger ones that can be more easily removed from suspension (AWWA, 1999). To insure maximum particle removal, proper mixing conditions and energy input must be provided in the flocculation tank. The mixing performance of mechanical mixers depends on the impeller type, impeller speed, reactor geometry, and the hydraulic residence time. The effects of these factors on full-scale flocculators are usually complicated and difficult to be predicted via traditional calculation approaches or lab-scale experiments.

In recent years, computational fluid dynamics (CFD) has come into use for evaluating water and wastewater treatment processes, such as disinfection contactors, air flotation units, sedimentation, coagulation and flocculation units (Lyn et al. 1999; Greene, 2002; Zhang et al., 2005). CFD is the science of predicting fluid flow, mass transfer, chemical reactions and related phenomena by solving the mathematic equations governing these processes using numerical algorithms (Versteeg et al., 2001). The use of CFD enables designers to obtain solutions for problems with complex geometry and boundary conditions. For flocculation processes, Luo (1997) applied the particle tracking method to predict mixing intensity of flocculation vessels. Essemiani and Traversay (2002) used the Eulerian approach to study mixing performance and residence time distribution of an experimental stirred vessel. However the majority of the previous CFD studies on flocculation treatment have focused on its applications on single impeller laboratory scale mixers.

The purpose of this research was to develop a three-dimensional CFD model and apply it to provide indications of the mixing performance of a complex full-scale flocculator

with a vertical shaft impeller mixer, which was being installed for the upgrading of the secondary flocculation process at the City of Toronto's R.L. Clark Water Treatment Plant. Because detailed design information was not available at the time of modelling and validation of the modelling results could not be performed, this research was considered to provide indications of expected behaviour, rather than quantitative predictions.

2. The CFD Modelling Approach

Computational fluid dynamics (CFD) works by solving the equations of fluid flow (the Reynolds averaged Navier-Stokes equations and turbulence transport equations) over a region of interest, with specified (known) conditions at the boundaries of that region. The commercial software CFX5.7.1 (ANSYS Canada Inc., Waterloo, Ontario, Canada) was chosen for this study. Using this software, the region of interest was divided into small elements, called control volumes. The equations were discretised and solved iteratively for each control volume. As a result, an approximation of the value of each variable at specific points throughout the domain could be obtained. In this way, a full picture of the behaviour of the flow could be derived (ANSYS, 2004).

2.1 Multiple Reference Frames (MRF) Model

To model impeller performance accurately, a 3D simulation was performed. The multiple frame of reference (MFR) model was used to simulate the impeller rotation. In the MFR modelling, the geometry of the flocculator was divided in two domains: a rotating frame was used for the region containing the rotating components (impellers) and a stationary frame was used for the regions that were stationary (tank walls and baffles). There are two commonly used models for connecting the two frames and incorporating the motion of the impellers. The first is called the frozen rotor interface

model, which produces a "steady state" solution to the multiple frame of reference problems. The two frames of reference connect in such a way that they each have a fixed relative position throughout the calculation, and the solution proceeds with steady transfer of information across the interface between the two frames. The second option is the transient rotor-stator model. With this model, the two grids slide past each other in a time-dependent manner, exchanging information at the cylindrical interface. The transient rotor-stator model is useful for examining start-up transients, or to accurately predict the periodic flow pattern in stirred reactors. The penalty is calculation time, which can be an order of magnitude longer than that needed for steady state calculations (Essemiani and Traversay, 2002). In this study, the frozen rotor interface model was chosen to be computationally effective.

2.2 Turbulence Models

Turbulence modeling is of crucial importance when describing flows in CFD modeling. The Shear Stress Transport (SST) model was used in this study. The SST model works by automatically applying the k-ε model in the bulk flow and the k-ω model at the walls. Previous research has shown that this model is superior to standard models in view of separation, lift and drag predictions (Gobby, 2004).

2.3 Local Velocity Gradient G

The performance of a flocculation vessel is commonly described by the global velocity gradient G (s^{-1}). This parameter is defined as:

$$G = [(P/volume)/ \mu]^{(1/2)} \quad (1)$$

Where P/volume is the power dissipated per unit volume and μ is the dynamic viscosity (Pa . s). This approach gives an average value; however, it does not provide any

information about the local shear rate distribution in the vessel. The rate of floc formation is directly proportional to the local velocity gradient distribution. The local G distribution is important as it controls particle suspension, distribution, coalescence and break-up efficiency.

In the present study, the local velocity gradient G was defined as:

$$G = (\mu_t / \mu)\sqrt{2\sum_i (\frac{\partial u_i}{\partial x_i})^2 + \sum_{i,j} [\frac{\partial u_i}{\partial x_j} + \frac{\partial u_j}{\partial x_i}]^2} \qquad (2)$$

Where, μ_t is the dynamic turbulent viscosity.

The local G value was calculated in CFX-POST using the simulated turbulence,(?) viscosity and flow velocity gradient data. It was used as a key parameter for evaluation of mixing performance of impeller mixers in this study.

2.4 Tracer Test Simulation

For flocculation processes, adequate residence time must be provided to allow generation of particles sufficiently large to allow their efficient removal in subsequent treatment processes. Residence time distribution (RTD) curves were simulated by solving scalar transport equations. First, a steady state CFD simulation was performed for calculating the fluid velocity fields. Then the tracer scalar was defined as an additional variable. The flow field obtained from the above simulation was used as the initial condition and was frozen when conducting unsteady state simulations to solve the tracer scalar transport equations.

2.5 CFD Modelling Procedures

The CFD modelling involves four sequential steps (ANSYS, 2004):

(1) Geometry and mesh generation

The geometry of the flocculator and impellers was built using a commercial CAD software: Solidworks^{TM} (SolidWorks Corporation, Massachusetts, USA). The geometry model then was imported into CFX-mesh to generate the mesh.

(2) CFD model setup

The flows in the flocculator were assumed to be isothermal. The frozen rotor model was used for the multiple frames of reference. The influent flow rate for the modelling was 2.55 m^3/s. The walls of the flocculation tank were set as no-slip walls and the top surface of the water was set as a free-slip wall. Impeller rotating speed were varied between 5 and 30 rpm. For steady state simulation, the time step was set at 0.1 to 10 s. The RMS (root mean square) normalised values of the equation residuals were set as 1×10^{-4}. For transient simulation, the total simulation time was 1200s. The time step was set between 1s and 20s.

(3) Simulation runs

In CFX 5.7, the governing equations for fluid flow and species transport are discretized in the computational domain by a finite volume method. Discretization of the non-linear differential equations yields a system of linear algebraic equations that are solved iteratively. A second order differencing scheme was applied to all equations to obtain high accuracy of computation.

(4) Post-processing

After a simulation has finished, CFX5.7 allows the presentation of results either graphically or numerically.

3. Case Study

The R. L. Clark Water Treatment Plant is a conventional treatment plant which treats water from Lake Ontario and has a rated capacity of 615,000 m^3/d. The treatment process consists of coagulation, flocculation, sedimentation, filtration, fluoridation and disinfection. This plant has three parallel coagulation/flocculation trains. After adding alum prior to rapid mixers, water flows through over-and-under hydraulic mixing chambers in series for coagulation, followed by flocculators. Each flocculation tank consists of a primary cell and a secondary cell. Currently, the primary flocculation tanks have been retrofitted with impeller-type mixers. The City of Toronto was replacing the old walking beam mixing equipment in the secondary cells with impeller mixers for flocculation. The current walking beam mixing system has functioned adequately to date but serious corrosion of moving parts and increased maintenance requirements necessitated the replacement of the mixing equipment.

3.1 Design of the Upgraded Flocculator

In the upgrading design, four impellers are being installed in each secondary flocculator. Each impeller has three hydrofoil blades, each being 2000 mm in diameter, with a minimum blade thickness of 12.7 mm and width of 300 mm with a tapered leading edge. Figure 1 shows the configurations of a flocculator and an impeller.

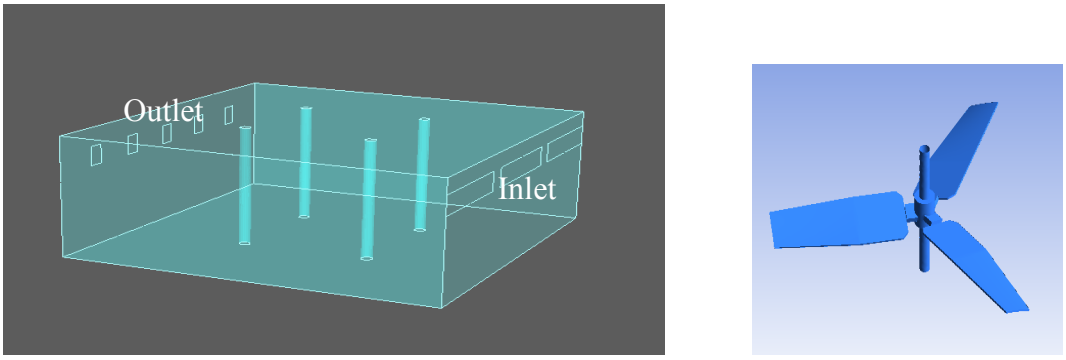

Figure 1 Three dimensional drawing of the existing flocculator (a) and impeller (b)

As mentioned previously, each flocculator consists of a primary flocculation cell and a secondary flocculation cell. Since the primary and secondary cells are separated by a wall, the effects of upstream mixing on downstream mixing can be considered to be negligible. Only the secondary flocculation cell was modelled in this study, and the modeling does not consider the upstream (primary cell) mixing conditions.

3.2 Geometry and Mesh Generation

In the actual secondary flocculation cell, there are four existing pillars for structural support. Preliminary modelling studies showed that the pillars have significant effects on the flow field in the flocculation tank. Therefore, the pillars were taken into account in the CFD modeling. Four impellers are being added beside each pillar. However, modelling the whole reactor is time consuming and computationally intensive. In this study, only half of the tank was modeled to reduce the computational time. Two geometry domains were set up via Solidworks. One is a stationary domain, and another is a moving domain. Fine tetrahedral three dimensional (3D) meshes were then created in CFX-mesh. For the stationary domain, meshing was done on multiple blocks to

obtain fine meshes at locations close to the moving domains. The mesh element numbers of the stationary domain and moving domain were 754,658 and 589,470×2 (two moving domains), respectively. The total number of elements for the flocculator was 1,933,598.

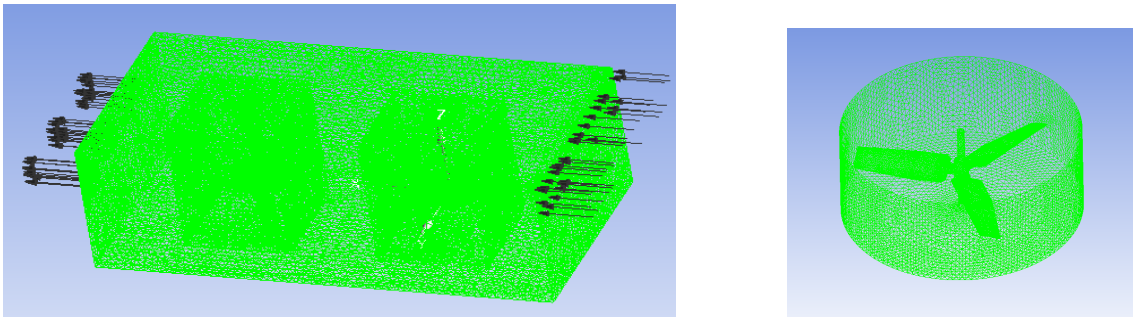

(a) Stationary domain (b) Moving domain

Figure 2 Mesh of two domains used in the frozen rotor interface model

4. Results and Discussion

4.1 Impact of Impeller Speed on Flow Fields

Figure 3 shows the simulated velocity fields when the rotating speed of both impellers was set at 5 rpm. The figure shows the locations of the potential dead zones and short-circuiting zones in the tank.

It was observed that the velocity of the incoming water could significantly influence the flow field and lead to serious short-circuiting and dead zone problems. This may be caused by the relatively low elevation of impeller A. Since the impeller and the inlet are at different heights, impeller A has reduced efficiency in mixing the incoming water in this configuration.

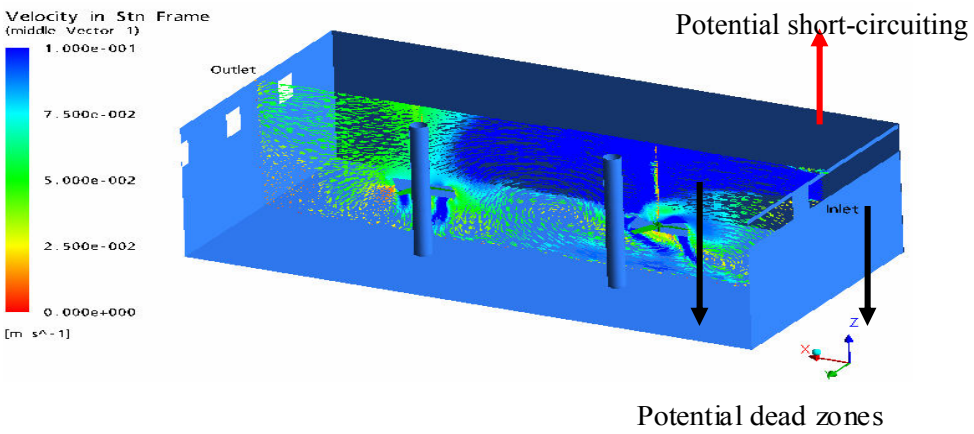

Figure 3 Velocity vectors inside the flocculator (impeller speed = 5 rev/min)

Figures 4 and 5 show the velocity fields simulated at higher rotating speeds (20 rpm and 30 rpm). It was observed that the impeller speed could significantly affect the flow fields. At higher impeller speed, the effects of influent water became smaller. However, local swirls were observed at the lower level of the tank. The existence of these swirls might reduce the mixing efficiency of the impellers.

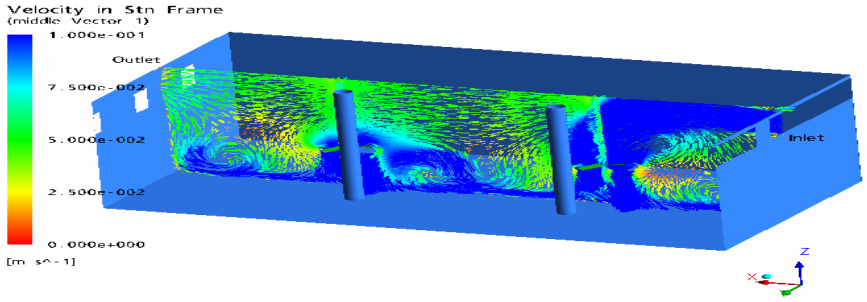

Figure 4 Velocity vectors inside the flocculator (impeller speed = 20 rev/min)

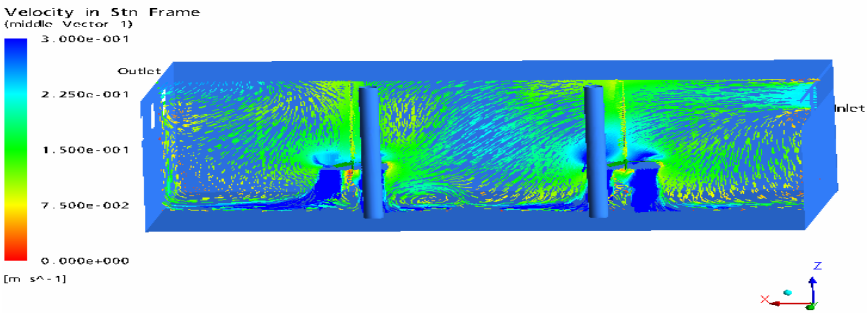

Figure 5 Velocity vectors inside the flocculator (impeller speed = 30 rev/min)

4.2 Residence Time Distribution

Figure 6 shows the effects of the impeller speed on the tracer residence time. The current results suggested that the flocculator had longer residence times at lower impeller speeds.

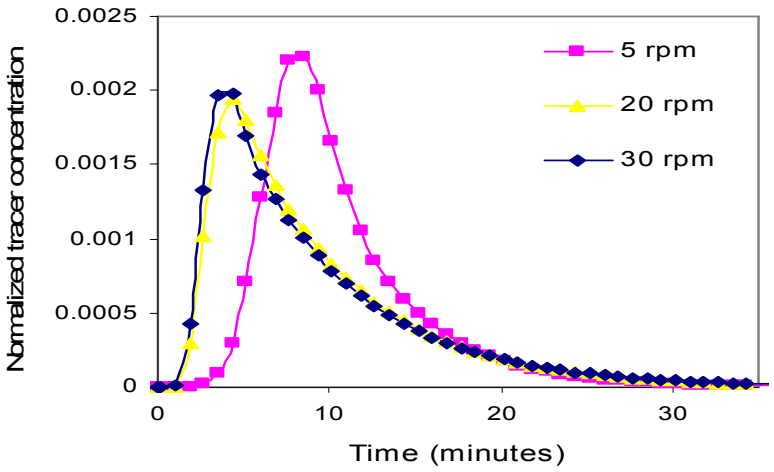

Figure 6 CFD predicted tracer residence time distribution curves

4.3 Local Velocity Gradient G

As discussed earlier, the local velocity gradient G was introduced in this study to describe local mixing intensity inside the flocculator. Figures 7, 8 and 9 show the local G value distributions inside the flocculator at different impeller speeds.

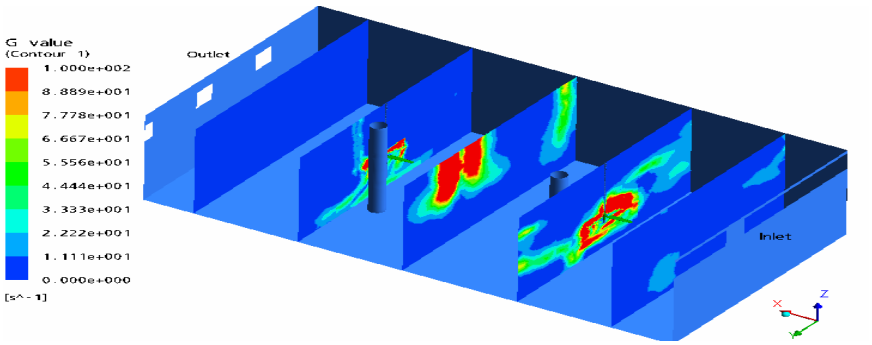

Figure 7 Local velocity gradient (G) distribution inside the flocculator (impeller speed = 5 rpm)

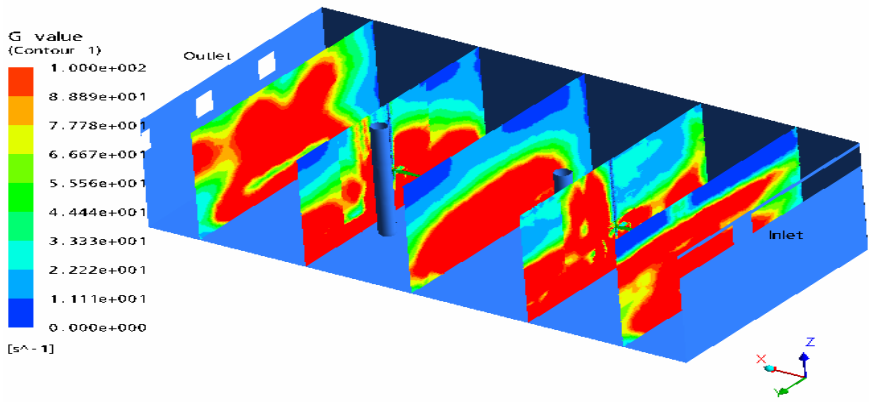

Figure 8 Local velocity gradient (G) distribution inside the flocculator (impeller speed = 20 rpm)

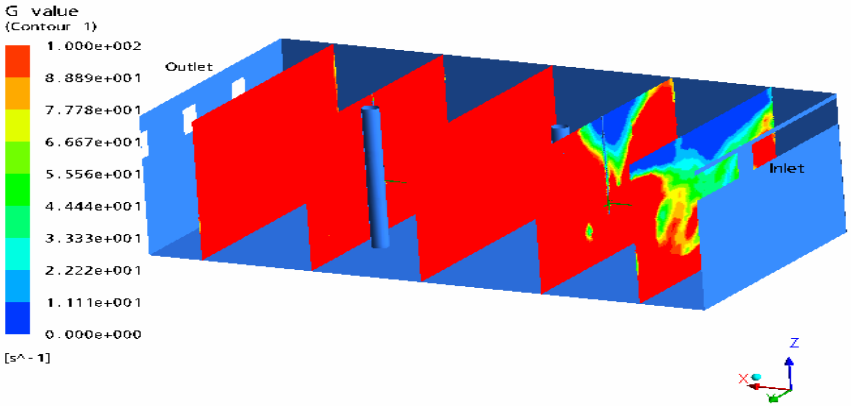

Figure 9 Local velocity gradient (G) distribution inside the flocculator (impeller speed = 30 rpm)

From the above figures, it could be observed that local G value varied with the monitoring location. When the impeller speed equalled to 5 rpm, the local G values at locations around the two impellers were in the range of 100 to 1000 s^{-1} and became significantly lower (less than 30 s^{-1}) at locations close to the walls. When impeller speeds equalled to 20 and 30 rpm, the local G values in most areas in the tank were higher than 100 s^{-1}. Based on drinking water treatment flocculation principles, mixing intensity values (average G values) for flocculators with vertical-shaft turbines should be in the range of 10 to 80 s^{-1} (MWH, 2005). The results suggested that for this flocculator configuration a more appropriate range of G values could be obtained at lower impeller speeds. Keeping in mind the fact that the modelled flocculators were in fact secondary flocculators, average G values in the lower part of the range cited would be more appropriate. This would also assist in minimizing breakup of flocs previously formed in the primary flocculation tank. However, at lower G values short-circuiting potentially existed near the inlet locations, as mentioned earlier, and this might reduce flocculation efficiency.

4.4 Effects of Baffle Walls on Impeller Mixing Performance

To obtain better G value distribution and reduce swirling in the flocculator, research was also conducted to study the benefits of installing baffle walls in the tank. Figure 10 shows the CFD simulation results of the flocculator with a baffle positioned in the middle of the tank. The length and width of the baffle wall was 4.7 m and 0.25 m respectively. The rotating speeds of impeller A and impeller B were 10 rpm and 5 rpm respectively. The higher speed for impeller A was chosen to reduce short-circuiting near the inlet. From the velocity profiles, it was found that the flow in the region downstream of the baffle had been improved; however the region upstream of the baffle was still poorly mixed. Therefore, installing a baffle wall in the middle of the flocculator might not be sufficient to improve the mixing efficiency.

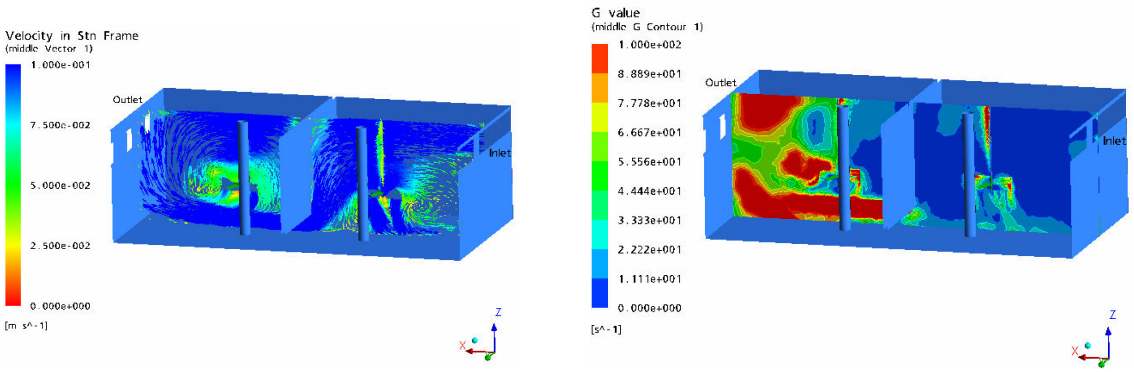

a) Flow field b) Local G value distribution

Figure 10 CFD simulation results of a baffled flocculator (baffle located at the middle of the tank, speeds of impeller A and impeller B are 10 rpm and 5 rpm, respectively)

Figure 11 shows the CFD simulation results of the flocculator with an alternative baffle location. A 3 m high baffle wall was located 1.5 m away from the inlet. The rotating speeds of impeller A and impeller B were 10 rpm and 5 rpm respectively, as for the other baffle location. This analysis suggested that the inlet baffle wall could substantially improve mixing. The inlet baffle could improve the G value distribution along the tank (decreasing from high to low). Under the current modelling conditions, the average G value of the half flocculator at the outlet side was 11.7 s^{-1}, which was in the range of 10 to 30 s^{-1}. At the inlet side, the average G value was relatively high (94.3 s^{-1}), which was caused by high G values in a small area around the impeller. The average G of the total tank was 43.8 s^{-1} which was in middle of the suggested G value range (10 to 80 s^{-1}) (MWH, 2005).

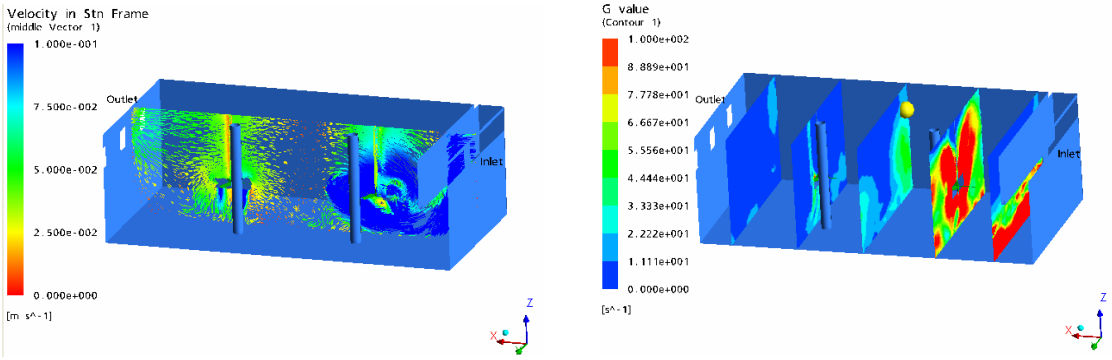

a) Flow field b) Local G value distribution

Figure 11 CFD simulation results of a baffled flocculator (baffle is close to the inlet, speeds of impeller A and impeller B are 10 rpm and 5 rpm, respectively)

4.5 Prediction of the G*t Value

A key design factor in a flocculation basin is the value of G*t (velocity gradient × detention time). From the CFD based tracer RTD and local G value analysis, it is possible to roughly predict the G*t value for the flocculator. For example, in Figure 11, the flocculation tank was divided into two regions by a middle plane between the two impellers. The spatial average G values of region 1 and region 2 were 94.3 s^{-1} and 11.7 s^{-1}, respectively. From tracer test simulation, it was found that the average residence times T_{50} for the two regions were 3.9 min and 4.6 min, respectively. Therefore, the G*t value of region 1 equaled 22066 (94.3 s^{-1} × 3.9 min), and G*t of region 2 was 3229 (11.7 s^{-1} × 4.6 min). The total G*t therefore was 25,295 (22,066 + 3,229), which was within the typically range (10,000 to 150,000), as cited by Qasim et al. (2000).

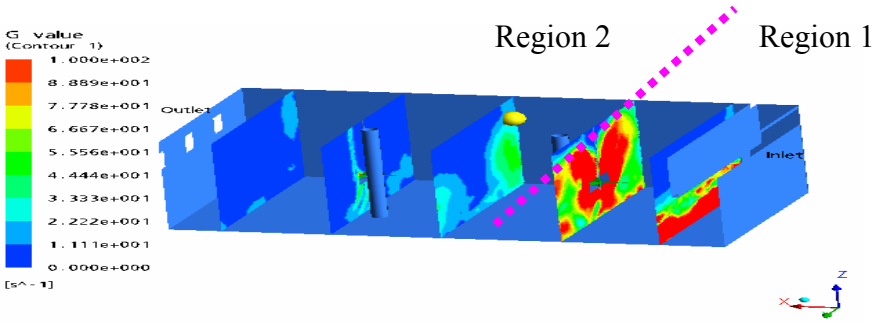

Figure 12 Method for prediction of the G*t value

5. Limitations of CFD Modelling and Future Work

Despite the significant advantages of CFD as a tool for predicting impeller mixing behaviour, it should be pointed out that current CFD techniques still have some limitations. CFD has to be used carefully and responsibly. The main sources of CFD error include the incorrect selection of numerical discretisation methods, improper turbulence model selection, incomplete description of geometry, computer round off, or poor definition of boundary conditions.

In the present research, the main uncertainty factor is the geometry of the impellers because limited information was available during the modelling work. A more refined prediction of system performance could be attempted if accurate design information is available for simulations and some sample results could be validated by full-scale or pilot scale testing. It is suggested that the sensitivity of mesh density, turbulence model selection, and boundary condition definitions should also be further studied to potentially improve the accuracy of prediction of mixing performance in the flocculation process. As with all CFD modelling, predictions should be validated with actual measured data. For the flocculators modelled, a comparison of actual tracer test results to model predictions would be the minimum level of validation that should occur. The validated model would then be able to be used in the future design and retrofit of similar flocculation systems.

In conducting further work it should be kept in mind the discrepancies between the global G values and CFD predicted local G values. A study of a laboratory-scale flocculator conducted by Essemiani and Traversay (2002) showed that the mean G value calculated from the local G distribution predicted by CFD was much higher than the one calculated by power input (Equation 1). This may be due to that, the local G value calculation (Equation 2) integrates turbulence effects through including a

turbulent viscosity term, however the global G value is derived based on a laminar shear flocculation rate equation and it is not a valid representation of the average velocity gradient in a turbulent fluid (AWWA, 1999, p 6.48; MWH, 2005, p 700). It would be necessary to conduct further studies to obtain an appropriate range for the CFD-predicted local G values and use this range to evaluate flocculation performance.

6. Conclusions

The mixing of a flocculator is affected by multiple factors including impeller speed, flocculator configuration, and inlet velocity. The CFD model described in this paper provided an efficient tool for understanding impeller mixing performance under various conditions and assists with the optimization of its design and operation. The application of the Local G values provided more detailed information for describing impeller mixing behaviour, compared with the use of the global G value.

This study demonstrated the potential of CFD as an efficient tool for understanding impeller mixing performance and may provide useful information for the design and operation of flocculation treatment processes. Because detailed design information was not available at the time of modelling and validation of the modelling results could not be performed, this research was considered to provide indications of expected behaviour, rather than quantitative predictions.

Initial CFD simulation results suggested that dead zones and short-circuiting might exist in the secondary flocculation tank after installing vertical shaft turbine impellers at the R.L. Clark Water Treatment Plant. These zones might influence flocculation efficiency. Installing baffles in the tanks might improve mixing performance in the flocculator. CFD simulation showed that installing a single baffle at the inlet location might be a

better choice than positioning a baffle in the middle of the tank. It was also suggested that experimental studies should be done in the future to validate the CFD modelling.

7. Acknowledgements

The authors would like to acknowledge the contribution of the City of Toronto. Funding for this project was provided by the Natural Sciences and Engineering Research Council of Canada (NSERC) in the form of an Industrial Research Chair at the University of Waterloo. The current Chair partners include: American Water Canada Corp., Brightwell Technologies Inc., the cities of Brantford, Guelph, Hamilton, Ottawa and Toronto, Conestoga-Rovers & Associates Limited, EPCOR Water Services, the Ontario Clean Water Agency (OCWA), PICA USA Inc., RAL Engineering Ltd., the Region of Durham, the Regional Municipalities of Niagara and Waterloo, Stantec Consulting Ltd., and Zenon Environmental Inc.

8. References

ANSYS (2004). CFX User manual, Ansys Europe Ltd.

American Water Works Association (1999). Water quality and treatment: a handbook of community water supplies. 5th Edition, Mcgraw-Hill, New York, USA.

MWH (2005). Water treatment: principles and design. 2th edition, John Wiley & Sons, Inc., New Jersy, USA.

Crozes G.F., Hagstrom J.P., Clark M.M., Ducoste J. and Burns C. (1999). Improving clearwell design for ct compliance. AWWARF and AWWA, Denver, Co.

Essemiani K. and Traversay C. (2002). Optimization of flocculation process using computational fluid dynamics. Chemical Water And Wastewater Treatment Vii. Proceedings of the 10th Gothenburg Symposium 2002, Gothenburg, Sweden.

Gobby D. (2004). Mixing of newtonian and non-newtonian fluids in a agitated baffled tank. CFX Validation Report, Ansys Europe Ltd.

Luo C. (1997). Distribution of velocities and velocity gradients in mixing and flocculation vessels: comparison between LDV data and CFD predictions. Ph.D Thesis, New Jersey Institute of Technology, New Jersey, USA.

Qasim S.R., Motley E.M. and Zhu G. (2000). Water work engineering planning, design and operation. Prentice-Hall Inc., New Jersy, USA.

Versteeg, H.K. and Malalasekera W. (2002). An introduction to computational fluid dynamics: the finite volume method. Longman Scientific & Technical Inc., Longman, UK.

Zhang, J., Anderson W.B., Smith E.F., Barbeau B., Desjardins R. and Huck P.M. (2005). Development, validation and implementation of a multiphase cfd model for optimization of full-scale ozone disinfection processes. AWWA Water Quality Technology Conference and Exposition (WQTC), Quebec City, Quebec. November 6-10, 2005, paper Mon14-3.